Geosynthetics '99

"Specifying Geosynthetics and Developing Design Details"

GEOSYNTHETICS 99 CONFERENCE
Boston, Massachusetts USA

Conference Proceedings

April 28-30, 1999

Organized by:

IFAI
Industrial Fabrics Association International

NAGS
North American Geosynthetics Society

GMA
Geosynthetic Materials Association

under the auspices of
IGS
International Geosynthetics Society

SPONSORED BY

Table of Contents

Reinforced Soil Walls II

Filtration and Drainage II

Geosynthetics in Waste Containment Applications II

Table of Contents

Reinforced Soil Walls I

SNAILBACK WALL—FIRST FABRIC WALL REVISITED AT 25-YEAR MILESTONE

DARYL GREENWAY
CH2M HILL, USA
J. RICHARD BELL
OREGON STATE UNIVERSITY, USA
BRUCE VANDRE
UTAH DEPARTMENT OF TRANSPORTATION, USA

ABSTRACT

The successful performance of a 3-m-high geotextile retaining wall, the Snailback wall, is reviewed 25 years after construction. This historic wall, constructed in 1974 on a forest road in southwestern Oregon, is the first geosynthetic wall built in North America. It is located on the Siskiyou National Forest near Cave Junction, Oregon. Built of geotextile and earth materials, the wall established precedents for design and construction methods developed by the U.S. Forest Service and others.

The paper reviews the design, construction, and performance of the wall, and compares and contrasts the ground-breaking methodologies used in 1974 with modern practice. Practical lessons learned from this historic wall are summarized in the paper. Today, the wall stands without visible degradation and, after 25 years, continues to support the Illinois River Road and its traffic. Like the wall, the basic design concepts still serve.

INTRODUCTION

Twenty-five years ago, in 1974, interest in the new plastic construction fabrics was developing rapidly in the northwestern United States. The terms "geotextile" and "geosynthetic" had not yet been coined. The Pacific Northwest Region (Region 6) of the U.S. Forest Service (Forest Service) was beginning the preparation of their landmark "Guidelines for Use of Fabrics in Construction and Maintenance of Low-Volume Roads" (Forest Service Guidelines) (Steward, Williamson, and Mohney, 1977). The Crown Zellerbach Corporation was constructing a manufacturing plant in Camas, Washington, to produce a continuous filament, needle-punched, nonwoven, polypropylene fabric to be marketed as Fibretex. (The Crown Zellerbach Corporation and Fibretex are identified in this paper for historical interest. Crown Zellerbach and Fibretex are no longer in the USA geosynthetics market.)

Crown Zellerbach was also sponsoring research at Oregon State University (OSU) to investigate possible civil engineering applications for this product. This coincided with an expanding interest in Reinforced Earth® in the United States. The key paper on Reinforced Earth® retaining walls by Lee, Adams, and Vagneron (1973) provided a simple practical design procedure and encouraged further development. One of the studies at OSU involved a series of model tests of geotextile-reinforced soil walls (Stilley, 1975), based on a design method modified from Lee, Adams, and Vagneron (1973).

In December 1974, the results of these efforts coalesced where the Illinois River Road crosses Snailback Creek in the Siskiyou National Forest of southern Oregon. At this site, the first geosynthetic-reinforced soil wall was built as a permanent part of a public facility. It was constructed to repair a storm-damaged roadway. A sand-cement mortar facing was later sprayed directly on the exposed fabric face of the wall to preserve it from sunlight attack and vandalism. Twenty-five years later, this wall is still in place and, without any maintenance, is admirably performing its intended purpose, as seen on Figures 1A and 1B.

FIGURE 1A. Snailback Wall, June 1998

Considering the economics and the requirement of limited disturbance to the adjacent slope, a fabric wall appeared suited to the Snailback site. The opportunity to build a geotextile-reinforced soil wall also satisfied the interest of Forest Service personnel in developing fabric wall technology. This type of wall was recognized as "unproven and untried" but its potential usefulness offset the uncertainties. A decision was made to proceed and to consider this reconstruction an experimental project. Even though it was deemed experimental, the budget was extremely limited and instrumentation was not included. All evaluations were to be visual.

2517_02

FIGURE 1B. Close-up of Snailback Wall Face, June 1998

Table 1. Snailback Geotextile Wall Project Summary

Project Name	Experimental Fabric Reinforced Soil Wall for Repair of Illinois River Road at Snailback Creek
Location	Near Cave Junction, Oregon, USA (approximate latitude and longitude are N-42-17.063 and W-123-41.817, respectively)
Owner	U.S. Department of Agriculture, U.S. Forest Service
Specifying Agency	Siskiyou National Forest, Grants Pass, Oregon
Project Engineer	Bruce Vandre
Designer	J. Richard Bell
Wall Dimensions	3 m in height and 20 m in length
Facing System	Sand-cement mortar sprayed directly on geotextile
Reinforcement	420 g/sq meter continuous filament, polypropylene, needle-punched, nonwoven geotextile
Alternative	Crib-wall
Construction Date	December 1974

John Steward of the Forest Service's regional office was one of the observers during the construction of the Snailback wall. At the time he was collecting information for what would become the Forest Service Guidelines (Steward, Williamson, and Mohney, 1977). He included the design procedure developed for the Snailback project in the guidelines. These Forest Service Guidelines, which were updated in 1983, were widely used in the United States and were influential in the development of American geotextile practice.

DESIGN, CONSTRUCTION, AND PERFORMANCE

Design

The design and construction of the historic geotextile wall at Snailback Creek has been described previously (Bell, Stilley, and Vandre, 1975; Bell and Steward, 1977). Road repair required a wall approximately 3-m-high and 10-m-long in steep terrain. To facilitate construction, the excavation was to be ramped down from either end, resulting in a wall approximately 20 m long overall.

Figure 2 shows the design cross section of the fabric wall as drawn in July 1974. The wall design considered only Fibretex fabric and onsite earth materials. Using the Rankine tie-back wedge design method, the geotextile dimensions were calculated for a factor of safety of 1.5. Because of the well-drained nature of the site, water pressures were assumed negligible in the design. The as-built section of the wall is shown on Figure 3.

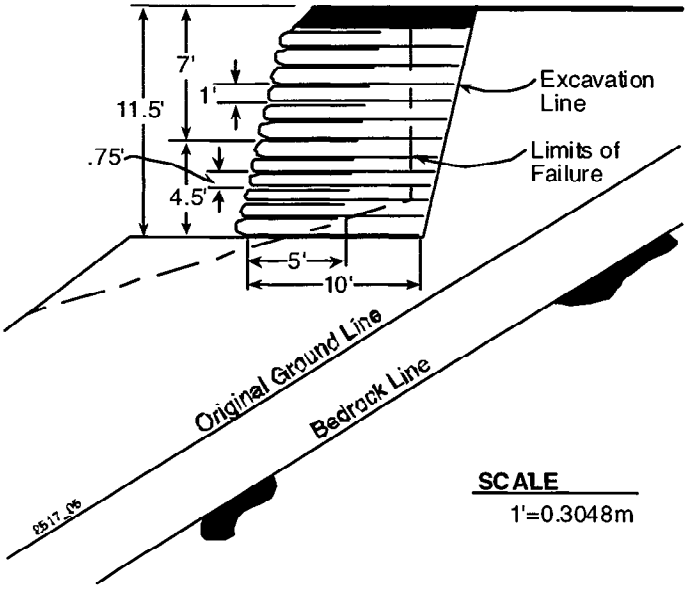

FIGURE 2. Section Through Tentative Design

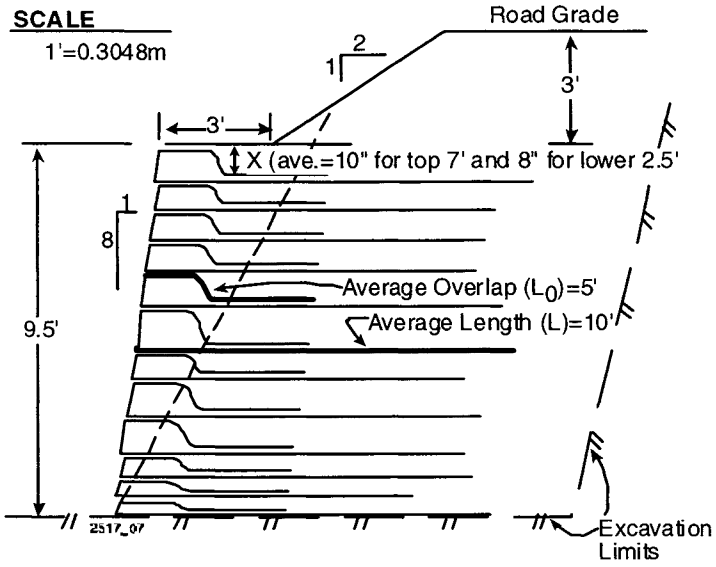

FIGURE 3. Completed Fabric Retained Earth Wall and Sketch of As-built Section

Construction

Figure 4A shows the nearly completed Snailback wall during construction. Additional pictures of the construction process were presented by Bell, Stilley, and Vandre (1975). A wrap-around fabric facing method of construction was planned for the Snailback wall because economics and the simplicity of not having to obtain additional facing components for the wall were important considerations. However, the wrap-around method created construction problems for which no prior experience existed; none of the individuals involved had experience building full-scale walls of this type. Building a berm and pulling the fabric back and anchoring it without using some temporary face support resulted in alignment problems; a support method using sand bags was employed after the first few layers. Figure 4B shows the wall during construction using sandbags. John Steward observed this construction problem and later developed the temporary movable form support system that was presented in the Forest Service Guidelines (Steward, Williamson, and Mohney, 1977). This support method is still widely used in current practice. The sand bag support method is still used in Japan.

2517_04

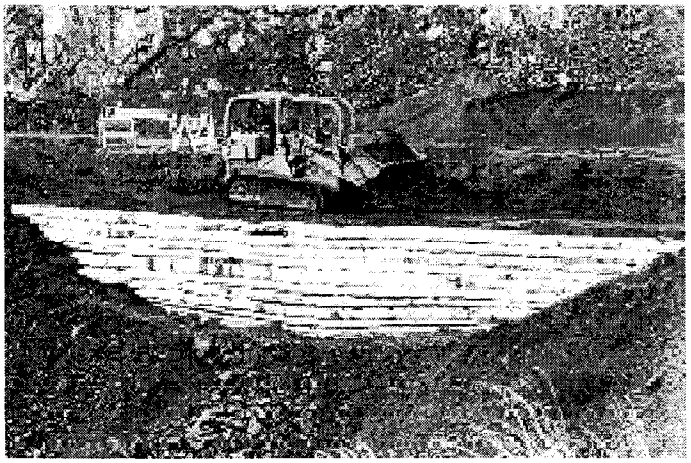

FIGURE 4A. Nearly Completed Wall During Construction, December 1974

2517_03

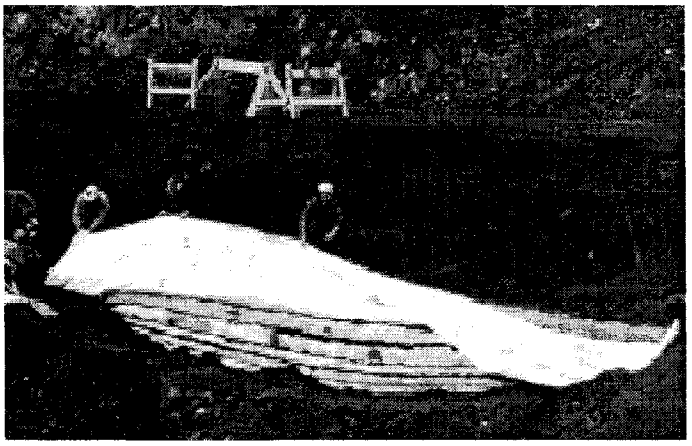

FIGURE 4B. Wall Construction Showing the Use of Sandbags

A sprayed mortar facing was applied during July 1975, eight months after the wall was constructed. The facing application was delayed to allow for backfill and geotextile deformation under service and environmental loading. At the time of the facing application, some of the geotextile exposed to sunlight had a powdery feel, indicating some deterioration. The wall face was first covered with 25-mm wire mesh attached with clips. The mortar consisted of seven sacks of cement per cubic meter of plaster sand and was applied with a stucco pump.

Performance

According to Forest Service records, no maintenance has been performed on the wall since construction in 1974. During a June 1998 inspection of the wall, only a few hairline shrinkage cracks were observed in the mortar facing and no spalling had occurred. The facing appeared to be in excellent overall condition. This indicates that no significant wall deformation had occurred after the placement of the facing, and generally illustrates the exemplary performance of the Snailback geotextile wall. The mortar facing has darkened with time, and in appearance the wall is very compatible with nearby rock outcrops. The facing was exposed to an environment where the average annual temperature is 12 degrees C, the average annual rainfall exceeds 1000 mm, and the average annual snowfall is less than 400 mm. The lowest average minimum monthly temperature is 0 degrees C, although daily and seasonal temperature changes at the wall site can be extreme. Detailed weather records for nearby Cave Junction, Oregon, since 1962 are available at http://www.wrcc.dri.edu/summary/climsmor.html.

GEOTEXTILE SELECTION: YESTERDAY AND TODAY

In 1974, less than 15 geotextile products were available for engineering uses, with approximately one-half being nonwovens (Steward, Williamson, and Mohney, 1977). Their properties were characterized primarily by mass-per-unit-area and some type of strength test inherited from the textile industry. The nonwoven, needle-punched, continuous filament, polypropylene fabric used was selected by the designer because he was familiar with it and it was available. A relatively heavy product with a nominal mass-per-unit-area of 420 g/sq m and a grab strength of about 1.1 kN (250 lb) was used (American Society for Testing and Materials (ASTM) D1682).

Today, according to the Geotechnical Fabric Report 1998 Specifier's Guide, more than 300 geotextiles are being produced and again approximately one-half are nonwovens. The relevant properties are characterized by several ASTM tests developed for specific engineering purposes. The wide-width tensile strength method (ASTM D4595) and creep-limited strength method (ASTM D5262) are the preferred methods for evaluating reinforcement applications. Less than 10 percent of the nonwoven fabrics are recommended for reinforcing use by their manufacturer. Approximately 5 percent of the nonwoven products have wide-width tensile strengths identified, and no creep-limited strength properties are listed. In contrast, about 55 percent of the woven geotextiles are recommended for reinforcing use by their manufacturer. Approximately 35 percent of the woven geotextiles have wide-width tensile strengths identified and 20 percent have creep-limited strength listed.

Today, woven fabrics are the geotextile most often recommended by manufacturers for reinforcement. For retaining walls, deformation is a critical consideration. However, the Snailback wall clearly shows that a nonwoven fabric can perform satisfactorily in retaining wall reinforcement application, and even with a low modulus fabric, wall movements are not necessarily large.

According to AASHTO M288, the Snailback geotextile would be rated at a high survivability level for erosion control and separation applications. Considering published mass-per-unit-area and wide-width tensile strength data, about 20 to 30 percent of the nonwoven geotextiles and most of the woven geotextiles would be expected to perform at least as well as the geotextile used in the Snailback wall. The selection of a geotextile for any reinforcement application should consider many factors including construction, durability, survivability, cost, and availability as well as mechanical properties. The choice of geotextile should be made according to the principle of design by function and not by whether the fabric is woven or nonwoven.

DESIGN BY 1974 AND CURRENT METHODS

Ratio of Fabric Tensile Resistance to Lateral Driving Load

The internal stability of geotextile reinforced walls with respect to fabric tensile failure can be reviewed by examining the ratio (R/L) of Allowable Tensile Resistance (R) to Lateral Driving Load (L) as determined by the Rankine tied-back wedge method:

$$R = Tu * \# / FTRF$$

Where:

- Tu = the ultimate tensile strength of the fabric;
- # = the number of sheets of fabric in a layer, and
- FTRF = the Fabric Tensile Reduction Factor.

$$L = z * \gamma * k * s$$

Where:

- z = the depth to the fabric layer with the lowest R/L ratio value;
- γ = the unit weight of the backfill material;
- k = the coefficient of lateral earth pressure; and
- s = thickness between fabric layers at the depth z.

Current Methods

The practice for determining some of the parameters used to calculate R/L have changed from those used on the Snailback wall in 1974 (Berg, Allen, and Bell, 1998). In 1998 the earth pressure coefficient used to determine loading is the active case (ka) rather than the at-rest (ko); the ultimate fabric strength is determined by the wide-width tensile strength test, not available in 1974; the allowable fabric tension incorporates reduction factors to account for creep, installation damage, and aging.

The current American Association of State Highway and Transportation Officials guidelines

(AASHTO, 1997) allow either a default Fabric Tension Reduction Factor (FTRF) of 7 or a best estimate of partial tension fabric reduction values. For Fibretex, our best estimate of the partial FTRFs from these guidelines are 2.5 for creep, 1.1 for installation damage, and 1.6 for aging. The product of these values yields a total FTRF of 4.4.

As-designed versus As-built

When an engineered structure performs satisfactorily for a considerable period of time, it is tempting to consider that fact a vindication of the design methodologies and assumptions. However, overly conservative design assumptions or deviations from the design during construction that significantly increase stability could result in satisfactory performance even with flawed design methodologies. Therefore, before conclusions are reached, an effort is made to estimate the factor of safety of the wall as actually built. This is done in terms of current practice because it includes the Fabric Tension Reduction Factor (FTRF).

Figure 2 shows the as-designed wall dimensions and Figure 3 shows the as-constructed dimensions. The design assumed a 3.5 m wall and called for 300 mm lifts in the top 2.3 m of the wall, 230 mm lifts in the lower portion of the wall, and a 1.0 m overlap of the wrap-around. This gives the critical layer at a depth of 3.4 m and a thickness of 230 mm. As Figure 3 shows, construction difficulties resulted in very thin lifts at the wall base, and thicker but variable lifts in the upper section. Because of the very thin lower lifts, the maximum fabric stresses are not in the lowest layers. The maximum fabric loads are in the fourth layer from the bottom, which is 2.1 m below the top of the wall and 290 mm thick. The actual fabric overlap is 1.5 m instead of 1.0 m. This resulted in embedment beyond the critical potential surface that is more than sufficient to fully develop the fabric strength. Therefore, two effective fabric sheets occur at each layer instead of one, as assumed in design.

As built, the wall was offset from the roadway so it was not subject to significant live loads, but during design large live loads from the transportation of logging equipment over the site were anticipated. As it worked out, live loads did not influence the design to any significant degree. At the bottom of the wall, the live load effect was small; in the upper part of the wall, the live load effect did not reduce layer spacing below that which was dictated by construction considerations.

Table 2 summarizes the values of the calculation parameters and the resulting R/L ratio values for three cases: (1) the original 1974 design assumptions; (2) the design assumptions revisited with current methodologies for FTRF, active earth pressure, and wide-width strength; and (3) the as-built dimensions, actual backfill parameters, and current methodologies. The table also presents the computed minimum R/L ratio for each case. This R/L ratio is equal to the factor of safety with respect to the maximum allowable fabric tension at the critical depth layer. Current practice requires a minimum R/L of 1.5. No surcharges, live loads, or pore water pressures are included. In the as-built case, the concrete facing and sandbags are assumed not to contribute to stability. During design, the backfill material was assumed to have a unit weight of

19.6 kN/m^3. The friction angle (ø) was assumed as 30 degrees, and this gave an at-rest lateral earth pressure coefficient (ko) as computed from 1-sin (ø) of 0.5 and an active coefficient (ka) of 0.33. Tests during construction indicated unit weights of 21.2 kN/m^3; post-construction strength tests of the imported backfill sand yielded a ø of 38 degrees (therefore an active coefficient of lateral earth pressure of 0.24).

Table 2. Comparative Wall Design Summary

	Case		
Method/Parameter	1	2	3
Method	1974	1998	1998
Geometry	As-designed	As-designed	As-built
Backfill	As-designed	As-designed	As-built
ø (deg)	30	30	38
k	0.50 (at-rest)	0.33 (active)	0.24 (active)
s (mm)	230	230	290
z (m)	3.4	3.4	2.1
γ (kN/m^3)	19.6	19.6	21.2
Tu (kN/m)	11.4	19.0	19.0
FTRF	1.0	4.4	4.4
#	1	1	2
R(kN/m)	11.4	4.3	8.6
L(kN/m)	7.8	5.1	3.2
R/L	1.5	0.8	2.7

The second set of parameters presented in Table 2 takes the design wall dimensions from Figure 2, uses the same original assumptions for backfill properties, but takes the modern approach and uses active earth pressures and an FTRF. This second set of parameters evaluates strength with the wide-width tensile test. In this case, R/L is 0.8, which is below the minimum of 1.5 required by current best practice (AASHTO, 1997). The higher strength and lower earth pressure coefficient both tend to increase R/L but the large FTRF overwhelms them and causes the large decrease.

The as-built conditions are also included in Table 2. In this case, the R/L of 2.7 exceeds the required minimum of 1.5. This reflects the stronger than assumed backfill and the construction of thinner than planned thicknesses between fabric layers. But even these would not result in an acceptable R/L without considering two fabric sheets in each reinforcement layer. As built, the factor of safety relative to the ultimate (FTRF = 1.0) wide-strip strength of the geotextile is 11.9.

The fabric overlap of the wrap-around of 1.5 m provides sufficient embedment behind the

critical Rankine surface to develop the full fabric strength, thereby providing two effective fabric sheets at each layer. This is not considered in the first two cases in Table 2 because it was intended to reflect the designers thinking in 1974. The decision to make the overlap 1.5 m was made for construction considerations after the design computations were completed. This factor is included in the as-built case to give the best comparison of the R/L of the actual Snailback wall for comparison to current practice.

A source of uncertainty in these analyses is the estimation of wide-width tensile strength. Wide-width test results were not available for the geotextile used in this wall (420 g/sq m Fibretex). The value used in Table 2 is from correlations with OSU Ring tests and 100 mm-wide strip tensile tests made of this fabric in 1974 and 1975. Five tests were selected and resulted in estimates for wide-width strength of 13.5; 15.5; 15.8; 15.8; and 16.9 kN/m. Actually the data supporting the correlation factors are very limited; however, after studying these data and test results on other fabrics similar to Fibretex, the authors believe that the actual value is in this range and the best value is 15.8 kN/m (plus or minus 10 percent), based on machine direction tests. In the Snailback wall, the critical direction was the cross-machine direction, which was the stronger direction for Fibretex. To account for this and to avoid being unjustifiably critical of the high FTRFs used in current practice, a value of 19.0 kN/m was chosen for the analyses presented in Table 2.

The apparent factor of safety of the as-built Snailback wall is almost 12, but the apparent factor of safety with respect to the allowable stress in the fabric after reduction for creep, survivability, and durability is probably less than 2.5, which is not a great deal larger than the minimum of 1.5 required by current practice. The history of this wall shows that a wall built to conform to AASHTO (1997) will perform satisfactorily. Some would argue that the fabric strength reduction factors required in modern practice are excessive. This cannot be supported or rejected by this case study because as built, the working stresses indicated by the R/L value are close to those dictated by current practice. This case should, however, give confidence that walls built according to current practice, even those built of nonwoven geotextiles, will perform satisfactorily.

1974 ISSUES AND ANSWERS

In 1974, those involved with the Snailback wall project had a number of questions and concerns. Back then, the most basic theoretical question was whether the simple Rankine tie-back wedge model was adequate for internal stability (geotextile rupture and pullout) calculations. The literature contained evidence that this model was reasonable for steel strap reinforcements (Lee, Adams, and Vagneron, 1973). The OSU model tests had shown good, somewhat conservative correlations with this methodology (Stilley, 1975); consequently, confidence was placed in the procedure but, as the designers knew, it still was untried with fabrics in a full-scale wall. This confidence has since been confirmed by many successful designs, and this model is the basis for most current design methods in American practice (Berg, Allen, and Bell, 1998).

Even in 1974 it was recognized that the Rankine tie-back wedge model overestimated the soil pressures on the wall face, but this was not a design issue with the wrap-around face used on the Snailback wall. However, a method for evaluating forces to be resisted by fabric reinforcing layers which is predicated on a theory for computing stresses in a soil mass assumed to undergo uniform lateral yield is suspect. Further, the simplistic model for distributing the stresses to the individual layers without allowing layers to share the load is questionable. This methodology is little more than an empirical procedure which, when used with recommended coefficients and factors, is known to provide stable designs. This is a well worn engineering paradigm but it is disappointing scientifically. Hopefully, the next 25 years will give a better understanding of the internal behavior of reinforced soil structures and lead to improved models for analysis.

The at-rest lateral earth pressure coefficient (ko) was used in the Snailback design because Chang, Forsyth, and Beaton (1974) had just reported field measurements in a Reinforced Earth® wall in California that indicated at-rest pressures. Also, the effects of vibrations from heavy logging trucks were a concern, and Lee et al. had just completed vibration experiments on Reinforced Earth® walls and noted reinforcement stresses greater than predicted for the active case (Lee, Adams, and Vagneron, 1975). Based on the results from a number of measurements from more recent experiments on geosynthetic reinforced wall that showed better correlations with the active case, current (1998) practice generally uses the active lateral earth pressure coefficient with "extensible" reinforcements such as geotextiles.

Durability of the fabric was a prime issue in 1974. Everyone knew the plastics were resistant to the agents likely to be encountered when buried in a wall backfill; however, no actual long-term experience existed. Would it really last? Many individuals were reluctant to trust the stability of significant structures to the durability of some untried material. The working load was not specifically reduced for survivability or degradation in the Snailback design. Survivability of Fibretex during construction had been demonstrated by previous use of the fabric in logging road subgrade stabilization projects. The fabric had been found to be very tough. The subrounded, fine to medium sand backfill material was judged not to be a construction concern. Current guidelines (AASHTO, 1997) suggest an installation damage reduction factor of 1.1 to 1.4 and a degradation factor of about 1.6 for the conditions at the Snailback site.

Geotextile strength was evaluated for the Snailback wall using the OSU Ring Test (Bell, Stilley, and Vandre, 1975). Creep data were not available but an effort was made to limit geotextile strain. Bell et. al. (1975) report the ultimate strength of the fabric as 12.3 kN/m and that a "yield" strength of 11.4 kN/m was used in the wall design. This would correspond to using a FTRF of 1.1. Because the load-deformation relationship from the ring test was curved from the origin, the "yield" point was taken where the rate of change of slope (second derivative) of the curve showed a marked increase. Today strength is evaluated by the wide-width strip tensile test, ASTM D4595, which was not available in 1974. Today, FTRF values used to account for creep may be as high as 4 or 5 in addition to FTRFs used for construction damage and aging, and then an additional general factor of safety of 1.5 is required.

In review, the most significant changes with respect to internal stability calculations in American design practice are the use of active lateral earth pressures (ka) instead of at-rest pressures (ko), and the use of reduction factors applied to geotextile strength to protect against creep, degradation, and installation damage. The reduction factor effect is usually larger and frequently much larger so the overall effect is a net increase in the factor of safety. In actual practice, this has contributed to a movement to strong woven geotextiles, geogrids, and proprietary wall systems.

CONCLUSIONS

Twenty-five years ago, it was concluded (Bell, Stilley, and Vandre (1975) that: (1) Geotextile walls were economical and practical; (2) The Snailback wall design method was a satisfactory preliminary method suitable for design of future experiments; (3) Unanswered design questions and construction problems existed, and (4) More study, tests, and work were needed.

Today, it has been concluded that: (1) Geotextile walls are economical and practical; (2) The design approach used for the Snailback wall is accepted practice with minor changes in method—the use of an active earth pressure coefficient that increases the ratio of fabric tensile resistance to lateral driving load and the use of a Fabric Tension Reduction Factor (FTRF) that reduces the ratio; (3) The primary design issue is deformation and creep; and (4) More study, tests, and work are needed to increase our confidence in design, provide a better model of soil-reinforcement interactions, and demonstrate that the very large FTRFs are justified for some materials.

It is a fact that the Snailback wall, built 25 years ago, is still in service and is showing no sign of distress. The 1974 decision to undertake this trial has certainly been vindicated. The wall was an economical solution to a specific problem and it has served its function admirably. More importantly, this project has contributed to the development of a new technology.

The design procedures used in 1974 were not greatly different from those in use today. By a combination of factors, the as-built R/L ratio of the wall is close to what would be required by current practice (AASHTO, 1997). The lessons learned at Snailback Creek are applicable to current practice.

This wall was built with what many people would today consider the worst possible geotextile for reinforcement – a nonwoven, needlepunched, polypropylene fabric. Yet, the wall is an unqualified success. This is not an endorsement of a specific geotextile; it is an endorsement for geosynthetics and the design methodologies used for geosynthetic reinforced soil walls. This case record should instill confidence in the technology and encourage its further use. This is especially true for organizations who build numerous low walls and can readily benefit from the cost savings from geotextile walls. It seems there could be thousands more geotextile walls built and millions of dollars saved every year. The walls need not use only wrap-around facing

covered with mortar, but could use timber, concrete block, and other facings (Wu, 1994).

ACKNOWLEDGEMENTS

The authors wish to acknowledge Richard Van Dyke II, geotechnical engineer with the Siskiyou National Forest, for his assistance in file searches. The opinions expressed in this paper do not necessarily represent the opinions of the U.S. Forest Service.

REFERENCES

AASHTO (1997) "Interims to Standard Specifications for Highway Bridges," 16th Edition, American Association of Sate Highway and Transportation Officials, Washington, DC, USA.

Barrett, R., A. Ruckman, and G. Richardson (1998) Designers Forum, "Geotextile - reinforced retaining walls using granular backfills." GFR, Geotechnical Fabrics Report, March 1998. Vol. 16, Number 2. pp 27-31.

Bell, J. R., A. N. Stilley, and Bruce Vandre (1975) "Fabric Retained Earth Walls," Proceedings of the Thirteenth Annual Engineering Geology and Soils Engineering Symposium. University of Idaho. Moscow, Idaho. pp 271 - 287.

Bell, J. R. and J. E. Steward (1977) "Construction and observations of fabric retained soil walls." Proceedings C. R. Coll. Int. Sols Textiles. Paris, France.

Berg, R. R., Allen, T. M., and Bell, J. R. (1998) "Design Procedures for Reinforced Soil Walls - A Historical Perspective." Proceedings, Sixth International Conference on Geosynthetics, Atlanta, GA, USA.

Chang, J. C., Forsyth, R. A. and Beaton, J. L. (1974) "Performance of Reinforced Earth® Fill," Transportation Research Record, No. 510, TRB, pp. 56-68.

Kelsay, H. S. (1975) Investigation of a Nonwoven Fabric as a Reinforcement for Gravel Paved Roads, Master's Thesis, Oregon State University, Corvallis, OR, USA. 63 p.

Lee, K. L., Adams, B.D., and Vagneron, J. J. (1973) "Reinforced Earth® Retaining Walls," Journal, Soil Mechanics Division, ASCE, Vol. 99. No. SM10, pp. 745-764.

Lee, K. L., Adams, B.D., and Vagneron, J. J. (1975) "Closure to Discussions, Reinforced Earth® Retaining Walls," Journal, Geotechnical Engineering Division, ASCE, Vol. 101. No. GT3, pp. 345-346.

Steward, Williamson, and Mohney (1977) "Guidelines for Use of Fabrics in Construction and

Maintenance of Low-Volume Roads," USDA, Forest Service, Region 6, Portland, OR, USA.Stilley, A. N. (1975) A Model Study of Fabric Reinforced Earth® Walls, Master's Thesis, Oregon State University, Corvallis, OR, USA, 64 p.

Wu, J. T. H. (1994) "Design and Construction of Low Cost Retaining Walls," Report No. CTI-UCD-1-94, Colorado Transportation Institute, Denver, CO, USA, 152 p.

INSTRUMENTED SOIL REINFORCED RETAINING WALL: ANALYSIS OF MEASUREMENTS

PAOLO CARRUBBA
UNIVERSITA' DI PADOVA, ITALY
NICOLA MORACI
UNIVERSITA' DI REGGIO CALABRIA, ITALY
FILIPPO MONTANELLI
TENAX SPA, ITALY

ABSTRACT

A vertical retaining wall, 4m high and 10m long, was constructed by reinforcing the backfill with geogrids. The reinforcing layers were instrumented with strain gauges, tensile geogrid load transducers and horizontal displacement sensors. In addition, total soil pressure transducers were installed inside the structure to monitor the internal state of stress of the reinforced wall.

The aim of this research is to better understand the behavior of reinforced structures. In particular, the development of slip surfaces and the tensile forces acting in the reinforcements were investigated. By this analysis it was possible to assess current design approaches and related safety factors in terms of either long term tensile failure, pullout, direct sliding or compound failures.

Data related to reinforcement tensile strains and loads, applied vertical pressures, rainfall and construction sequences were collected for two different geogrids over a period exceeding 10,000 hours.

INTRODUCTION

Until now several reinforced structures have been constructed and monitored, but most of them were reinforced with metallic strips since they are easily instrumented. Structures reinforced with geosynthetics are more difficult to be instrumented. Consequently, little data are available on their behavior as loading approaches failure. Therefore, some aspects related to the behavior of these structures remain unclear, including the location and shape of the slip surfaces and the tensile forces acting on the reinforcements.

Several design methods which are based on a limit equilibrium approach have been proposed to address the uncertainties associated with geosynthetic reinforced structures. (Jewell, et al., 1984; Jewell, 1991; Bonaparte, et al., 1987; Broms, 1988; Collin, 1986; Simac, et al., 1990; Leshchinsky and Perry, 1987; Schmertmann, et al., 1987). These methods consider different hypothesis and failure surfaces. So, the factors of safety against failure varies with the design method used.

This paper discusses an instrumented geosynthetic reinforced wall constructed in Italy near the town of Vicenza (Cereda site). The structure was monitored from the initial phase of construction, during the service phase and at failure. Failure was achieved by surcharging the wall with 3.5 m of soil.

This study provides valuable insight in reinforced wall behavior, including the location of failure surfaces, tensile stresses and strains distribution, and factors which can affect short and long term factors of safety such as geosynthetic creep and aging, rain effects and consolidation.

SOIL AND GEOSYNTHETIC PROPERTIES

The soil used for the construction of the wall, is called "Cereda tout venant", and was excavated from a quarry located near the site of construction. Ten percent of the soil passes the 0.075 mm sieve. It has a uniformity coefficient (C_u) of 130 and a curvature coefficient (C_c) of 19. The grain size distribution is shown in Figure 1. The Atterberg limits were evaluated on the fine fraction and are as follows: liquid limit LL = 28, plastic limit PL = 20; and plasticity index PI = 8. According to the unified soil classification system USCS classification system, this soil is a clayey gravel (GC).

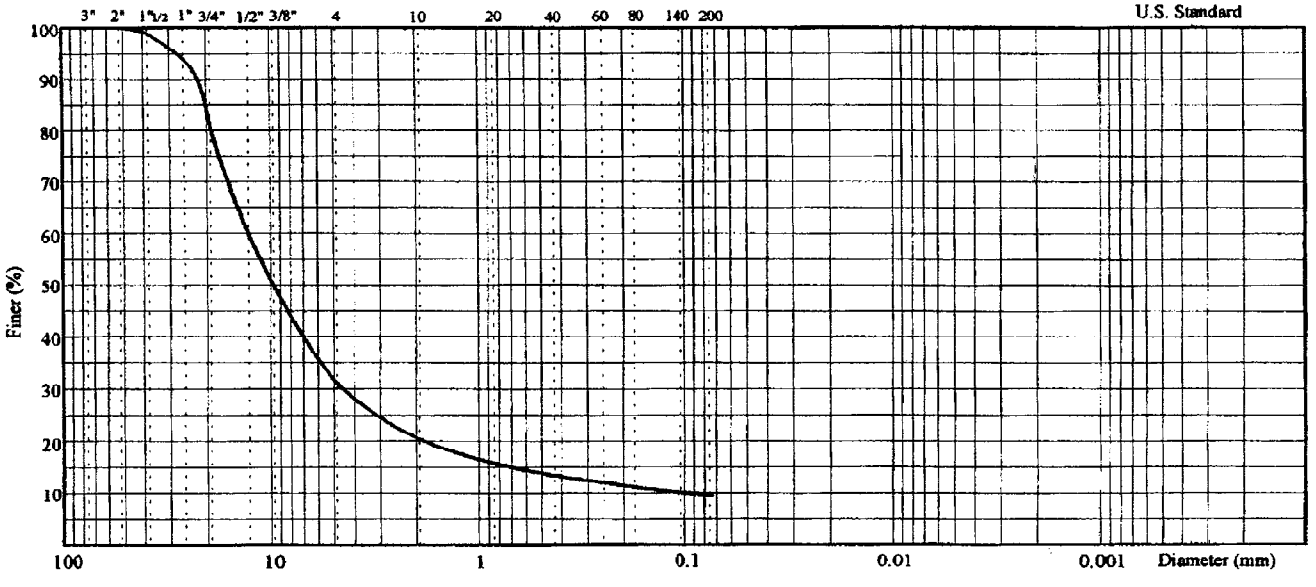

Figure 1. Grain size distribution for the fill soil.

Laboratory compaction tests were carried out following the modified AASHTO method. The results are showed in Figure 2. Maximum dry density ($\gamma_{d\ max}$) values of 22.25 kN/m^3 were obtained at an optimum water content (w_{opt}) of 5.5percent.

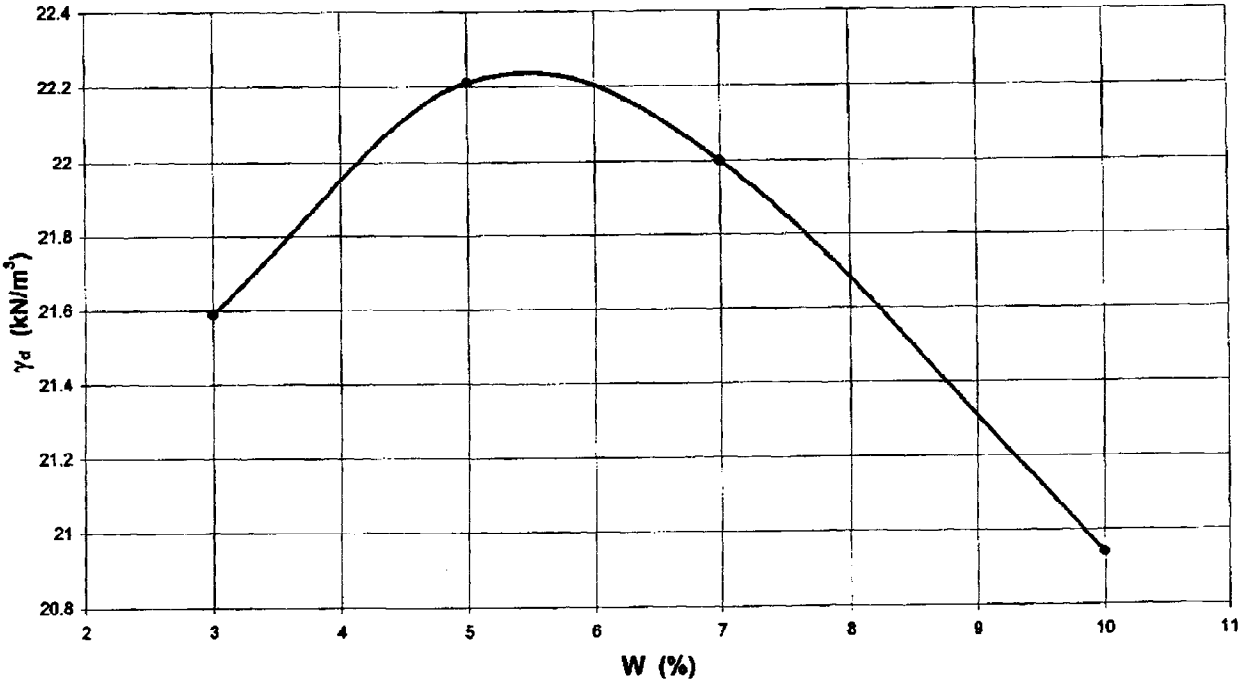

Figure 2. Laboratory compaction test results.

The permeability tests were performed in a triaxial apparatus under constant hydraulic load (corresponding to an hydraulic gradient equal to 1.0) and under confinement pressures of 50 and 100 kPa. The test results of specimens compacted at optimum water content indicate the soil has a permeability coefficient ranging from 2.0 10^{-4} to 2.5 10^{-4} cm/s.

To evaluate the soil's shear strength, different laboratory tests were performed. Triaxial tests on large diameter specimens (100 mm) were conducted to determine the shear strength at low strain and confining stress levels. The test results indicate a very high shear strength for confining stresses (σ) between 20 kPa and 100 kPa due to the dilatant behavior of the soil subjected to compaction effort.

Direct shear tests were performed on the portion of soil finer then 0.425 mm using the Casagrande shear box and the Bromhead ring shear apparatus to evaluate its large-displacement shear strength. The tests results indicate a residual shear strength angle (coincident with constant volume shear strength angle Φ_{cv}) of approximately 40 degrees.

The wall was built using two different reinforcement geogrids. One section was 5.0m in

width, and was reinforced with high density polyethylene (HDPE) uniaxial oriented extruded geogrids. The second section was also 5.0m in width and was reinforced with polypropylene (PP) biaxially-oriented extruded geogrids. The geogrids' nominal properties are reported in Table 1.

DESIGN AND CONSTRUCTION

The reinforced wall was designed using a limit equilibrium approach (Leshchinsky 1995) and with the RESLOPE design software. An internal soil friction angle (Φ_{cv}) of 40 degrees was used for the reinforced soil. The two sections of the wall were designed based on to two different failure mechanisms: 1) tie-back tensile failure for the portion of wall reinforced with GG20PP geogrids; and 2) pullout failure for the other portion reinforced with GG45PE geogrids. The design parameters used are listed in Table 2. All the Safety Factors were deliberately set to 1.00 to design a wall at limit equilibrium stage and consequent failure during surcharge loading.

Table 1. Geogrids' nominal properties.

Product Name	Tenax LBO 220 SAMP	Tenax TT 201 SAMP
Product Code	GG20PP	GG45PE
Polymer Type	Polypropylene	High Density Polyethylene
Nominal Tensile Strength, MD	20 kN/m	45 kN/m
Strain at Peak, MD	11%	12%
Tensile Strength at 2% Strain	7 kN/m	13 kN/m
Tensile Strength at 5% Strain	14 kN/m	26 kN/m
Unit Weight	270 g/m^2	450 g/m^2
Mesh Sizes	41 x 31 mm	130 x 15 mm
Junction Strength	18 kN/m	36 kN/m

The long term allowable design tensile strength of the geogrids was assumed to be equal its peak tensile strength as determined by the wide width tensile test method (ASTM D4595). Since geogrids with different strengths were used in the designs, the vertical spacing and reinforcement lengths of these two sections were also different. For the section reinforced with GG20PP geogrids, three layers, each 2.20m long, were necessary. The first layer was installed at elevation 0.00m with respect to the base, the second at 0.80m and the third at 2.40m elevation. For the section reinforced with GG45PE geogrids, three layers, each 2.00m long, were necessary. The first layer was installed at elevation 0.00m with respect to the base, the second at 1.30m and the third at 2.90m elevation.

Table 2. Retaining wall design parameters.

GEOMETRY AND LOADING DATA	
• Height of the slope, H (m)	4.0
• Height of soil surcharge at failure, H (m)	3.5
• Face inclination, β	85°
FACTORS OF SAFETY	
• Factor of safety for direct sliding	1.0
• Factor of safety for geosynthetic uncertainties	1.0
• Factor of safety for geosynthetic pullout	1.0
• Factor of safety for installation damage	1.0
• Factor of safety for chemical degradation	1.0
• Factor of safety for biological degradation	1.0
• Factor of safety for creep	1.0
INTERACTION COEFFICIENTS	
• Pullout interaction coefficient	0.9
• Direct sliding coefficient	1.0

To ensure the face stability and geometry, the structure was constructed using "left in place" welded wire formworks. They are composed of wire mesh precut to an height of about 1.5m and bent to the face at an angle of 85 degrees. The fill soil was compacted in layers of 0.3m thick using a vibrating roller (80 kN). The structure is shown in Figure 3.

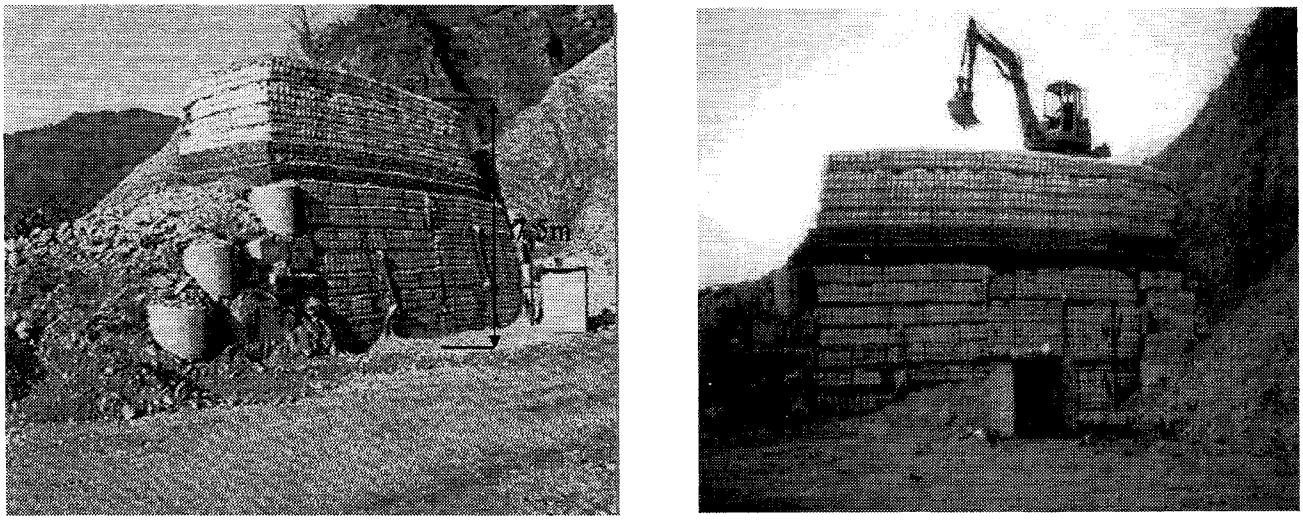

Figure 3. View of the two reinforced walls.

The geogrids were instrumented with self-temperature compensated strain gauges having a nominal gauge length of 5mm and a maximum strain of 10% with a measurement accuracy of 0.5%. The strain gauges were glued to the geogrid ribs with cyanoacrylate adhesive using a multi-step method. This procedure allows the measurement of the geogrid strains up to 10%, over a period in excess of two years and during freezing temperatures. Ten strain gauges were installed on each reinforcement layer at a spacing of about 0.20m. The strain gauges were protected with silicon rubber and with a 0.10m-thick sand layer. The effectiveness of this procedure has been demonstrated by the low mortality rate of the sensors (only one out of 63 sensors malfunctioned). The electrical connection was made using a three wires Whetstone quarter bridge. The strain gauges were connected to an automatic data acquisition unit which is capable of recording up to 100 sensors every 15 minutes. The actual recording frequency was reduced to once per day after the construction was completed. Additional specimens of geogrids, were instrumented with strain gauges, were prepared and tested in the laboratory to provide a basis for calibration and correlation between strain and tensile stress The stress-strain curves and modulus for both geogrids were established with laboratory testing. These relationships are function of time, temperature, stress and strain. The following tests were performed to define the time dependent properties of the geogrids: in isolation index single rib tensile tests, low strain rate tensile tests, and different load ratio creep tests.

Three tensile load cells, each having a physical profile similar to the shape of the uniaxial geogrid, were installed at each GG45PE reinforcement layer to record the actual confined tensile loads in the material. Three vertical total stress cells, each having a diameter of 300mm, were installed at each GG45PE reinforcement layer to record the actual vertical total stress in soil. These cells were located 1m inside the wall face. Horizontal multiple base displacements sensors were installed on the GG45PE geogrid layers to monitor absolute and differential movements of the reinforced mass and its face.

ANALYSIS OF THE RECORDED DATA

The change of total vertical pressures over time at the different reinforcing layers during construction and surcharging is shown in Figure 4 for the section of wall reinforced with GG45PE. These data demonstrate a good response of instrumentation to the vertical pressure changes, even if some discrepancies may be noticed with respect to theoretical values. This behavior may be attributed to the proximity of the cells to face (1.0m), the flexibility effects of the face itself, the position of the cells with respect to the surcharge and finally, to the presence of a rigid base on which the wall was founded.

The change of the total vertical pressures over time are compared to the recorded rainfall in Figure 5. The figure shows that the change of the unit weight over time has a little influence on recorded data. A comparison between the applied total vertical pressures and the associated strains in reinforcing layers is shown in Figure 6 for both geogrids. This comparison is made for selected points (Table 3) which are approximately at the same position with respect to the wall

face. The data in Figures 4 & 5 indicates a good response with respect to time of loading of the two independent monitoring systems. For a given stress level, the dependence of recorded strain on geogrid stiffness is clearly shown in Figure 6.

Figure 7 shows the development of tensile strain over time in the upper layer of both GG45PE and GG20PP. The data indicate a marked dependence of the tensile strain in geogrids on the stress level achieved during surcharging, the geogrid stiffness and its creep properties. Moreover, for a given temperature, creep became more important as the tensile stress in reinforcement increases. Finally, it is possible to observe that the effect of creep is more significant in GG20PP geogrids than in GG45PE geogrids. This is due to the different polymer, manufacturing process, and the involved failure mechanisms. The development of tensile strains over time for strain gauges located at different locations is shown Figures 8 and 9 for the GG20PP and the GG45PE geogrids, respectively.

Table 3. Designation and location of strain gauges installed on reinforcing geogrids.

GG45PE Channel N. Vs. Face Distance, m						GG20PP Channel N. Vs. Face Distance, m					
BASE		MEDIUM		UPPER		BASE		MEDIUM		UPPER	
CH 11	0.06	CH 21	0.18	CH51	0.07	CH 01	0.10	CH 41	0.10	CH 31	0.16
CH 12	0.21	CH 22	0.45	CH52	0.35	CH 02	0.32	CH 42	0.29	CH 32	0.39
CH 13	0.35	CH 23	0.73	CH53	0.63	CH 03	0.54	CH 43	0.49	CH 33	0.83
CH 14	0.49	CH 24	1.01	CH54	0.77	CH 04	0.77	CH 44	0.70	CH 34	1.06
CH 15	0.62	CH 25	1.12	CH55	0.90	CH 05	1.00	CH 45	0.91	CH 35	1.29
CH 16	0.76	CH 26	1.30	CH56	1.04	CH 06	1.23	CH 46	1.13	CH 36	1.52
CH 17	0.90	CH 27	1.45	CH57	1.18	CH 07	1.46	CH 47	1.34	CH 37	1.72
CH 18	1.17	CH 28	1.59	CH58	1.32	CH 08	1.69	CH 48	1.54	CH 38	1.95
CH 19	1.45	CH 29	1.73	CH59	1.46	CH 09	1.92	CH 49	1.74	CH 39	2.05
CH 20	1.73	CH 30	1.88	CH60	1.73	CH 10	2.06	CH 50	1.94	CH 40	----

The maximum tensile strain achieved in each reinforcing layer indicates the location in which tension is greatest. Using this information, the location of the internal failure plan can be identified. The two slip surfaces obtained by this analysis are shown in Figures 10 and 11 as well as the failure surfaces considered in the design step, and the tensile strains measured. Moreover, the data in Figures 10 and 11 indicate that the reinforcing layers are stressed in a different way.

The actual mechanism of failure for GG45PE is pullout, as indicated by the multibase displacement data and by the low values of measured tensile strains (0.6-1.6% in Figure 9). The actual failure mechanism for GG20PP is tensile stress in the upper reinforcing layer as indicated by the high tensile strains measured (about 4.0 percent in Figure 8).

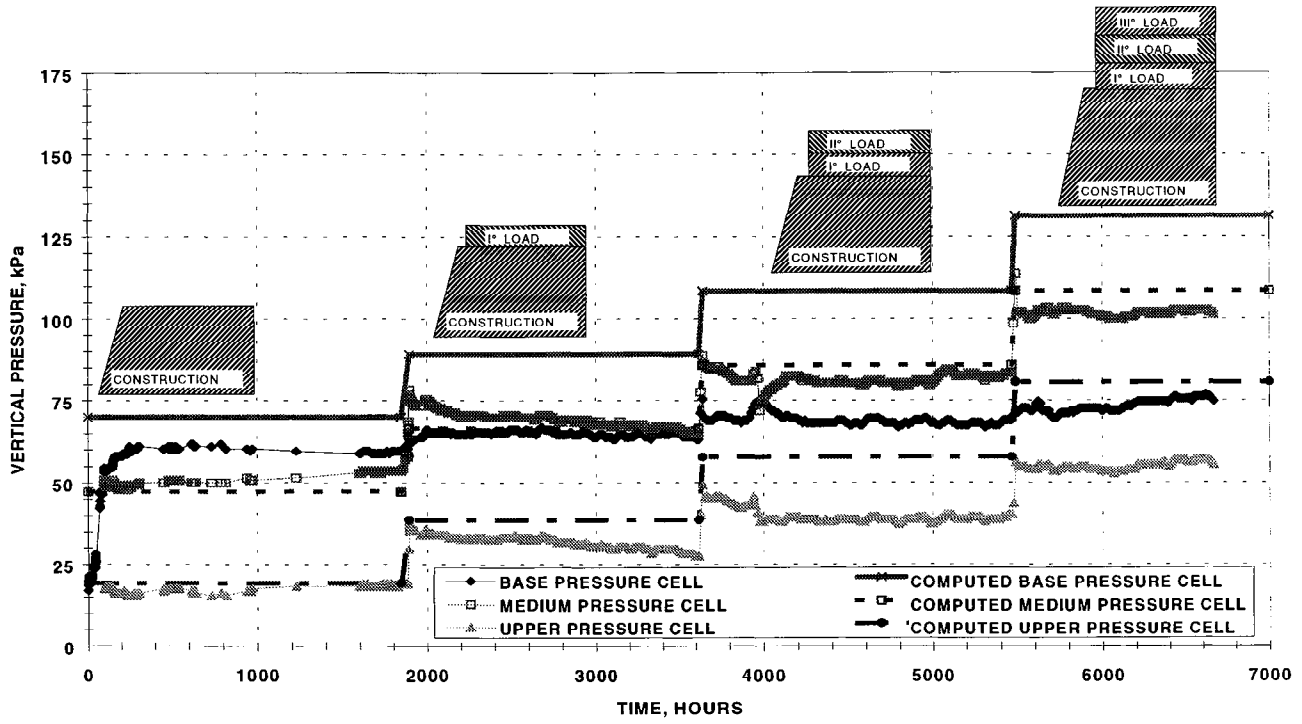

Figure 4. Variation of total vertical pressure during construction and surcharging for the GG45PE geogrid reinforced wall.

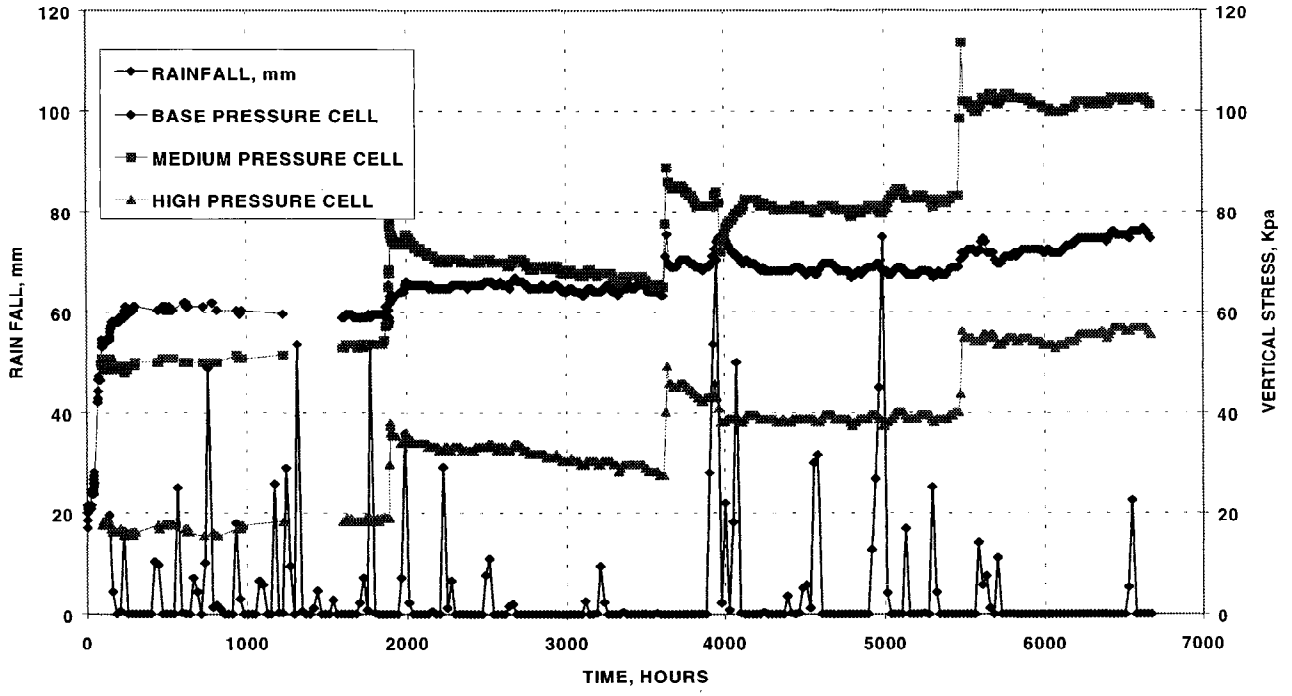

Figure 5. Total vertical pressure and rainfall during construction and surcharging for the GG45PE geogrid reinforced wall.

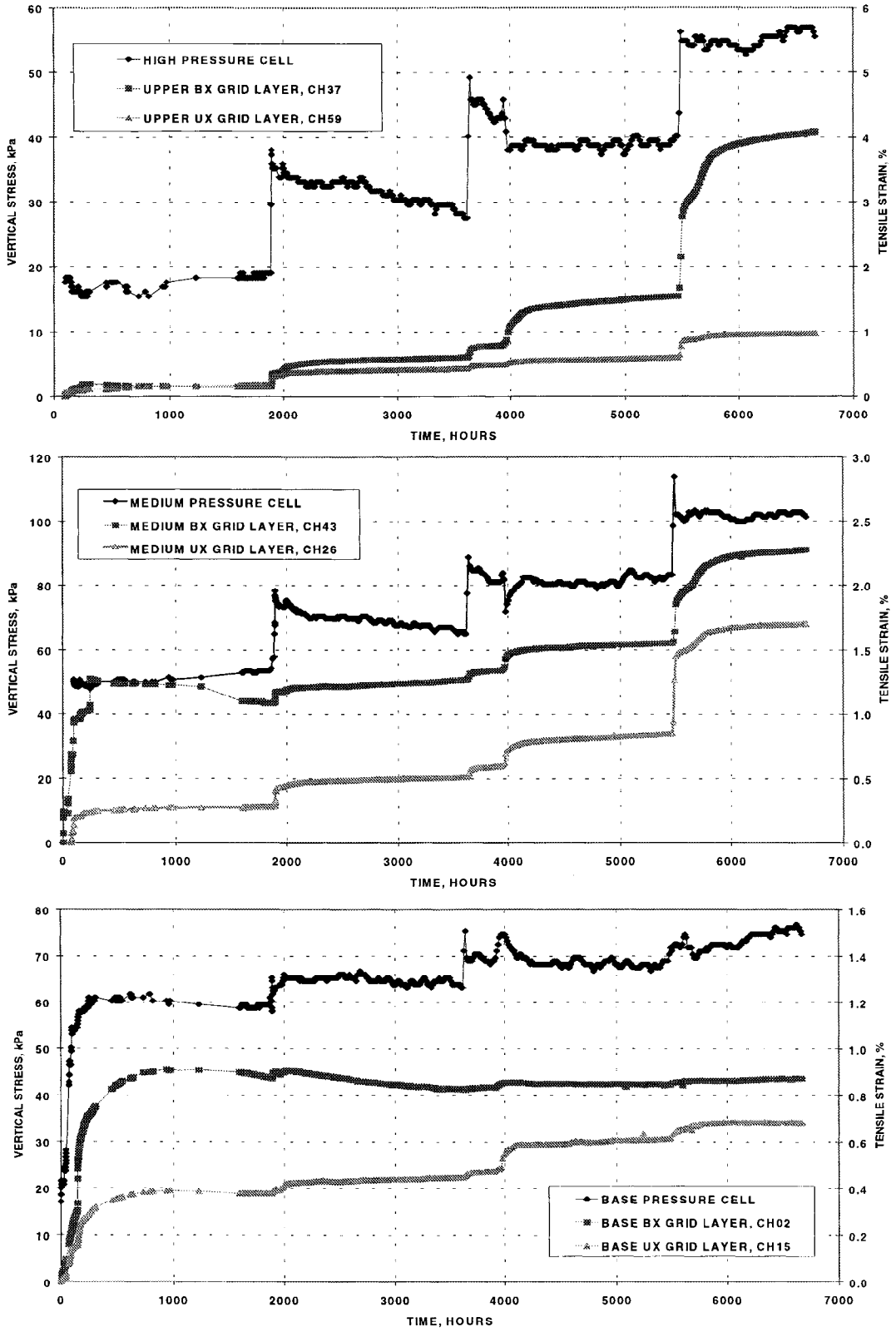

Figure 6. Comparison between total vertical pressure and strains at some instrumented locations of the GG45PE and the GG20PP geogrids.

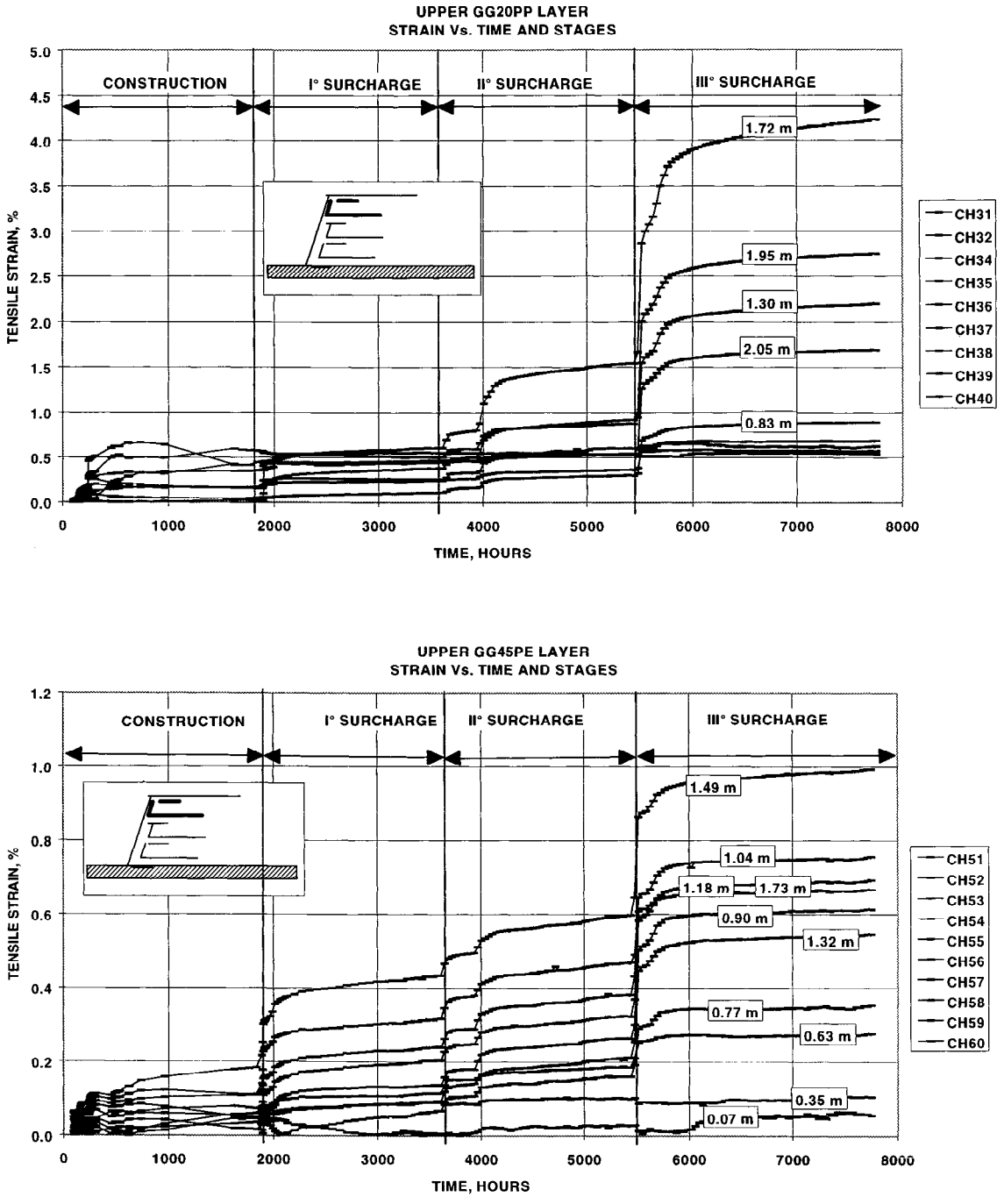

Figure 7. Tensile strains vs. time in the upper reinforcing layers for the GG45PE and the GG20PP geogrids. On the curves are shown the strain gages face distance (Table 3).

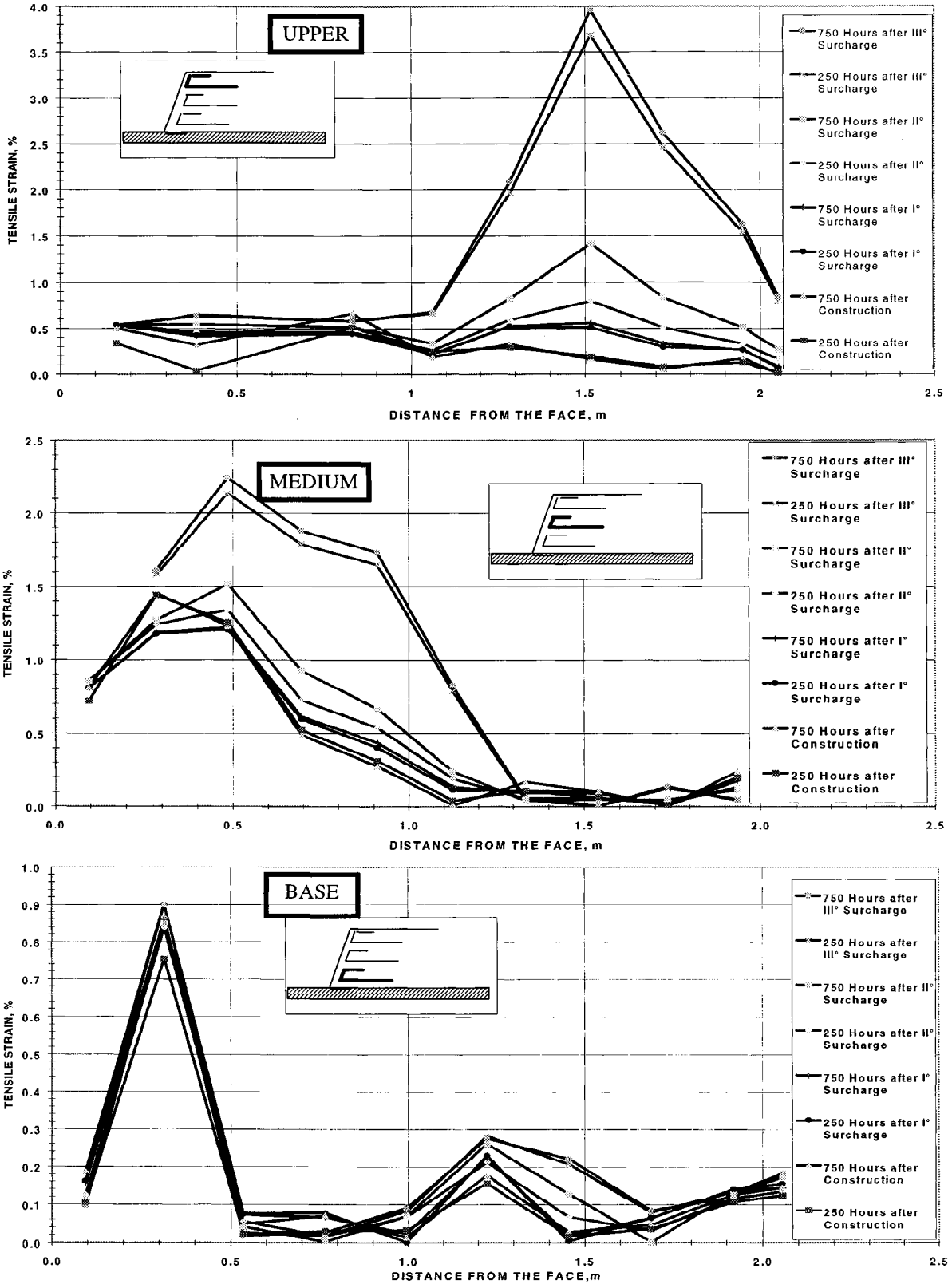

Figure. 8 Tensile strains vs. time along the GG20PP geogrid reinforcing layers.

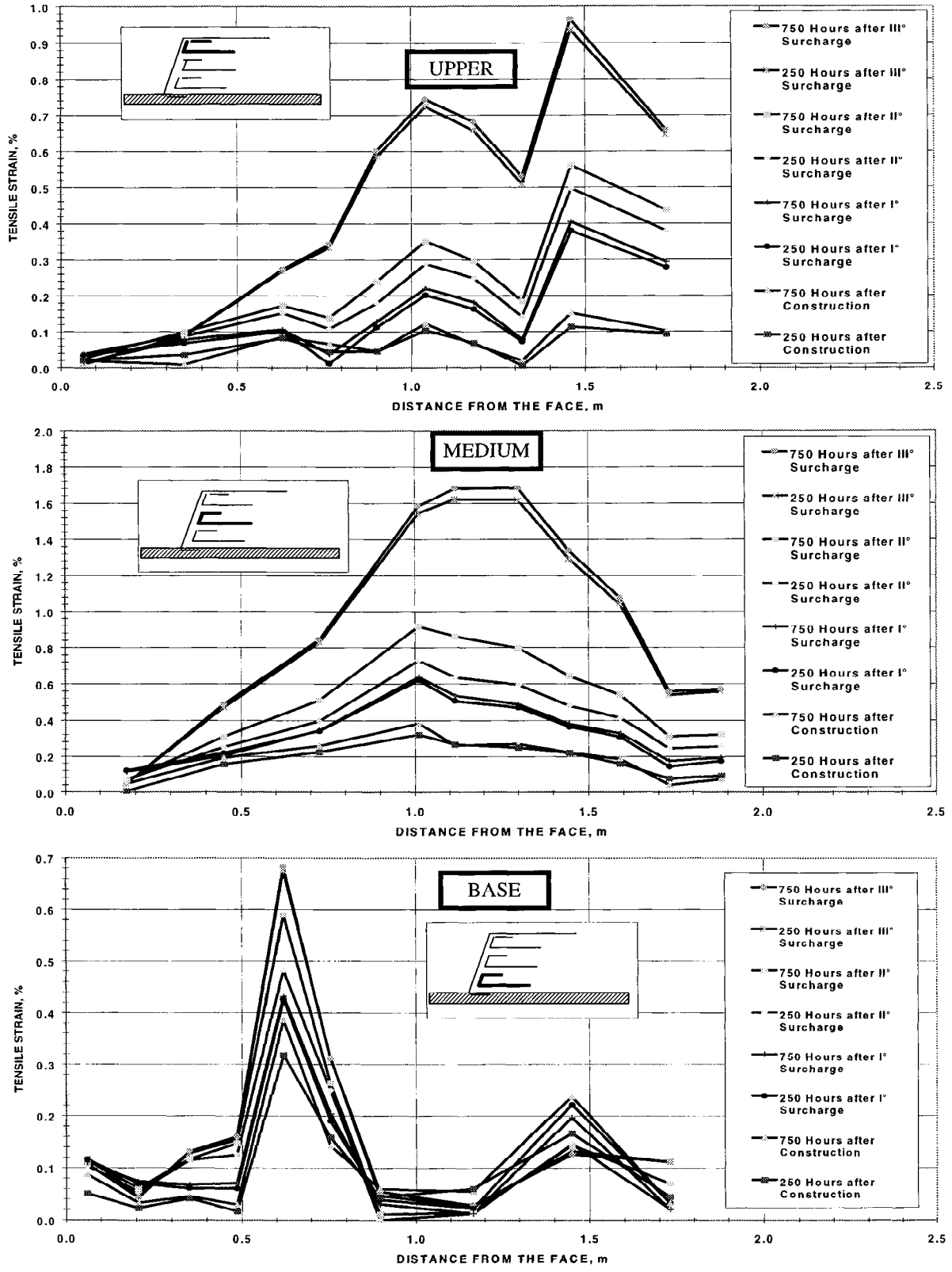

Figure 9. Tensile strains vs. time along the GG45PE geogrid reinforcing layers.

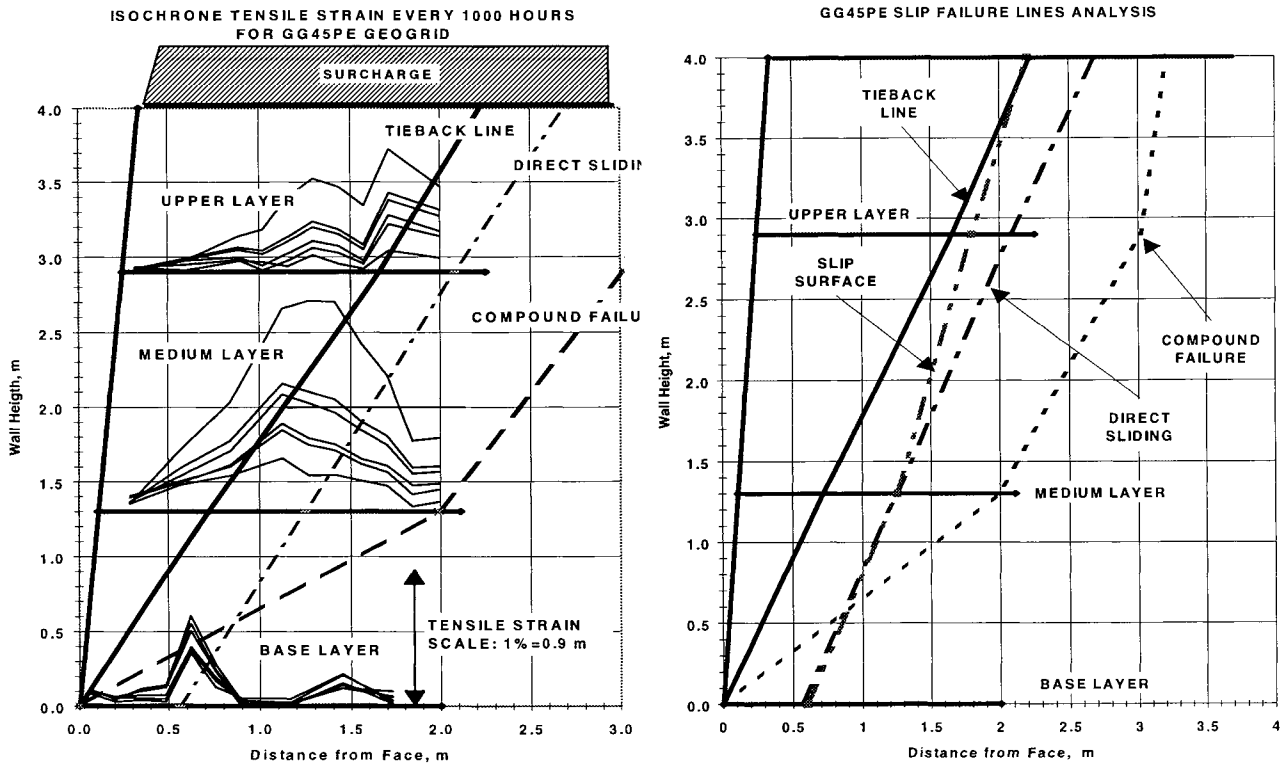

Figure 10. Localization of the actual slip surfaces inside the GG45PE reinforced wall.

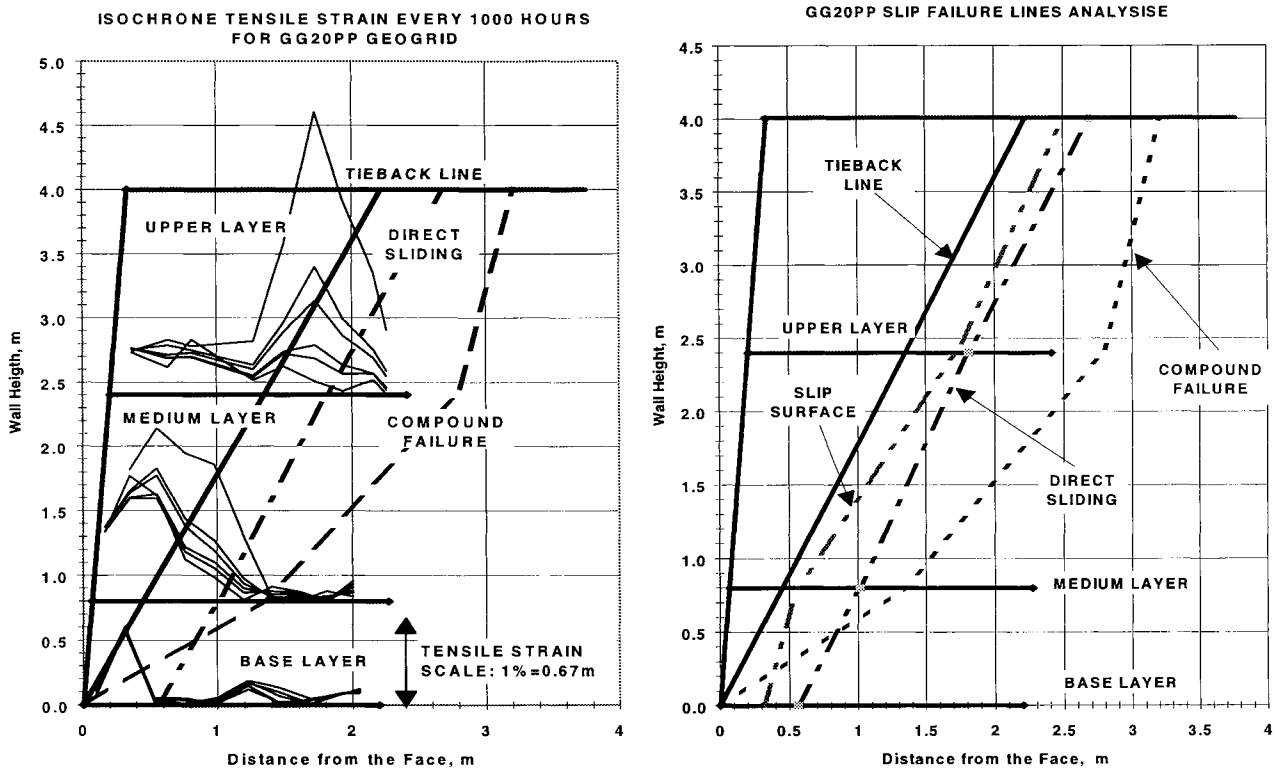

Figure 11. Localization of the actual slip surfaces inside the GG20PP reinforced wall.

CONCLUSIONS

A vertical retaining wall, 4m high and 10m long, was constructed by reinforcing the backfill with two different type of geogrids. The reinforcing layers were instrumented with strain gauges, tensile geogrid load transducers and horizontal displacement sensors. Moreover, in order to measure the internal state of stress of the reinforced walls, total soil pressure transducers were installed inside the structure. Finally, the walls were brought to failure by surcharging with 3.50m of loose soil. The tensile strains collected inside the reinforced structures allowed the location of failure surfaces to be clearly identified. Two different failure mechanisms were identified: a pull-out mechanism failure, in the case of GG45PE reinforced wall, and a tensile reinforcing failure, in the case GG20PP reinforced wall. The paper shows that the instrumentation and the long term observation of a large scale model may be considered a valuable tool in understanding the behavior of such a complex structures.

REFERENCES

Bonaparte, R., Holtz, R.D. and Giroud, J.P. (1987) " Soil Reinforcement Design Using Geotextiles and Geogrids", Geotextile Testing and the Design Engineer, ASTM STP 952, pp.69-116.

Collin, J.G. (1986) " Earth Wall Design", Ph.D. Thesis, University of California, Berkley; U.S.A.

Jewell, R.A (1991) " Application of Revised Design Charts for Steep Reinforced Slopes ", Geotextiles and Geomembranes, Vol.10, n.4, pp.203-233.

Jewell, R.A., Paine, N., Woods, R.I. (1984) " Design Method for Steep Reinforced Embankments ", Polymer Grid Reinforcement in Civil Engineering, Thomas Telford, London, U.K., pp.70-81.

Leshchinsky, D., Perry, E.B. (1987) " A Design Procedure for Geotextile-Reinforced Walls ", Proceeding Geosynthetic '87, New Orleans, U.S.A., pp.95-107.

Leshchinsky, D. (1995) " RESLOPE " Design Manual, Department of Civil Engineering , University of Delawere, U.S.A.

Schmertmann, G.R., Chouery-Curtis, V.E., Johnson, R.D. and Bonaparte, R. (1987) " Design Charts for Geogrid-Reinforced Soil Slopes ", Proceeding Geosynthetic '87, New Orleans, U.S.A., pp.108-120.

Simac, M.R., Christopher, B.R., and Bonczkiewicz, C. (1990) " Instrumented Field Performance of a 6 m Geogrid soil wall " Proceeding 4th International on Geotextiles Geomembranes and Related Products, The Haughe, Holland, Vol.1, pp.53-59.

FULL SCALE GEOSYNTHETIC REINFORCED RETAINING WALLS: A NUMERICAL PARAMETRIC STUDY

WEI F. LEE, RESEARCH ASSISTANT
UNIVERSITY OF WASHINGTON, U.S.A
ROBERT D. HOLTZ, PROFESSOR
UNIVERSITY OF WASHINGTON, U.S.A
TONY M. ALLEN, STATE GEOTECHNICAL ENGINEER
WASHINGTON STATE DEPARTMENT OF TRANSPORTATION, U.S.A

ABSTRACT

In order to improve our understanding of the behavior of the geosynthetic reinforced soil (GRS) retaining walls, numerical models of a well-instrumented full scale GRS wall were first developed using a finite difference program. A parametric study was then performed to evaluate the behavior of GRS walls with different reinforcement stiffnesses. Performance of two full scale steel reinforced soil retaining soil walls was also simulated to verify the result of the parametric study. The modeling results matched the instrumentation measurements with reasonable accuracy. This paper presents the results of the numerical models and parametric study, and discusses the influence of reinforcement stiffness on GRS wall performance.

INTRODUCTION

The most common design procedure for the internal stability of GRS retaining structures is the U.S. Forest Service or tie-back wedge technique, although available evidence of GRS performance to date indicates that this technique tends to overestimate the reinforcement stresses within the structure (Bell, et. al., 1983, Rowe and Ho, 1993). In order to improve internal stability design procedures, reliable information on the internal stress-strain distribution of GRS structures is necessary. In an effort to improve our understanding of this distribution and therefore improve internal stability design procedures, research has been conducted that includes (1) developing numerical models of GRS retaining structures that are capable of reproducing field instrumentation measurements, and (2) performing parametric analysis using the developed numerical models to examine the influence of the reinforcement stiffness on the wall performance.

Although numerous finite element analyses of reinforced soil have already been performed and with reasonably good results, the computer finite difference program FLAC was chosen for this research because of its excellent ability to analyze geotechnical problems, especially those involving stability. Numerical models of one of the U.S. Federal Highway Administration (FHWA) test walls built in Algonquin, Illinois, were developed and results were compared to the measurements from instrumentation installed in the walls. The numerical models were able to reproduce the instrumentation measurements quite well. A parametric study was then performed by systematically varying the reinforcement stiffness in order to investigate its influence on wall performance. The shape and magnitude of face deflections, and the reinforcement strain distributions were observed and analyzed in the parametric study. This paper presents and discusses these analyses and the implications of the results on our understanding of internal reinforcement behavior and design.

FHWA ALGONQUIN TEST WALLS

Three of the FHWA test walls built in Algonquin, Illinois (Christopher, 1993) were used as the objects for the numerical modeling in this research. Table 1 summarizes the reinforcement types and properties used in each wall. Figure 1 shows the wall geometry, material properties, and instrumentation details for the geogrid wall (Wall 2). The wall geometry was identical for all three walls, and the instrumentation details were similar. All three walls used the same type of wall facing, precast concrete panels of the Reinforced Earth Company design. Backfill materials were a well graded sand and gravel (Figure 1). In this research, numerical models were first developed to simulate the instrumentation measurements of the geogrid reinforced wall, Wall 2. Walls 1 and 3 were used as verifying cases in the parametric study.

Table 1. Construction and reinforcement information of the modeling wall cases (Christopher, 1993).

Wall Names	Wall 1	Wall 2	Wall 3
Reinforcement Name and Type	Reinforced Earth Company- Ribbed Steel Strip	Tensar SR2- Polyethylene Extruded Geogrid	VSL Steel Bar Mat using W11 bars
Reinforcement Strength, Strain, and Stiffness	T_{yield}= 67.9kN/m ε_{yield}=0.12% J=54690kN/m [a]	T_{peak}= 67.7kN/m ε_{peak}=16.0% J=2040kN/m [b]	T_{yield}= 44.4kN/m ε_{yield}=0.12% J=37860kN/m [a]

a: per meter of wall, calculated based on the coverage ratio (the width of the reinforcement divided by the center to center horizontal spacing).

b: from wide width strip tensile tests (ASTM D 4595)

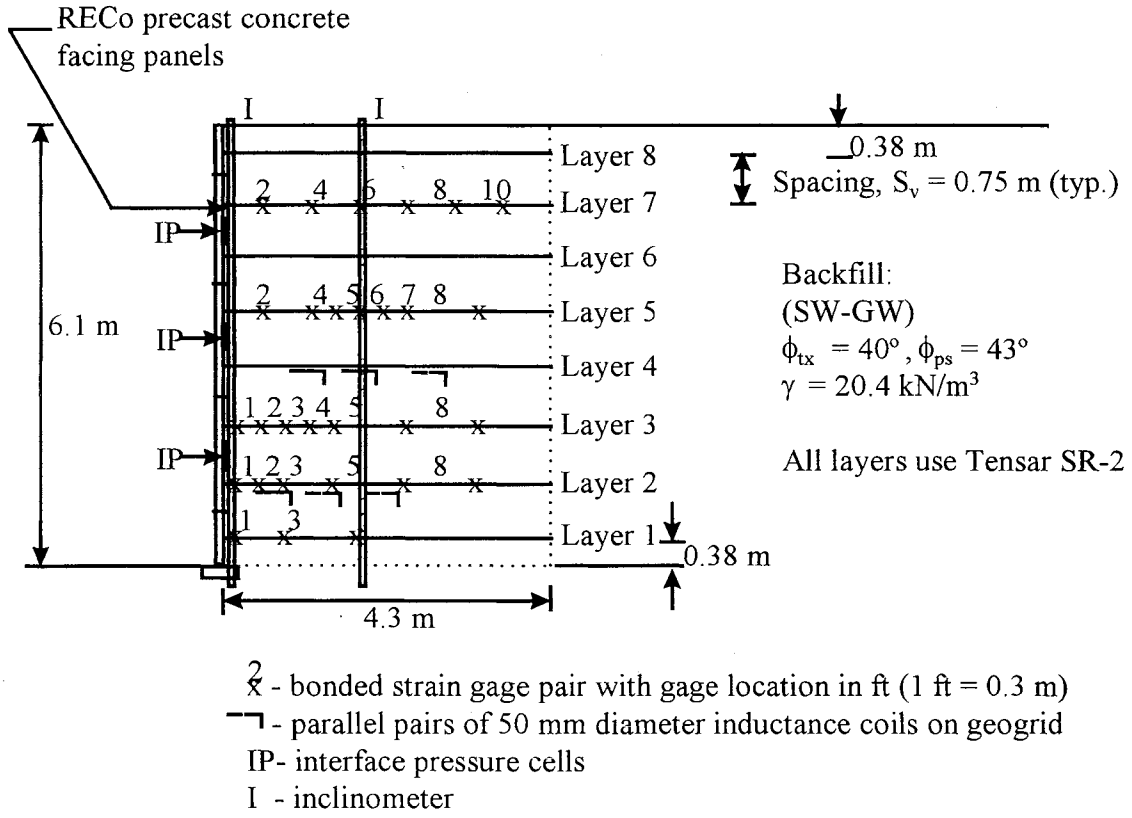

Figure 1. Wall geometry and instrumentation plan for Wall 2 (after Christopher, 1993).

NUMERICAL MODELS

A commercial computer program FLAC (Fast Lagrangian Analysis of Continua, Itasca Consulting Group, 1993) was used to develop the numerical models of the retaining walls. FLAC is a two-dimensional explicit finite difference program. In FLAC, materials are represented by elements that form a grid to fit the shape of the modeling object. All FLAC model analyses were performed on IBM-compatible personal computers.

FLAC Model Alg-W2 was developed to simulate the instrumentation measurements of Wall 2, the geogrid reinforced test wall. In FLAC Model Alg-W2, material elements with a linear elastic stress-strain behavior were used to represent the precast concrete panels. The backfill and foundation soils were represented using material elements with elasto-plastic stress-strain behavior and Mohr-Coulomb failure criteria (Mohr-Coulomb material elements). Cable elements were used to represent the geogrid reinforcement. These elements are one of the built-in structural elements of the FLAC program that consists of an elastic material element with interfaces around its perimeter. Interface elements were also placed between the wall face elements and the soil elements to represent the interfaces between soil and the concrete panels.

The input properties of Model Alg-W2 were as follows:

1. Soil moduli (Mohr-Coulomb material) elements were determined using procedures described by Lee and Holtz (1998) from test data obtained in the Unit Cell Device (UCD) by Boyle (1995). The UCD is able to test soil and GRS specimens under plane strain conditions.
2. The soil friction angle was obtained from triaxial test data converted into a plane strain soil friction angle for the soil elements (Lade and Lee, 1976). The cohesion of the soil elements was set to zero, which reflected the triaxial test results.
3. High strength concrete material properties (Cook and Young, 1985) were used as the input properties for the concrete panel (elastic material) elements.
4. For the geogrid reinforcement, 50% of the in-isolation modulus obtained from the wide-width tensile test (ASTM D 4595) was used as the modulus of the cable elements. This 50% reduction was chosen to account for the difference between the actual rate of loading of the reinforcement in the field during wall construction, which may be five or six orders of magnitude slower than the standard D 4595 wide width testing rate of 10%/min. Although there is strong evidence that nonwoven geotextiles do in fact have greater moduli and strengths when confined in soil, soil confinement has little effect on wovens and geogrids. For example, Boyle (1995) found that the tensile moduli of woven geotextiles were not significantly influenced by confinement in the UCD device. On the other hand, wide width tensile and UCD tests conducted at strain rates which are similar to that which is typical in full scale structures have indicated that reductions of about 50% relative to the ASTM D4595 modulus are needed to account for slower rates of loading, especially for polypropylene geotextiles (Boyle, 1995; Boyle, Gallagher, and Holtz, 1996). Thus, for this research, a modulus reduction of 50% relative to the ASTM D4595 modulus was a reasonable adjustment to make.
5. Plane strain soil friction angle and reinforcement stiffness were used as the friction angle and shear stiffness of the interface of cable elements (Holtz and Lee, 1998).
6. For the interface elements between soil and concrete panels, a friction angle equal to two-thirds of the plane strain soil friction angle and a stiffness equal to the stiffness of the soil at the same stress level were used.

MODELING RESULTS

Wall face deflections can be measured incrementally as is the case for deflection measurements using survey methods, or they can be measured relative to a single fixed reference point, as is the case for inclinometer deflection measurements. The results of FLAC Model Alg-W2 are compared to the face surveys in Figure 2, and except for one survey point, they show reasonable agreement with the measurements. Figure 3 shows the predicted deformation of Wall 2 in comparison to the measurements obtained from an inclinometer located 1.8m behind the wall face. Although the inclinometer measurements at 4m height had an abnormal shift, the

overall prediction still shows very good agreement with the measurements in both shape and magnitude below that height.

In Figure 3, "folds" or "jogs" of about 3mm were obtained in the upper portion of the predicted soil deflection curve. When the concrete panel facing deformed, it also pulled the reinforcement, whose front portion was embedded in the concrete panel, toward the front of the wall. As a result of this drag force, soil elements located next to reinforcements had larger deformations than soil elements located in between the reinforcements. This situation became more obvious in the upper portion of the wall because deflections accumulate. The same situation was also observed in the parametric study, as discussed later in this paper.

Model Alg-W2 was also able to reproduce the axial strain in the reinforcement quite well, as shown in Figure 4. The peak strain locations, the peak strain magnitudes, and the strain distributions agree quite well with the measurements obtained from reinforcement layers 1, 2, 3, and 5. For reinforcement layer 7, Model Alg-W2 tends to underpredict the reinforcement strain by about 0.25%.

Generally speaking, the results shown in Figures 2, 3, and 4 indicate that Model Alg-W2 is capable of providing reasonable working stress-strain and deformation information of a GRS wall.

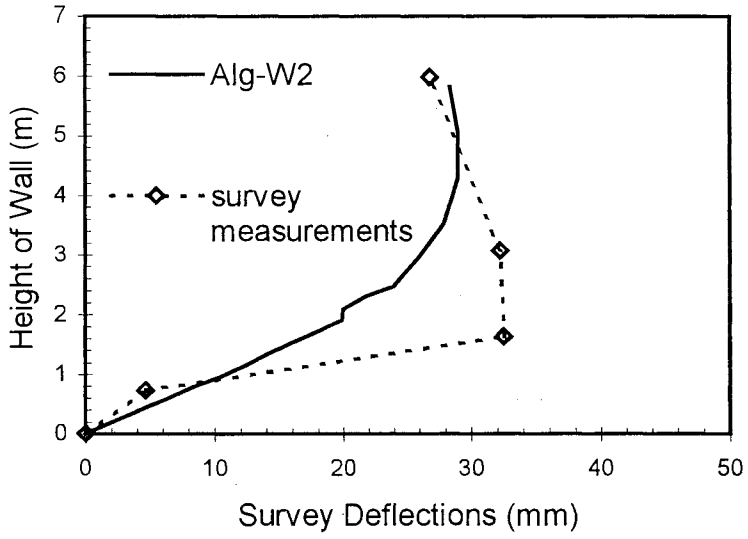

Figure 2. Predicted and measured wall face deformation for Wall 2.

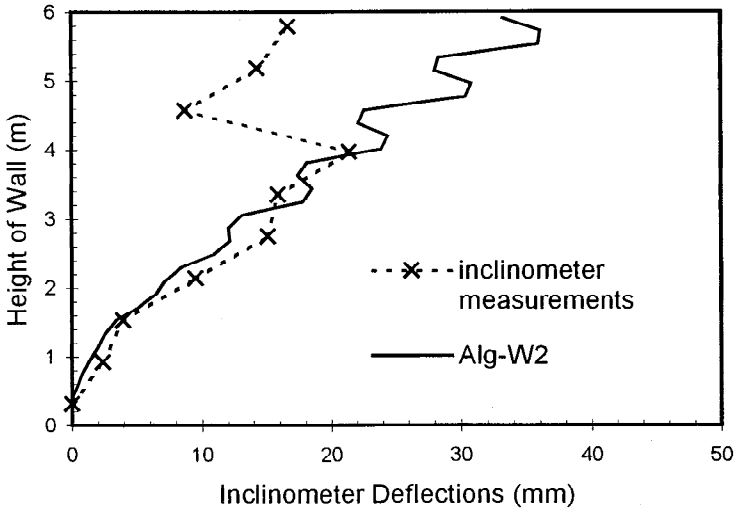

Figure 3. Predicted and measured inclinometer deflections at 1.8m behind wall face for Wall 2.

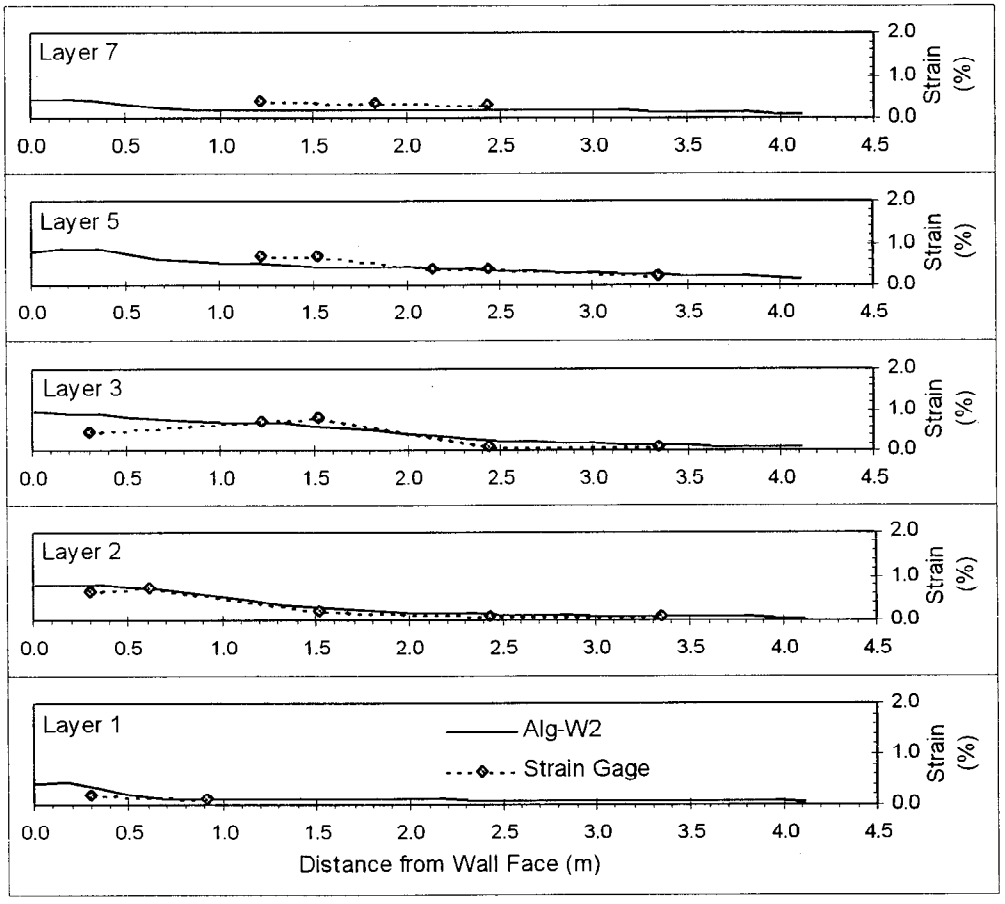

Figure 4. Predicted and measured reinforcement strain distribution for Wall 2.

PARAMETRIC STUDY

In this study, reinforcement stiffness was chosen as the controlling factor. A set of FLAC models was created based on Model Alg-W2. They had the same geometry, reinforcement layout, input soil properties, and input concrete panel properties as that model. Different stiffnesses and therefore the properties of the built-in interface of the reinforcement (cable elements) were systematically introduced into these FLAC models, as given in Table 2; a total of six FLAC models were developed for this parametric study. Both wall performance and working stress-strain distribution were monitored and analyzed.

Table 2. Summary of the models of the parametric study.

Model Name	Reinforcement Modulus, (kN/m)	Interface Shear Stiffness, (kN/m)	Notes
Alg-W1	54690	54690	Reinforcement modulus was equal to the modulus of steel strip (Algonquin Wall 1)
Alg-W3	37860	37860	Reinforcement modulus was equal to modulus of bar mat (Algonquin Wall 3)
Alg-W2-200%	2040	2040	Reinforcement modulus was 200% of Wall 2 geogrid modulus
Alg-W2	1020[a]	1020[a]	same input properties as Model Alg-W2
Alg-W2-50%	510	510	Reinforcement modulus was 50% of Wall 2 geogrid modulus
Alg-W2-25%	255	255	Reinforcement modulus was 25% of Wall 2 geogrid modulus

a: Including 50% reduction because of strain rate effects

PARAMETRIC STUDY RESULT AND DISCUSSIONS

Because of the high stiffness reinforcement of Walls 1 and 3, the magnitudes of face deflection are very small and not easy to predict. The potential error in the measurements due to the accuracy of the method could be very close to the magnitude of the measurements themselves. As shown in Figure 5, Models Alg-W1 and Alg-W3 both predicted very small survey face deflections, and difference between predicted and measured maximum deflection is only about 5mm. Figures 6 and 7 show the reinforcement strain distributions of Walls 1 and 3 compared with the modeling results of Models Alg-W1 and Alg-W3. The predicted reinforcement strains show reasonable agreement with the measurements of Walls 1 and 3.

Maximum survey face deflections were plotted versus the reinforcement modulus in Figure 8. The results indicate that increasing reinforcement stiffness significantly decreases maximum face deflections. This tendency was further verified by the results shown in Figure 9, in which accumulative inclinometer deflections at 1.8m behind the wall face decreased as the

reinforcement stiffness increased. Also observed in Figure 9, walls reinforced with very high stiffness reinforcement such as steel strips and bar mats (Walls 1 and 3) have almost the same deflections. This shows that there is a point of diminishing return where increasing reinforcement stiffness does not reduce the overall wall face deflection. As explained in the above section on modeling results of Model Alg-W2, "folds" or "jogs" were also observed in the predicted soil deflection curves of Models Alg-W2-200%, Alg-W2-50%, and Alg-W2-25% (Figure 9). The magnitude of these jogs increased as the stiffness of the reinforcement decreased.

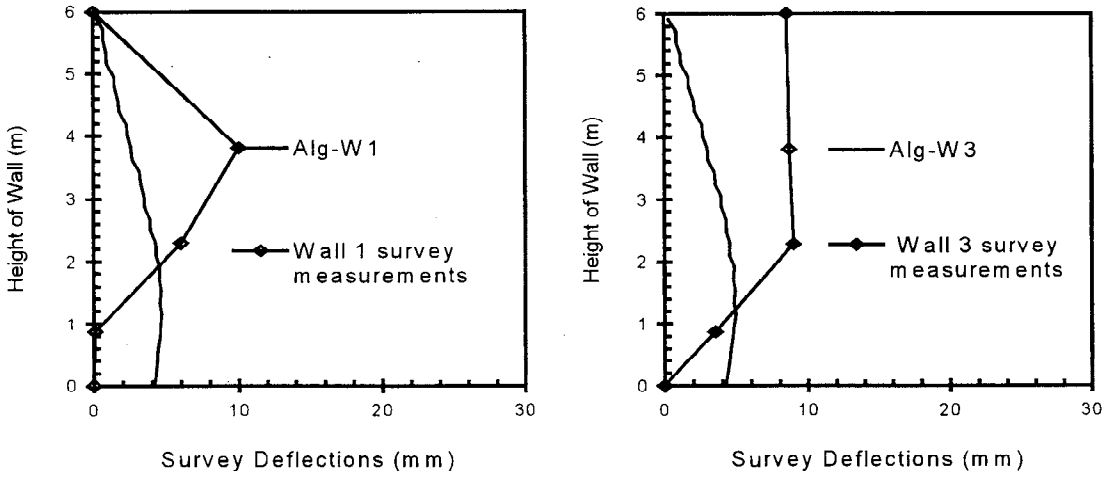

Figure 5. Predicted and measured wall face deflections of Walls 1 and 3.

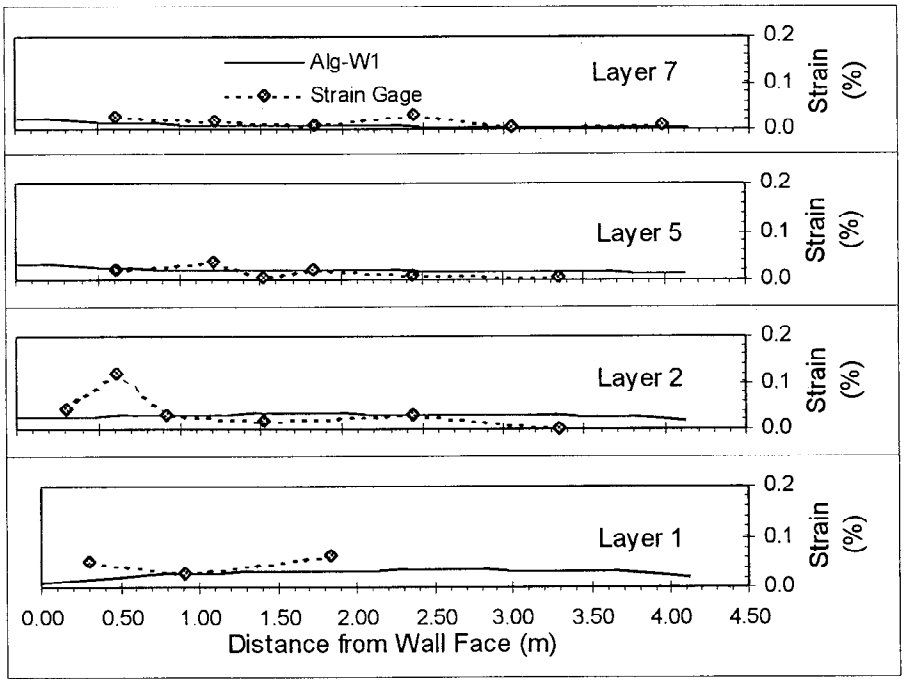

Figure 6. Predicted and measured strain distribution for Wall 1 (Model Alg-W1).

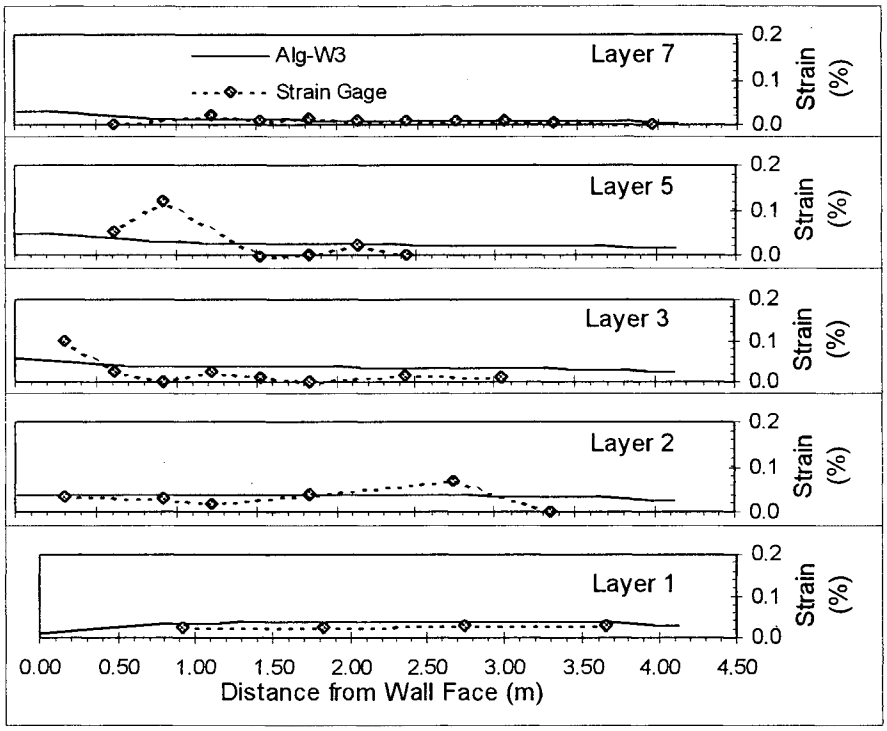

Figure 7. Predicted and measured strain distribution of Wall 3 (Model Alg-W3).

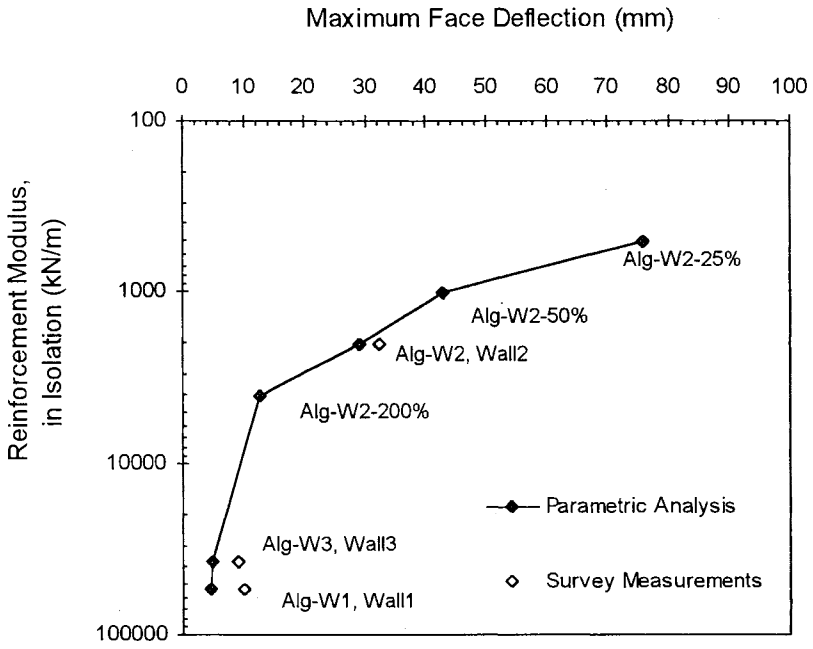

Figure 8. Maximum face deflection from survey vs. reinforcement modulus.

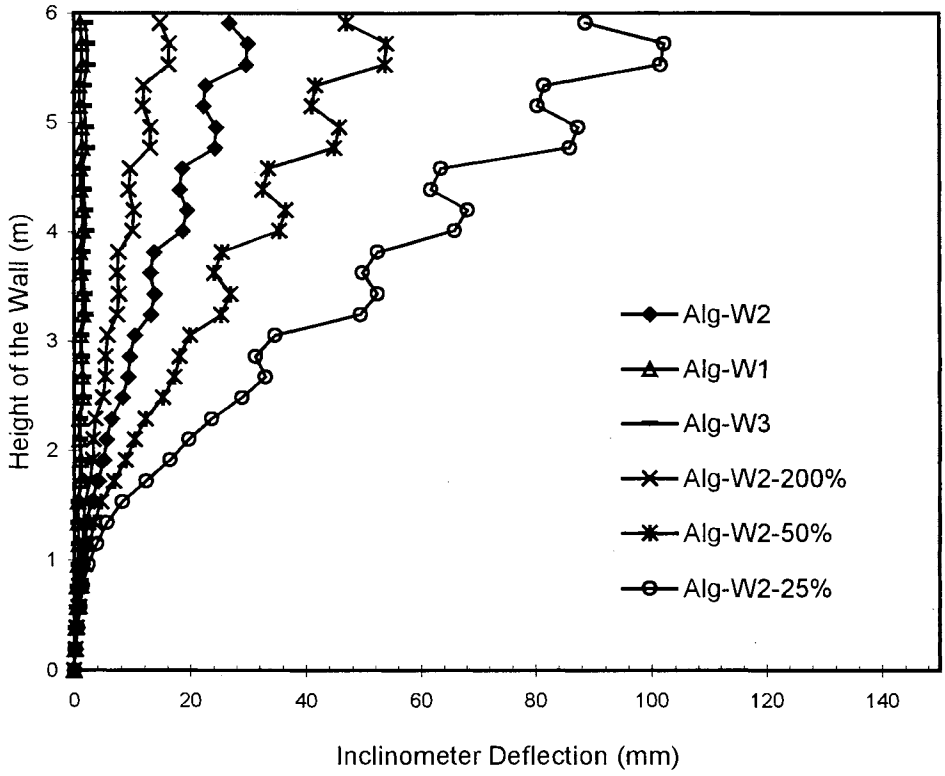

Figure 9. Modeling result of accumulated inclinometer deflection, at 1.8m behind wall face.

Figure 10 summarizes the reinforcement strain distribution obtained for all the reinforcement stiffnesses analyzed. Both peak strain and overall strain in the reinforcement increased as the reinforcement stiffness decreased. All the peak strains occurred at the wall facing except at layer 1 of Model Alg-W2-25% (case with low reinforcement stiffness). Results of Model Alg-W2-25% shows that the peak strain of layer 1 was located at about 0.17m from wall face. Moreover, results of parametric models indicate that decreasing the reinforcement stiffness tends to cause the high strain zones of the reinforcements to extend from the wall face into the backfill.

Figure 11 shows the relationship of the maximum reinforcement load as a function of the reinforcement stiffness. It shows that reinforcement with relatively high stiffness such as steel reinforcement attracts larger reinforcement loads than does low stiffness reinforcement such as geosynthetic reinforcement. By synthesizing the results shown in Figures 10 and 11, it appears that as the reinforcement stiffness decreases enough to result in having peak reinforcement strains of 3 to 4% or more, the load in the reinforcement does not continue to decrease, but instead begins to increase as reinforcement stiffness decreases. Interestingly, the peak shear strain for the soil was on the order of 2 to 4% strain, based on triaxial tests conducted on this wall backfill (Christopher, 1993). Figure 11 also shows that the maximum reinforcement load occurs in the middle of the wall (layers 3 and 5) for all the reinforcement stiffnesses analyzed.

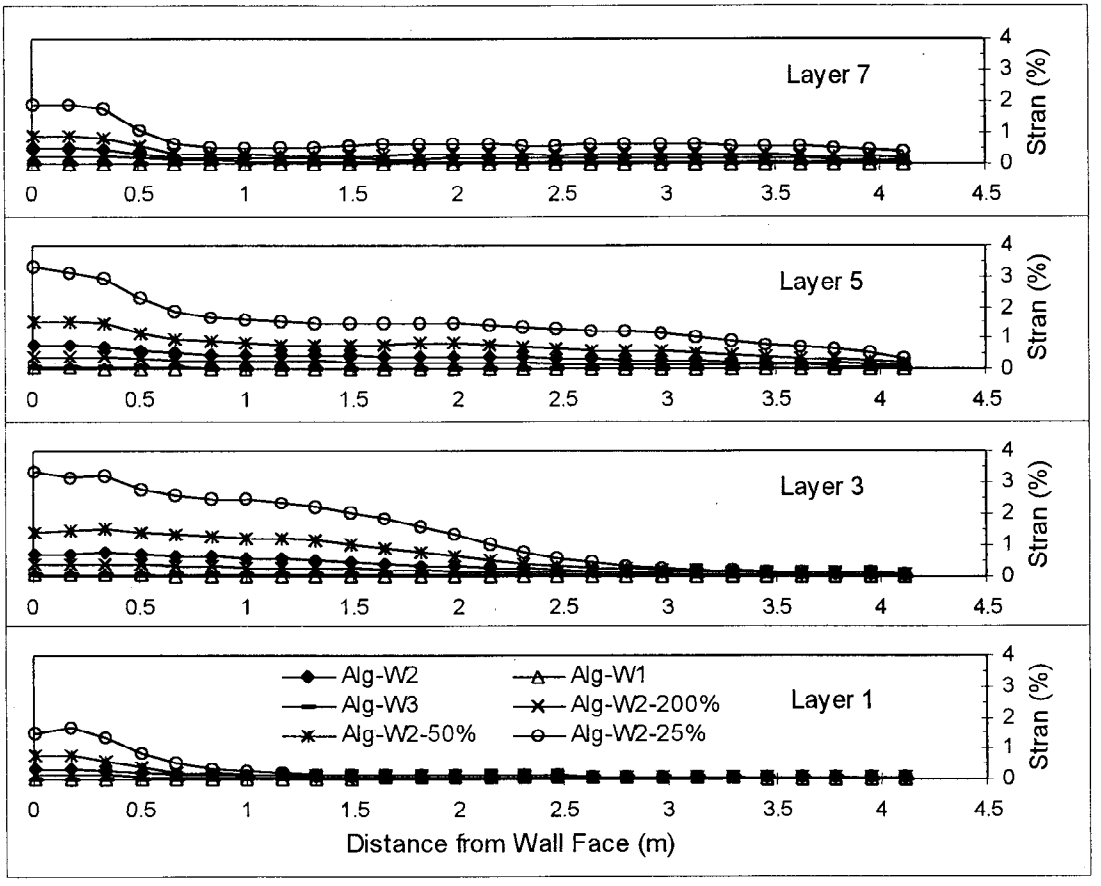

Figure 10. Reinforcement strain distribution.

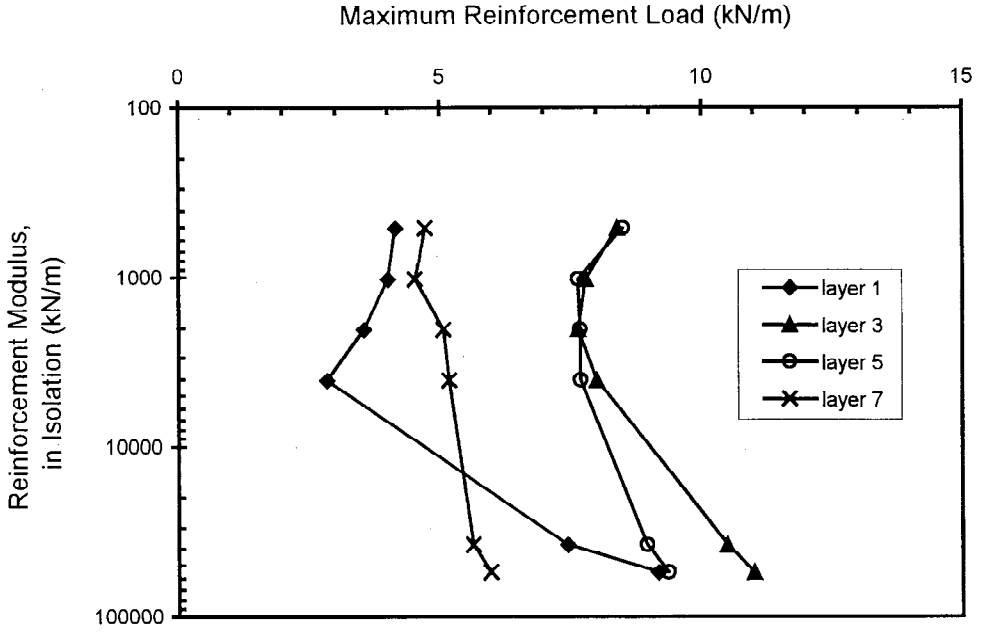

Figure 11. Maximum reinforcement axial loads.

CONCLUSIONS

Numerical models have been developed to help improve our understanding of internal stress-strain conditions inside GRS retaining walls. Three MSE retaining walls with identical geometries, facings, and soil properties but with different reinforcement stiffnesses were modeled and results were compared to the measurements obtained from instrumentation installed in those walls. Then a parametric analysis was performed to evaluate the effect of varying the reinforcement stiffness on reinforcement strains, and overall deformations. This research is applicable to GRS systems with well-compacted granular backfills with moderate to high friction angles and small strains in the soil and reinforcement.

Based on these analyses, the following can be concluded:

1. The results indicate that FLAC Models Alg-W1, Alg-W2, and Alg-W3 are capable of modeling deformations and internal wall behavior with reasonable accuracy.

2. Increasing the reinforcement stiffness results in decreasing the overall wall deflection. This tendency diminishes when very high reinforcement stiffness is used.

3. Both peak and overall reinforcement strains increase as the reinforcement stiffness decreases. This conclusion coincides with the conclusions obtained from observing the result of overall wall deflection analysis.

4. High stiffness reinforcement such as steel reinforcement attracts much higher reinforcement loads than low stiffness reinforcement such as geosynthetics.

5. For the wall cases analyzed, when reinforcement stiffness is higher than about 2000 kN/m, reinforcement loads increase as reinforcement stiffness increases. However, when reinforcement stiffness is less than this value, reinforcement loads also increase as reinforcement stiffness decreases. This situation is the result of the dramatic increase in reinforcement strains when low stiffness reinforcement is used.

6. Based on the parametric analysis, it appears that a lower modulus geosynthetic could have possibly been used and still have strains and deformations within an acceptable range. For example, results of Model Alg-W2-50% indicates that, with only 50% of the designed reinforcement modulus, the wall performance would still be in a tolerable range (maximum face deflection = 43mm, maximum accumulative deflection at 1.8m behind wall face = 50mm, and maximum peak reinforcement strain = 3.3% at layer 3).

7. Considering that the results of the parametric study compared well to the measured strain and deformation data for all three walls, the feasibility of using analytical modeling tools,

like FLAC, to analyze reinforced soil wall behavior for different design factors is demonstrated.

ACKNOWLEDGMENT

The Washington State Department of Transportation provided funding for this research. This support is greatly appreciated. The authors also thank B.R. Christopher, R.J. Bathurst, and R. Kimmerling for helpful advice.

REFERENCES

Bell, J. R., Barrett, R. K., and Ruckman, A. C., 1983, "Geotextile Earth-Reinforced Retaining Wall tests: Glenwood Canyon, Colorado," Transportation Research Record 916, Washington, DC, pp. 59-69.

Boyle, S.R., (1995), "Deformation Prediction of Geosynthetic Reinforced Soil Retaining Walls", Ph.D. Dissertation, University of Washington. 391p

Boyle, S.R., Gallagher, M, and Holtz, R.D., (1996), " Influence of Strain Rate, Speciemen Length and Confinement on Measured Geotextile Porperties," Geosynthetics International, Vol. 3, No. 2, pp. 205-225.

Christopher, B.R., (1993), "Deformation Response and Wall Stiffness in Relation to Reinforced Soil Wall Design", Ph.D. Dissertation, Purdue University, 354p.

Cook, R.D. and Young, W.C., (1985), "Advanced Mechanics of Materials," Macmillan, Inc., New York. 539pp.

Holtz, R.D., and Lee, W.F., (1998), "Geosynthetic Reinforced Wall Analysis, Phase II: Use of In-Soil Geosynthetic Behavior to Predict Deformation", Report No. WA-RD 452.1, Washington State Department of Transportation, 32p

Itasca Consulting Group, (1993), "Fast Lagrangian Analysis of Continua Version 3.2", Itasca Consulting Group, Inc., Minneapolis, MN, U. S. Vol. I, II, III,

Lade, P.V., and Lee, K.L., (1976), " Engineering Properties of Soils," Report UCLA-ENG-7652, 145pp.

Lee, W. F., and Holtz, R.D., (1998), "Analysis of Geosynthetic Reinforced Soil Retaining Walls Using Composite Material Properties", Proceedings of the Thirteenth South East Asia Geotechnical Engineering Conference, Taipei, Taiwan, Vol. 1, pp. 349-354.

Rowe, R. K., and Ho, S. K (1993), "Keynote Lecture: A Review of the Behavior of Reinforced Soil Walls," Earth Reinforcement Practice, Ochiai, Hayashi, and Otani, ed's, Balkema, Rotterdam, pp. 801-830.

STUDY ON THE INTERACTIVE EFFECT BETWEEN GEOGRID AND WEATHERED MUDSTONE

DAVE TA-TEH CHANG
Professor, Civil Engineering Dept. Chung Yuan University, Chung Li TAIWAN 32023, R.O.C
SHI-WEI CHEN
Master, Civil Engineering Dept. Chung Yuan University, Chung Li TAIWAN 32023, R.O.C.
SHYANG-JIUN SHIEH
Graduated Research Assistant, Civil Engineering Dept. Chung Yuan University,Chung Li TAIWAN 32023, R.O.C.

ABSTRACT

The interactive behavior between the geogrid and the soil mass is one of the major factors determining the viability of the reinforced structure.This study performed a number of pullout tests on geogrids of differing specimen and aperture size to simulate the pullout failure mechanism of the geogrid under different conditions.The results indicate that specimen size affects the pullout resistance and the tensile force-displacement behaviors. Moreover, no matter if the spacing between or the length of the transverse ribs, were modified, altering the aperture of the geogrid had a significant effect on pullout test results. Generally, pullout resistance development can be categorized in the following three stages: (1) The period of frictional resistance development. (2) The period of passive resistance development. (3) The period of soil mass plasticity.

INTRODUCTION

In general, the three major problems associated with the interaction between the soil and reinforcement materials of a reinforced structure are: (1) The appearance of frictional resistance, (2) The passive resistance provided by the reinforcement material, (3) The twisting of the reinforcement material. Of these three, the latter can be ignored for geosynthetics. Thus, the problems of the interactive behavior of the soil/reinforcement material are simplified to the consideration of the sliding of the soil, and the material being pulled from out of the soil mass. For an illustration of the direct shear failure mechanism and the pullout failure mechanism, as shown in Figure. 1.

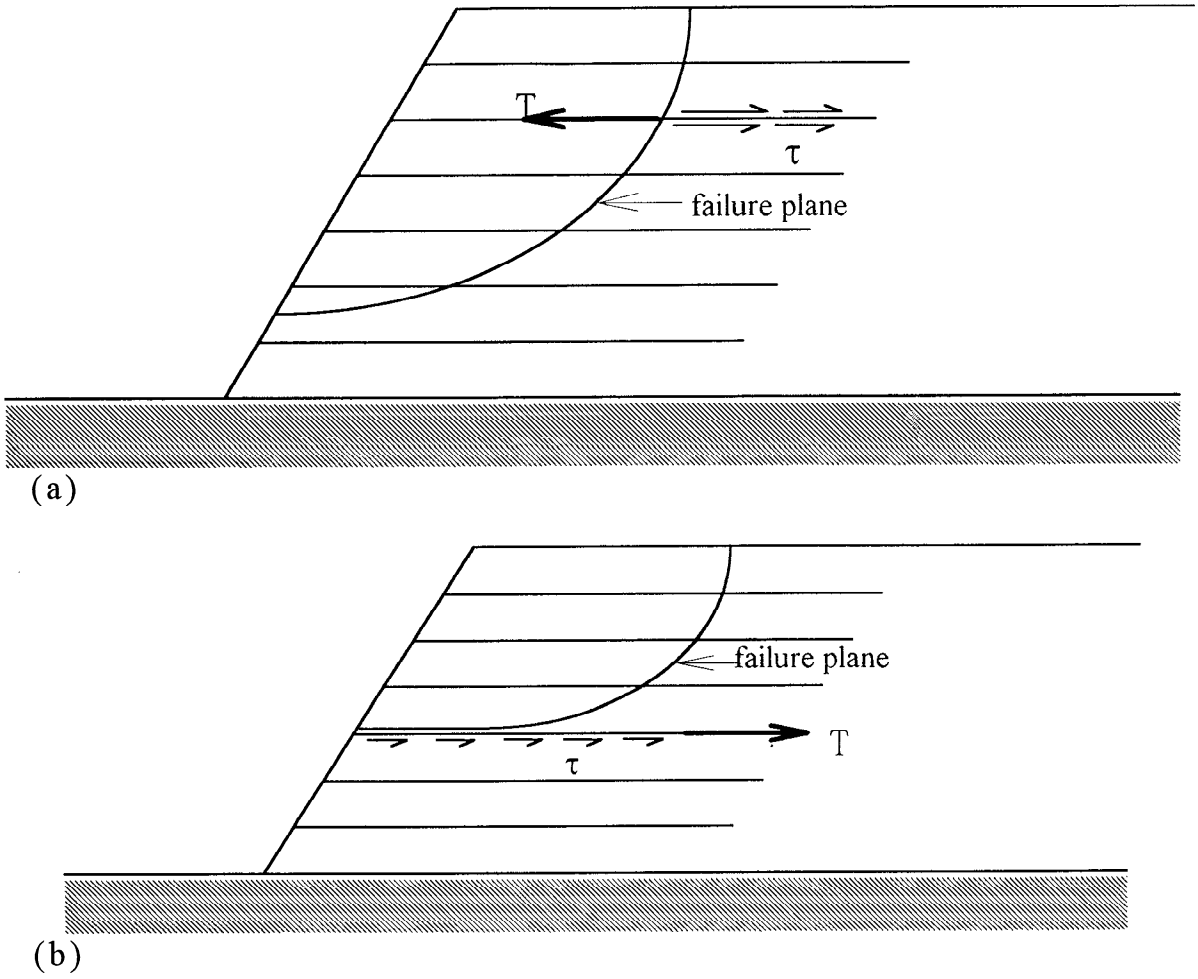

Figure 1 Illustration of Failure Mode of the Reinforced Earth
(a)Pullout Failure(b)Shear Failure

The interactive behaviors between the soil and geogrid are usually simulated by the direct shear and pullout tests. The two sources of pullout resistance for geogrids are the frictional resistance between the geogrid and the soil, and the passive resistance produced from the squeeze of soil by the transverse ribs. Using a completely different shape and size, Schlosser and Elias (1978) found: (1) Merely 0.05 in. of displacement was necessary to mobilize the frictional resistance between the reinforcement material and the soil. (2) 4 in. of displacement was needed to completely mobilize passive resistance. Using metal wire to perform pullout tests, Bergado (1992) found that passive resistance comprised 80 % or more of total pullout resistance.

In the early days, reinforced earth techniques used non-cohesive soils with a relatively higher frictional angle. Yet, economic considerations warrant the use of backfill materials available on site. Therefore, as the National Highway No. 2 in Taiwan passes through a mudstone formation, lots of weathered mudstone may be used in reinforced structure. This study tests the pullout resistance behaviors between geogrid and weathered mudstone backfill in order to better understand the mechanical properties between geogrid and cohesive soil.

PLAN AND CONTENTS OF EXPERIMENT

To accomplish its objectives, this study concentrates on the following three parts: (1) Testing the basic properties of the geogrid in order to control each characteristic of the geogrid. (2) Performing pullout tests of the geogrid to determine the amount of influence factors such as geogrid type, aperture size, specimen dimensions, and so on. (3) To organize testing results to discuss the influence of different types of pullout resistance behaviors. Generally, the shape and size are the most significant factors concerning the geogrid specimen.

Shape of Reinforcement

Using Bangkok clay, Bergado (1992) conducted pullout tests on metal grids. The results show that when spacing ratio (s/d; s = the space between transverse ribs, d = thickness of transverse ribs) was between 8 ~ 50, then $f_b \leqq 1$. When s/d = 9, f_b = 0.45; s/d = 50, f_b = 0.2. (f_b: represents the adherent coefficient, the result of the pullout strength of the geogrid divided by soil strength is used to evaluate the interactive capability between the soil and geogrid). The results of the pullout testing of Mallick et al. (1995) showed that the larger the aperture size, the greater the pullout resistance. Using particulate soil backfill material, Bauer et al. (1990) determined that when aperture ratio (= d_{50} / aperture width) was in the 0.25 ~ 0.35 range, a greater amount of pullout resistance was mobilized. From the above findings it can be clearly seen that the relationship between soil particles and aperture size have a great effect on pullout resistance. Sarsby (1985) suggested that this relationship be expressed as:

$$B_{GG} / d_{50} = 3.5 \quad (1)$$

where, B_{GG}: Smallest width of geogrid aperture

d_{50}: Average grain size of soil backfill

Reinforcement Specimen Size

Using specimens of different size, Imaizumi et al. (1994) conducted direct shear tests on soil/geosynthetics. The findings show that the larger the specimen size, the lower the shear strength, and the large displacement of the development of peak strength. This phenomenon was due to the following two reasons: (1) The frictional effect between the soil and the boundary, which was most evident in low normal stress, the smaller the specimen size, the less the friction of boundary. (2) The larger the specimen size, the greater the plane of failure, and the longer the extent of the failure plane.

TESTING MATERIALS AND INSTRUMENTS

This study makes use of weathered mudstone taken from Tienliau Village, Kaohsiung County, the basic properties of which are shown in Table 1.

During the course of this study the size of the geogrid aperture had to be changed, and because they have to meet the necessary requirements, flexible grids are adopted. The basic properties of the flexible geogrids used can be seen in Table 2.

A detailed description of the pullout testing device used in this study can be seen in Figure 2. The internal dimensions of the testing box measure 40 cm in width by 50 cm in length by 30 cm in height. A rubber air bag was used to exert pressure above and below simultaneously. The weathered mudstone was compacted of standard 95 % compaction ($0.95\gamma_{dmax}$), with moisture controlled at OMC $\pm$ 2%. Thus controlled, the soil was placed in the box in separate layers.

Table 1 Factors Involved in the Interactive Effect

Instrument	Soil Specimen	Reinforcement
· Height of Box · Testing Spee · sleeve Length · Confining pressure · Boundary Condition	· Shear Strength · Compaction Ratio · Grain Size Distribution · Swelling	· Size · Shape · Aperture Size · Stiffness

Table 2 Basic Properties of Weathered Mudstone

Gs	2.7
LL (%)	34
PL (%)	22
PI (%)	12
γ_{dmax} (kg/m^3)	1.68
ω (%)	17.5
f (degree)	17.14
c (kN/m^2)	50.5
d_{50} (mm)	0.007

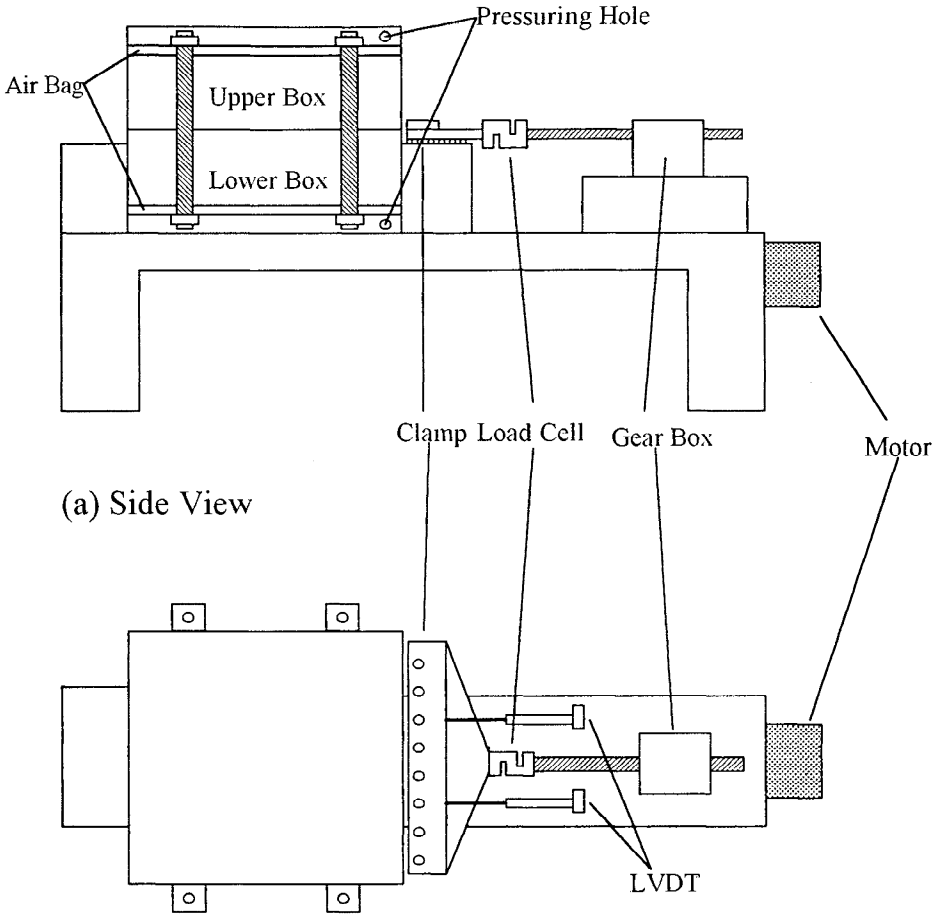

Figure 2 Illustration of the Pullout Testing Device
(a) Side View (b) Overview

TEST RESULTS

Effects of Specimen Size

This study embeded specimens of geogrid width, geogrid length, different area, and to perform pullout tests; the results of which are shown in Figures 3 ~ 5. The force-displacement curves of pull-out test of each specimen had its own characteristics. When resistance peaked, the corresponding displacement followed increase in the length of the specimen. As seen in Figure 3, increases in specimen width corresponded with increases in resistance, but the amount of increase tended more slowly. From Figure 4 it can be seen that the relationship between resistance and specimen length has the same contribution as that of width. The results displayed in Figure 5 show that for each increase in specimen area there is a corresponding increase pullout resistance in unit area, and the amount of increase also follows reductions. When area is approximately 0.035 m^2 or greater, resistance tends toward stability and does not increase further. If normalization is a consideration, 17.5 % (ratio of specimen to box area $-$ 0.035 m^2/0.2 m^2) is the maximum value that can be discarded

concerning the specimen size effect. When this value is exceeded, the front wall and the boundary of the box will constrain the development of full failure plane of the soil mass, which causes no further increases in resistance. Therefore, this limitation must be observed during the design phase.

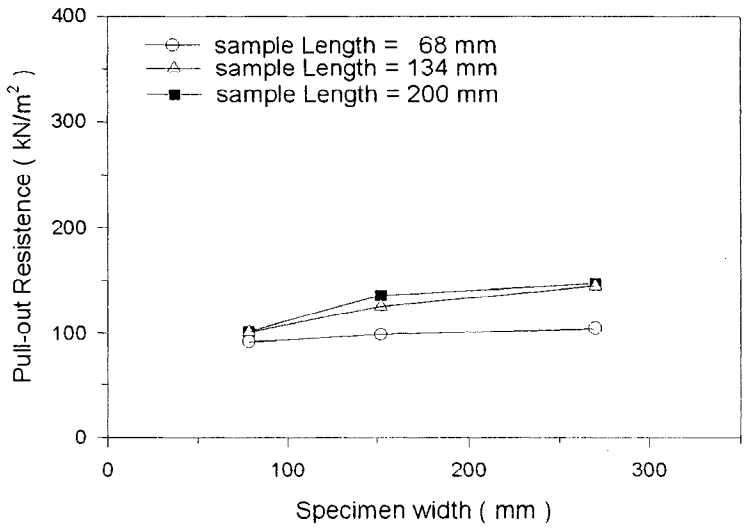

Figure 3 Relationship Between Pullout Resistance and Specimen Width

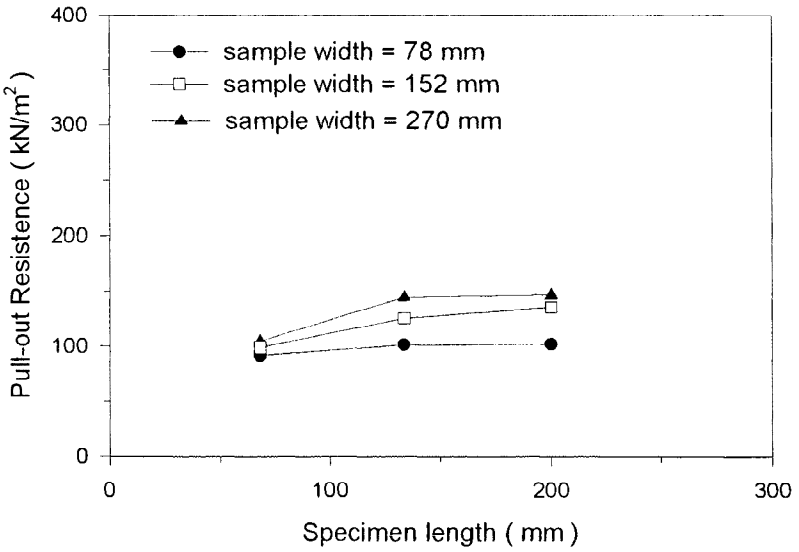

Figure 4 Relationship Between Pullout Resistance and Specimen Length

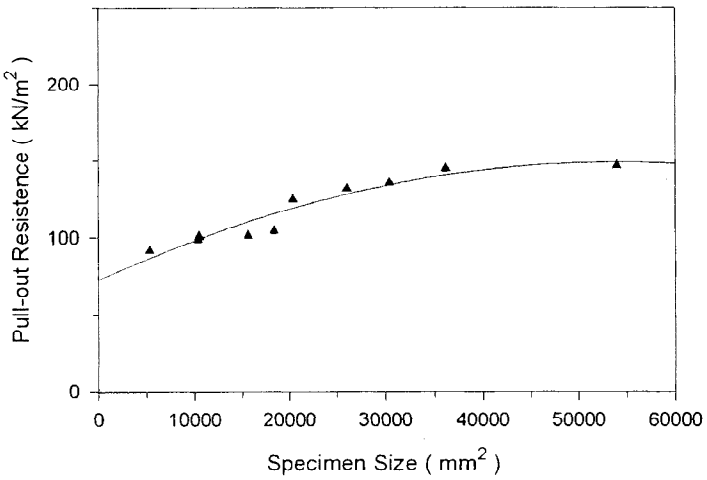

Figure 5 Relationship Between Pullout Resistance and Specimen Area

Aperture Size Effects

Overall Pullout Behaviors

In order to better understand the interactive relationship between aperture and soil mass, specimens were cut to change the spacing of the transverse ribs (s) and to alter the length of the transverse ribs (l) (see Figure 6).

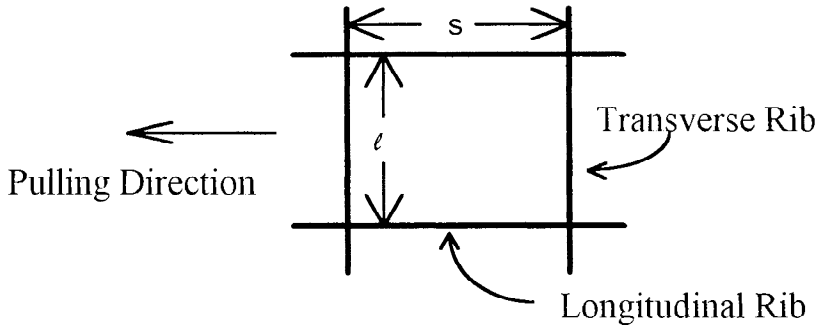

Figure 6 Symbols of the Longitudinal and Transverse Ribs

As testing results were too numerous, only a typical representative example is provided in Figure 7 for consideration. From the pullforce-displacement cure shown in the figure, the development of pullout resistance can be seen to fall into three stages. The first of these is the period of frictional resistance development, second is the period of passive resistance development, and finally the third stage is the period the soil reaches plasticity. To clearly define the above description, a non-scaled illustration is provided in Figure8. .

In the first stage, the frictional resistance development period is not affected by alterations in aperture size. In the second stage, the passive resistance development period will differ in

accordance with changes of transverse rib spacing and transverse rib length; the longer the length of the transverse rib (l), and the greater the spacing (s), the longer the period of passive resistance development. This is due to the transverse ribs pushing out the soil in front which causes the soil behind the rib to loosen when the spacing between the transverse ribs (s) is small. This in turn causes the next rib to push out the soil in front of it with an even greater amount of force, thus influencing the mobilization of passive resistance. Palmeria (1989) called this phenomenon the interference effect. From the figure it can also be seen that the greater the spacing between the transverse ribs (s), the less the spacing influence will have on the development of passive resistance. In the third stage, the amount of pullout resistance follows the length of the transverse ribs (l) (i.e. it increases in corresponding proportion in length). The ratio of the passive resistance comprises of total resistance follows the increase; the greater the spacing of the transverse ribs, the greater the pullout resistance.

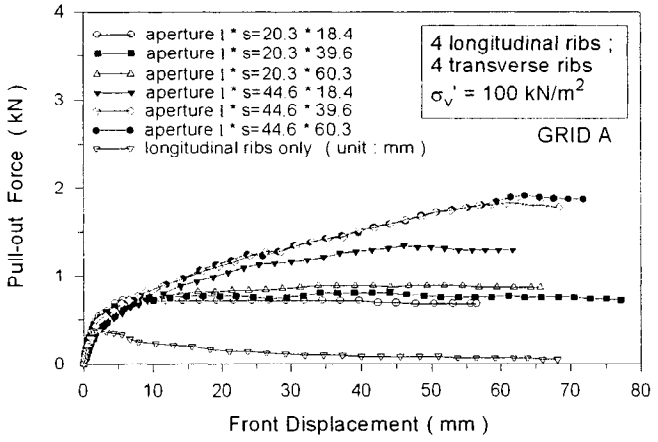

Figure 7 Chart of the Pullout Force — Displacement Curve of Geigrid A with Different Apertures(σ_V=100kN/m^2)

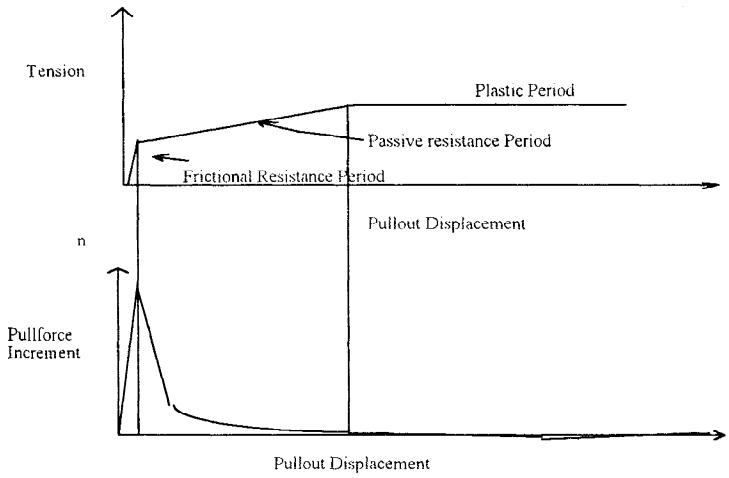

Figure 8 Scheme of the Resistance Development in each Stage

Effects on Passive Resistance

In addition to the aforementioned consideration of the total amont of resistance, ultimate passive resistance is also used for evaluation. Using the results from the longitudinal ribs only, ultimate passive resistance is found by subtracting the frictional resistance from the value of total resistance. Results show that the greater the spacing between transverse ribs, the greater the normal stress, and the greater the passive resistance (see Figure 9 for details).

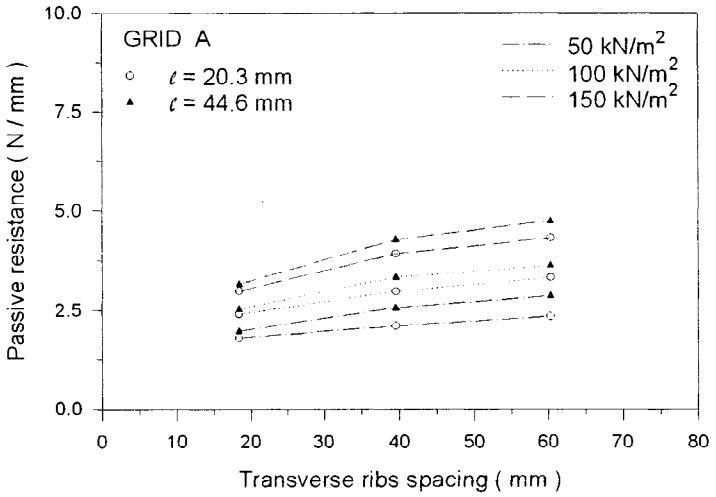

Figure 9 Comparison Chart of Passive Resistance and Transverse Rib Length for Geogrid A

As the transverse rib is pushing out soil, the transverse rib is assumed to bearing uniform force all along the rib body, and the rib joint is assumed not to undergo failure. Moreover, the if the flexible rib is unable to bear bending, then the rib will receive force in the same way as a simple beam. As in Figure 10, "q" equals passive resistance, the dip angle is (θ_i) and the flexure is (δ_i).

Assume that the direction of the passive resistance produced is normal to the transverse rib. The part of the pullout direction has on passive resistance should be $P_i\cos\theta_i$ (see Figure. 10); which the greater the dip angle, the smaller the part of pullout resistance. Depending on the length of the transverse rib, changes in the dip angle of the rib after undergoing the pulling force will also affect the curvature. Thickness is also one of the factors affecting the transverse ribs. The length to specing ratio of the geogrid specimens used in this study were: 2.2 for grid A, 2.3 for grid B, and 2.4 for grid C. After bearing force, the greater the length in relation to the specing, the greater the disparity in the curvature for the short rib. In addition, as the transverse rib of geogrid C was thicker than the other two specimens, its ribs had the greatest amount of passive resistance. In summary, the unit length passive resistance of the three types of geogrid is related to changes in length, shape, and amount of pulling force borne by the transverse rib.

The definition of spacing ratio is the spacing distance between transverse ribs divided by the thickness of the transverse rib (s/d). From the pullout test results and the spacing ratios shown in Figure 11, it can be seen that under three types of normal stress, unit area pullout resistance follows increases in spacing ratio. If more data were available, results would be even better.

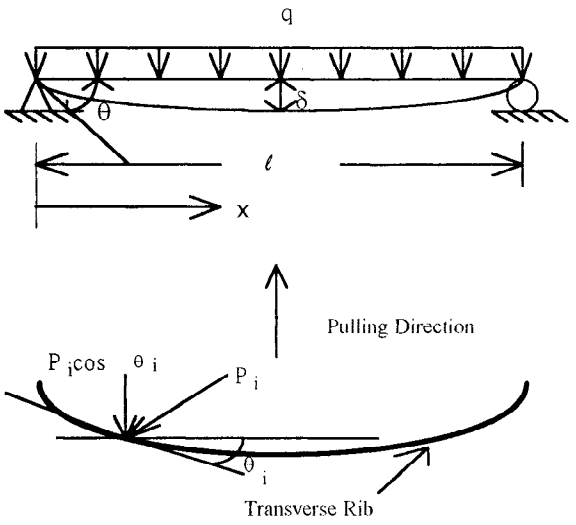

$$\theta = \frac{ql^3}{24EI} \quad , \quad \delta = \frac{5ql^4}{384EI}$$

Figure 10 Restraint of Pulling Force by the Transverse Rib

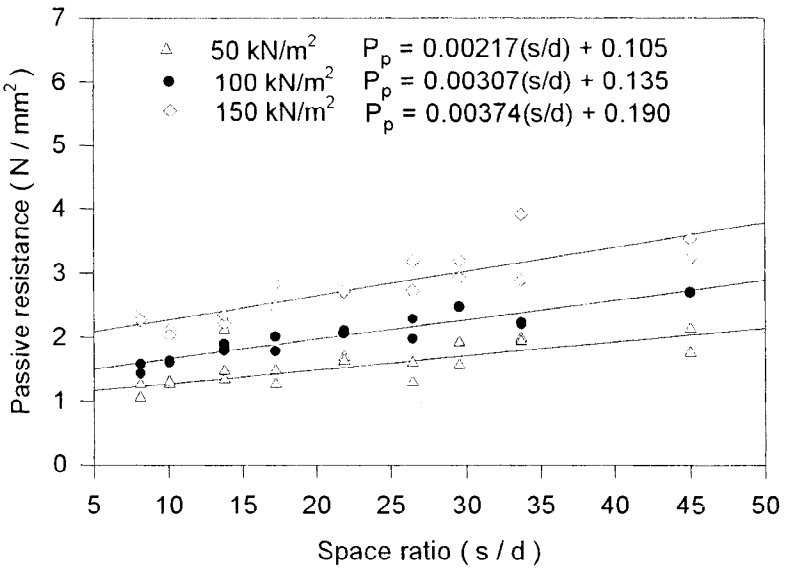

Figure 11 Relationship Between Unit Area Passive Resistance and Spacing

Bond Coefficient f_b

Shown in Figure 12 is the relationship between the corresponding displacement of ultimate pullout resistance and the spacing of the transverse ribs. From this figure it can be seen that increases in displacement follow increases in the spacing of the transverse ribs; the longer the transverse rib, the greater the displacement. When all the three geogrid samples are comparatively shorter, the influence of normal stress is relatively small. However, for comparatively longer transverse ribs, the corresponding displacement of ultimate pullout resistance will mirror increases in normal stress. In addition to this phenomenon, the extreme resistance value can be normalized; the formula for which is defined as:

$$f_b = \frac{\text{ultimate pullout resistance}}{\text{shear strength of soil}} \qquad (2)$$

Figure. 13 illustrates the relationship between the value of f_b and normal stress. The size of all three geogrid types were the same, and for all types, an increase in normal stress followed with a corresponding decrease in the amount of f_b. A reduction in the rate of normal stress increase follwed with a more gradual reduction in f_b. This phenomenon is due to: (1) The failure envelope is nonlinear, so that it is neither in a strait line nor is it in direct proportion to the normal stress. (2) While the pullout stress is dispersed for a geogrid buried in the soil, the definition for f_b assumes the value for f_b is uniform,but it is not in reality. Furthermore, as spacing of the transverse ribs increases, the value for f_b decreases. This is due to the fact that as spacing increases, area also increases, but the amount of increase in resistance does not keep pace with the increase in area. Therefore, the value of f_b decreases.

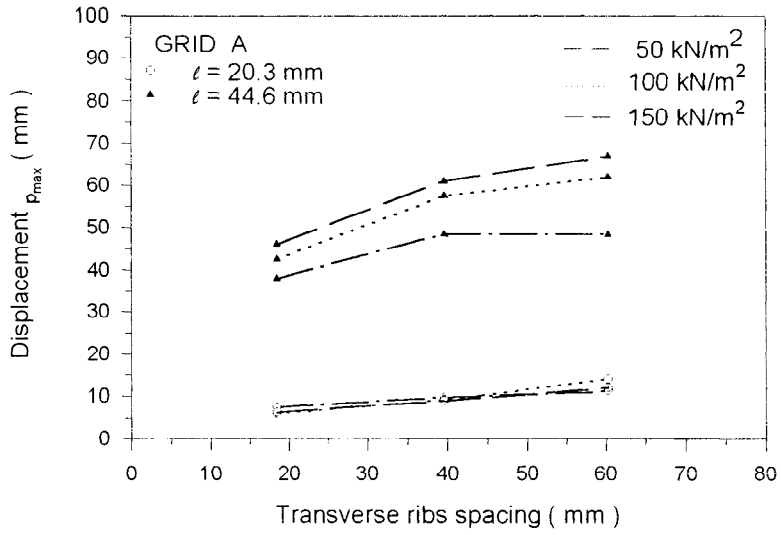

Figure 12 Relationship Between f_b and Normal Stress for Geogrid A

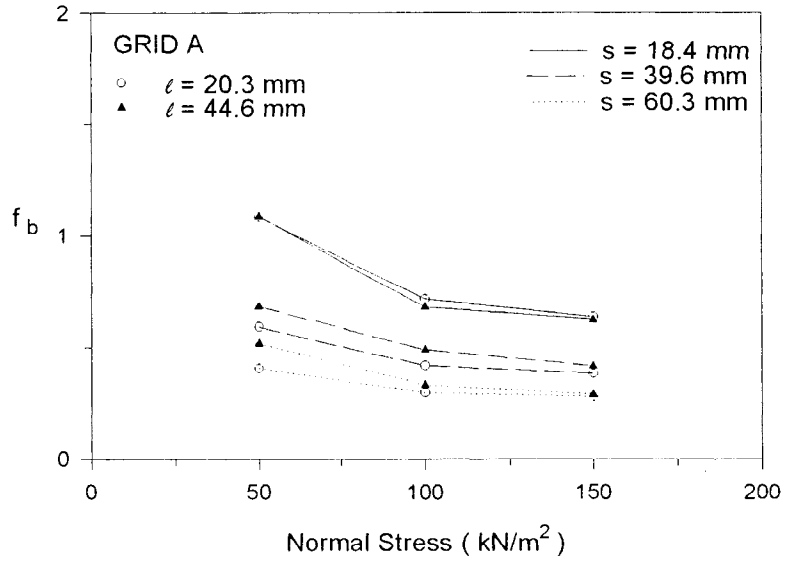

Figure 13 Relationship Between Max. Pullout Resistance Displacement and Transverse Rib Spacing for Geogrid A

SUMMARY AND CONCLUSIONS

Using cohesive particulate soils to perform pullout testing ,it was found that the influence of the front wall effect for cohesive soils was less than that for non-cohesive soils.

The size of the geogrid specimen had a certain degree of effect on the pullforce-displacement curve of pullout resistance. The longer the specimen, the greater the displacement needed to reach the ultimate resistance; the greater the area, the smaller the effect of size on pullout test results. Therefore, when cohesive soils are used to perform pullout testing, the size of the confinement box should be adapted to suit the specimen.

Using weathered mudstone, the development of pullout resistance can be separated into the following three stages: (1) The period of frictional resistance development. (2) The period of passive resistance development. (3) The period of soil plasticity. Each of these phases is largely influenced by grid aperture (both by spacing of the transverse ribs and by length of the transverse ribs).

Passive resistance makes up 90 % or more of total pullout resistance. This ratio of total pullout resistance is related to soil type, length and thickness of transverse ribs, and the ratio of projected area to the total area of the ribs.

Wider spacing of the transverse ribs can reduce the interference effect of the geogrid, thus increasing passive resistance. However, if spacing is too great then the speed of passive

resistance development will be affected. The, unit area resistance provided by the contribution of the geogrid will be reduced; thus impairing reinforcement effectiveness.

The magnitude of the cooresponding displacement of the peak pullout resistance will be affected by differences and changes in aperture. The greater the spacing and the longer the transverse ribs, the greater the displacement. Normal stress only influences displacement for comparatively longer transverse ribs.

When the length of the transverse ribs increases, passive resistance increases, the force undergone by the grid joints increase, and the amount of tension on the logitudinal ribs increases. When the length of the transverse is increased and the strength of the soil is great enough, grid joint strength and longitudinal rib strength are two major factors which allow the geogrid to perform its function.

Using a cohesive soil (weathered mudstone), this study performed testing to determine the effects of grid aperture. The results of such testing have shown that the aperture ratio provided by Bauer (1990) is unsuitable for cohesive soils.

REFERENCES

Bauer , G.E. and Mowafy , Y.M., (1990) "The Effect of Grid Geometry and Aaggregate Size on the Stress Transfer Mechanism" 4th International Conference on Geotextile, Geomembrane and Related Products, Netherlands, pp.801-801.

Bergado D.T., Cisneros, C.B., Sampaco, C.L., Alfaro, M.C., and Shivashankar R., (1990) "Effect of Compaction Moisture Contents on Pullout of Steel Geogrids with Weathered Clay Backfill" 4th International Conference on Geotextile, Geomembrane and Related Products, Netherlands, pp.803.

Bergado, D.T., Chai, J.C., and Balasubramanism, A.S., (1992) "Interaction between Grid Reinforcement and Cohesive-Frictional Soil" Proc. of the Internation Symposium on Earth Reinforcement Practice , Asian Institute of Technology, Bangkok, Thailand , pp.29-34.

Fannin, R.J. and Raju, D.M., (1993)"Large-Scale Pull-Out Test Results on Geosynthetics." Proc. of Geosynthetics Conference, Vancouver, British Columbia, Canada, pp.633-643.

Geosynthetics Research Institude, (1991)"GRI Test Method GG5, Standard Test Method for Geogrid Pull-Out", GRI Test Methods & Standards, Drexel University.

Hong, F. Y., (1992) "Study on the Mechanical Properties of the Pullout Testing of Geogrids under Confined Conditions" Master's Degree Thesis Presented to the Department of Civil Engineering, Chung Yuan University, Chungli, Taiwan, R.O.C.

Huang, S. L., (1995) "Mechanical Behaviors of Geogrids under Soil Confinement" Master's Degree Thesis Presented to the Department of Civil Engineering, Chung Yuan University, Chungli, Taiwan, R.O.C.

Imaizumi, S., Nishigata, T., Iimura, K., (1994) "Effect of Variation in Sample Sizes on Soil-Polymer Interface Strength" The Fifth International Conference on Geotextiles,Geomembrane and Related Products, Singapore, pp.423-426.

Juran , I. , Knochenmus , G. , Acar , T.B. , and Atman, A.,(1988) "Pull-out Response of Geotextiles and Geogrids" , Geosynthethics for Soil Improvement , Geotechnical Sepecial Publication No.18 , New Yark , pp.92-111.

Mallick, S.B., Zhai, H.,(1995) "A Laboratory Study on Pull-Out Performance of Woven Geotextiles." Proc. of Geosynthetics Conference, Nashville, Tennessee, pp.1169-1178.

Palmeria, E. M. and Milligan, G.W.E., (1989) "Scale and Other Factors Affecting the Results of Pull-Out Tests of Grid Beried in Sand" Geotechnique, Vol.39, No.3, pp.511-524.

Sarsby, R.W. (1985) "The Influence of Aperture Size/Particle Size on the Efficiency of Grid Reinforcement." Proc. 2nd Canadian Symp. on Geotextiles and Geomembranes, Edmonton, Alberta, pp.7-12.

Schlosser, F. and Elias, V., (1978) "Friction in Reinforced Earth." Proc. ASCE Symposium on Earth Reinforcement, Pittsburgh, Penn., pp.735-763.

Sun, T. S., (1995) "Pullout Behaviors and Numerical Analysis of the Reinforcement Grids Buried under Weathered Mudstone." Master's Degree Thesis Presented to the Department of Civil Engineering, Chung Yuan University, Chungli, Taiwan, R.O.C.

Transportation Research Board (1987) " Reinforcement of Earth Slopes and Embankments" NCHP 290.

NUMERICAL STUDY OF THE INFLUENCE OF BASE SHAKING ON REINFORCED SOIL RETAINING WALLS

R.J. BATHURST and K. HATAMI
ROYAL MILITARY COLLEGE OF CANADA, CANADA

ABSTRACT

The paper reports results of numerical simulation of reinforced propped panel walls subjected to base shaking. The paper extends the results of earlier simulation work reported by the writers. In the current study the effects of wall height, reinforcement stiffness and spacing on the dynamic response of model walls are reported. The simulated reinforced wall structures were 3, 6 and 9 m in height and seated on a rigid foundation. The facing panels were pinned at the toe. A variable-amplitude harmonic motion with the frequency of 3 Hz and a peak horizontal acceleration of 0.2 g was applied at the foundation. The two-dimensional, explicit dynamic finite difference program Fast Lagrangian Analysis of Continua (FLAC) was used to carry out the numerical experiments. Numerical simulations of the type reported here hold promise to verify or modify current pseudostatic methods of seismic analysis and design of reinforced soil walls.

INTRODUCTION

In North America and Japan, geosynthetic and metal strip reinforced soil walls in earthquake areas are routinely designed using limit-equilibrium pseudostatic methods. In the United States, pseudostatic design methods are limited to sites with peak horizontal ground acceleration (PGA) $\leq 0.29g$, where g is the acceleration due to gravity (AASHTO 1996; FHWA 1996). A disadvantage of pseudostatic seismic design methods is that they are dependent on a single characteristic of ground motion (peak ground acceleration). These methods cannot capture wall response effects due to duration of seismic loading, frequency content, acceleration amplification, foundation condition, facing type, and stiffness of the reinforcement amongst many other factors. In addition, current pseudostatic seismic design methods in the USA are based on the results of limited experimental and numerical simulation work that was focused on reinforced soil walls constructed with relatively stiff steel strip reinforcement (Bathurst and Alfaro 1997). The results of numerical simulation work of the type reported in this paper are useful to guide the development of seismic design methods that are applicable to a range of reinforcement products, including geosynthetics, and to identify the influence of a wide range of factors on seismic response of reinforced soil retaining walls.

PREVIOUS RELATED WORK

Bathurst and Hatami (1998a,b) have reported the results of numerical simulations carried out to investigate the influence of base shaking on simulated reinforced soil retaining walls. The numerical simulations were carried out using the two-dimensional, explicit dynamic finite difference program Fast Lagrangian Analysis

of Continua (FLAC) (Itasca 1995). The simulation runs were restricted to a single height of wall (H = 6m), a single reinforcement layout (6 layers at a vertical spacing of S_v =1.0m) and a rigid foundation. The influence of reinforcement stiffness was investigated by carrying out simulations with a reinforcement stiffness of J = 500 to 69000kN/m. The wall facings were simulated as single reinforced concrete panels that are externally supported (propped) during construction and released prior to base shaking. Simulations were carried out for cases with a fixed toe and sliding toe condition. Horizontal base shaking was simulated by applying a variable-amplitude harmonic motion with the following characteristics: PGA = 0.2g; frequency f = 3Hz that is close to the fundamental frequency of the reference structure and; a duration of 6 seconds. The following principal conclusions were reported in the papers by Bathurst and Hatami (1998a,b).

- Wall displacements and reinforcement loads accumulated during base shaking. The amplitudes of wall deformation and reinforcement load during base shaking were small compared to permanent values calculated at the end of the input record. Similar qualitative responses were calculated when the first 6 seconds of the El Centro earthquake accelerogram scaled to 0.2g were applied to the structure.
- The magnitudes of total wall displacement at the wall crest and relative wall displacement with respect to the wall toe at the end of base excitation were less for a reinforced wall that was free to slide at the base than for a wall that could only rotate about the toe.
- The magnitude of permanent wall displacement diminished with increasing reinforcement stiffness and increasing reinforcement length. However, for models subjected to the reference harmonic base input motion at 3Hz, the greatest influence on the magnitude of wall displacement was the foundation condition (i.e., whether the wall facing panel was free to slide or was constrained to only rotate at the toe).
- The reference harmonic base input record resulted in additional tensile loads being generated in reinforcement layers that were significantly larger than values resulting from static loading alone. The magnitude of additional dynamic-induced loads in reinforcement layers was observed to increase with increasing stiffness of the reinforcement.
- The single most important influence on the magnitude of dynamic response of the simulated reinforced soil structures was the base input accelerogram. In particular, the relationship between fundamental frequency of the simulated structure and predominant frequency of the base input record was judged to have a major influence on structure response.

OBJECTIVES OF THE CURRENT STUDY

The current paper extends the previous work by the writers by investigating the influence of wall height, a wider range of reinforcement stiffness values and the influence of reinforcement density (i.e., spacing) on the response of reinforced propped panel walls (pinned toe condition) to base shaking. The current study allows the general observations reported above to be re-examined based on a wider range of parametric analyses.

NUMERICAL MODELS

Numerical Grid and Problem Geometry An example numerical grid used in the current study is shown in Figure 1. Simulated wall heights were H = 3, 6 and 9m (Table 1). The wall facing was modelled as a stiff continuous panel connected to uniformly spaced reinforcement layers at vertical spacings S_v = 0.5 and 1.0m. The height of the walls and the number of reinforcement layers are typical of actual structures in the field. The ratio of the reinforcement length to the height of the wall models was L/H = 0.7 which is a typical

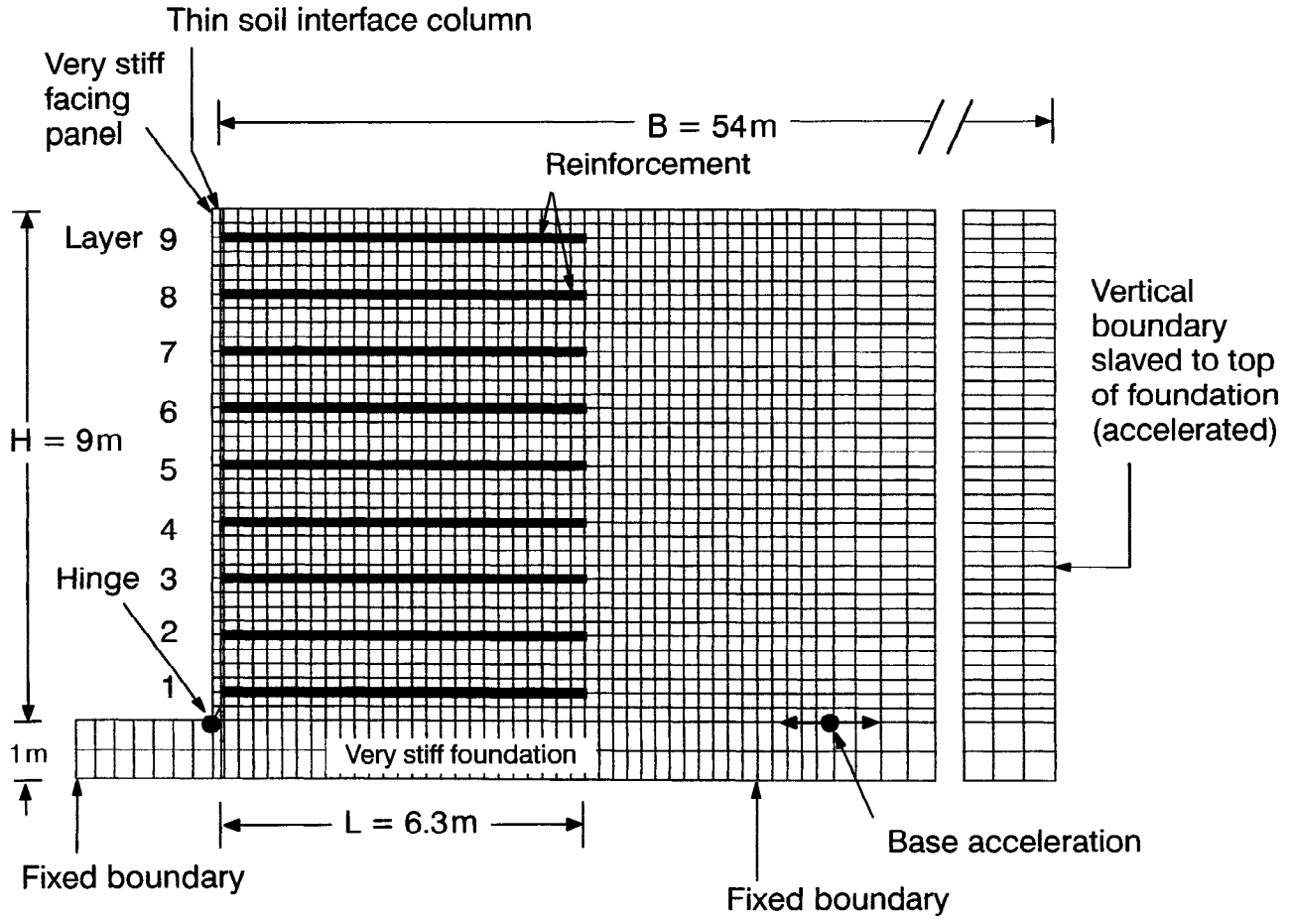

Figure 1. Example numerical grid for reinforced soil wall.

minimum reinforcement ratio for static design of reinforced soil walls (e.g., FHWA 1996). The wall and soil regions were connected directly to a foundation base comprising a 1 m-thick layer of very stiff material. The base of each facing panel was pinned (i.e., the toe of the wall was slaved to the foundation but was free to rotate). The width of the backfill, B, was extended to a large distance beyond the back of the facing panel so that the truncated boundary remained well beyond the wedge of failed soil that was observed to develop through and behind the reinforced soil zone during base shaking.

Model Properties The wall facing was modeled as a continuous concrete panel with a thickness of 0.14 m. The bulk modulus, shear modulus and Poisson's ratio values of the panel material were K_w = 11,430 MPa, G_w = 10,430 MPa, and μ_w = 0.15, respectively. The soil was modeled as a purely frictional, elastic-plastic material with a Mohr-Coulomb failure criterion and nonassociated flow rule. The friction angle of the soil was $\phi = 35°$, dilatancy angle $\psi = 6°$, and unit weight $\gamma = 20\,kN/m^3$. The soil material was assigned constant values of bulk modulus K_s = 27.5 MPa and shear modulus G_s = 12.7 MPa. The foundation zone was assigned the same material properties as the concrete facing panel.

The wall-soil interface was modeled using a thin (0.05 m-thick) soil column directly behind the facing panel. A no-slip boundary was used between the thin soil column and the facing panel. The friction angle and the dilatancy angle of the interface soil column between the reinforced soil zone and the panel wall were set to $\phi_i = 20°$ and $\psi_i = 0$, respectively. The remaining soil properties of the interface soil column were the same as the properties of the backfill soil.

The reinforcement layers were modeled using linear, elastic-plastic cable elements with negligible compressive strength and an equivalent cross-sectional area of $0.002\,m^2$. The tensile yield strength of the reinforcement in all cases was kept constant at $T_y = 200\,kN/m$, which is well above the magnitude of the maximum reinforcement load recorded in the simulations. Consequently, reinforcement rupture was not a possible failure mechanism in this study. In the parametric analyses, the equivalent linear elastic stiffness value for the cables was kept constant at J = 100, 500, 3000 and 69000 kN/m (Table 1). The stiffness values over the range J = 100 to 3000 kN/m are typical values for the initial index stiffness of (extensible) geogrid products from constant rate of displacement tensile tests. This range of stiffness values also captures the magnitude of the initial stiffness value of a typical woven polyester geogrid and a typical high density polyethylene (HDPE) geogrid under cyclic loading at a frequency of 3 Hz (Bathurst and Cai 1994). A stiffness value of J = 69000 kN/m corresponds to the stiffness of steel strip reinforcement. The interface between the reinforcement (cable elements) and the soil was modeled as a grout material of negligible thickness and an interface friction angle $\delta_g = 35°$. The bond stiffness and bond strength of the grout were taken as $k_b = 2 \times 10^6\,MN/m/m$ and $s_b = 1 \times 10^3\,kN/m$, respectively. To simplify constitutive models and numerical modeling results, the interface and grout properties were selected to simulate a perfect bond between the soil and reinforcement layers. Hence, yielding of the interface was restricted to the adjacent (elastic-plastic) soil zone (i.e., no strain softening). The end of each cable element (reinforcement) was connected to a single grid point at the back surface of the continuous panel region to simulate a fixed connection in the field.

Table 1. Parametric analyses values.

Wall height H (m)	Model width B (m)	Reinforcement spacing S_v (m)	Reinforcement stiffness J (kN/m)	Reinforcement stiffness density $\Omega = J/S_v$ (kN/m/m)
3	30	0.5, 1.0	100, 500, 3000, 69000	100, 200, 500, 1000, 3000, 6000, 69000, 138000
6	42	0.5, 1.0	100, 500, 3000, 69000	100*, 200, 500, 1000, 3000, 6000, 69000, 138000
9	54	0.5, 1.0	100, 500, 3000, 69000	100*, 200, 500, 1000, 3000, 6000, 69000, 138000

* excessive outward deflection at end of construction.

Construction The backfill soil and the reinforcement were placed in layers, while the continuous panel was braced horizontally using rigid external supports. The panel supports were then released in sequence from the top of the structure.

Base Shaking After static equilibrium was achieved, the full width of the foundation was subjected to the variable-amplitude harmonic ground motion record illustrated in Figure 2. This acceleration record was applied horizontally to all nodes at the bottom and the right-hand side (truncated) boundary of the backfill soil zone at equal time intervals of $\Delta t = 0.05$ s. The resulting peak acceleration amplitude at the foundation level was 0.2 g. The applied acceleration at the right-hand side boundary was based on the assumption of a uniform distribution of horizontal acceleration over the depth of the backfill away from the facing panel. The frequency of the base excitation was f = 3 Hz and was selected to represent a typical predominant frequency of medium- to high-frequency content earthquakes. The combination of problem geometry and magnitude of linear elastic material properties influences the fundamental (critical) frequency of the simulated wall structures (Bathurst and Hatami 1998b). The fundamental frequency of each numerical model can be accurately estimated from the theory proposed by Wu and Finn (1996) that considers a linear elastic medium

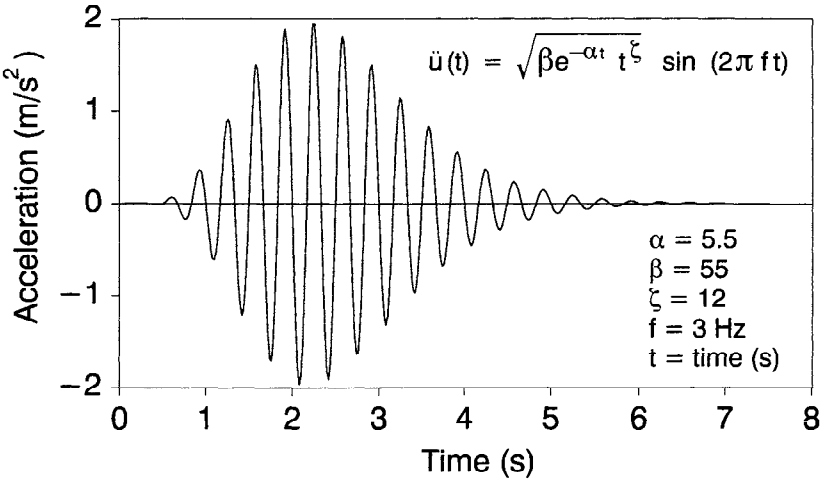

Figure 2. Base acceleration history.

of finite width and height. Based on this theory, the predominant frequency, f_H , of each wall model was calculated to be: $f_3 = 6.67$Hz, $f_6 = 3.38$Hz and $f_9 = 2.28$Hz, where the subscript denotes the height of the wall model in meters. Hence, the influence of input acceleration frequency on structure response can be investigated by simulating wall models with different heights. The frequency of input acceleration is below the fundamental frequency of models with height H = 3m, close to the fundamental frequency of models with height H = 6m and, above the fundamental frequency of models with H = 9m. A damping ratio of ξ = 5% was chosen for both the soil and facing panel regions in the parametric analyses reported in the current study. The influence of type of truncated boundary, width of numerical model, magnitude of damping ratio and base input ground motion record on numerical results using program FLAC has been described in the paper by Bathurst and Hatami (1998b).

RESULTS OF BASE SHAKING

Displacements Example horizontal displacement histories at the top of the wall facing due to base excitation are presented in Figure 3. The datum for the calculated maximum horizontal wall displacement, Δx_{top} , is taken at the end of construction following prop release. The displacement histories show that the permanent outward displacement of the wall increases monotonically with time during application of the input acceleration. The amplitudes of motion are small compared to the magnitude of the permanent outward displacement at the end of base shaking. Similar qualitative trends have been reported in the literature from the results of reduced-scale model reinforced wall shaking table tests (Matsuo et al. 1998, Koseki et al. 1998).

The largest permanent displacements and largest vibration amplitudes for walls with the same reinforcement stiffness and spacing occur for walls with height H = 6m. This trend is attributable to the base excitation record which is close to the fundamental frequency of the 6m-high wall structures. The data also show that as the stiffness of the reinforcement increases, for a given wall height, the magnitude of permanent deformation decreases.

Normalized facing panel displacement profiles predicted at the end of base shaking are shown in Figure 4 for the range of parameter values summarized in Table 1. The datum for panel displacements is taken as the end of construction (i.e., displacements do not include values from initial static loading). Simulation results for walls with height H = 6 or 9m, and very low values of reinforcement stiffness density $\Omega = J/S_v = 100$kN/m/m are not reported in the figure since these structures developed excessive outward wall deflections at end of construction. The plotted data show that total panel displacements diminish with increasing rein-

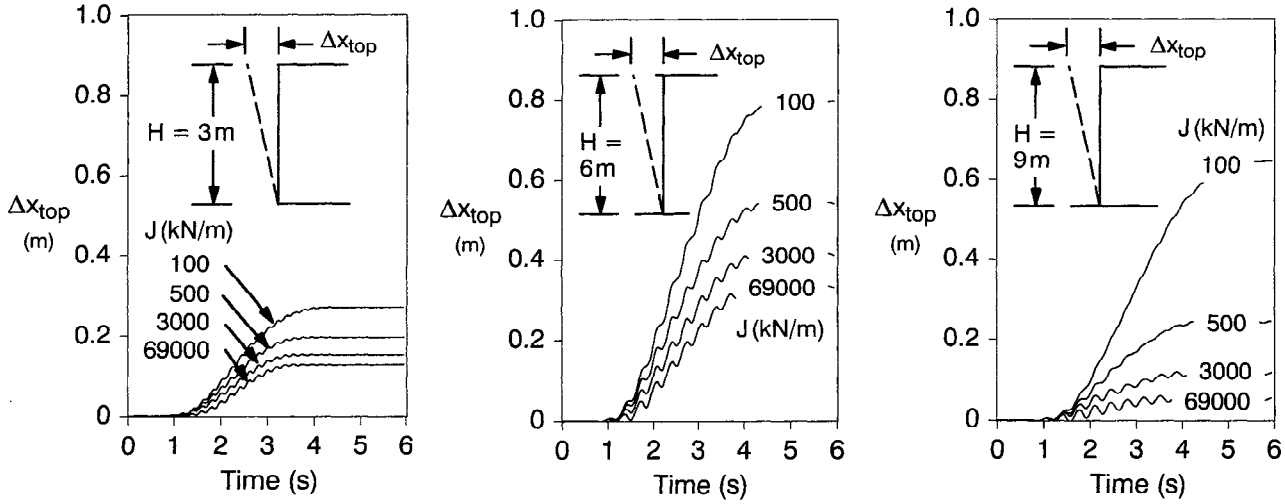

a) H = 3m b) H = 6m c) H = 9m

Figure 3. History of horizontal displacement at top of wall, Δx_{top} , for different reinforcement stiffness values, J, and wall height H. Note: S_v = 1.0m.

forcement stiffness for all three wall height cases. Not unexpectedly, for a given reinforcement stiffness, there is less total wall displacement for S_v = 0.5 as compared to configurations with a lower number of reinforcement layers (i.e., S_v = 1). Reductions in wall displacements with increasing reinforcement stiffness and decreasing spacing have also been reported by Koga and Washida (1992) from shaking table tests.

The results of Figure 4 are combined and re-plotted in Figure 5 as a function of reinforcement stiffness factor, $\Lambda = J/K_a\gamma HS_v$, introduced by Rowe and Ho (1998) for statically loaded walls. Parameter K_a is the coefficient of (static) active earth pressure calculated according to Rankine theory. Similar to numerical simulation results reported by Rowe and Ho using the finite element method, the curve for all data corresponding to the end of construction condition can be seen to vary smoothly with changes in Λ . These results confirm that Λ is a useful parameter to illustrate the influence of a large number of model parameters on wall dis-

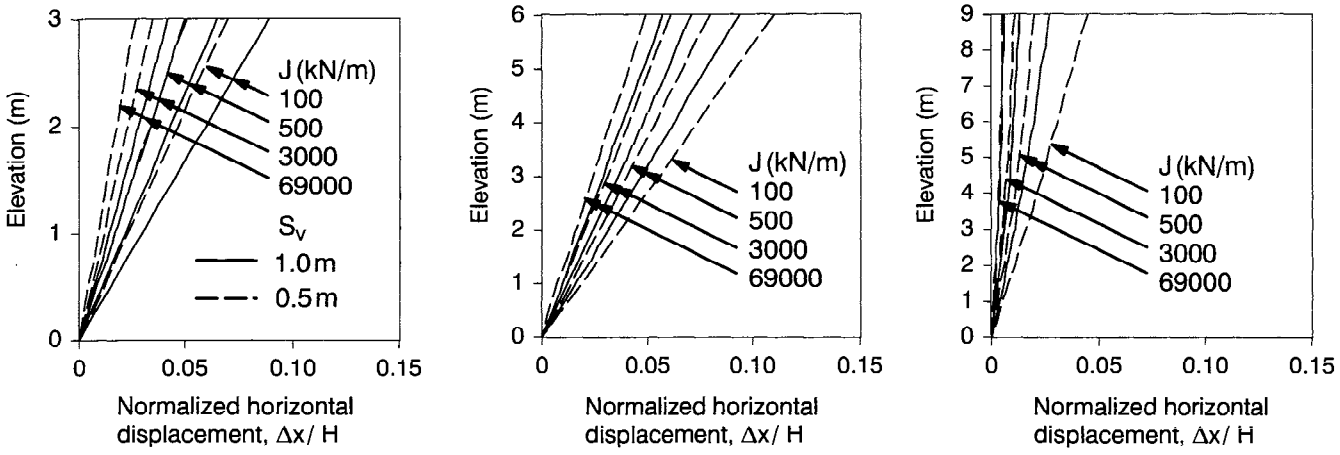

a) H = 3m b) H = 6m c) H = 9m

Figure 4. Normalized facing panel displacements at end of base shaking for walls with different reinforcement stiffness, J, and spacing S_v .

placements under static loading conditions. After base shaking, however, the dynamic response of the model walls is more complicated and the reinforcement stiffness factor $\Lambda = J/K_a\gamma HS_v$ (or another similar dimensionless quantity) is not a unique parameter with the exception of models with H = 9m. The data in Figure 5 shows that for walls with H = 3 and 6m, the magnitude of reinforcement spacing, S_v, does influence wall deformation. For walls constructed to a height of 9m, the frequency of the selected input ground motion is greater than the fundamental frequency of the structure and relatively low magnitudes of normalized outward wall crest movements were observed. This may explain why there was no significant influence of reinforcement spacing on wall deformations in these simulation runs.

The largest normalized wall displacements plotted in Figure 5 after base shaking occurred for the wall with H = 6m illustrating again that the predominant frequency of the base input acceleration in relation to the fundamental frequency of the structure may have a greater influence on seismic wall response than the height of the structure, reinforcement spacing and stiffness. Nevertheless, the general trend of decreasing wall deformations with increasing reinforcement stiffness factor for the same wall height and reinforcement spacing is preserved in the results of all simulation runs.

Reinforcement Loads Example cross sections showing the true-scale deformation of the reinforced zone after base shaking are presented in Figure 6. The cross sections are shown for two wall heights with reinforcement stiffness values of J = 100 and 3000kN/m and vertical spacing S_v = 1.0m. Superimposed on the figure are bar graphs of reinforcement loads at the same point in time. In all simulations, reinforcement loads were greatest at the connections after base shaking. This trend can be attributed to the progressive downward movement of the reinforced soil zone relative to the continuous wall panel at end of construction and during base excitation. This pattern of reinforcement load is the result of the pinned reinforcement-wall connection detail adopted in the models. Peak reinforcement loads at the connections have been observed in static load physical experiments with propped panel walls (Bathurst and Benjamin 1990, Andrawes and Yogarajah 1994) and in a field instrumented wall with a pinned full-height concrete facing panel (Bathurst 1991). In-

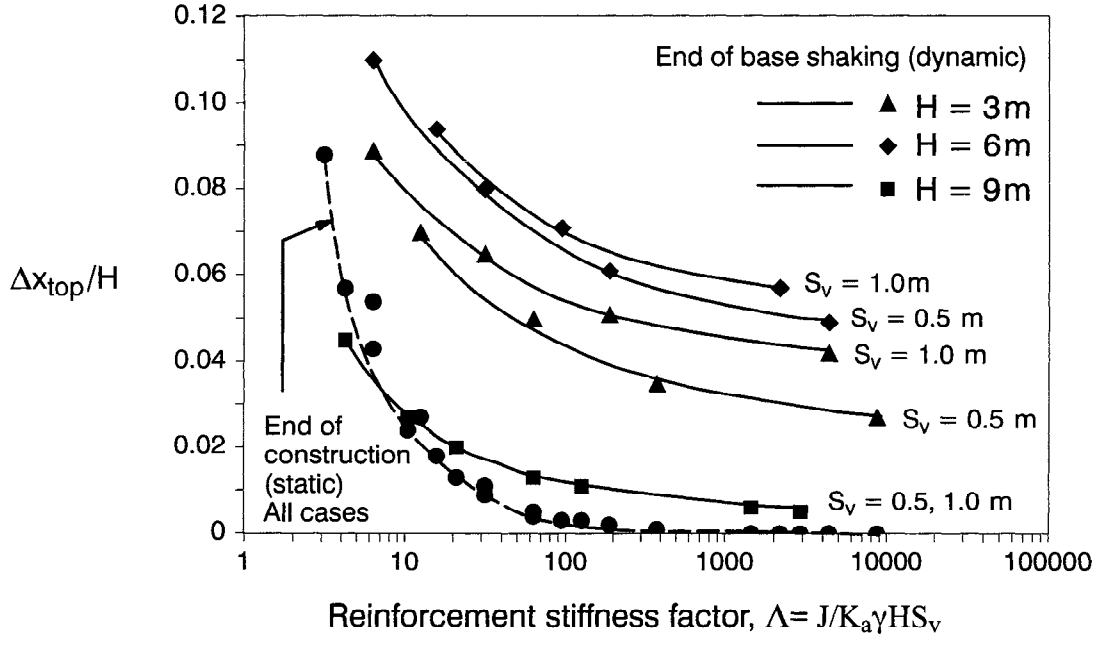

Figure 5. Influence of reinforcement stiffness factor, Λ, on normalized wall displacement measured at wall crest, $\Delta x_{top}/H$, at the end of construction and after base shaking.

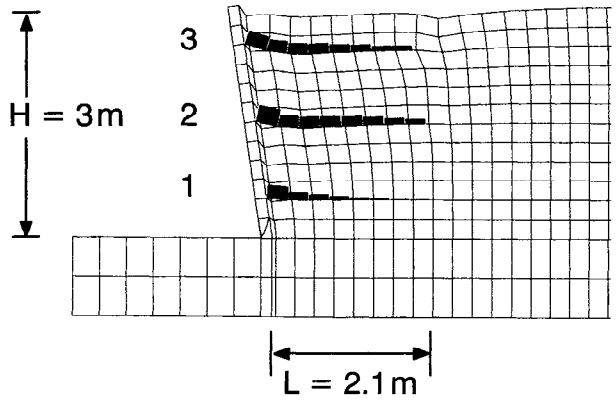

Note: Maximum reinforcement load = 13.4kN/m

a) H = 3m, J =100kN/m, S_v = 1.0m

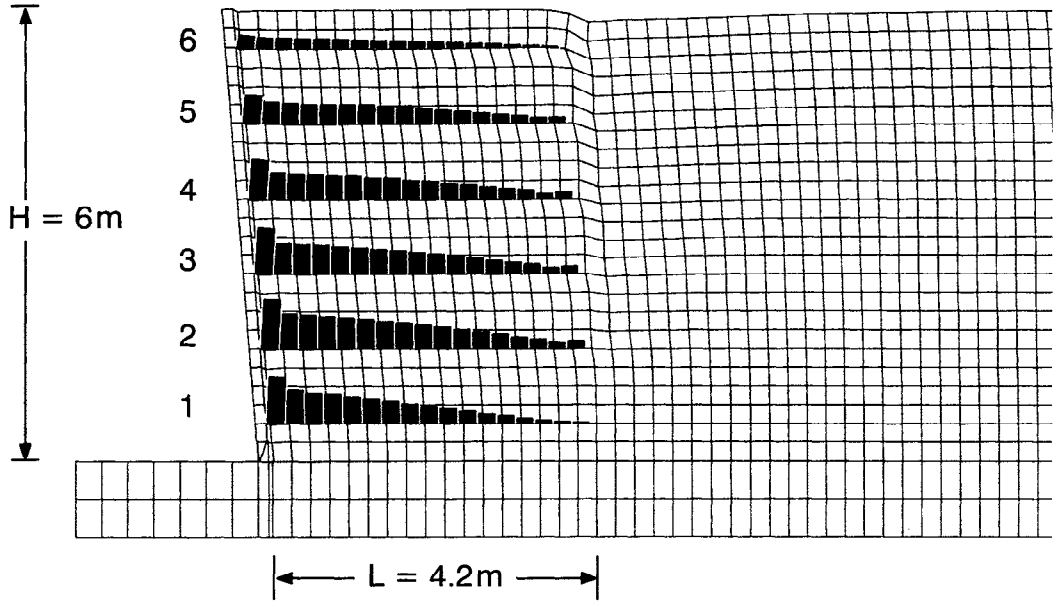

Note: Maximum reinforcement load = 68.4kN/m

b) H = 6m, J =3000kN/m, S_v = 1.0m

Figure 6. Example wall deflections and reinforcement loads at end of base shaking.

creases in the magnitude of reinforcement load toward the front of walls with fixed connections to hard facings have been noted by Murata et al. (1994), Matsuo et al. (1998) and Koseki et al. (1998) from shaking table tests of reduced-scale reinforced wall models.

Examples of axial load histories in the reinforcement layers at the connections are shown in Figure 7 for simulation runs with H = 3, 6 and 9m and J = 100, 3000 and 69000kN/m. Connection loads, T_c , can be seen to accumulate with time during shaking. This qualitative feature was observed in all simulation runs. The same trend has been observed in numerical simulations reported by Cai and Bathurst (1995) who used a dynamic finite element method code to simulate the response of a reinforced segmental retaining wall to actual (scaled) seismic accelerogram records. Figure 7 shows that the amplitude of reinforcement load vibration and magnitude of reinforcement load at the end of base shaking increase with increasing reinforce-

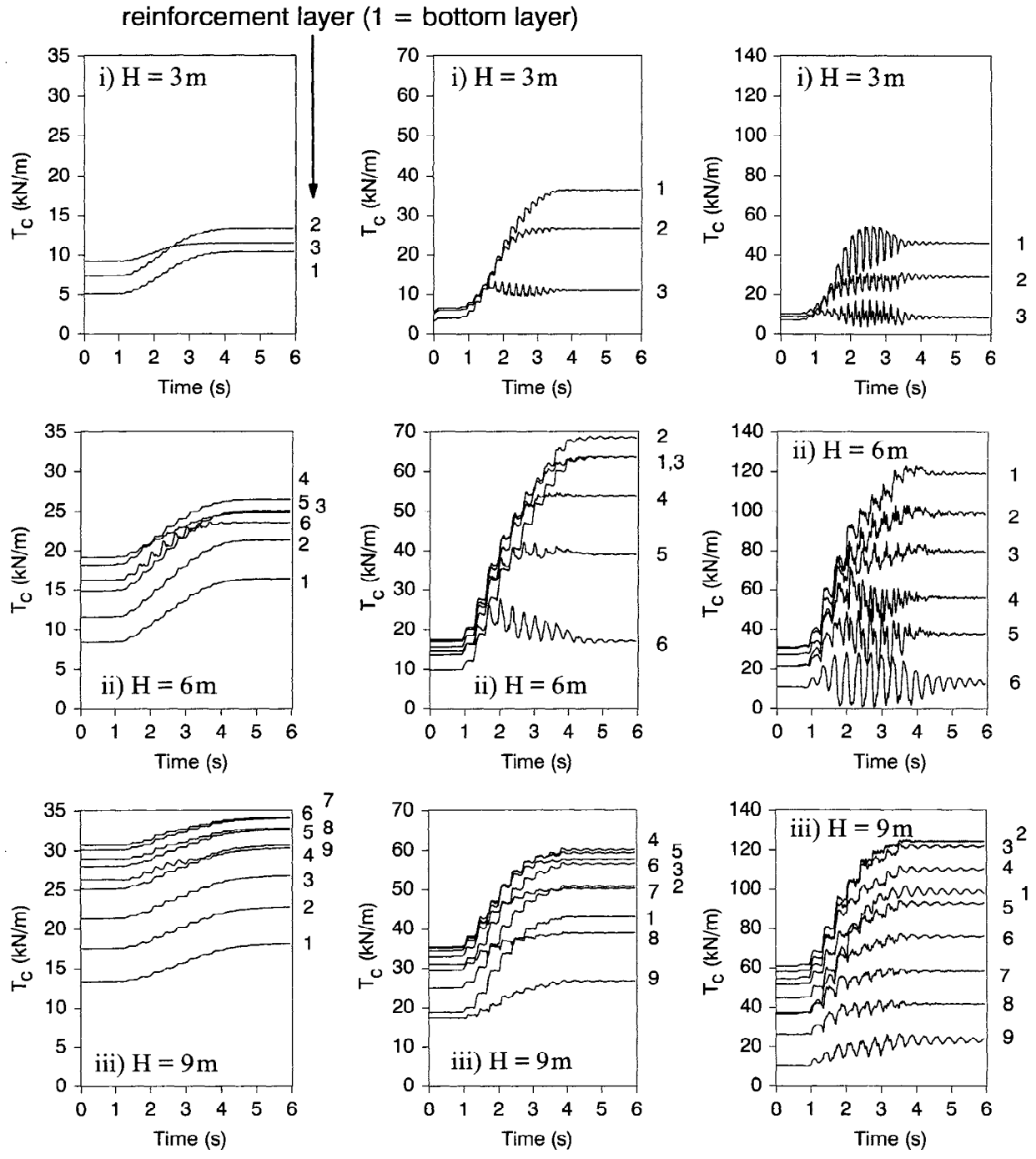

Figure 7. History of connection load, T_c , in reinforcement layers. Note: S_v =1.0m.

ment stiffness for the same wall height. In an actual wall, cumulative tensile loads in a reinforcement layer after base shaking would be expected to diminish with time (due to visco-elastic stress relaxation). This mechanism was not modelled in the current study. Taken together, the data from all plots in Figure 7 illustrate the complex interaction of the parameters investigated in the current study (i.e., there is no systematic

trend in the pattern of load-time response or rank order of reinforcement load level for walls constructed with the same reinforcement stiffness).

The distributions and magnitudes of the maximum recorded load, $T_{i\,max}$, in each reinforcement layer, i, at the end of construction (static loading) and during base shaking (dynamic loading) are plotted in Figure 8. Each maximum load value corresponds to the maximum tensile load recorded along the entire length of that layer. It should be noted that maximum tensile loads in reinforcement layers during base shaking are not necessarily time coincident (e.g., see Figure 7c).

The data in Figure 8 show that at end of construction (static) the differences in the shape and magnitude of reinforcement loads in the curves become more pronounced with increasing reinforcement stiffness and wall height. However, in comparison with the same curves representing response to base shaking, it can be argued that the effect of reinforcement stiffness on load distributions for a given wall height is not significant for values of J = 100, 500, 3000kN/m. The trends in the reinforcement load curves at end of construction are qualitatively similar to those reported by Rowe and Ho (1997) who investigated the influence of reinforcement stiffness on the distribution and magnitude of reinforcement loads in numerical simulations of similar propped panel wall models under static conditions.

Also shown in Figure 8 are the theoretical values for the static load in each reinforcement layer using limit-equilibrium methods based on Rankine ($K_a = f(\phi)$) and Coulomb ($K_a = f(\phi, \phi_i)$) earth pressure theories, and a tributary area approach to distribute reinforcement loads. The linear distribution values from theory contain the range of predicted reinforcement loads but do not capture the general trend for geosynthetic stiffness range. The limit-equilibrium solutions under-predict the reinforcement loads close to the top of the wall and over-predict the magnitude of loads toward the base of the wall. The effect of the pinned toe in combination with increasing reinforcement stiffness can also be identified in the figure. As reinforcement stiffness increases, less load is carried by the base of the wall and the distribution of reinforcement loads becomes less uniform with depth (i.e., closer to a triangular distribution as predicted by Rankine/Coulomb theory). These qualitative observations are also consistent with the results reported by Rowe and Ho (1997).

The solid lines in Figure 8 correspond to the maximum reinforcement load recorded in each layer during base shaking. In all cases, the reinforcement loads were larger during dynamic loading than for the end-of-construction (static) condition. Under dynamic loading, the maximum reinforcement loads increased with reinforcement stiffness for all cases.

The differences in the relative distributions of reinforcement load for static and dynamic cases can be quantified by calculating the reinforcement load resultant above the toe of the wall. The variation in elevation of the reinforcement load resultant with reinforcement stiffness is summarized in Figure 9. In general, for both static and dynamic loading conditions, the resultant reinforcement load elevation decreases as the reinforcement stiffness value increases. For static load conditions and a given reinforcement stiffness, the normalized elevation of the load resultant, m_s, decreases with increasing wall height. Hence, the lowest normalized elevations are recorded for the highest walls (H = 9m) and the stiffest reinforcement (J = 69000kN/m). An important implication of the trend in the data in Figure 9a to limit-equilibrium based design of walls under static loading is that the assumption of a triangular load distribution may be most applicable for very stiff reinforcement systems (i.e., steel strip reinforced walls) and may not be applicable for extensible reinforcement systems (i.e., geosynthetic reinforced soil walls).

The curves in Figure 9b show that the normalized elevation of the load resultant during base shaking is always lower than the corresponding static load case. For dynamic load conditions and a given reinforcement stiffness, the normalized elevation of the load resultant, m_d, increases with increasing wall height for extensible reinforcement systems (opposite trend to static loading case). It should be noted that the value of m_d for the dynamic case is based on total reinforcement loads recorded along each reinforcement layer during

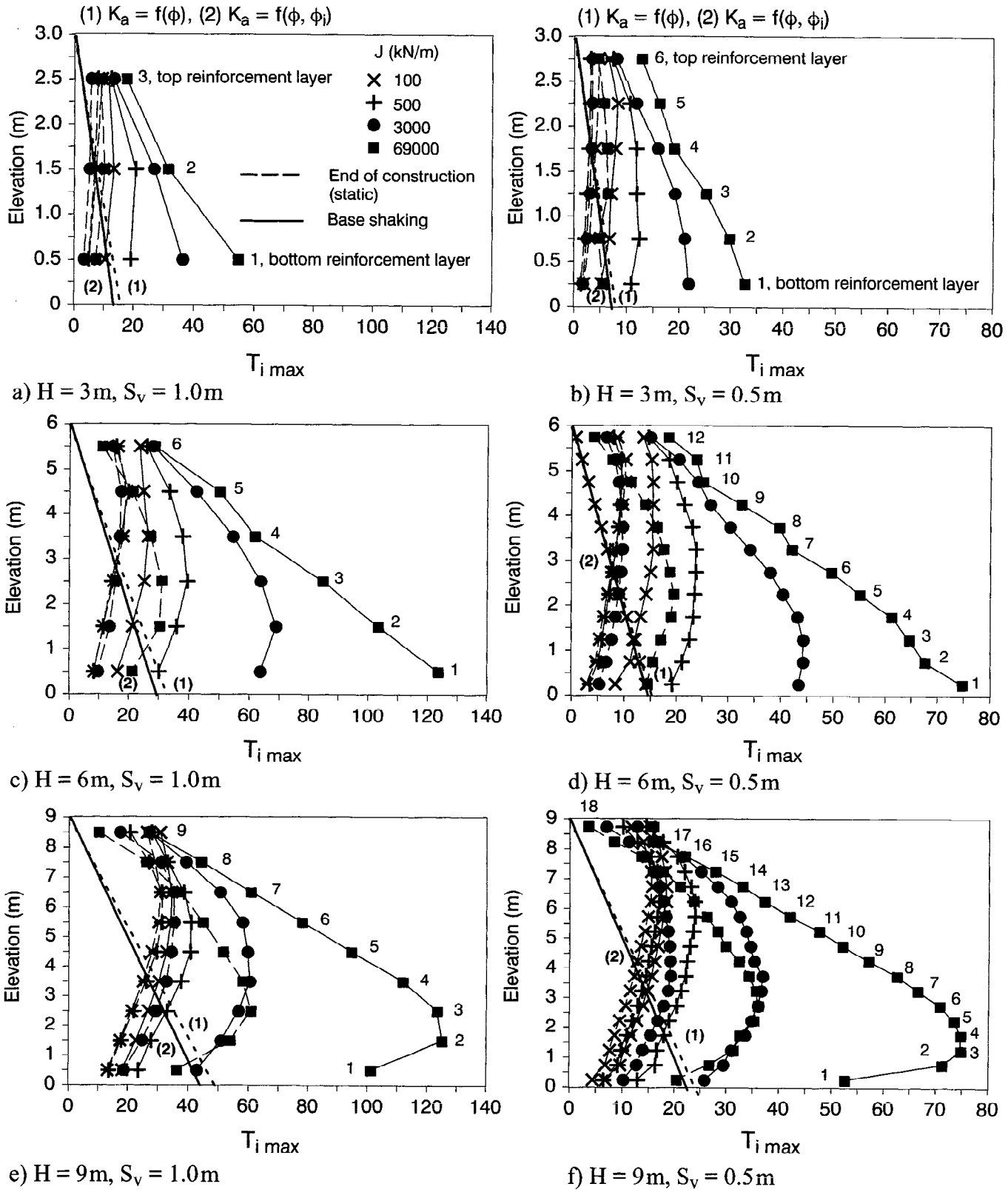

Figure 8. Influence of reinforcement stiffness, J, and spacing, S_v , on reinforcement loads at end of construction (static) and during base shaking (dynamic).

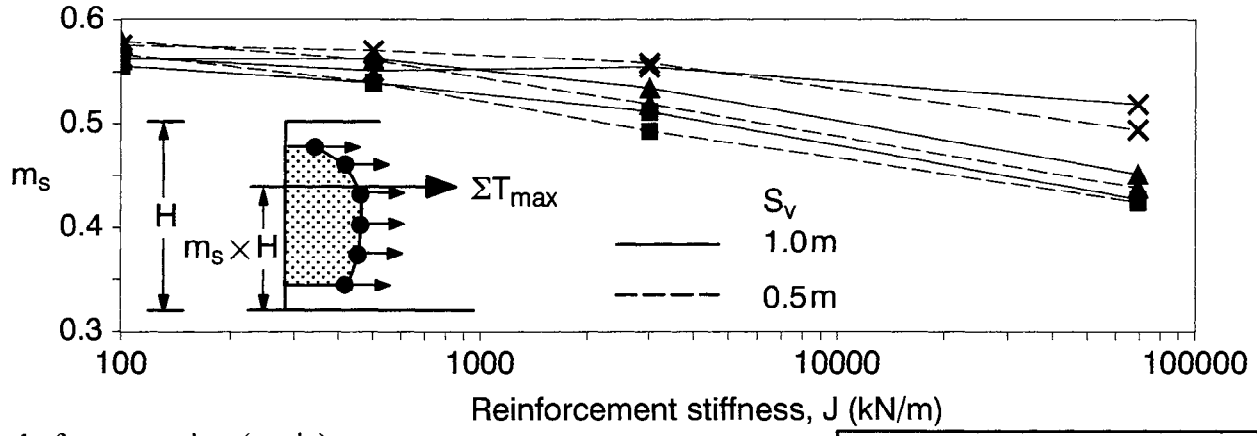

a) End of construction (static)

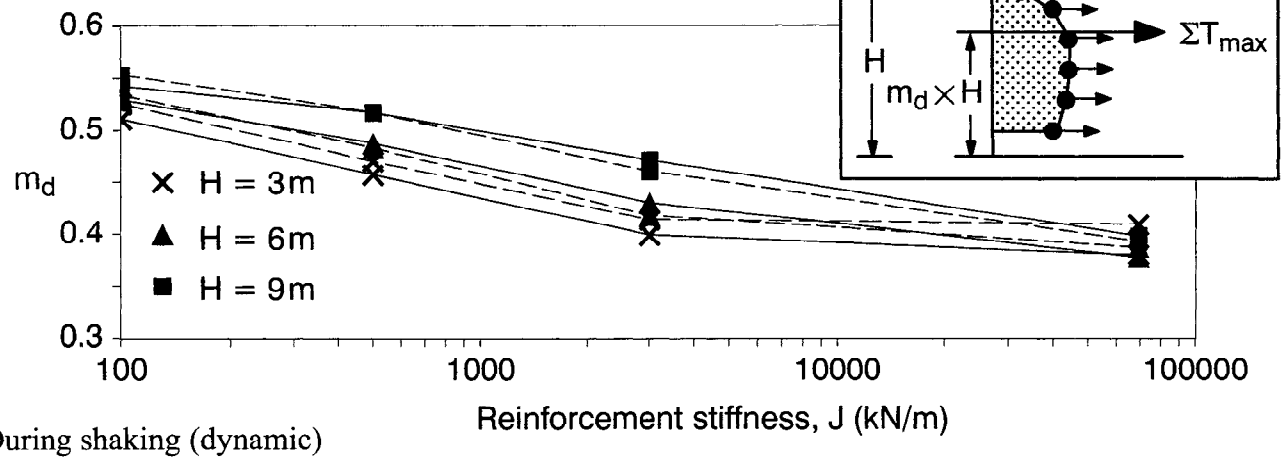

b) During shaking (dynamic)

Figure 9. Influence of reinforcement stiffness, J, and spacing, S_v , on location of reinforcement load resultant.

base shaking and that these peak loads are not necessarily concurrent. The numerical results discussed here have potential implications to conventional limit-equilibrium seismic design of reinforced soil walls with propped panel wall facings. AASHTO/FHWA (1996) guidelines recommend that a trapezoidal distribution be assumed for the total dynamic pressure distribution in reinforced retaining wall design. This distribution is used to partition apparent dynamic earth pressures to individual reinforcement layers using a tributary area approach. The method limits m_d to $0.33 \leq m_d \leq 0.6$. The data in Figure 9b falls within this range but illustrates how the selection of m_d may be refined to consider the effect of wall height and reinforcement stiffness.

IMPLICATIONS TO DESIGN OF REINFORCED SOIL RETAINING WALLS

The results of the current study illustrate that large dynamic-induced reinforcement loads may be developed behind reinforced soil retaining walls. However, it is important to note that the choice of input record has a significant influence on the magnitude of reinforcement loads and wall displacements. The use of an input ground motion with a single frequency close to the fundamental frequency of some retaining wall models is largely responsible for the large loads and displacements predicted from numerical simulations in the current study. In a previous study (Bathurst and Hatami 1998b), it was observed that a true earthquake record scaled to a peak horizontal ground acceleration of 0.2g gave similar qualitative responses for model walls

subjected to the harmonic record in Figure 2 but with lower magnitude reinforcement loads and displacements. Hence, the focus of the results of the current study is on the relative distribution of reinforcement loads and wall displacements rather than their magnitude. It should also be noted that the stiffness and depth of the foundation can be expected to have a major influence on the seismic response of reinforced soil wall models. The results of the current study may not apply to the seismic response of reinforced soil walls built on less rigid foundation soils. The influence of foundation depth and stiffness on dynamic response of simulated wall structures is currently under investigation by the writers.

The results of numerical simulations reported here have important implications to design of reinforced soil walls. The choice of distribution pattern will control the assignment of active forces to reinforcement layers in pseudostatic seismic design methods that use the tributary area approach. The current study shows that the stiffness of the reinforcement has a significant effect on the relative distribution of reinforcement loads during base shaking. For very stiff reinforcement (e.g., steel strip reinforcement) a triangular distribution of load may be more accurate, while for less stiff (extensible) geosynthetic reinforcement products, a uniform distribution may be applicable. Current pseudostatic methods of design do not distinguish between reinforcement materials based on stiffness. For geosynthetic reinforced segmental retaining walls, which must be designed to resist local facing modes of failure, the selection of a representative load distribution pattern is particularly important (Bathurst and Cai 1995).

CONCLUSIONS

Program FLAC has been used to extend the range of parametric analyses reported in earlier papers by the writers. The qualitative results from this previous work on the response of reinforced soil walls to simulated seismic shaking has been confirmed using numerical models with different wall heights, reinforcement stiffness values and reinforcement spacing. Numerical simulations of the type reported here hold promise to verify or modify current pseudostatic methods of seismic analysis and design of reinforced soil walls. However, the results reported here have not been checked against the results of any physical measurements (such as shaking table tests). Nevertheless, the data is valuable to assist researchers to design physical experimental programs (1 g or centrifuge shaking table tests) that can quantify the influence of wall geometry, type and reinforcement stiffness, and characteristics of applied ground motions to the seismic response of reinforced soil wall structures.

ACKNOWLEDGMENTS

The funding for the work reported in the paper was provided by grants from the Natural Sciences and Engineering Research Council and Department of National Defence (Canada).

REFERENCES

AASHTO, (1996) "Standard Specifications for Highway Bridges", *16th Edition, American Association of State Highway and Transportation Officials*, Washington, DC, USA, 677 p.

Andrawes, K.Z. and Yogarajah, I., (1994) "Effects of Reinforcement Connections on the Behaviour of Reinforced Soil Retaining Walls", *Computer Methods and Advances in Geomechanics*, (Siriwardane and Zaman Eds.), Balkema, Rotterdam, pp. 1313-1318.

Bathurst, R.J., (1991) "Case Study of a Monitored Propped Panel Wall", *Proceedings of the International Symposium on Geosynthetic-Reinforced Soil Retaining Walls*, Denver Colorado, August 1991, pp. 159-166.

Bathurst, R.J. and Alfaro, M.C., (1997) "Design, Analysis and Performance of Geosynthetic Reinforced Walls, Slopes and Embankments", Keynote Paper, *Earth Reinforcement, Vol. 2, Proceedings of Internation-*

al Symposium on Earth Reinforcement, (Ochia, Yasufuku and Omine, Eds.), IS-Kyushu'96, Balkema, Fukuoka, Kyushu, Japan, November 1996, pp. 887-918.

Bathurst, R.J. and Benjamin, D.J., (1990) "Failure of a Geogrid-Reinforced Soil Wall", *Transportation Research Board 1288*, pp. 109-116.

Bathurst, R.J. and Cai, Z., (1994) "In-isolation Cyclic Load-Extension Behavior of Two Geogrids", *Geosynthetics International,* Vol. 1, No.1, pp. 3-17.

Bathurst, R.J. and Cai, Z., (1995) "Pseudostatic seismic analysis of geosynthetic-reinforced segmental retaining walls", *Geosynthetics International*, Vol. 2, No. 5, pp. 787-830.

Bathurst, R.J. and Hatami, K., (1998a) "Influence of Reinforcement Stiffness, Length and Base Condition on Seismic Response of Geosynthetic Reinforced Retaining Walls", *6'th International Conference on Geosynthetics,* Atlanta, GA, March 1998, Vol. 2 pp. 613-616.

Bathurst, R.J. and Hatami, K., (1998b) "Seismic Response Analysis of a Geosynthetic Reinforced Soil Retaining Wall", *Geosynthetics International*, Vol. 5, Nos. 1&2, pp. 127-166.

Cai, Z. and Bathurst, R.J., (1995) "Seismic response analysis of geosynthetic reinforced soil segmental retaining walls by finite element method", *Computers and Geotechnics*, Vol. 17, No. 4, pp. 523-546.

FHWA, (1996) "Mechanically Stabilized Earth Walls and Reinforced Soil Slopes Design and Construction Guidelines", *Federal Highway Administration (FHWA) Demonstration Project 82*, (Elias, V. and Christopher, B.R.), Washington, DC., USA, 364 p.

Itasca Consulting Group, (1995) "FLAC - Fast Lagrangian Analysis of Continua", Version 3.30, *Itasca Consulting Group, Inc.*, 708 South Third Street, Minneapolis, Minneapolis, USA.

Koga, Y. and Washida, S., (1992) "Earthquake resistant design method of geotextile reinforced embankments", *Earth Reinforcement Practice, Proceedings of International Symposium on Earth Reinforcement Practice*, IS-Kyushu'92, (Ochiai, Hayashi and Otani, Eds.), Balkema, Fukuoka, Japan, November 1992, pp. 255-259.

Koseki, J., Munaf, Y., Tatsuoka, F., Tateyama, M., Kojima, K. and Sato, T., (1998) "Shaking and Tilt Table Tests of Geosynthetic-Reinforced Soil and Conventional-Type Retaining Walls", *Geosynthetics International*, Vol. 5 Nos. 1&2, pp. 73-96.

Matsuo, O., Tsutsumi, T., Yokoyama, K. and Saito, Y., (1998) "Shaking Table Tests and Analyses of Geosynthetic-Reinforced Soil Retaining Walls", *Geosynthetics International*, Vol. 5 Nos. 1&2, pp. 97-126.

Murata, O., Tateyama, M. and Tatsuoka, F., (1994) "Shaking table tests on a large geosynthetic-reinforced soil retaining wall model", *Recent Case Histories of Permanent Geosynthetic-Reinforced Soil Walls* (Tatsuoka and Leshchinsky, Eds.), Proc. Seiken Symp., Tokyo, Japan, pp. 289-264.

Rowe, R.K. and Ho, S.K., (1997) "Continuous Panel Reinforced Soil Walls on Rigid Foundations", *Journal of Geotechnical and Geoenvironmental Engineering*, Vol. 123, No. 10, pp. 912-920.

Rowe, R.K. and Ho, S.K., (1998) "Horizontal deformation in reinforced soil walls", *Canadian Geotechnical Journal*, Vol. 35, No. 2 pp. 312-327.

Wu, G. and Finn, Liam W.D., (1996) "Seismic Pressures against Rigid Walls", *ASCE, Proceedings of sessions on Analysis and Design of Retaining Structures against Earthquakes*, Washington, D.C., November 1996, S. Prakash (Ed.), pp. 1-18.

THIRTY-YEAR PERFORMANCE EVALUATION OF A GEOTEXTILE FILTER

BARRY R. CHRISTOPHER, PH.D., P.E. – CHRISTOPHER CONSULTANTS (USA)
STEPHEN N. VALERO, P.E. – SYNTHETIC INDUSTRIES, INC. (USA)

ABSTRACT

The 79th Street Causeway Project in Miami, Florida represents one of the earliest applications of geotextiles in North America. A woven monofilament geotextile was installed as a filter beneath a rip-rap slope revetment designed to protect a bridge abutment and the causeway from erosion. Performance of this geotextile was originally examined in 1979 (Christopher, 1983). Observations made during this previous evaluation indicated that the revetment was performing well, requiring no maintenance through 10 years of service. In late 1997, the site was reevaluated to examine geotextile performance after nearly three decades of service. The recent study consisted of visual performance characterization and exhumation, recovery, and laboratory testing of a geotextile sample. Visual observations indicate that the geotextile continues to perform well (the revetment has not required maintenance since 1969). Multiple specimens from the recovered sample were subjected to Scanning Electron Microscopy (SEM) analysis and tested for physical, mechanical, hydraulic, and durability characteristics. This paper presents results of all assessments and conclusions regarding the geotextile's performance, aging characteristics, durability, and the effects of installation damage.

INTRODUCTION AND BACKGROUND

The first recorded use of synthetic fabrics as geotextiles was in Florida (USA) in the late 1950's. These applications involved placement of woven monofilament fabrics (geotextiles) beneath coastal erosion control rip-rap revetments in place of graded-granular filters. The success of these early projects spurred development of the modern geosynthetics industry. Since then, geosynthetics, have been effectively used to improve cost-effectiveness, increase safety, shorten construction periods, and comply with environmental regulations on millions of construction projects. However, 40 years represents a relatively short history with respect to civil engineering applications. Although long-term performance evaluations of geotextiles in drainage/ erosion control applications exist (e.g., Christopher, 1983; Koerner, et. al., 1994;

Mannsbart and Christopher, 1996), they are relatively few compared to those for traditional construction materials.

The focus of this paper is the 79th Street Causeway Project in Miami, Florida. In 1969, the Florida Department of Transportation (DOT) replaced a portion of the causeway with a bridge. Rip-rap protected revetments were constructed at the same time to prevent erosion around the new bridge abutment and along remaining portions of the causeway (Figure 1). Revetments of this type are common in coastal erosion protection applications. The rip-rap provides a rough surface to dissipate impacting wave energy and substantial mass to avoid displacement. However, large voids between the cobble and boulder size rip-rap allow fine foundation soil particles to be drawn out under the action of waves and seepage. If allowed to occur, this action will eventually lead to collapse and failure of the revetment. In 1969, it was standard practice to include a graded-granular filter underlayment beneath such structures to preclude the loss of fine soil particles. However, portions of the 79th Street Causeway revetment were constructed using a polypropylene, woven monofilament geotextile in lieu of the standard granular filter.

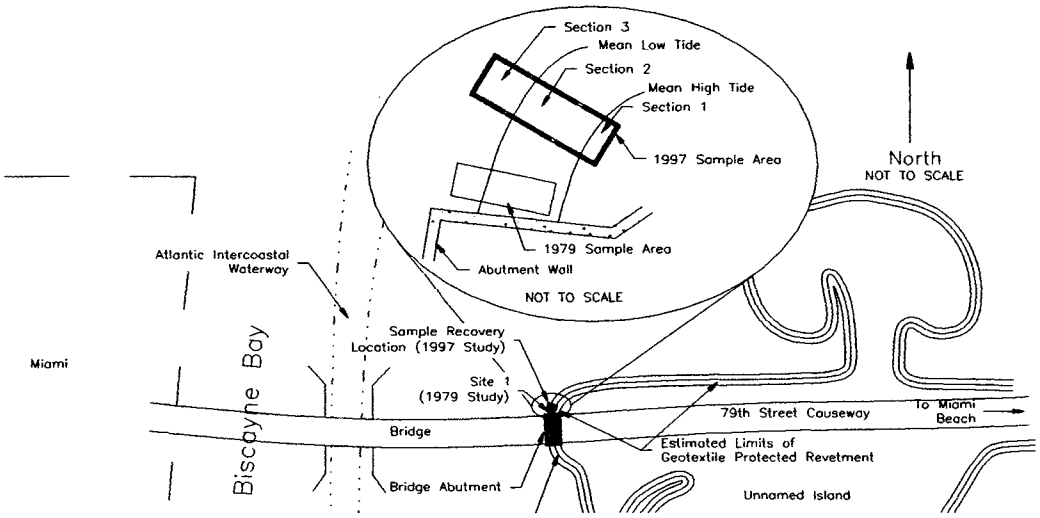

Figure 1. Field Study Site Plan (Miami, Florida)

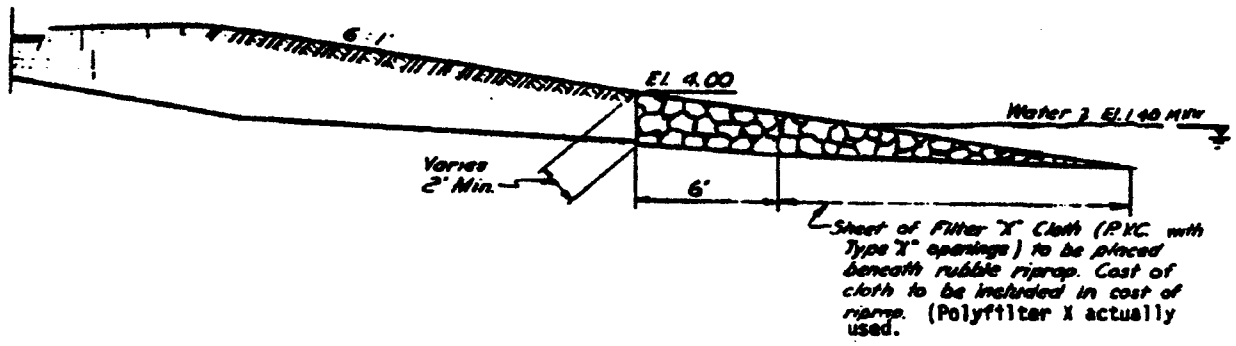

Figure 2. Proposed Design of Revetment from the Original Drawings (Christopher, 1983)

Figure 2 illustrates the original revetment design. The protected section was designed for approximately one meter of wave and tidal fluctuation. It should be noted that details regarding subgrade preparation or geotextile placement and anchorage at the head or tow of slope were not included. At that time, the importance of anchorage and construction quality control when using geosynthetics was not widely understood.

This site was originally studied in a detailed performance evaluation conducted in October 1979, approximately 10 years after installation (Christopher, 1983). The evaluation included observations of revetment and geotextile performance and laboratory analysis of geotextile and soil samples recovered from the site. Observations indicated that the structure and the geotextile were functioning as originally intended. Laboratory test results indicated that the geotextile had not suffered significant loss of strength or hydraulic capacity in the first 10 years of operation. In October 1997, the 79th Street Causeway was reevaluated to document geotextile performance after nearly three decades of service. As in the previous study, a detailed visual evaluation of the site was conducted and geotextile samples were retrieved. A description of the field and laboratory evaluations and observations concerning geotextile performance, aging, and durability are presented in the following sections.

FIELD STUDY AND OBSERVATIONS

Prior to excavation and sampling activities, visual observations regarding apparent maintenance/repair activities, erosion, tidal fluctuation, wave action, geotextile exposure, etc. were noted and documented with photographs. No significant erosion of the revetment or evidence of maintenance was observed in areas protected by a geotextile filter. In contrast, a portion of the revetment protecting the southern side of the bridge abutment (Figure 1) where no geotextile filter was used has experienced significant erosion and piping since construction. Erosion problems in this area were also recorded in the 1979 study (Christopher, 1983). It was reported that concrete had been poured against the abutment and over the adjacent exposed soil to stop erosion. It was also noted that large voids were present within and beneath this concrete mat where the foundation soil and portions of the concrete had eroded. In 1997, substantial portions of this concrete mat were observed to have broken and failed due to erosion. In addition, it appears that the non-geotextile protected site has required maintenance several times since 1979.

During the recent field study, approximately one meter of tidal fluctuation was observed. The site is continuously exposed to mild wave attack (0.2 to 0.3 meter high) and regularly subjected to commercial/recreational boat traffic (0.3 to 1.0 meter wave heights). Tidal and wave conditions appeared to be consistent with those reported in the 1979 study and the original design. However, multiple hurricanes and tropical storms have occurred in the Miami area since 1969. During these events, the revetment structure was subjected to water levels and wave attack well beyond intended design levels. Florida DOT records indicate that several unprotected areas of the causeway required maintenance to correct erosion problems after these storm events (where the geotextile protected revetments required none).

Although the geotextile protected revetments have functioned effectively, evidence of inadequate anchorage and construction quality assurance were readily noticeable. About one-half meter of geotextile material was observed protruding from the surface of the rip-rap near the slope head and along the abutment wall in several areas (Figure 3). This was most likely the result of insufficient anchorage of the geotextile's up-slope termination. In 1979, exposed geotextile was noted in the same areas. Thus, it is reasonable to assume that this material (or portions thereof) has been directly exposed to sunlight and the environment for up to 28 years. Although the edge of the exposed fabric was tattered, faded, and easily torn by hand, folded sections protected from direct sunlight were relatively pliable and not capable of being torn by hand.

A site near the north side of the bridge abutment was selected for geotextile sample recovery. The excavation site was located approximately three meters north of the bridge abutment corner. The size of the sample area was approximately 1.5 by 4.5 meters and oriented with the long dimension perpendicular to the direction of tidal fluctuation. T his area and orientation was selected to allow recovery of geotextile material subjected to varying exposure conditions and submergence. The top of the sample area encompassed the exposed fabric near the top of slope while the bottom was below mean low-tide level. This site was also selected to be in close proximity to (without overlapping) the sample area designated Site 1, in the 1979 study (Figure 1).

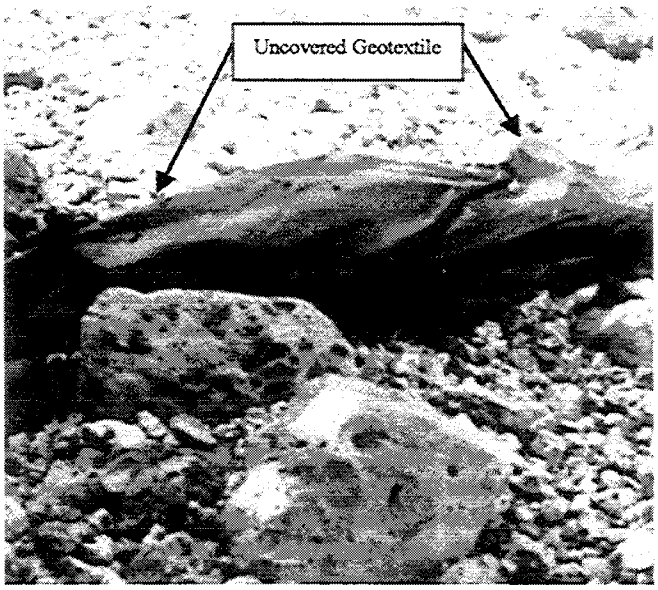

Figure 3. Uncovered Geotextile Near Top of Slope (10/97)

To exhume the geotextile for sampling, boulder size rip-rap was carefully removed with steel pry-bars. Most surface boulders had a mean diameter between 300 and 450 mm. Beneath the surface layer, a layer of 150 to 300 mm diameter rip-rap was encountered. All rip-rap at the site consisted of highly weathered, fossiliferous limestone. The rip-rap was highly angular with many sharp edges and protrusions. Directly above the geotextile, a 80 mm thick layer of coarse sand and gravel was present in most areas. However, in some cases large rip-rap boulders were in direct contact with the geotextile. It is doubtful that this thin layer of finer material was placed during construction. It is more likely that it resulted from natural sediment deposition and weathering of the rip-rap boulders. This layer also contained various sharp objects such as broken glass, remnants of steel and aluminum cans, etc. It is felt that the area removed was representative of typical site conditions and observed revetment/subgrade materials were consistent with those reported in the 1979 study. As in 1979, several pairs of heavy duty-work gloves were destroyed by sharp edged stones during exhumation activities. Following removal

of all large stones, the surface of the geotextile was carefully cleaned using plastic gardening implements, hand sweeping, and water.

Once exposed, the geotextile was photographed and marked to indicate apparent mean high- and low-tide elevation, and slope direction. In several areas, it was noted that large boulders were present in the subgrade immediately beneath the geotextile. These locations were also marked on the fabric. In most cases, small holes (10 to 50 mm in diameter) where noted directly above the protruding subgrade stones. However, the majority of the geotextile remained undamaged and intact. For sampling, the geotextile was carefully cut around the perimeter of the exhumed area and peeled away from the subgrade. Care was taken to leave at least 150 mm of clean material exposed around the perimeter for overlap with the replacement geotextile.

Observations of subgrade appearance were noted and recorded photographically (Figure 4). Sand with gravel was observed directly beneath the fabric in most areas (where subgrade boulders were not present). This material was found to progressively decrease in grain size to very fine silty sand with depth indicating that a natural "soil bridge" has developed beneath the fabric. These observations agreed with those of the 1979 study. Although this particular installation was not "designed" based on geotextile filtration principals, it is interesting to note that it meets criteria established by several common filter design and selection methods (Calhoun, 1972; Holtz, et. al., 1995; AASHTO, 1998) based on the subgrade soil gradation presented by Christopher (1983). Table 1 illustrates the properties in comparison to AASHTO default requirements for erosion control Geotextiles in Highway Applications.

Table 1. 79th Street Causeway Geotextile Properties Compared to AASHTO Requirements

Property[1]	Original Geotextile[2] - Carthage Mills POLY-Filter X®	AASHTO M 288-96 Requirements[3] – Class 2 (AASHTO, 1998)
Structure	Woven Monofilament	- -
Polymer	Polypropylene	- -
Grab Strength, N	1244	1100
Trapezoidal Tear Strength, N	267	250
Puncture Strength, N	689	400
Mullen Burst Strength, kPa	3652	2700
Permittivity, sec^{-1}	0.37	0.2
Apparent Opening Size, mm	0.212	0.25 (max)
Ultraviolet Stability, %	90	50

NOTES: [1] Minimum Average Roll Values (MARVs) according to test method current at time.
[2] As listed in Geotechnical Fabrics Report (IFAI, 1992).
[3] Woven, monofilament geotextiles – subgrade soil 15 to 50% pass 0.075 mm sieve.

Following exhumation, the geotextile sample was gently rinsed with salt water to remove loosely attached soil particles. No tears, punctures, or abrasions larger than approximately 50 mm were observed. Considering the roughness of the subgrade and angularity of overlying stones, this is quite remarkable (remember the work gloves). However, several clusters of 10 to 50 mm punctures were observed. In all cases, the clustered puncture locations corresponded to

the areas where significant subgrade boulders and protrusions were noted prior to sample removal. In addition, 15 to 20 small holes (less than 6 mm diameter) were observed per square meter of geotextile (Figure 5). Based on field observations, it is likely that the observed damage was the result of installation stress and not wear or abrasion over time.

A qualitative evaluation the geotextile's hydraulic characteristics was also made in the field. Water passed through the plane of the fabric unimpeded and light was readily observed through the section (Figure 5). Although limited particle retention was noted, the majority of the openings were clear and uniform indicating that the geotextile has not clogged after nearly 30 years of service. Significant staining was observed on portions of the geotextile which had been removed from beneath the normal low tide level. After field examination and air drying, the geotextile sample was carefully rolled and placed into a container for shipment to the laboratory. A new piece of comparable woven monofilament geotextile (manufactured at the same plant as the original geotextile) was cut and placed over the sample area. The sand, gravel and rip-rap boulders were then replaced in the appropriate order to conclude the field study.

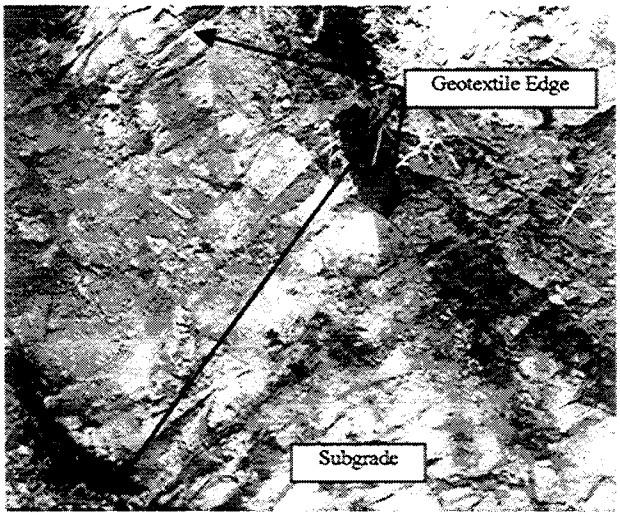

Figure 4. Subgrade After Geotextile Removal – Note Large Protrusions

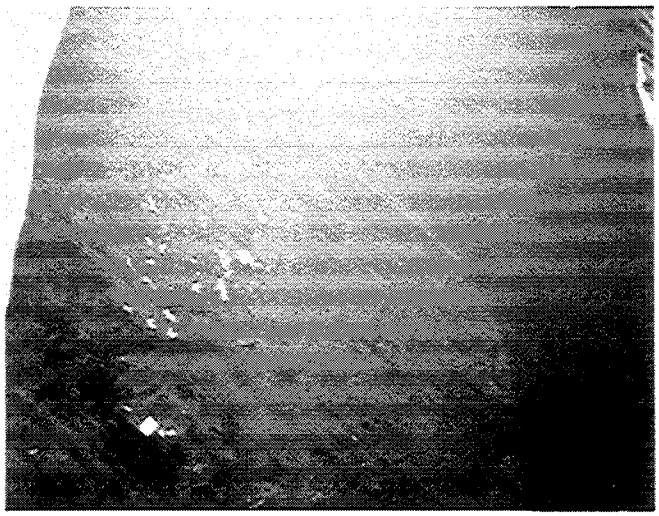

Figure 5. Exhumed Geotextile Specimen – Note Light Passage and Hole Clusters

LABORATORY EVALUATION

The laboratory program consisted of tests to evaluate durability and filtration characteristics of the exhumed geotextile. The test results on the exhumed sample could then be compared to the properties of new geotextiles at the time of installation as well as results from the 1979 study. In order to identify the influence of exposure conditions, the sample was divided into three distinct areas: (Section 1) the uncovered section that had been exposed to air, extremes in temperature and ultraviolet light over the life of the specimen; (Section 2) the section covered by soil and in the tidal region where the material would have been cyclically exposed to air and water; and (Section 3) the region below mean low-tide which was essentially under water for the entire life of the project. This also provided a basis for comparison with

laboratory results from the previous study that indicated some change in characteristics relative to position along the length of slope perpendicular to the water line. A series of laboratory tests were conducted on each of the three sections.

Perforations in the exhumed geotextile sample made it apparent that some mechanical degradation had occurred in all three sections. Therefore, a series of laboratory tests was performed to determine the extent and mechanism of this degradation. The potential degradation mechanisms were considered to be installation damage and long-term abrasion from movement of the sharp rocks. Some cyclic loading may have also occurred under wave action which may have repeatedly pulled the material against the sharp rocks. In addition, strength loss and/or embrittlement could have also occurred through polymer aging, making the material more susceptible to mechanical damage over time.

The principle aging mechanism for polypropylene is oxidation (Elias, 1996). Considering that oxidation varies with exposure to oxygen (i.e. air), different levels of oxidation were anticipated for each of the three sections (Section 1 had the highest air exposure due to the uncovered condition, Section 2 had less exposure due to soil and periodic water cover, and Section 3 had the lowest air exposure due to soil and water cover). Aging is accelerated due to heat and ultraviolet light exposure (Elias, 1996), as is the case for specimens from Section 1. Direct sunlight exposure is also known to cause rapid deterioration of geotextiles as was evident from the field observations of exposed material in Section 1. Direct exposure to sunlight also increases the temperature of black geosynthetics (Koerner et. al., 1995) To reduce the influence of exposure to direct sunlight in Section 1, test specimens were taken within the folds of the geotextile. Oxidation can be evaluated through chemical tests, however the procedures to perform such tests and interpret the results are still in a research phase and not well established. The actual strength loss due to oxidation has been attributed to the formation of circumferential cracks in the filament (Elias, 1996). These cracks can be observed in scanning electronic microscope (SEM) photos of aged polypropylene material as shown in Figure 6. The onset of these cracks would be indication of significant oxidation.

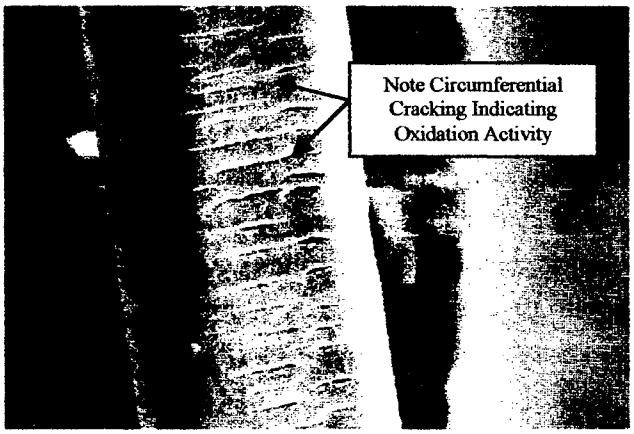

Figure 6. Example SEM Photo of Aged Geotextile (Elias, 1996)

SEM Evaluation

In order to assist in distinguishing aging from mechanical degradation, a series of scanning electronic microscope (SEM) photos were taken at various locations along the length of the sample (in representative portions of each of the three sections of the sample. The photos were taken at different magnifications with low magnifications used to provide visual signs of mechanical damage and abrasion and high magnification used to indicate signs of oxidation. In

addition, SEM photos were taken of virgin material removed from the manufacturer's brochures dating from the period the project was constructed (Minimum oxygen exposure was anticipated for the virgin sample as it had been stored between the pages of a booklet). Figure 7 presents an SEM photo of the virgin material while Figures 8 through 10 show representative SEM photos from the exhumed geotextile.

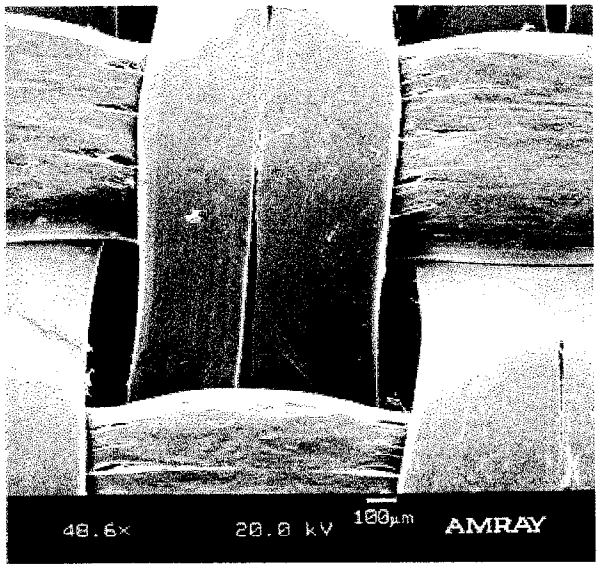

Figure 7. SEM Photo of Virgin Geotextile

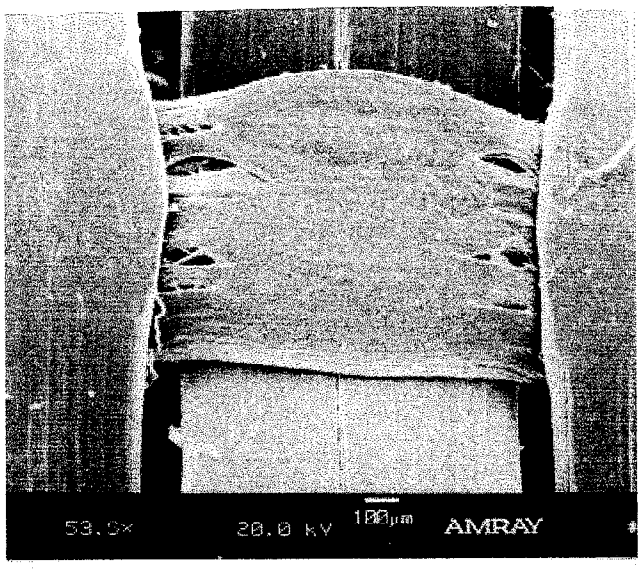

Figure 8. SEM Photo of Geotextile Recovered from Middle of Slope – Covered (Section 2)

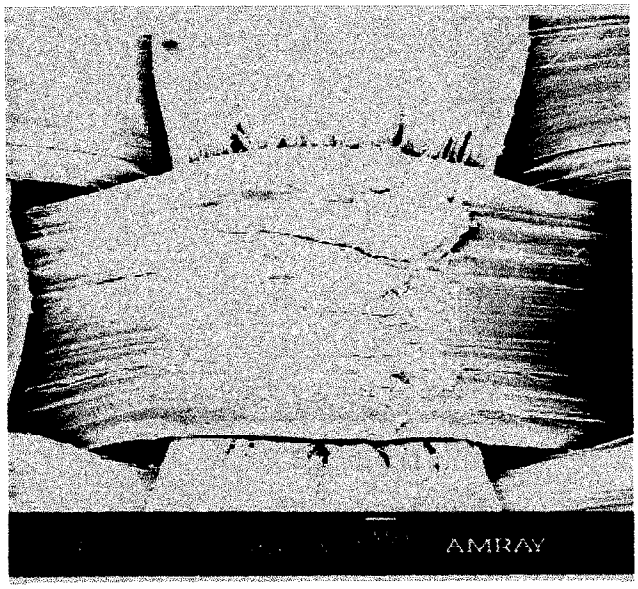

Figure 9. SEM Photo of Geotextile Recovered from Bottom of Slope - Underwater (Section 3)

Figure 10. SEM Photo of Geotextile Recovered from Top of Slope – Uncovered (Section 1)

The photos indicate some surface abrasion (Figure 9), However, the magnitude of these abrasions does not appear significant. With the exception of the SEM photos from Section 1 (Figure 10), the uncovered section, circumferential cracking was not prevalent in any of the materials. This indicates that noticeable oxidation did not occur in any area that was covered by soil. Some cracking was observed parallel to the filaments (for example see Figure 8). However, photos of virgin material (Figure 7) illustrate identical cracking indicating that this parallel cracking apparently occurs during the manufacturing process, most likely when the polymer is over heated during calendering. Although the SEM photos are not conclusive concerning aging (as surface and internal aging may be occurring), they do not show signs of significant oxidation. The mechanical evaluation discussed in the following paragraphs provide more information regarding degradation due to aging.

Mechanical Evaluation

In order to determine if mechanical degradation has occurred, strength tests were performed in each section of the sample. Two types of strength tests were performed: grab tensile (ASTM D 4632) and wide strip tensile (ASTM D 4595). Grab tensile tests were performed on randomly selected specimens to provide a basis for comparison with the manufactures' original specifications and results from the 1979 study. Wide strip tests (both 200 mm and 100 mm wide) were performed (this test is used in the current practice (ASTM D 5818 and Elias, 1996) for evaluating installation damage). The 200 mm wide tests were performed on randomly selected specimens as per FHWA installation damage evaluation procedures (Elias, 1996). This width allows for some averaging of the influence of perforations on the test results. The 100 mm wide tests were performed on select specimens located outside the areas where large rip-rap had been located directly above or below the geotextile (as described in the Field Study and Observations section) and containing no apparent perforations. The select specimen results would provide an indication as to whether any loss in strength was due to perforations or abrasion that might have occurred due to scour. By eliminating the influence of perforations, these test results would also allow for a better evaluation of loss in strength and elongation that could have occurred due to aging.

Results of strength tests are summarized in Figures 11 through 14 with respect to the location down the slope. With the exception of Section 1, Figures 12 and 13 show that randomly selected specimens have approximately the same strength as specimens recovered during the previous study, indicating that no apparent additional loss in strength has occurred over the past 20 years. The results also show that select materials with no perforations possessed essentially the same strength as new materials, indicating that a majority, if not all of the strength loss can be attributed to the holes. Since no additional strength loss has occurred over time, it is likely that all of the damage occurred during installation. Evidently no significant movement of the rip-rap (that would induce long term abrasive damage) has occurred since it was placed. Moreover, the results confirm that some aging degradation has occurred in the uncovered section (Section 1). As previously indicated, aging would have been accelerated in this section due to exposure to higher oxygen, heat, and ultraviolet light levels.

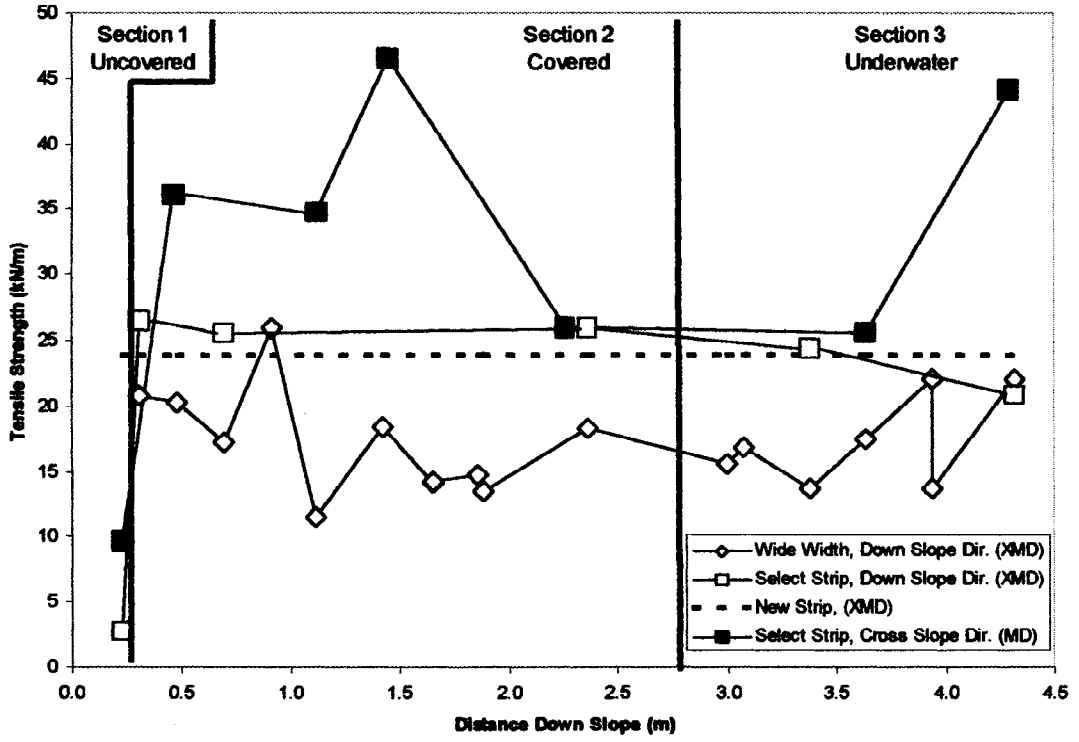

Figure 11. Geotextile Strip Tensile Strength

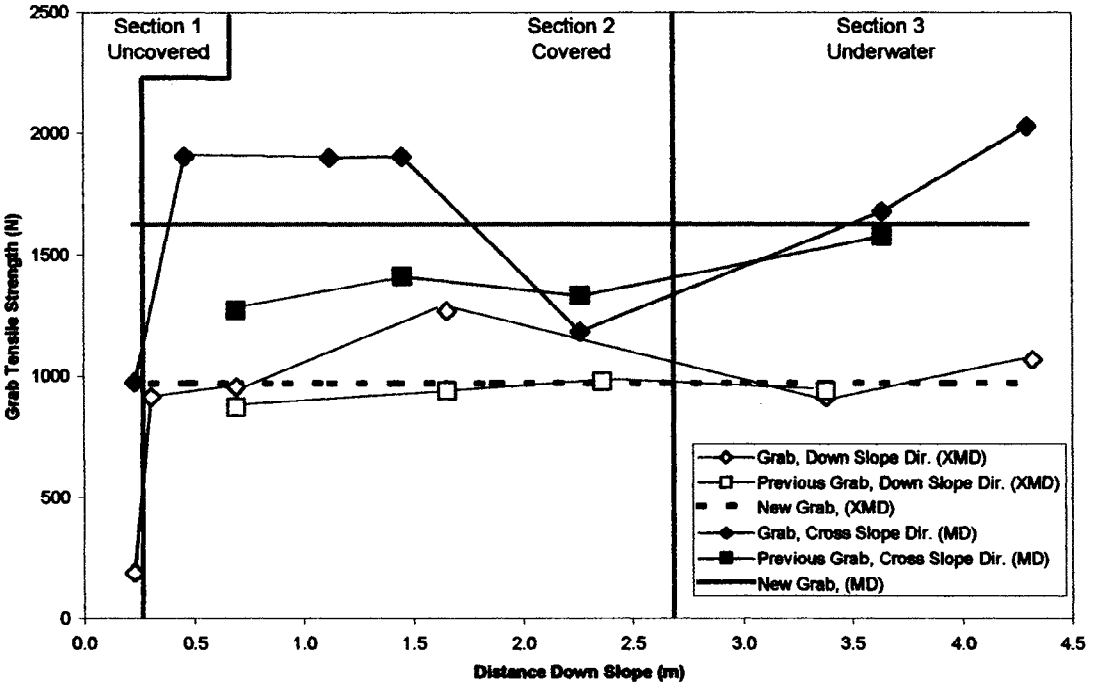

Figure 12. Geotextile Grab Tensile Strength

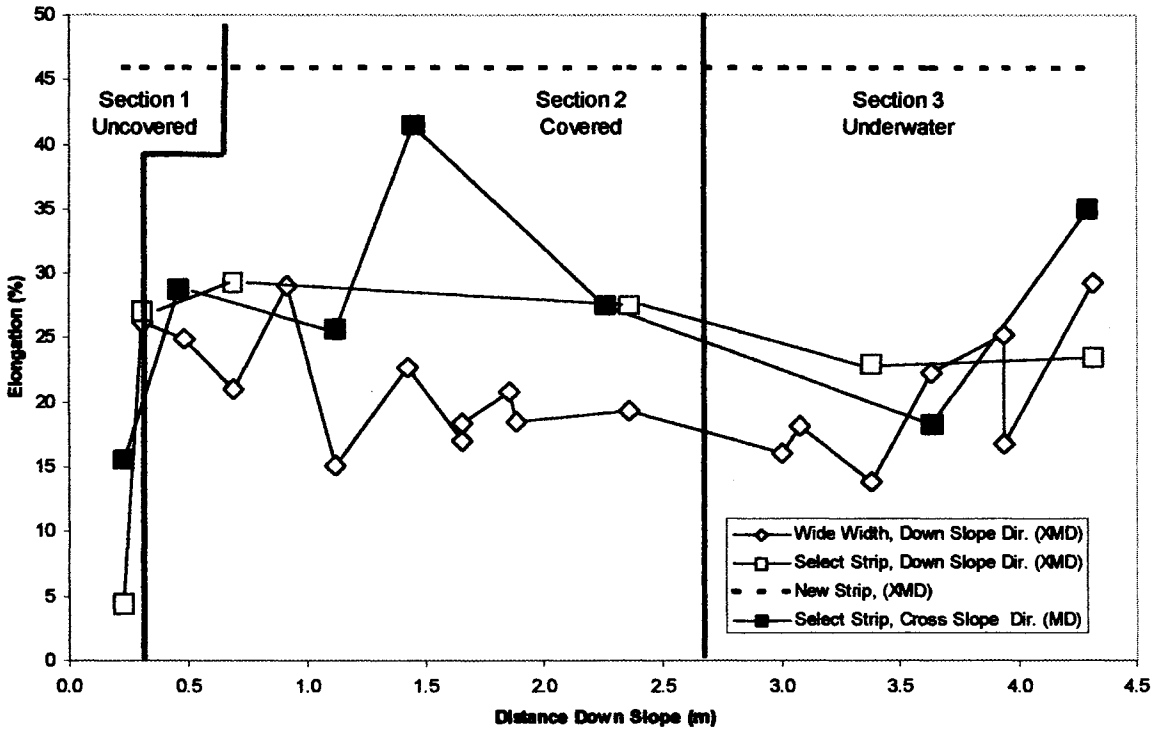

Figure 13. Geotextile Strip Tensile Elongation

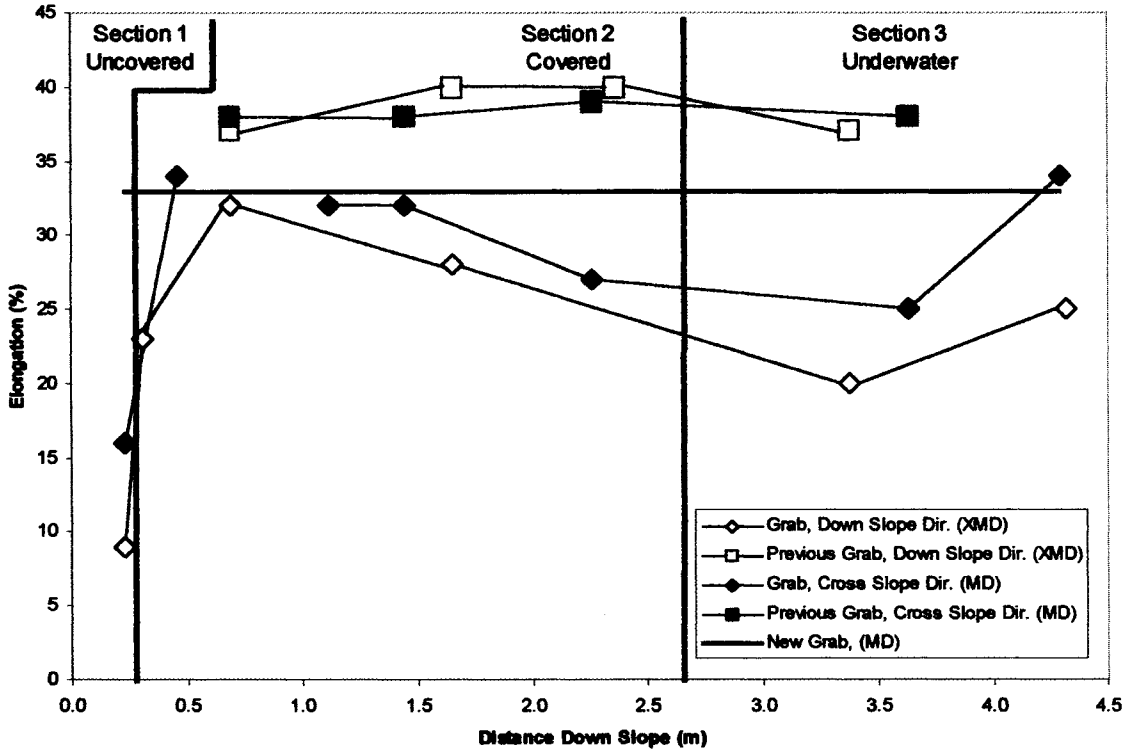

Figure 14. Geotextile Grab Tensile Elongation

Figures 14 and 15 indicate some reduction in the extensibility of the materials has occurred over the past 30 years. This sign of embrittlement would imply that some aging is taking place (perhaps in terms of loss of plasticizers). However, an additional period of time (perhaps another 30 years) will be required to evaluate the significance of this finding since the SEM photos did not indicate strong signs of oxidation.

Filtration Evaluation

The filtration test program was focused on characterization of the hydraulic properties of the exhumed sample, again with the purpose of obtaining comparative data to the 1979 study and virgin materials. Percent open area tests with an emphasis on particle retention were performed in accordance with CW02215. The percent of openings containing particles compared to the total POA of the geotextile provided a relative indication of clogging. Permittivity/permeability tests were performed in accordance with ASTM D 4491. Tests were performed using a J-tube permeameter identical to that used in the previous study. These tests were performed on the same specimen used for POA tests so that values could be compared to the magnitude of particle retention and to evaluate the influence of clogging on flow reduction. Tests were performed on randomly selected specimens along the down slope length. In order to avoid unrepresentative values, only portions of the specimen not containing perforations were evaluated for permeability.

Average POA and permeability results for each section of the sample are compared to the 1979 study and new materials in Table 2. The POA and permeability values remain relatively unchanged indicating no loss in functional performance over the life of the system. There appears to have been some reduction (approximately 10 percent) in the POA of the geotextile in the lower section of the slope (Section 3). Since there is less tidal activity in this section, some of the reduction may be due to deposition of particles and incrustation. As previously indicated, heavy staining was observed on the geotextile in the lower section of the slope. Regardless of the cause, the magnitude is insignificant with respect to performance. The permeability is still much greater than the underlying soil (estimated at $1x10^{-5}$ m/sec) and greater than would be required by most current design methods. For example, using a high factor of safety for a critical structure, the FHWA criteria (Holtz et. al., 1995) would require a permeability of $1x10^{-4}$ m/sec. Likewise, the geotextile in the lower portion of the slope exhibited a measured permittivity of 0.4 to 0.6 sec^{-1} while the current AASHTO criteria (AASHTO, 1996) only requires a permittivity of 0.2 sec^{-1} for this application.

Table 2. 79th Street Causeway Geotextile Hydraulic Property Evaluation Results

Section	Distance Down Slope (m)	Open Area (%)			Average Permeability (m/sec x 10^{-4})		
		1997	1979	New	1997	1979	New
2	0.3 to 0.5	5.5	5.5	6.0	5.7	2.6	3 to 4
2	1.0 to 1.5	5.3	5.7	6.0	5.6	2.2	3 to 4
2	2.0 to 2.8	4.3	5.4	6.0	2.2	1.9	3 to 4
3	3.5 to 4.0	4.4	4.8	6.0	2.8	2.3	3 to 4

SUMMARY AND CONCLUSIONS

This study was undertaken to document the performance and durability of a geotextile installed in 1969. The study consisted of visual observations of geotextile performance, sample exhumation, and laboratory evaluation of the exhumed sample. Results and observations were compared to those of a similar study conducted at the same site in 1979 (Christopher, 1983). The following statements summarize the findings of this study:

- Strength loss in the geotextile after nearly 30 years of performance appears to be primarily, if not entirely, due to damage during initial installation in 1969.

- Insufficient understanding of geotextile anchorage and geosynthetic construction quality control on this early installation lead to eventual exposure of the geotextile along the top of the revetment and installation damage.

- Significant aging (sufficient to cause a loss in strength) does not appear to have occurred over the life of the geotextile where it has been properly installed and covered.

- While the geotextile was visible damaged, its ability to conform to the rip-rap and the underlying soil apparently prevented soil migration and associated problems at these isolated locations.

- Relatively little change has occurred in the hydraulic geotextile's hydraulic properties over the past 30 years. The measured permeability/permittivity of the material still exceeds design requirements of several accepted filtration design procedures.

Despite the severe conditions of this application, the continued effective performance observed during this field study illustrates the exceptional durability and robust nature of polypropylene, woven monofilament geotextiles (and geosynthetics in general). From this study, we know that properly designed and installed woven monofilament geotextiles can provide at least 30 years of performance with no significant deterioration in performance or physical properties. It appears that we will have to wait a considerably longer period of time to provide an assessment of how long the geotextile will continue to perform effectively. In the mean time, at least in this project, the geotextile keeps going, and going and going.

ACKNOWLEDGEMENTS

The authors wish to thank the following for support during this study: The Florida DOT for their cooperation in allowing this exhumation to take place, Carthage Mills for pioneering efforts and initiating the original study (Christopher, 1983), Synthetic Industries for financial support of this study and providing the replacement geotextile, Pedro Giralt of Giralt Enterprises for field assistance in the exhumation, Victor Elias and the Federal Highway

Administration (FHWA) for providing the SEM photos, and TRI Environmental for performing the laboratory testing.

REFERENCES

AASHTO, 1996, "Standard Specifications for Geotextiles - M 288," Standard Specifications for Transportation Materials and Methods of Sampling and Testing, American Association of State Transportation and Highway Officials, Washington, D.C., pp. 745-755.

ASTM, 1994, Annual Books of ASTM Standards, American Society for Testing and Materials, Philadelphia, Pennsylvania: Volume 4.08 (I), Soil and Rock; Geosynthetics and Volume 4.08 (II), Soil and Rock; Geosynthetics.

Calhoun, C.C., 1972, Development of Design Criteria and Acceptance Specifications for Plastic Filter Cloths, Tech. Report S-72-7, U.S. Army Corps of Engineers Waterways Experiment Station, Vicksburg, MS, 105 p.

Christopher, B.R., 1983, "Evaluation of Two Geotextile Installations in Excess of a Decade Old", Transportation Research Record 916, Transportation Research Board, Washington, D.C., pp. 79-88.

Elias, E., 1996, Corrosion/Degradation of Soil Reinforcements for Mechanically Stabilized Earth Walls and Reinforced Soil Slopes, U.S. Department of Transportation, Federal Highway Administration, Washington DC, Publication No. FHWA-SA-96-072, 104 p.

Holtz, R.D., Christopher, B.R., and Berg, R.R., 1995, Geosynthetic Design and Construction Guidelines, U.S. Department of Transportation, Federal Highway Administration, Washington DC, Report No. HI-95-038, 396 p.

IFAI, 1992, "1992 Specifier's Guide", Geotechnical Fabrics Report, Industrial Fabrics Association International, Roseville, MN, pp. 82-83.

Koerner, G. R. and Koerner, R. M., 1995, "Temperature Behavior of Field Deployed HDPE Geomembranes," Proceedings, Geosynthetics '95 Conference, Nashville, USA, Industrial Fabrics Association International Publisher, pp. 921-938.

Koerner, R.M., G.R. Koerner, A.K. Fahim and R.F. Wilson-Fahmy, 1994, Long-Term Performance of Geosynthetics in Drainage Applications, NCHRP Report 367, National cooperative Highway Research Program, Transportation Research Board, National Research Council, Washington, D.C.

Mannsbart, G. and Christopher, B.R., 1996, "Long-term Performance of Nonwoven Geotextile Filters in Five Coastal and Bank Protection Projects", Proceedings of the 10th Geosynthetics Research Institute Conference on Field Performance of Geosynthetics and Geosynthetic Related Systems, Philadelphia, Pennsylvania, pp. 26-38.

DUAL-GEOTEXTILE INSTALLATION FOR SEDIMENT FILTRATION

DARREN QUILLEN
ARCADIS GERAGHTY & MILLER, UNITED STATES
JAMES BEDESSEM, P.E.
ARCADIS GERAGHTY & MILLER, UNITED STATES

ABSTRACT

In the summer of 1997, an environmental response action was implemented at an industrial legacy site to improve the water quality of stormwater discharging from a 6,900-square-meter (1.7-acre) settling pond. During implementation, unexpected field conditions, including an elevated volume of suspended pond sediments, threatened the success and completion of the project. Therefore, an engineered alternative was developed to expedite particle settlement and ensure separation between the sediments and clean backfill. A 10,100-square-meter (2.5-acre) dual geotextile panel was placed over the entire pond area to act as the filter/separator. The geotextile consisted of a 0.5 kilogram (15-ounce) woven and a 0.4-kilogram (11-ounce) non-woven fabric sewn together. The geotextile was pulled across the 46-meter (150-foot) wide pond and backfilled in a manner to uniformly sink the fabric while ensuring sediment did not "squeeze" from under the geotextile. The dual-fabric successfully filtered-out the underlying settled sediment particles during backfilling and aided in preventing unacceptable discharge into the river.

INTRODUCTION

At a former integrated steel mill where operations included coke production, iron and steel making, casting, primary rolling and roughing, hot and cold finishing and galvanizing, a 6,900-square-meter (1.7-acre) pond served as a receiving water for stormwater and wastewater from the "cold" side of the integrated steel mill, including the wire mill and the merchant mill (Figure 1). The pond was used as a treatment basin during active operations of the steel mill from 1915 to 1986. The pond was used to hold wastewater to allow sediment, oil and greases to be removed prior to discharge to a river that is a tributary to a major lake. Since operations ceased in 1986, the pond has continued to receive stormwater runoff from the site.

Sediments in the pond were identified as an area of concern during site environmental investigation activities. The pond sediments contained oils and greases and, depending on the weather conditions, a sheen would develop on the surface of the pond. Because the pond is continuously fed by groundwater and stormwater runoff from the site, the state regulatory agency was concerned about the potential discharge of oil to the downstream receiving water. In a voluntary agreement with the state regulatory agency to address this concern, the site owner committed to removing approximately 7,600 cubic meters (10,000 cubic yards) of sediment from the pond and then backfill the pond to create a wetland treatment unit.

During excavation, a tremendous volume of sediment was suspended in the water column and remained suspended due to its colloidal nature. The original design for backfilling and wetlands construction did not anticipate the elevated volume of suspended sediment. To keep these suspended solids contained in the pond, to prevent the sediments from cross-contaminating the clean backfill, and to minimize construction delays, an engineered remedy using a dual geotextile was implemented.

BACKGROUND

The excavation of the oil-laden pond sediments was performed through the water column using a dragline. A cross-section showing the pond excavation plan is shown in Figure 2. To prevent discharge from the pond during excavation, a temporary water treatment system consisting of bag filters and granular activated carbon (GAC) contactors was used to pump water from the pond and into the river. This pumping initially lowered the water level in the pond by approximately 2.1 meters (7 feet) so that discharge over the outlet weir would not occur during excavation.

Figure 1. Overview photo of wire mill pond.

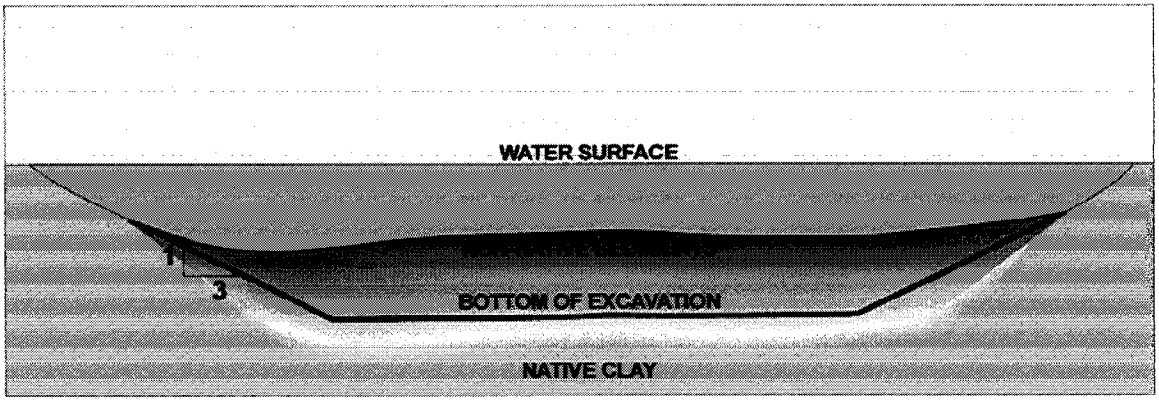

Figure 2. Cross section prior to excavation.

The excavation of several meters of pond sediments using the dragline was performed over two months. During this time, groundwater, and periodically stormwater, continued to flow into the pond causing the water level to rise. The dragline excavation activities suspended sediment throughout the pond depth.

After the initial lowering of the water level in the pond, the temporary water treatment system was unusable because the suspended sediment would clog the filters and GAC contactors. At the conclusion of excavation, the pond had regained its original water surface elevation and consisted of sediment-laden water. Since backfilling through this water column would potentially compromise the objective of the project by cross-contaminating the entire depth of the clean fill, the commencement of backfilling operations was postponed until an engineered solution was identified.

ALTERNATIVES ANALYSIS

The objective of the engineered solution, at a minimum, was to establish a separation between the pond sediments and the top 0.6 meters (2 feet) of the backfill while ensuring that any displaced pond water and sediment from filling activities did not overflow into the river. This objective permitted a transition zone within the bottom 1.5 meters (5 feet) of the backfill in which limited sediment contamination was permissible. Various parameters that required consideration and needed to be overcome to effectively achieve the objective include the following:

- Tests indicated up to 260,000 parts per million (ppm) total suspended solids (TSS) were in the pond water column at the conclusion of excavation. The high volume of TSS was directly related to the clogging and breakthrough of the water treatment system.
- The sediment stayed in suspension upon disturbance due its colloidal nature. The particle grain size of the sediment yielded 97 percent less than 0.074 millimeter (No. 200 sieve) and 57 percent less than 0.01 millimeter.

- Prior dewatering activities indicated that significant resources and costs would be incurred in an effort to dewater the pond entirely.
- Implementation of the selected remedy needed to be commenced and completed expeditiously to avoid significant standby costs and freezing seasonal temperatures.

A preliminary evaluation of numerous alternatives was conducted to determine the feasibility of completing the project within the estimated one month of remaining permissible construction weather. The alternatives were grouped into two categories: 1) partially dewatering the pond to limit the zone of sediment/clean fill cross-contamination and to reduce the potential for pond overflow during filling; and 2) backfilling through the full pond depth while ensuring separation of sediments and clean backfill. Various alternatives were eliminated from further consideration strictly due to the schedule constraints of the upcoming winter season; however, it was determined that one or a combination of alternatives warranted further consideration due to the possibility of project completion within the estimated time frame. Subsequent analyses further reduced the list of alternatives based on uncertainty and lack of confidence for achieving the stated objective. Some of the alternatives that were eliminated include the following:

- Enhanced filtration system to remove sediment as water is pumped to the treatment system;
- Construction of a separate settling basin or settling tanks to temporarily hold the sediment-laden water;
- Using a perimeter well-point system for intercepting groundwater and dewatering the pond;
- Adding centrifuges, thickeners, or rotary drum components to the treatment system;
- Installation and filling of geobags along the pond bottom; and,
- Backfilling during the winter season using the frozen pond surface for separation.

Three alternatives remained for consideration; however, after further evaluation, including on-site field studies, it was determined that none of these options could individually accomplish the objective. Each of the remaining alternatives, their function, and the overall objective analysis is presented in Table 1.

The combination of these three alternatives were then considered and, ultimately, selected for implementation to complete the project. Field and laboratory test results indicated that a proprietary coagulant and flocculant mixed in the pond would yield a TSS content of less than 50 ppm. Since dissolved-phase contamination of the pond water was minimal, the removal of sediment from the water column enabled the constituent concentrations in the pond water to meet the pretreatment standards set forth by the local municipality for the POTW. Therefore, the pond water could be partially evacuated and direct discharged to the sanitary sewer in a timely manner to facilitate geotextile installation and satisfy pond overflow concerns during filling operations while meeting the schedule constraints. It was believed that the larger, flocculated sediment

particles would enable sufficient filtration by a geotextile. Laboratory tests were not conducted to determine the particle size of the flocculated sediment, but pilot tests indicated that the AOS of selected non-woven geotextiles would provide sufficient separation characteristics. The pilot tests were carried out using approximately 1-liter samples of sediment-laden pond water that were subject to coagulation and flocculation to generate large, settleable solids. The water and flocculated solids were then filtered through samples of typical non-woven geotextiles to determine if the material was capable of retaining the flocculated solids. The solids retained on the geotextile were examined and the filtrate was collected and compared visually to the supernatant of a settled water sample. Although these preliminary geotextile analyses satisfied the separation criteria required for the project, upon further evaluation, it was determined that the tensile loads applied during fabric installation and those anticipated during backfill operations would have to be considered to ensure the integrity of the alternative.

Table 1. Final Alternatives Analysis

Alternative	Function	Analysis
In-place pond flocculation	Remove sediment from suspension to permit dewatering or pond overflow	Flocculated particles may re-suspend during backfilling
Discharge to the publicly owned treatment works (POTW) through the sanitary sewer	Partially dewater the pond	Sediment-laden water exceeded pretreatment standards for the POTW
Geotextile separation	Physical barrier between sediment and clean backfill	Sediment particles much smaller than geotextile apparent opening size (AOS) Installation through 3-meter (10-foot) water column

The selected alternative presents a unique combination of components to address the various criteria inherent with the situation. Unable to solely accomplish the complete objective, the geotextile was the key component of the combined remedy because it provided a degree of confidence in establishing separation and prohibiting cross-contamination between the pond sediments and clean backfill and enabled project completion in a timely manner.

ALTERNATIVE DESIGN

Several considerations went into the design of the geotextile component of the alternative. In selecting the geotextile material, the two main considerations were:

- Filtering capability — The geotextile needed a sufficiently small AOS to keep the flocculated sediment separate from the clean backfill.
- Strength — The geotextile needed to be strong enough to support the tensile forces applied during fabric installation and placement of the clean backfill.

Geotextiles are available in woven and non-woven styles. Non-woven geotextiles are thicker and offer a smaller AOS, which resulted in an acceptable filtering capability, while woven geotextiles offer much higher tensile strengths. Additionally, the geotextiles are manufactured of polypropylene filaments with specific gravities of less than 1.0. Therefore, the geotextile floats, reducing the tensile load required to install the fabric over the pond. Selected properties of two readily available geotextiles, one non-woven and one woven, are provided in Table 2.

Table 2. Selected Properties of Geotextiles

Geotextile Property	0.4-Kilogram (11-Ounce) Non-Woven	0.5-Kilogram (15-Ounce) Woven
Apparent Opening Size	0.150 mm (100 sieve)	0.595 mm (30 sieve)
Tensile Strength	1.11 kN (250 lbs)	1.82 kN (410 lbs)
Ultimate Wide Width Tensile	--	70.0 kN/M (4,800 lbs/ft)

Notes:

kN	kilonewtons
kN/m	kilonewtons per meter
mm	millimeters
lbs	pounds
lbs/ft	pounds per foot

Dr. Jack Fowler, a recognized expert in the use of geotextiles, and TC Mirafi, a geotextile manufacturer, were consulted on the use of woven versus non-woven geotextile for this application. After extensive consideration, it was decided that while the non-woven geotextile would provide sufficient filtration capabilities, it may not possess acceptable strength characteristics. Alternatively, the woven geotextile would possess sufficient strength characteristics, but would not achieve the filtration requirements. Therefore, to ensure that both the strength and filtration requirements would be met, a dual-geotextile consisting of a 0.4-kilogram (11-ounce) non-woven geotextile sewn to a 0.5-kilogram (15-ounce) woven geotextile was selected (Figure 3). A sufficient quantity of the dual-geotextile was fabricated at the manufacturing facility to cover the 6,900-square-meter (1.7-acre) pond. The fabrication consisted

of first sewing three 4.6-meter (15-foot) wide by 46-meter (150-foot) long rolls of the woven fabric together to create a panel 13.5 meters (45 feet) wide by 46 meters (150 feet) long. This procedure was repeated using the non-woven fabric. The two large panels were then overlaid and sewn together to create the dual-geotextile. Sixteen of the large dual-geotextile panels were shop fabricated and shipped to the site.

Figure 3. Close-Up Photo of Dual-Geotextile.

The design of the installation plan for the dual-geotextile evaluated and accounted for the following concerns:

- The geotextile needed to be in-place over the entire surface of the pond prior to any backfilling to ensure that the sediment remained trapped below the geotextile.
- The installation process needed to have minimal water disturbance so that the settled sediment would remain at the bottom of the pond.
- There was a limited amount of space along the perimeter of the pond.
- The backfilling needed to progress in such a manner as to sink the dual-geotextile as uniformly as possible to minimize tensile stresses in the fabric and induction of sediment waves underneath the fabric.

The installation plan successfully addressed each of these concerns and is discussed below.

CONSTRUCTION

Approximately two weeks were required to flocculate and partially dewater the pond. The pond contained 10 ppm TSS after coagulation and flocculation; approximately 21 million liters (5.5 million gallons) of water were evacuated from the pond to lower the water surface elevation to within 1.2 meters (4 feet) of the pond bottom. To maximize the rate of dewatering, water was pumped both to the sanitary sewer and to the temporary water-treatment system, which discharged to the river. Immediately following flocculation and dewatering, the dual-geotextile installation commenced.

The geotextile was delivered to the site in 16 pre-sewn panels 13.5 meters (45 feet) wide by 46 meters (150 feet) long. Due to the physical boundary constraints of the site including wetlands, the river, and elevated topography, the geotextile panels were stacked along the 122-meter (400-foot) long by 7.6-meter (25-foot) wide north perimeter road. The 16 panels were then sewn together in the stacked formation to comprise one 10,100-square-meter (2.5-acre) geotextile panel capable of completely covering the 6,900-square-meter (1.7-acre) pond. After sewing, the fabric remained stacked in an accordion fashion to facilitate installation (Figure 4).

Figure 4. Geotextile on bank.

Polypropylene ropes were tied to straps sewn to the leading edge of the fabric every 7.5 to 15 meters (25 to 50 feet) and extended to the south perimeter to enable pulling of the geotextile for installation. The specific gravity of the geotextile was intentionally selected as less than 1.0 so that the fabric would float and minimize the drag force during installation. Five pieces of traditional construction equipment, including dozers and backhoes, were equally positioned along

the south perimeter with a laborer between each piece of equipment. All equipment and workers uniformly pulled their ropes to extend the accordion-stacked fabric across the pond (Figure 5). Throughout the process, several ropes or straps ripped due to concentrated tensile loads as a result of non-uniform pulling; however, the majority of ropes and straps remained intact and permitted installation without major interruption. Once the geotextile was completely across the pond and the fabric was maneuvered to minimize wrinkles and assure complete coverage of the pond (Figure 6), the geotextile was anchored at the top of the sideslope along the southern perimeter road. The north perimeter was not anchored to permit the north edge to form-fit to the pond by sliding down the slope during filling; this reduced tension within the geotextile.

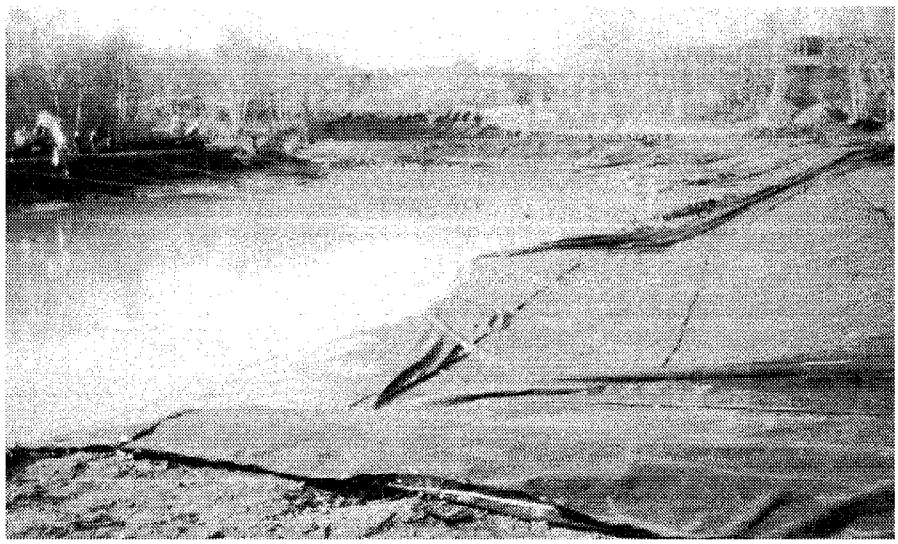

Figure 5. Installation of Geotextile Fabric.

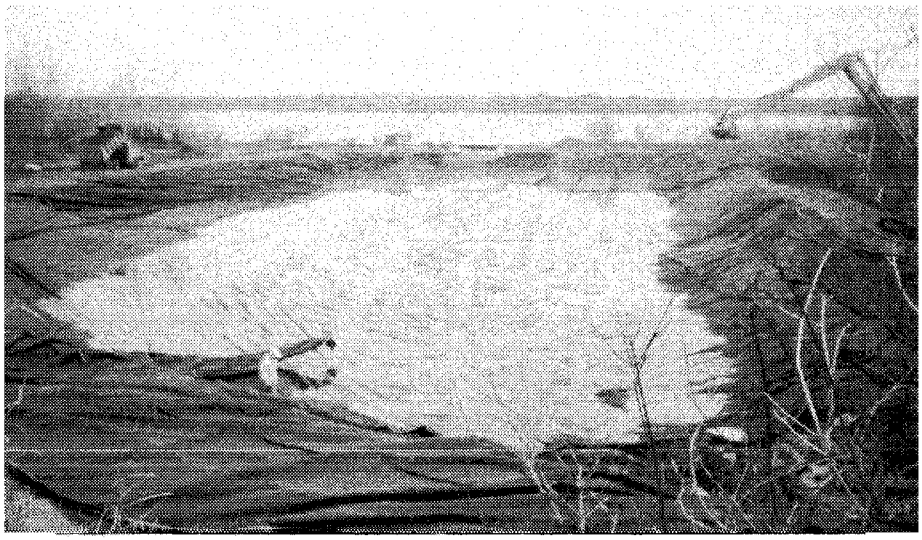

Figure 6. Geotextile Placement Complete.

Geotextile sewing and installation required three days. A completed panel layout is shown in Figure 7(a). Upon completing the installation of the geotextile and permanently anchoring the material along the southern perimeter road, backfilling activities commenced. An engineered and controlled backfilling sequence plan was implemented to ensure uniform loading of the geotextile and to reduce mud wave propagation and stresses transmitted throughout the geotextile. The backfilling sequence described below is also portrayed in Figure 7(b).

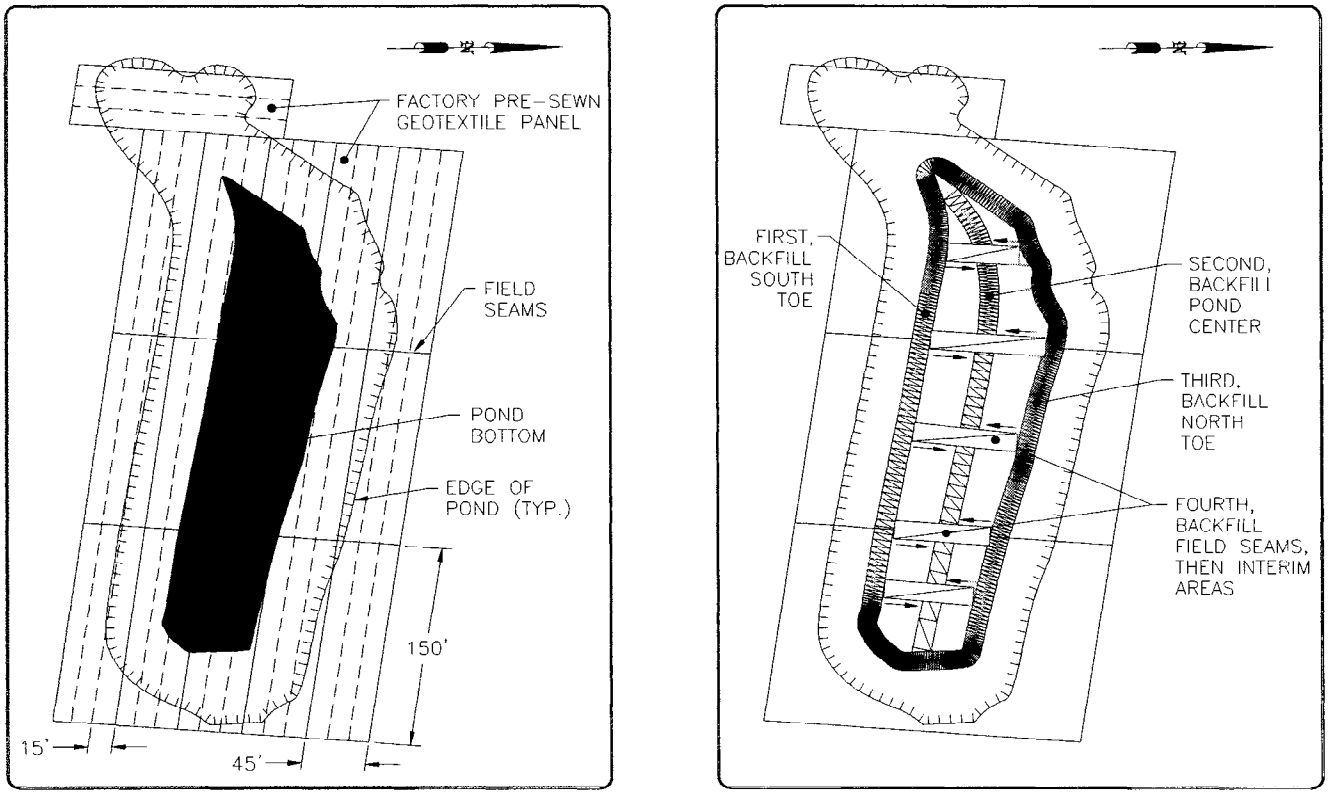

a) Completed Panel Layout

b) Backfilling Sequence

Figure 7. Geotextile Installation and Backfilling Plan.
(1 foot = 0.3048 meter)

Initially, the toe of the sideslope along the southern perimeter was backfilled to sink the geotextile to the bottom of the pond along the southern perimeter while maintaining intimate contact between the sideslope and the geotextile. An approximate 0.6- to 0.9-meter (2- to 3-foot) thick lift was required. Care was taken and observations made to ensure that the perimeter lift was not excessive and would not initiate mud waves. This initial filling along the perimeter was intended to minimize the potential for sediment to "squeeze-out" between the pond bank and the geotextile throughout the remainder of filling operations. Throughout backfilling, the geotextile along the northern perimeter was permitted to slide as the material sank to the bottom of the pond.

Following completion of the initial lift along the southern perimeter, an approximate 0.3-meter (1-foot) thick lift of fill was placed along the centerline of the pond to facilitate sinking of the geotextile. Backfill placement in the middle of the pond was conducted to contain future mud wave development and reduce stresses on the floating geotextile. Subsequently, the northern perimeter was backfilled similar to the southern perimeter.

Backfilling in the interior of the pond was first completed along the field seams with an approximately 4.6-meter (15-foot) wide by 0.3-meter (1-foot) thick lift which progressed from the perimeter toward the centerline to control and contain any mud wave development. Once the field seams sunk to the bottom of the pond, the midpoints between the field seams were located and filled in a similar manner. This type of filling progression was intended to uniformly fill on the geotextile and minimize potential stresses. Upon completion of filling at the midpoints located between the field seams, the remainder of the first 0.3-meter (1-foot) thick lift was placed to fill in the gaps between midpoints.

Backfilling progressed in the interior of the pond with two additional 0.3-meter (1-foot) thick lifts placed in a similar manner to that described above for the interior of the pond. Following placement of the three 0.3-meter (1-foot) thick lifts, 0.6-meter (2-foot) thick lifts were uniformly placed throughout the pond to complete the backfilling activities. A photograph of the backfilling operations is shown in Figure 8. A cross-section of the backfilled pond complete with the dual-geotextile separator is shown in Figure 9. A total of 2.1 meters (7 feet) of fill was placed over the geotextile through the water column in approximately 3 weeks using a long-stick backhoe and a crane.

Figure 8. Photograph of Pond Backfilling.

Construction quality assurance (CQA) activities verified sediment filtration through analytical testing of the pond water. Testing was conducted once every 2 days. Additionally, CQA observations noted a 15-meter (50-foot) long tear of the geotextile along a field seam on the slope of the northern perimeter. The rip occurred after the first 2 lifts of fill were placed and was attributed to localized overloading due to construction of a soil access pad approximately 1.8 meters (6 feet) thick to enable the contractor to reach the middle of the pond for filling operations. Several meters of fill were placed over the tear to minimize the potential for sediment re-suspension from below the geotextile.

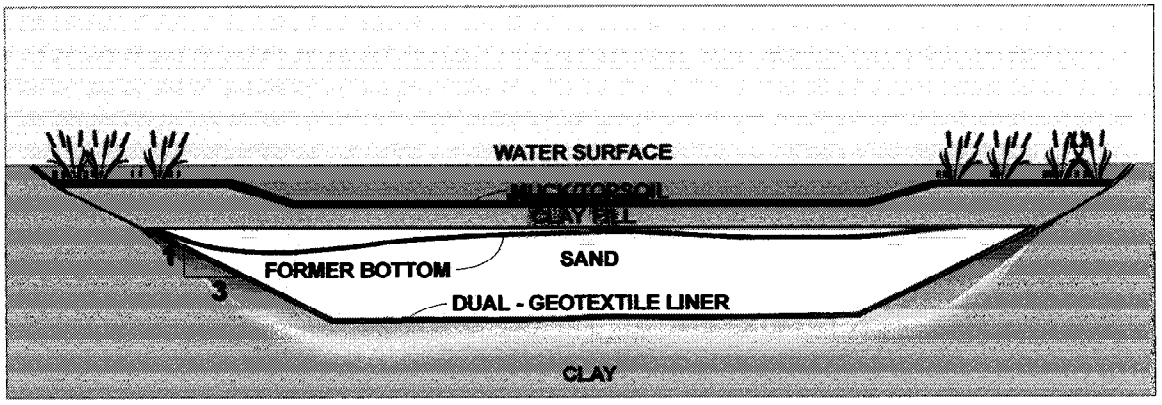

Figure 9. Cross Section of Backfilled Pond.

CONCLUSIONS

The response action objective for the site was to protect water quality of the nearby river by improving the quality of water discharging from the site through the pond. The response action included the removal and disposal of up to 3 meters (10 feet) of contaminated sediments from the pond during the course of the project, followed by backfilling and establishing a wetland treatment unit. Because the excavation activities suspended a tremendous volume of sediment in the pond water column, an engineered solution was required prior to backfilling. The selected alternative, specifically the separation component, was instrumental in determining the outcome and timely completion of the project. Both the filtration and strength characteristics of the dual-geotextile were critical to ensure that sediment would neither pass through the fabric nor seep through a rip or tear resulting from installation and/or backfilling.

Throughout backfilling operations, CQA analytical test results indicated that the pond water was free of sediment contamination. These results were a preliminary indication that the dual-geotextile was properly functioning as a physical separation barrier between the sediments and clean backfill. However, the ultimate measure of project success was, and continues to be, post-construction response action monitoring. To date, the pond water constituents are below the concentrations set forth in the response action report. Therefore, since the geotextile's role was

simply to separate sediment from clean backfill during the agitation of construction, it may be stated that the dual-geotextile component of the remedy met its performance objective.

REFERENCES

Fowler, S., (1985) "Fabric Reinforced Dikes, Craney Island," Proceeding of the Geotoechnical '85 Fabrics Conference, Cincinnati, Ohio, June 1985, pp. 118-128.

Guglieimetti, J.L., Koerner, G.R. and Battino, F.S., (1955) "Geotextile Reinforcement of Soft Landfill Process Sludge to Facilitate Final Closure: An Instrumented Case Study," Proceedings of the 9th GRI Conference, Philadelphia, pp. 185-193.

ACKNOWLEDGMENTS

The expeditious development, implementation, and success of the prescribed alternative is directly attributable to various entities involved. They include the following:

- Owner: confidential client
- Engineer: ARCADIS Geraghty & Miller
- Contractors: WATEC, Bird Treatment Services, Dr. Jack Fowler (Geotec Associates), and TC Mirafi

INITIAL EVALUATION OF GEOTEXTILES FOR WASTEWATER FILTRATION AT TEMPORARY BASE CAMPS

C. James Martel
U.S. Army Cold Regions Research and Engineering Laboratory, USA.
Deborah K. Pelton
U.S. Army Cold Regions Research and Engineering Laboratory, USA.
Karen S. Henry
U.S. Army Cold Regions Research and Engineering Laboratory, USA.

ABSTRACT

The Army has identified a need for a deployable wastewater treatment system for use at temporary base camps such as those in Bosnia. In this study we evaluated a new concept for wastewater treatment that features the use of disposable geotextiles for filtration of wastewater. The advantage of this concept is that it eliminates the need for large settling tanks and sludge dewatering operations. Cost estimates indicate that geotextile filtration of wastewater is approximately one-third the cost of conventional treatment. In this bench scale study, up to 70% of the total suspended solids (TSS) and 40% of the biochemical oxygen demand (BOD) from raw wastewater (sewage) were removed, demonstrating that nonwoven geotextiles are very good filters. The hydraulic capacity varied from 646 L/m^2 to 3138 L/m^2 depending on the TSS concentration. Approximately one-half of the hydraulic capacity was restored by cleaning. Calculations indicate that the graywater (sewage minus water from latrines) produced by a 550 soldier unit would require 116 m^2 of geotextile per day, which would mean several manual filter changes each day. The alternative is to automate the filter change as it becomes clogged.

INTRODUCTION

As the Army is called upon to keep the peace in many parts of the world, soldiers will be stationed at temporary base camps for several months and possibly years. The waste generated by these soldiers will require some degree of treatment prior to discharge or disposal. In some cases, treatment will be provided by the existing facilities of the host country. In other cases, treatment facilities may be too far from base camp or they may be inoperative, as was the case in Bosnia. In these cases where no treatment facilities are available, present doctrine calls for constructing latrines where human wastes are buried or burned in half-barrel containers (U.S. Army Field Manual 21-10). This practice may be acceptable for short term operations of six months or less. During longer operations, odors from latrines, the lack of hand washing facilities, and pollution caused by

graywater discharges can become a serious health problem. To safeguard the health and safety of the soldiers, a deployable water and wastewater treatment system is needed.

According to an extensive report by Remson and Gallion (1997), the Army has a continuing requirement for disposing graywater produced by Force Provider. Force Provider is a tent based facility developed to give the front-line soldier a brief respite from the austere conditions in a combat theater. It is also intended for use in support of disaster relief and humanitarian missions. It is designed to provide each soldier with three hot meals per day, laundered clothing, shelter, showers, latrines, and recreation facilities. Each Force Provider package contains all materials necessary to support 3,300 soldiers per rotation. It is subdivided into six 550 soldier modules, with each module capable of independent operation. Consequently, each module must have its own capability for treating graywater. The volume of graywater generated by a module is expected to be 100,000 L/day.

Conventional methods of wastewater treatment require the construction of large reinforced concrete tanks for aeration and sedimentation. For temporary base camps, this approach would be expensive because of the large amount of onsite construction needed. Package plants would require less onsite construction, but they are also quite expensive because they are designed for more permanent installations like suburban subdivisions and mobile home parks. For temporary base camps, a temporary and deployable method of treatment is needed. To be deployable it must be compact, light, and reusable. From the soldiers point of view, it should be simple to operate and maintain.

Our proposed method of wastewater treatment to meet these requirements is the Wastewater Filtration and Treatment Unit (WFTU). Basically, this unit (Figure 1) consists of three sections: a top filter that removes large objects, grit, and other suspended solids; a trickling filter section where attached microorganisms remove the organic pollutants in the wastewater; and a bottom filter which catches any sloughed biological growth. The advantages of this approach areas follows:

1. No in-ground structures would be required,
2. The unit is self-contained and light making deployment and setup easy,
3. There would be no need for sludge dewatering since all solids would be captured and dewatered on the filters. When the geotextile filter becomes clogged, it would be removed and replaced with a new filter. The clogged filter could either be cleaned and reused, or incinerated.
4. The unit would be easy to operate because it has no mechanical equipment except a pump to deliver the wastewater to the unit.

The main question concerning the feasibility of the WFTU concept is the performance of the top and bottom geotextile filter in terms of removal efficiency and hydraulic capacity. The trickling filter section is of less concern because its characteristics and performance are already well known. In this application the trickling filter media could be made from rock or plastic, or perhaps a different geotextile (Buisson and Rollin, 1989; Valentis and Lesavre, 1990; Mlynarek et al., 1993). The

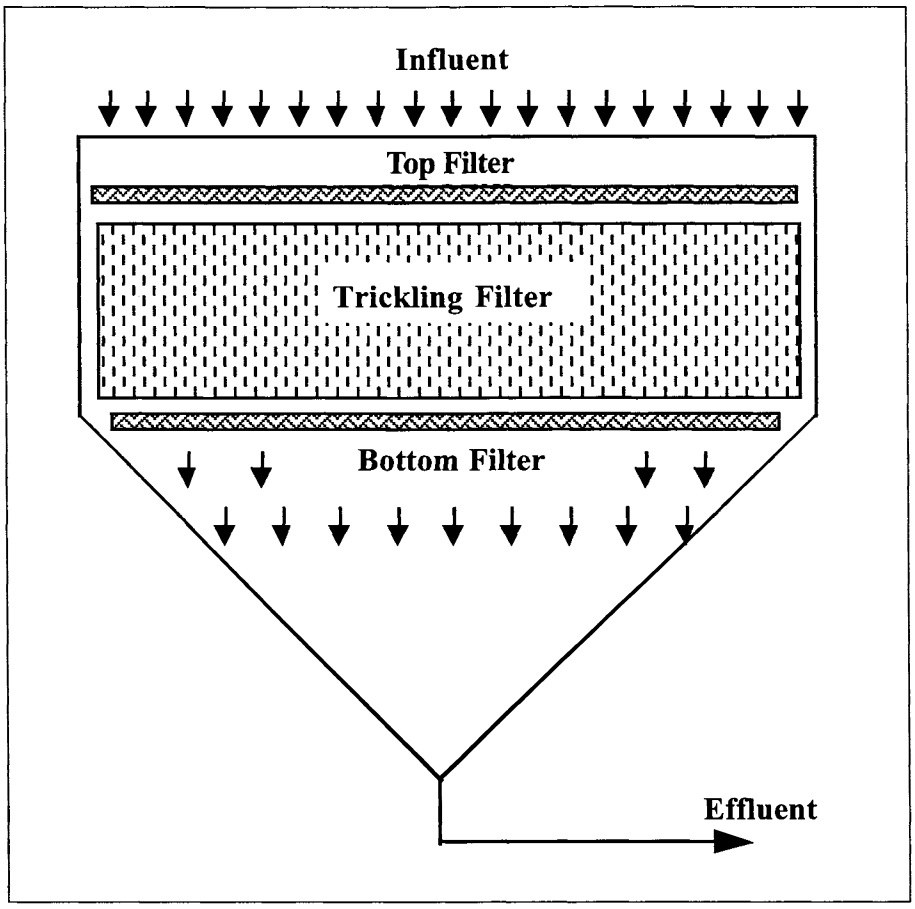

Figure 1. Conceptual sketch of wastewater filtration and treatment unit (WFTU).

main characteristics of a good trickling filter medium are that it has a high surface area per unit volume, is low in cost, has a high durability, and does not clog easily (Metcalf and Eddy, 1979).

We found no previous work on direct filtration of raw sewage with geotextiles. However, there are published papers on related applications in water treatment and sludge dewatering. The operational performance of slow sand filters was significantly improved by placing a layer of nonwoven synthetic fabric on the top surface (Graham and Mbwette, 1991; Klein and Berger, 1994). The geotextile prevented algae and other organic and inorganic byproducts from clogging the filter. As a result, the sand filter operated for longer periods of time. Replacement of the geotextile was simpler and less expensive than skimming the top layer of sand.

Another application of geotextiles in wastewater treatment is the use of geotextile bags and tubes to dewater sludges. Fowler et al. (1997) found that nonwoven polypropylene bags dewatered digested wastewater sludge (typically containing 6% solids) to 21.4% total solids content in 65 days. The advantage of this method is that it does not require extensive labor and maintenance of equipment.

The purpose of our study was to evaluate the ability of geotextiles to perform the function of primary and secondary settling tanks. Specifically, our objectives were to determine the a) BOD and TSS removal efficiency, b) hydraulic capacity, and c) merits of cleaning the geotextiles after use. To accomplish these objectives, bench scale tests were conducted at the U.S. Army Cold Regions Research and Engineering Laboratory (CRREL) during the spring and summer of 1997.

MATERIALS AND METHODS

Because the main function of the geotextile is to filter out settleable solids, we decided to base our selection on apparent opening size (AOS). According to Metcalf and Eddy (1979), settleable solid particles range in size from 10 μm and up. Because of the small size of these particles, we decided to select geotextiles with the smallest apparent opening sizes. Based on the 1997 Specifier's Guide, none of the geotextiles had AOS's as small as 10 μm but we found several nonwoven, polypropylene geotextiles with openings in the 106 to 212 μm range. We assumed that this was still small enough to remove a significant portion of the particles. The Apparent Opening Size (AOS), mass, permittivity, grab tensile strength, and cost, of the ten geotextiles we randomly selected are shown in Table 1.

A 20-cm (8-inch) diameter U.S. Standard Sieve no. 20 was used as the bench scale support screen for the geotextile (Figure 2). The openings on this sieve are 0.85 mm. Samples were cut to fit snugly within the sieve so that none of the wastewater could bypass the geotextile. Wastewater was carefully poured into the sieve to avoid any overflow.

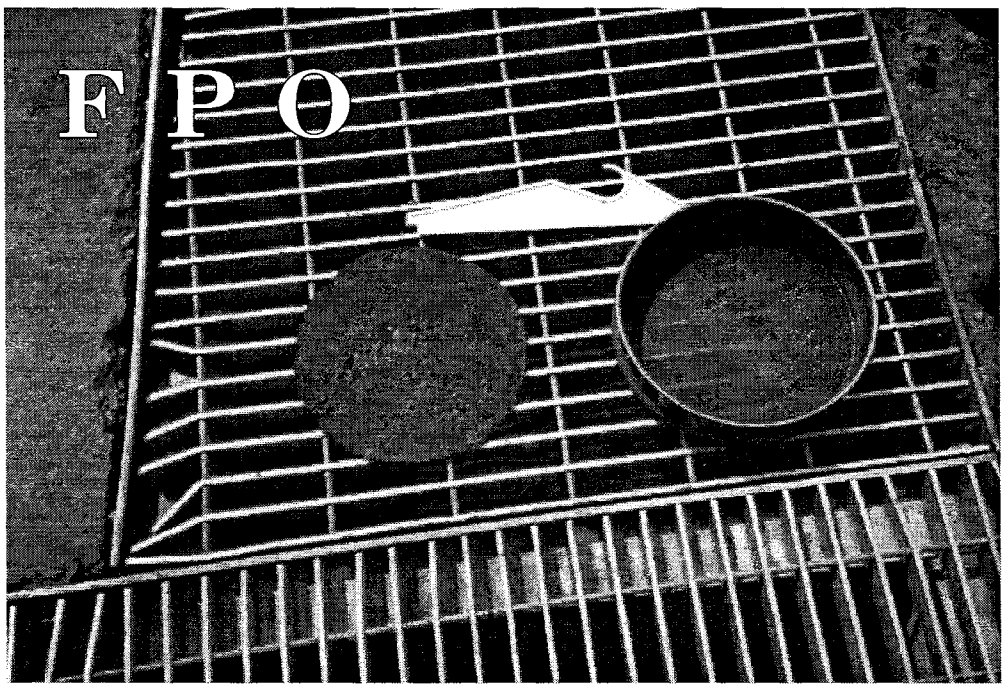

Figure 2. Support screen, geotextile sample, and scraper used in wastewater filtration and hydraulic capacity tests.

Table 1. Properties of selected nonwoven, polypropylene geotextiles (1997 Specifiers Guide).

Geotextile Number	**Construction**	**Apparent Opening Size** mm (US sieve)	**Mass per Unit Area,** g/m^2 (oz/yd^2)	**Permittivity** L/min·m^2 (gal/min·ft^2)	**Grab Tensile/ Elongation** kN (lb)/%	**Cost** \$/m^2 (\$/yd^2)
1	needle-punched, staple fibers	0.212 (70)	135 (4)	5700 (140)	0.42 (95)/15	0.72 (0.60)
2	needle-punched, staple fibers	0.150 (100)	339 (10)	3460 (85)	1.11 (250)	1.61 (1.35)
3	needle-punched, staple fibers	0.150 (100)	540 (16)	2037 (50)	1.78 (400)/50	2.03 (1.70)
4	thermally spun-bonded, continuous filament	0.100 (140)	Not Reported	448 (11)	1.07 (240)/60	0.87 (0.73)
5	needle-punched, staple fibers*	0.150 (100)	339 (10)	2442 (60)	1.27 (285)/50	1.24 (1.04)
6	needle-punched, staple fibers	0.149 (100)	339 (10)	3056 (75)	1.11 (250)/50	1.28 (1.07)
7	needle-punched, staple fibers	0.149 (100)	407 (12)	2648 (65)	1.34 (300)/50	1.83 (1.53)
8	needle-punched, staple fibers	0.149 (100)	543 (16)	2037 (50)	1.69 (380)/50	2.37 (1.98)
9	needle-punched, staple fibers*	0.150 (100)	314 (9.25)	3460 (85)	1.11 (250)/50	1.09 (0.90)
10	needle-punched, staple fibers*	0.106 (140)	575 (17)	2645 (65)	1.82 (420)/60	1.85 (1.55)

* Heat set on one side.

The treatment efficiency of each geotextile was determined by measuring the BOD and TSS concentrations in the wastewater before and after filtration. These tests were conducted at the wastewater treatment plant in Hanover, New Hampshire. Raw wastewater from the influent channel was pumped into a large container and manually mixed to maintain homogeneity. Ten liter buckets of wastewater were taken from the container and poured onto each geotextile filter (Figure 3). Samples of the influent and effluent were taken and analyzed at the plant for BOD and TSS according to Standard Methods (1992).

Based on the results of the previous tests, Geotextile 1 was selected for hydraulic capacity tests. In this case, the hydraulic capacity was defined as the maximum volume of wastewater per unit area that a geotextile can effectively filter before it becomes clogged. A filter was judged to be clogged when, for all practical purposes, the flow was reduced to a trickle. The wastewater application procedure was the same as before except that several buckets were applied until it was apparent that the filter was clogged. The sum volume of the buckets was recorded as the total volume of wastewater filtered.

Six different wastewaters containing various TSS concentrations were tested: raw wastewater, raw wastewater after 15 minutes of settling, raw wastewater after 30 minutes of settling, raw wastewater after 1 hour of settling, primary effluent, and trickling filter effluent. As in the previous test, the raw wastewater and primary effluent were obtained from the Hanover plant. The trickling filter effluent was obtained from the treatment plant in Newmarket, New Hampshire.

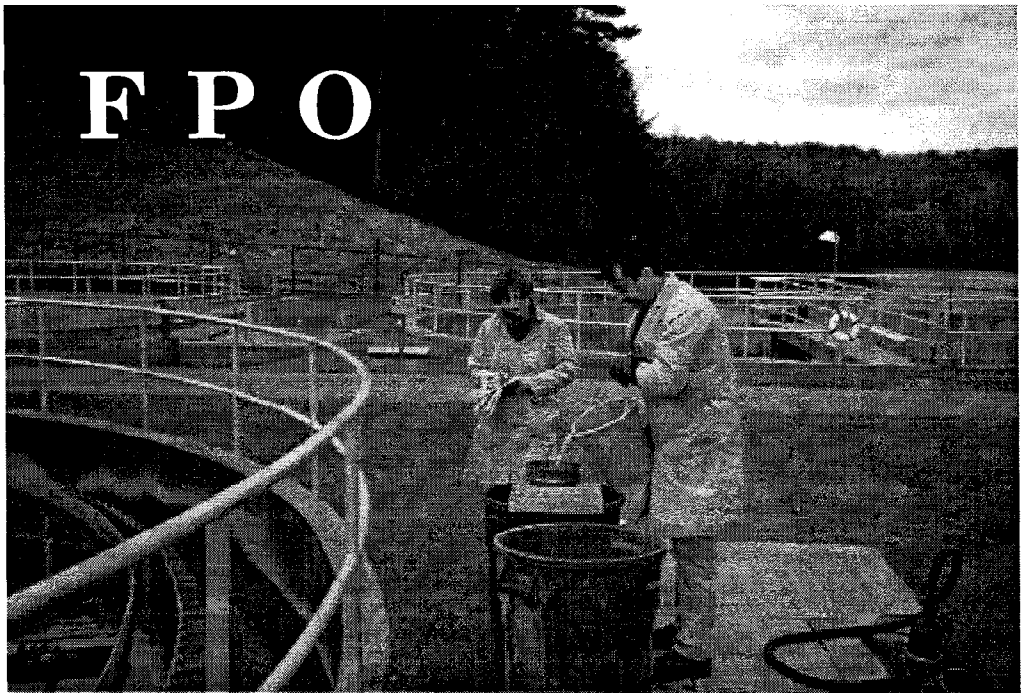

Figure 3. Pouring of wastewater from Hanover, New Hampshire, treatment plant on geotextile sample in support screen.

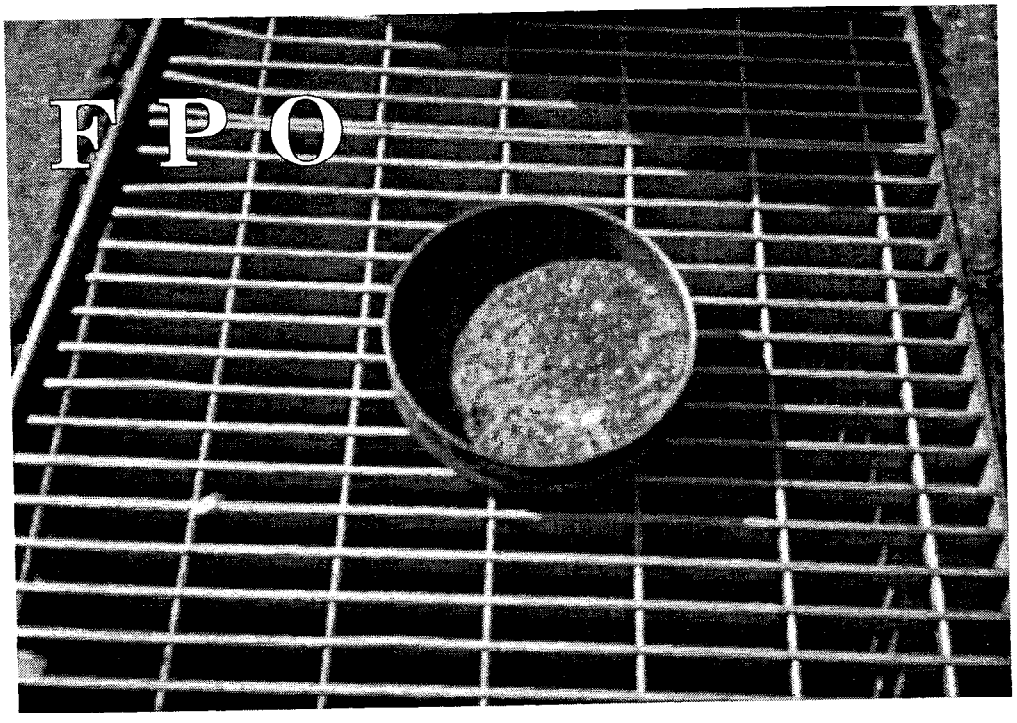

Figure 4. Clogged geotextile after filtration of several liters of raw wastewater.

To determine whether cleaning and reusing the filter increased the hydraulic capacity, we applied raw wastewater to Geotextile 8 until it was clogged (Figure 4). It was then removed from the sieve and scraped with a rubber squeegee. This technique is similar to the "doctor blade" used to scrape solids from a vacuum filter media. A high pressure spray was directed at the back of the fabric to dislodge any attached solids. The filter was then placed back in the sieve with the same side facing up. More wastewater was applied until the filter was clogged for a second time and the cleaning process was repeated. Geotextile 8 was selected for this test because it has a high mass per unit area and appeared to be durable enough to withstand repeated cycles of filtration and cleaning.

RESULTS

Filtration Tests.

All the selected geotextiles except Geotextile 4 performed as well as a conventional primary treatment process. As shown in Table 2, the percent removals of BOD and TSS were well within the performance range of primary treatment (50 to 70% removal of TSS and 25 to 40% removal of BOD). Geotextile 4 repelled water thus producing no filtrate. In general, the heavier fabrics had a slightly higher removal efficiency than the lighter fabrics.

Table 2. BOD and TSS Removal by Selected Geotextiles.

Geotextile Number	**Filtrate BOD Concentration** mg/L	**Filtrate TSS Concentration,** mg/L	**BOD Removal[1],** %	**TSS Removal[2],** %
1	167	56	40	59
2	168	60	39	56
3	164	50	40	64
4	Not measured	Not measured	Not calc.	Not calc.
5	169	64	39	53
6	163	52	41	62
7	157	40	43	71
8	163	40	41	71
9	165	52	40	63
10	172	42	38	69

1. Based on influent BOD concentration of 276 mg/L.
2. Based on influent TSS concentration of 137 mg/L.

Table 3. Results of hydraulic capacity tests on Geotextile 1.

Wastewater Source	**Wastewater Filtered,** L	**Wastewater TSS,** mg/L	**Filtrate TSS,** mg/L	**TSS Removal,** %
Raw Wastewater	21	225	73	68
R. W. after 15 min. settling	38	126	70	44
R. W. after 30 min. settling	36	122	64	48
R. W. after 60 min. settling	40	111	56	50
Primary Effluent	102	62	50	19
Trickling Filter Effluent	74	60	20	67

Hydraulic Capacity Tests.

Because all the geotextiles except Geotextile 4 were able to achieve primary treatment, we selected the least expensive one (Geotextile 1) for the hydraulic capacity tests. As expected, these tests confirm the notion that hydraulic capacity increases as the TSS concentration in the applied wastewater decreases. As shown in Table 3, the filter was able to process only 21 L of raw wastewater before it became clogged. This volume almost doubled after the raw wastewater was allowed

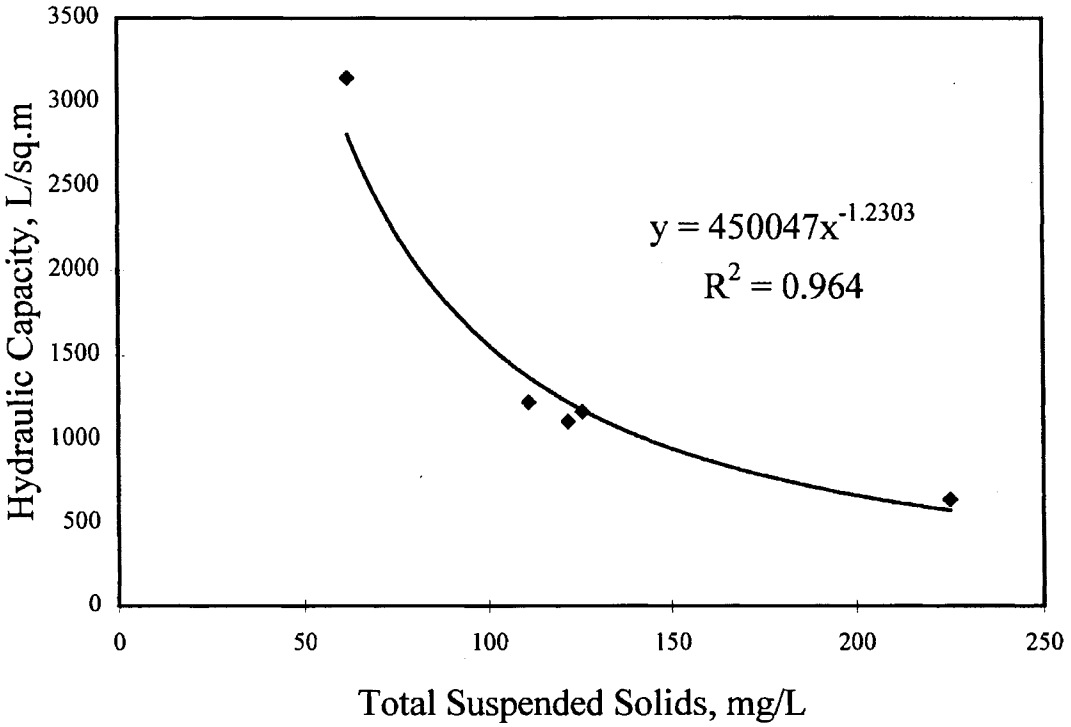

Figure 5. Hydraulic capacity of needle-punched polypropylene geotextile, 135 g/m^2 and 0.212 mm AOS (Geotextile 1) for filtration of raw wastewater.

to settle for as little as 15 minutes prior to filtration. The primary effluent contained very little filterable solids as indicated by the low percentage of TSS removal. Therefore, the geotextile was able to process 102 L, which is approximately 5 times more than the volume of raw wastewater. Although the TSS in the trickling filter effluent was slightly lower than in the primary effluent, the percent removal was higher. Consequently, the geotextile was able to process only 74 L of trickling filter effluent before clogging.

Based on the data in Table 3, the hydraulic capacity of Geotextile 1 was calculated by dividing the volume of wastewater filtered by the surface area of the sieve (0.0325 m^2). A plot of this data is shown in Figure 5. The equation of the line of best fit is

$$y = 450047x^{-1.2303} \quad (1)$$

where y is the hydraulic capacity in L/m^2 and x is the TSS concentration in the raw wastewater. The correlation coefficient (R^2) for this equation is 0.964, indicating a high degree of correlation between TSS and hydraulic capacity. Although this correlation is based on only 5 data points, we feel quite confident that it is valid for the case of a raw wastewater applied to Geotextile 1. Other geotextiles may produce a different equation.

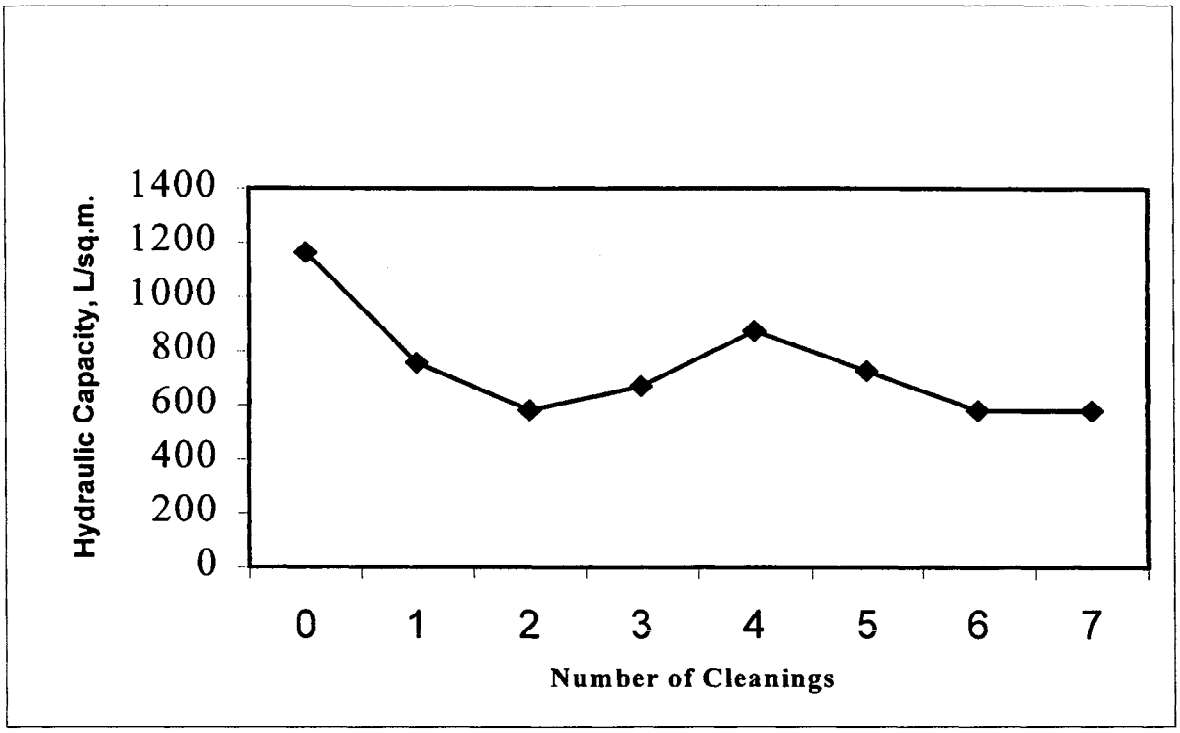

Figure 6. Effect of cleaning on hydraulic capacity of Geotextile 8.

Cleaning Tests.

About one-half of the hydraulic capacity was restored to each of the geotextiles after cleaning. As shown in Figure 6, the hydraulic capacity of Geotextile 8 decreased from approximately 1200 to 600 L/m^3 after two cleanings. The hydraulic capacity remained about the same for the next 5 cleanings.

DISCUSSION

Based on the results of this study, we estimate that the top filter of the WFTU unit will require 116 m^2/day of Geotextile 1, or equivalent, for a 550 soldier module generating 100,000 L/day. This estimate is based on Equation 1 and an assumed graywater TSS concentration of 162 mg/L (Salvato, 1992). Only 44 m^2/day would be needed for the bottom filter assuming a trickling filter effluent concentration similar to that of the Newmarket, New Hampshire, plant, i.e., 60 mg/L. If the diameter of the filter is 2.4 m, the width of a standard ISO container (2.4 m wide, 2.4 m high and 6.1 m long), then the surface area of each WFTU unit would only be 4.5 m^2. This means that the top filter of the WFTU unit will require 26 filter changes per day since the total amount of geotextile needed to filter the graywater from a 550 soldier module is 116 m^2/day. Similarly, the bottom filter will require 10 changes per day. Obviously, this would not be acceptable from a operational point of view.

One way to overcome this problem would be to make the filter change a mechanical operation rather than a manual one. This could be accomplished by separating the geotextile filter sections from the trickling filter section and operating them independently. One potential configuration would be to dispense the geotextile from a roll through a special chamber similar to a traveling screen used for grit removal. This is a simple and proven technology. Because geotextiles are normally sold by the roll, acquisition and shipment would be simplified. Typically, nonwoven geotextiles like Geotextile 1, come in rolls 4.6 m wide by 365 m long. Thus one roll contains 1672 m^2 of filtration area. At the usage rates cited previously, a roll would last over two weeks for filtering graywater, and over a month for filtering trickling filter effluent. Longer periods of use may be possible as suggested by the cleaning tests.

CONCLUSIONS

This study demonstrated that nonwoven geotextiles can remove suspended solids from wastewater. Some geotextiles performed better than others, but they were all capable of achieving primary treatment. Thus, the selection of which fabric to use in this application will be based largely on cost. At \$0.72/m^2 (\$0.60/yd^2), the cost of primary treatment, including sludge dewatering, would be \$0.83/m^3 (\$3.14/1000 gal). Based on a report by EPA (1978), adding a trickling filter would increase this cost to \$1.02/m^3, which is approximately one-third of the average cost of conventional wastewater treatment at Army installations (Red Book, 1995).

The cost of filtration could be lowered even further by developing a special geotextile that has a lower mass per unit area than 135 g/m^2 because the light geotextiles performed as well as the heavier geotextiles. Also, it would be beneficial to have a biodegradable fabric that could be composted along with the trapped solids.

Based on the positive results of this study, the next step is to build and test a pilot scale unit. These tests would provide a better understanding of the operational parameters and design criteria for the WFTU concept. Unfortunately, there are no plans to continue this research because of a reallocation of funds.

ACKNOWLEDGMENTS

The authors would like to thank Don Elder, Superintendent of the Hanover, New Hampshire, Wastewater Treatment Plant, and Dick Kingston, Chief Operator, for allowing us to use their facility and analyzing our samples for BOD and TSS. This study was funded by U.S. Army Corps of Engineers Work Unit AT42-CO-E03, *Water Supply and Waste Treatment in Cold Regions Theater of Operations–Phase I.*

REFERENCES

EPA (1978) Analysis of operations and maintenance costs for municipal wastewater treatment systems. Report MCD-39, 430/9-77-015.

Buisson, H. and Rollin, A. (1989) The use of geosynthetics as bacteria support in fixed film bioreactors. Paper No. 892175, ASAE/CSAE Meeting, Quebec, Canada, June 1989. p.14.

Fowler, J., Bagby, R.M., and Trainer, E. (1997) Dewatering sewage sludge with geotextile tubes. Geotechnical Fabrics Report, Sept., 26–30.

Geotechnical Fabric's Report. Specifier's Guide (1997) Vol. 14, no. 9.

Graham, N.J.D., and Mbwette, T.S.A. (1991) Protected slow sand filtration: specification of non-woven synthetic fabric layers. Water Supply, 9, 157–164.

Klein, H.P. and Berger, C. (1994) Slow sand filters covered by geotextiles. Water Supply, 12, 3/4, 221–230.

Metcalf & Eddy, Inc. (1979) Wastewater Engineering 2nd Ed., McGraw Hill, New York.

Mlynarek, J., Barabe, Y., Bisaillon, J-G., Marchand, G., and Roy, C. (1993) Biotextile potential for domestic wastewater treatment. Joint CSCE-ASCE National Conference on Environmental Engineering, July 12–14, Montreal, Canada, 461–468.

Red Book (1995) Annual Summary of Operations, Directorates of Public Works, Department of the Army.

Remson, A. and Gallion, C. (1997) Cost and operational effectiveness analysis (COEA) for graywater treatment to support Force Provider and DEPMEDS. Report prepared for U.S. Army Tank Automotive Command, Warren, Michigan.

Salvato, J. A. (1992) Environmental Engineering and Sanitation, 4th Ed. John Wiley & Sons, New York.

Standard Methods for the Examination of Water and Wastewater. 18th Ed. (1992) APHA, AWWA, WEF, Washington, DC.

U.S. Army (1992) Field Manual 21-10. Field Hygiene and Sanitation.

Valentis, G. and Lesavre, J. (1990) Wastewater treatment by attached-growth micro-organisms on a geotextile support. Wat. Sci. Tech. 22, 1/2, 43.

DEWATERING CONTAMINATED, FINE-GRAINED MATERIAL USING GEOTEXTILES

D.A. GAFFNEY, P.E.
SYNTHETIC INDUSTRIES (USA)

S.M. MARTIN, EIT, CPESC
SYNTHETIC INDUSTRIES (USA)

M.H. MAHER, PH.D.
RUTGERS, THE STATE UNIVERSITY OF NEW JERSEY (USA)

T.A.BENNERT
RUTGERS, THE STATE UNIVERSITY OF NEW JERSEY (USA)

ABSTRACT

The ability of geotextiles to retain solids while passing liquid has lead to their use in dewatering fine-grained materials. Fine-grained materials such as dredged material from waterways, lagoon sediment or industrial waste products tend to have long and inefficient dewatering periods when allowed to dry by simply leaving the surface open to the atmosphere.

When fabricated into a tube, geotextiles act to contain the material and provide faster dewatering due to several factors. The objective of this paper is to provide basic information regarding the consolidation and dewatering of fine-grained materials within permeable tubes of various polymeric fibers and the retention of solids and pollutants within the geotextile tube.

Several laboratory tests and full scale projects have been conducted which are providing basic filtration, retention, consolidation and effluent water quality data. Additionally, these tests are verifying the efficacy of geotextile tubes and the cost effectiveness of this technology when compared to other methods of dewatering. An understanding of how dewatering occurs within a geotextile tube can be matched to specific project objectives to design the most appropriate and cost-effective application.

INTRODUCTION

The need for improved dewatering technology stems from the basic premise that saturated, fine-grained materials are typically bulky, have little or no value in their saturated state, and do not dewater efficiently on their own. For example, fine-grained cohesive dredged material consolidates to an equilibrium moisture content somewhat above the liquid limit with a relative consistency of warm axle grease (Haliburton, 1977). After reaching this state, the stress deformation relationship of the material is such that little additional settlement occurs from self-weight consolidation. In the dredging industry, this means that very large areas are required for the containment of dredged material. In other industries, sludge is the end product of a wastewater treatment system. Dealing with this sludge can be a costly problem.

Through laboratory testing and actual field use of geotextile tubes, it has been found that dewatering of fine-grained materials is enhanced when encapsulated within a permeable, woven geotextile. While this has been known for some number of years, the use of geotextile tubes for this purpose has not been widespread due to the lack of design guidance. In fact, most applications rely on trial and error. Even so, geotextile tubes provide a viable solution for some very difficult engineering problems.

This paper will present the results of field use and laboratory testing, and relate the data to the physical parameters of the geotextile tube/soil composite system. Dewatering concepts, geotextile properties and pertinent geotechnical principles are reviewed below.

RETENTION AND FILTRATION

During filtration, water in an encapsulated soil will seep through the manufactured plane of a geotextile driven by gradient and soil self weight while solid particles are retained. In traditional geotechnical filtration applications, a certain compatibility between the sizes of the soil particles and the sizes of openings through the geotextile is required when using a geotextile to retain solid particles while allowing water to escape (U.S. Army Corps of Engineers, 1997).

The method generally used to assure the retention of soils having a particular grain size distribution is based on the Apparent Opening Size (AOS) of the geotextile and is as follows (Task Force #25, American Association of State Highway and Transportation Officials (ASSHTO, 1990):

For soil with 50% or less particles by weight passing U.S. No. 200 sieve, the AOS of the geotextile must be less than 0.595 mm (AOS > No. 30 sieve).

For soil with more than 50% particles by weight passing U.S. No. 200 sieve, the AOS of the geotextile must be less than 0.297 mm (AOS > No. 50 sieve).

Apparent Opening Size is defined as the 95% opening size and is specifically measured using ASTM standard test ASTM D 4751-95. This test is conducted dry, using glass beads, and in some respects, does not replicate a wet geotextile under tension as would be the case while pumping a geotextile tube.

Several other criteria to assure retention have been developed. These often rely on the coefficient of uniformity of the soil ($CU=d_{60}/d_{10}$). It is unclear whether these have been applied to soil retention within geotextile tubes, but it is generally believed that a highly-uniform, fine-grained sediment can pipe through a tube under dynamic loads such as wave action. For filtration applications subject to cyclical loading such as in a wave or tidal environment, Schiereck (1998) provides the following criteria:

$$O_{98} < 2\, d_{85}$$

Where O_{98} = 98 percent of the grain size retained by the geotextile
and d_{85} = the 85^{th} percentile of the soil to be retained.

Leshchinsky (1992) notes that when the soil being filtered by a geotextile is a slurry containing clay, experience shows that the escape of particles through the geotextile stops rapidly and the seepage water becomes clear. This may occur due to clogging or blinding of the geotextile, and in a tube, can result in a filter cake which increases the filtration capability and decreases the permeability.

Clogging and Blinding. Clogging is the movement of soil particles into the voids of a geotextile, thereby reducing the hydraulic conductivity (also known as permeability) of the geotextile (Koerner, 1994). Schiereck (1998) states that clogging is a time dependant process which stabilizes after a certain period of time. Blinding similarly reduces the hydraulic conductivity by blocking the openings in the geotextile. A soil/geotextile composite which has blinded will typically have permeabilities very close to the soil itself and will exhibit very small amounts of fines passing through the geotextile (Austin, et al., 1997).

When discussing dewatering with geotextile tubes, the term "clog" tends to imply that water has completely stopped passing through the geotextile. Blinding is more often the case since soil particles build up a restrictive layer (filter cake) on the inside surface of the geotextile thus reducing the permeability of the geotextile but usually not eliminating water seepage. In fact, polyester fabrics being hydrophilic, tend to wick, allowing moisture to be removed from the tube through evaporation. Sludge within a polypropylene tube on the other hand, tends to desiccate against the geotextile shell.

Filter Cake and the Importance of Viscosity. The term filter cake comes from the use of specific cake resistance, often considered to be the key factor in the characterization of sludge dewaterability (Tosun, et al., 1993). The cake filtration equation is based on an analogy to Ohm's law for two resistances in series, one resistor being the filter and the other being the mass of solids forming the cake. Time, viscosity, pressure drops and resistance are the key parameters in the cake filtration equation. Darcy's law, however, is not used in the derivation of the cake filtration equation, with the result that when the permeability of the cake is compared to resistance, mathematical inconsistencies are noted (Tosun, et al., 1993).

From field experience with geotextile tubes, grain size alone is not a reliable parameter to predict the filtration capability of a particular geotextile. Viscosity appears to play a role. When considering the consolidation of clay (or extremely fine-grained particles), the water surrounding the particle must deform (Dunn et. al, 1980). This deformation is viscous in nature and the speed of the deformation is a function of the magnitude of the load placed on the material. The time lag associated with viscous resistance is called viscous lag, and when acting with hydrodynamic lag, form the processes by which consolidation occurs. The Terzaghi theory of consolidation, however, recognizes only hydrodynamic lag in determining settlement.

Multiphase filtration theories, which are improvements on the cake filtration equation, indicate that the high drag which occurs at the cake-filter interface controls the filtration rate (Tosun, et. al, 1993). The newer equations include a resistance function that relates the drag force to the velocity difference and is dependent on the viscosity of the liquid and the surface area of the solids.

Background. Previous tests conducted by the U.S. Army Corps of Engineers provide a background on the ability of geotextiles to provide for filtration and retention of soils. Filtration data were collected for a geotextile tube project at Nippersink Lake, Illinois (U.S. Army Corps of Engineers, 1997). The

dredged material contained volatile organics and was described as a peaty clay. The geotextile system was a composite of a nonwoven inner liner and a woven polypropylene tube. Test results showed that Total Suspended Solids (TSS) in the seepage water were a small fraction of the background water (meeting the Illinois Environmental Protection Agency regulation of no more than 15 PPM) and, that TSS decreased during the pumping process. This was reasoned to be due to blinding or clogging of the inside of the geotextile's openings.

There may not, however, be a need for an inner liner in most cases. Testing conducted by Moo-Young, et. al., (1998) indicated that a composite of geotextiles increased the filtering efficiency by, at most, 0.01%. Filtering efficiency (FE) was defined as:

$$FE = \frac{TSS_{initial} - TSS_{final}}{TSS_{initial}} X\ 100 \qquad (1)$$

Similar results were found during testing described herein using dredged material. This work will be described in more detail under the laboratory testing section.

PERMITTIVITY AND PERMEABILITY

Filtration is one of the most important functions of a geotextile. The relationships between permittivity, permeability and water flow are important in understanding filtration. To dewater fine-grained materials, the liquid must flow through the geotextile and the dewatering soil itself. Permittivity describes the cross-plane permeability (or hydraulic conductivity) and is defined as:

$$\psi = \frac{k_n}{t} \qquad (2)$$

where ψ = permittivity,
k_n= the permeability coefficient (hydraulic conductivity) normal to the geotextile, and
t = the thickness of the geotextile.

Substituting the above equation into Darcy's formula yields the following:

$$q = k_n iA$$
$$= k_n \frac{\Delta h}{t} A$$
$$\frac{k_n}{t} = \psi = \frac{q}{(\Delta h)(A)} \qquad (3)$$

where q = the flow rate,
i = the hydraulic gradient = Δh/t,
Δh = the head loss, and
A = the total area of geotextile test specimen.

This implies that water flow rate and permittivity are directly proportional assuming the head loss and area are constant (see table 1).

As with soil permeability testing, the above formula is used for constant head tests. The flow rate (q) is measured at different values of Δh, and when ΔhA versus q is plotted, the slope of the resulting straight line yields the desired value of ψ (Koerner, 1994).

Sample	Type	AOS (Sieve No.)	Permittivity (sec^{-1})	Water Flow Rate (gal/min/ft2)
A	PP, nonwoven, 12 ounce	100	1.00	75
Separation Fabric	PP, woven slit film	40	0.07	6
Filtration Fabric	PP, woven monofilament	70	0.28	18
Reinforcement Fabric	PP, woven, 400 X 400 #/in tensile strength	30	0.60	45
B	PP, woven, 400 X 600 #/in tensile strength	40	0.3	20
C	PET, woven, 1200 X 1200 #/in tensile strength	40	0.1	3
D	PET, woven, 1000 X 1000 #/in tensile strength	40	0.3	18
E	PET, woven, 1000 X 1000 #/in tensile strength	60	0.1	6

Table 1 - Minimum Average Roll Values of drainage properties of tested geotextiles

In the laboratory tests described herein, the permeability of the soil/geotextile mass was found to change both with time and distance away from the surface during the lab testing.

CONSOLIDATION WITHIN A GEOTEXTILE TUBE

Tubes achieve a natural height dependent on the pressure of pumping and the density of the fill material. For sandy materials, the tube will consolidate quickly and will retain nearly its original height. For fine-grained sludges and dredged material having a high water content (low percent solids), tubes will decrease in height as water is expelled and the material consolidates within the tube. The amount of consolidation (settlement) is typically related to the void ratio of the material. The void ratio is defined as the volume of the voids divided by the volume of the soil solids. The void ratio and load (or pressure) are two parameters typically used to calculate settlement.

Rate of Consolidation. Terzaghi and Peck (1948) presented the traditionally used theory to describe the time rate of consolidation of clay soils. A coefficient of consolidation, c_v, is calculated for each load increment based on consolidation tests, and is a function of the permeability and the coefficient of

volume decrease. The rate of consolidation can be estimated using a time factor, T, which is a function of the degree of consolidation, U.

In dredge disposal studies the length of the shortest drainage path is particularly important and results in the following equation (Salem, et al., 1977):

$$c_v = \frac{T\,h^2}{4\,t} \tag{4}$$

where t = time
h = the length of the shortest drainage path
T = time factor which is a function of the degree of consolidation

Several filtration and consolidation factors are enhanced by dewatering within a geotextile tube. The filtration surface area is increased by encapsulating the material in an oval container. Drainage paths are optimized and pressure (or self weight) is maximized due to the geometry of the tube.

Tubes filled with various sludges during the field testing portion of this study decreased in height at rates and magnitudes similar to Fowler, et al. (1996) and Miki, et al. (1996). That is, height decreased rapidly during the initial hours and days and slowed with increasing time. Both lagoon waste from a pig farm and sludge from a waste water treatment facility reached acceptable levels of percent solids in two to three weeks.

The equation for predicting consolidation within a tube developed by Leshchinsky, et al., (1996) is based on the experience that the height of the tube drops while the maximum width changes very little. When plotted for various ratios of initial slurry unit weight to the unit weight of water, equation 5 provides an approximate estimate of the average drop in height:

$$\frac{\Delta h}{h_o} = \frac{G_s(\omega_o - \omega_f)}{1 + \omega_o G_s} \tag{5}$$

where Δh = decrease in the height of the tube
h_o = initial height of the tube
G_s = specific gravity of the solids
ω_o = initial water content of the fill material
ω_f = final water content of the fill material

None of the preceding theories or equations can be used to predict which style of geotextile will dewater best for a particular sludge, or help the project designer determine the optimum tube size and geometry. Laboratory testing was conducted to lend further insight into the interaction of the geotextile and fine-grained material during dewatering.

LABORATORY TESTING

Dredged material from New York Harbor was used for laboratory testing of various geotextiles. The purpose was to determine the optimum geotextile for confining this potentially contaminated fine-grained material within a tube. Filtration testing was conducted under accelerated conditions to simulate long term dewatering.

Grain size analysis was conducted on the dredged material via sieve and hydrometer. The dredged material was comprised of 85 % silt, 12 % clay, and 3 % fine sand and shell fragments (Figure 1). The dredged material was placed in a column and allowed to drain through a geotextile. Accelerated conditions were achieved by drawing a vacuum below the geotextile to collect effluent water. Water was collected for a standardized 24 hours. After this period of time, visible dewatering had ceased and

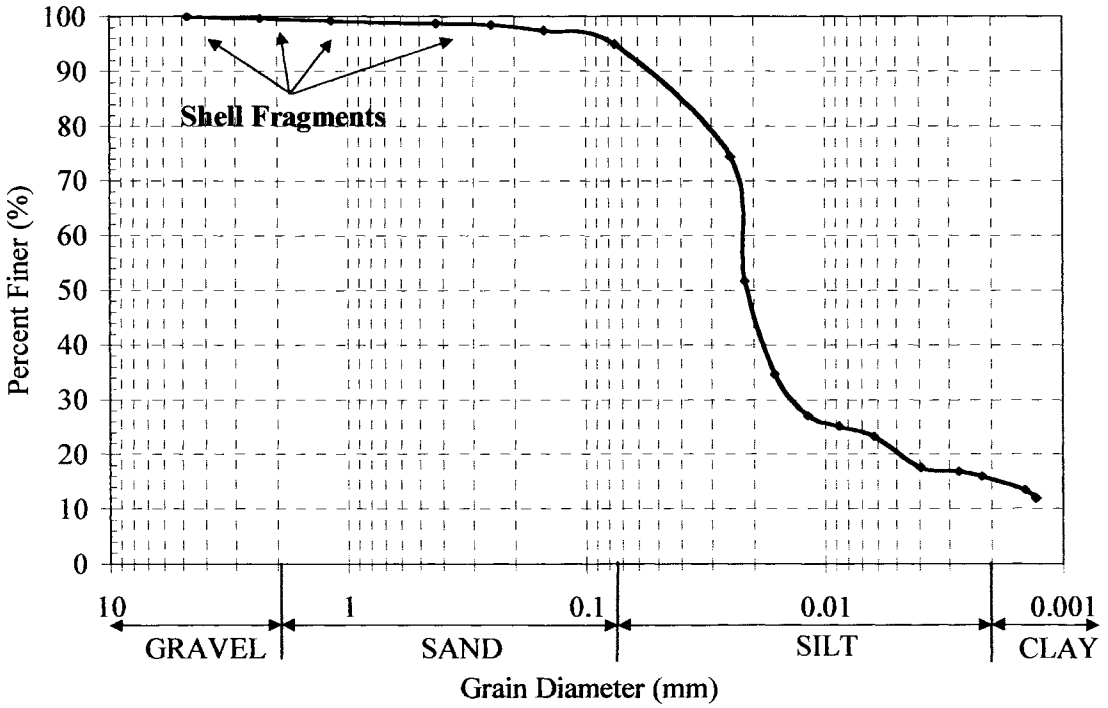

Figure 1 – Grain Size Distribution of New York Harbor Dredged Material

the effluent was sent to a water quality lab for testing. Table 2 shows the characteristics of the dredged material before filtration and the collected effluent after the 24-hour period. All of the geotextile styles performed well, however it is important to note that the addition of a nonwoven (A+B) did not provide a significant increase in performance and may have hindered volume reduction (ie. consolidation).

The retained dredged material was analyzed for its moisture content and percent solids. It was found that material closest to the geotextile had the highest percent solids. This change in void ratio with distance (i.e. dynamic vertical consolidation) is believed to result in a decreasing permeability of the soil/geotextile interface. This factor, plus probable blinding of the material, retarded further dewatering of the dredge mass.

Sample	% Solids of Contained Mat'l		Volume Reduction	TSS mg/L	Chromium ug/L	Lead ug/L
	Initial	Final				
Raw	n/a	n/a	n/a	38,541	84,800	88,700
A+B	34.0	42.3	19.0	74	Not Detected	410
B	32.8	43.0	24.3	80	Not Detected	520
C	33.6	42.5	17.5	145	250	460
D	34.1	43.6	26.2	98	Not Detected	1200
E	32.6	42.1	20.0	90	Not Detected	660

Table 2 – Characteristics of Raw Dredged Material and Filtered Effluent Water

Figure 2 illustrates the phenomena of decreasing permeability and blinding in dredged material from New York Harbor. To eliminate units in the analysis, the parameters of 'moisture content' and 'distance from geotextile/dredge interface' are divided by 'initial moisture content' and 'diameter of dredge contact area (dia_{ca})', respectively. A logarithmic increase in moisture content develops as the distance from the geotextile/dredge interface increases. If the trendline is extended, as shown in the figure, an interesting situation can be postulated. If evaporation were not to occur, the moisture content at a distance 1.3 times the dia_{ca} away from the geotextile/dredge interface, would remain constant. This would imply that smaller circumference tubes would dewater to a greater percent solids on average than larger tubes. Since the polyester continues to wick away moisture, however, dewatering is not expected to completely stop. Experience shows that given sufficient time, very-fine grained dredged material will continue to dewater to a very low moisture content.

If the data points representing the composite A+B filter are removed, R^2 increases. This may point to the added complexity of the cake-filter interface when two geotextiles are used.

The result of both the laboratory testing and field applications for some fine-grained materials used in geotextile tubes, is that dewatering results in a drier, outer layer surrounding a higher moisture content center. Miki et al. (1992) reported similar findings for fill material with a very high percentage of clay (82.4%). A schematic of this scenario is shown in Figure 3.

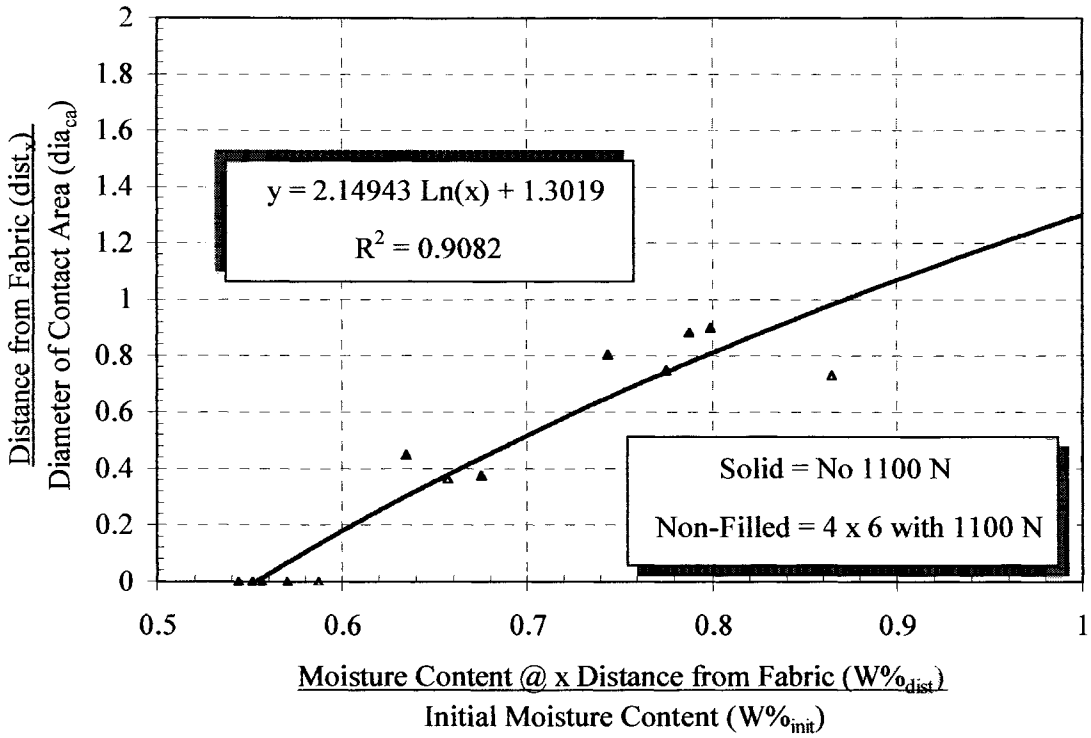

Figure 2 – Normalized Illustration of Decreasing Permeability and Blinding of Dredged Material (for moisture content above 0.87 the curve is extrapolated)

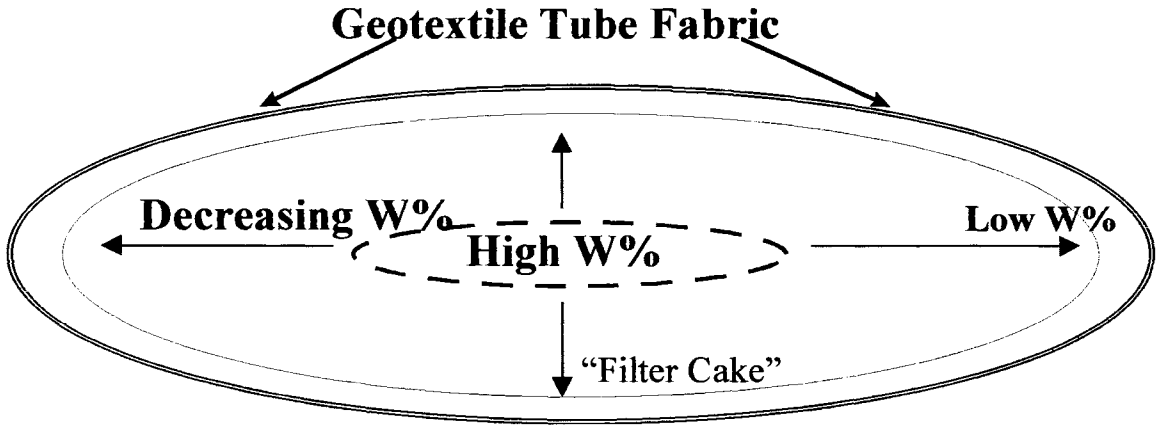

Figure 3 – Possible Dewatering Characteristic of Geotextile Tube/Dredge Material Drainage

Drainage distance (see equation 4) is therefore an important consideration. A geotextile tube will contain a certain volume (cross sectional area times a unit length) depending on its initial circumference and the height to which it is pumped (see Figure 4). A thirty-foot circumference (9.15m) tube costs more than a fifteen-foot (4.57m) tube, but will contain much more sludge. For the same unit volume however, a fifteen-foot circumference tube would have a shorter drainage distance and could be expected to dewater faster and more completely than the thirty-foot tube. For the same total volume, however, a fifteen-foot circumference tube would need to be roughly four times as long, therefore requiring more space for dewatering.

For the dredged material used in the laboratory testing, the most efficient retention and dewatering occurred with a single layer of woven polypropylene (style B). Since polypropylene does not wick, it is unknown how this fabric would compare to polyester over the long term in a field situation. Further testing of various types of fine-grained materials need to be tested and compared to field results in order to determine the relationship of accelerated testing to field dewatering in a tube.

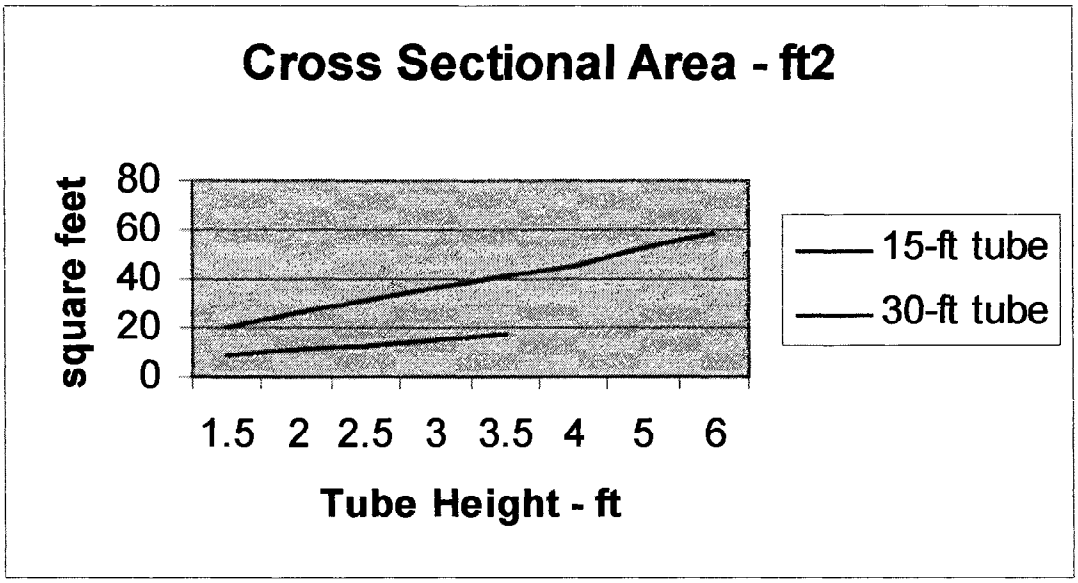

Figure 4 - Geotextile tube capacity for 15-ft (4.57m) and 30-ft (9.15m) circumference tubes

FIELD TESTING

Industrial Retention Project. Geotextile tubes were used in two recent projects which demonstrate the ability to dewater and contain contaminated materials. The first was a project in Seattle, Washington, in October of 1997, where a dewatering system was used to dewater chemically-treated stormwater to improve the overall quality of water entering the environmentally sensitive waterway. The Port of Seattle, responsible for managing the SEATAC International Airport, was having a problem meeting water quality standards from their stormwater discharge. The port was in the process of constructing a 30-acre parking lot when the fall rains started. Construction was still in the grading stages. The existing stormwater control system failed and was not capable of treating the stormwater to the desired level to meet water quality standards. Fine sediments from the site exceeded the turbidity.

A water quality criterion used by the Department of Ecology to measure contaminant concentration is based on total suspended solids measured in Nephelometric Turbidity Units (NTU). An NTU is a qualitative, rather than quantitative way of measuring turbidity. It is calculated by measuring the dispersion of a light beam passed through a water sample. Fine particles such as clay, silt, organic and other suspended matter will cause a beam of light passing through the water sample to be scattered. It has been determined that the amount of scattering is proportionate to the amount of turbidity present. The higher the NTU number, the more the beam of light is scattered. There is a direct correlation between the higher NTU value and particle size distribution within the water sample. Since clay and silt

particles (<0.00195 mm and 0.047 to 0.00195 mm, respectively) remain in suspension for longer periods of time, a higher NTU value indicates a higher concentration of these particles from urban areas. The acceptable range for human consumption is 1 to 5 NTUs.

The Department of Ecology's Water Quality Standards require that the turbidity in the receiving stream not exceed 5 NTUs above background from the source. This limit translated into a treatment standard of 25 NTUs for parking lot storm water discharge. Parametrix, Inc., an environmental consulting firm, designed a treatment system to meet the criteria. During the one-month design and construction stage, stormwater was hauled to Port property and disposed of on land at considerable cost, or be faced with a potential penalty of $10,000 per day.

A batch chemical treatment system was designed and installed which included three 20,000-gallon settling tanks, one 20,000 gallon sludge storage tank, and two geotextile tubes to dewater the contents in the sludge tank. Alum and caustics were injected into the stormwater prior to the settling tanks. The sludge from the bottom of the settling tanks was pumped to the sludge tank and allowed to settle again. Sludge from the sludge tank was pumped periodically into the geotextile tubes for further dewatering.

The tubes were 15.2 m (50 feet) long and 9.15 m (30 feet) in circumference, consisting of a woven polypropylene inner tube (sample fabric B) and a non-woven outer shell. When pumped full with sludge, tube heights were about 1 m (3.1 feet) high. Two tubes were used so that they could be filled on an alternating basis. It took up to 12 hours before the tubes were filled. Analysis of the discharge water (effluent) from the tube system was measured to be less than 8 NTUs.

For a short period, before the installation of the geotextile tubes, the sludge from the sludge tanks was hauled to a landfill at a cost of $66 per ton of sludge (approximately 10% solids) plus $125 per hour handling charge.

The geotextile tubes provided a significant cost savings. The cost per tube was $900. Only three tubes were needed for the seven month operation of the treatment system. For final disposal of the tube contents, the tubes were slit open, and the dirt was used for fill at the site. The empty tubes were hauled to the local landfill for disposal.

Waste Water Treatment Project. In a second project, geotextile tubes were successfully used to contain and dewater approximately 1,400 cubic yards (288,800 gallons) of tannery waste. Production at the tannery had outpaced the capacity of the wastewater treatment system. Tubes were used as a cost-effective alternative to belt presses and filter presses because of their capacity, and the ability to be filled quickly. Presses can only treat small amounts of waste at a time, therefore this method did not allow adequate response time to get ahead of the problem. Rental of this equipment was proving to be very expensive when compared to material costs, mobilization and pumping of the geotextile tubes.

The tube dewatering site was prepared by grading the area and lining it with an impermeable plastic sheet. Water draining from the tubes during dewatering was to flow into a sump to be pumped back into the waste collection system.

Five permeable geotextile tubes of various fabrics and weaves were used. One tube was fabricated from polypropylene, and the remaining tubes were made of high strength polyester (see figure 5). The

polypropylene tube was made from sample fabric B and was 40 feet (12.2 m) in length and 15 feet (4.57 m) in circumference. This tube was originally pumped to a height of approximately 3 feet (0.9 m). As it dewatered, the tube decreased in height and was able to be pumped full a second time.

Figure 5 – On site dewatering of sludge within polyester and polypropylene geotextile tubes

The polyester tubes were 30 feet (9.15 m) in circumference, with lengths ranging from 40 to 200 feet (12.2 to 61.0 m). Geotextiles used were sample fabrics C, D, and E. Two of the shorter tubes were pumped three times. The 200 linear foot tubes were placed in a "U" shape.

Polyester has different hydraulic properties than polypropylene. The polyester fibers are hydrophilic. During pumping, the polyester geotextile becomes wet and the weave becomes very tight. Effluent solids as small as 0.45 microns in size were retained within the tube. During dewatering, the polyester continues to weep water and lose moisture to evaporation. Polypropylene on the other hand, is hydrophobic, and apparently retains solids by forming a surface tension at the wall of the tube.

A sample of sludge pumped into the tube had a Total Suspended Solids (TSS) of 441 grams/liter. The water seeping from the tube during pumping had a TSS of 0.65 g/l. Using equation 1, a filtering efficiency of 99.998% was obtained. As one might expect, there was no significant difference in the Total Dissolved Solids. Chromium within the sludge was reduced from 3.370 mg/l to 0.8437 mg/l in the water seeping from the tube.

Two types of sludge were pumped into the tubes. Primary waste from the plant was pumped directly into the 200-foot tubes bypassing the oxidation ditch. Biological (anaerobic) sludge was pumped from the secondary clarifier into the smaller tubes. Both sludges experienced rapid dewatering of bulk water during the pumping process. Once in the tubes, however, the two sludges behaved differently. The primary effluent released water held by surface tension quicker than the biological effluent. After two

weeks, the primary effluent had reached a percent solids of greater than 25%. The criteria for landfilling is 17%, therefore the primary effluent was ready to be excavated from the tube and disposed of.

Two types of dewatering occurred in the tubes. Initially, the dewatering was mechanical due to pumping, then, passive dewatering occurred over a period of weeks. Dewatering was apparently uniform throughout the tube filled with primary waste (see table 3). For the biological sludge, greater desiccation occurred near the surface of the tubes. The sludge in the center of the fifteen foot (4.57 m) circumference tube dewatered slightly better than the 30 foot (9.15 m) circumference tube, presumably due to a shorter drainage distance.

Sludge	Geotextile Tube	Percent Solids (after 2 weeks)
Original sludge pumped into the tubes		10.38%
Primary waste. Consistent density throughout tube.	Sample fabric C, polyester, 30-ft circumference. 200 linear feet.	25%
Biological sludge. Top of tube.	Sample fabric B, polypropylene, 15-ft circumference	30%
Biological sludge. Middle of tube.	Sample fabric B, polypropylene, 15-ft circumference	21%
Biological sludge. Top of tube.	Sample fabric C, polyester, 30-ft circumference. 100 linear feet.	24%
Biological sludge. Middle of tube.	Sample fabric C, polyester, 30-ft circumference. 100 linear feet.	18%

Table 3 – Dewatering results for various geotextiles and sludges

Fowler (1996) reported similar measured percent solids for dewatering sewage sludge in a geotextile tube. Of interest is that measured values were higher than calculated. Fowler suggested that the increase was due to the three-dimensional drainage and consolidation which occurs in a tube.

Geotextile tubes provided a cost-effective alternative to sludge presses when quick containment of a large volume of sludge was required. When one considers the cost of regulatory fines and a potential plant shut down, the use of tubes was far more cost effective than traditional technology which was unable to accomplish the intended purpose.

CONCLUSIONS

The results of this work, and particularly the full scale field projects successfully demonstrate the use of geotextile tubes for retaining and dewatering various fine-grained materials as well as the containment of various contaminants. In both field tests the client saved money over traditional methods. With a material cost of approximately $900.00 per tube, the Seattle system provided significant cost savings over alternative methods of treating stormwater runoff from urban environments and prevented fines of $10,000 per day.

The tannery project successfully solved a problem for which no other practical alternative existed. By containing large quantities of tannery sludge in a cost-effective manner, the plant was able to return to optimal operating conditions. This allowed the plant operator to re-establish proper waste management parameters such as odor, pH, and acceptable solids level in the oxidation ditch and the secondary clarifier bringing the company back into regulatory compliance.

When added to existing literature in this field, the data collected is clarifying how fine-grained materials dewater when contained within a geotextile tube. Typical geotextile parameters such as Apparent Opening Size were not found to be significant when compared to the permeability of the geotextile/soil system. It appears that tube dewatering will eventually be described by a combination of filter cake and Terzaghi consolidation theories. In laboratory testing, fabric style had small impacts on the ability to retain solids and contaminants. In the field, dewatering was apparently related more to the content and consistency of the fill material than to its size relationship to the geotextile. Additionally, drainage path distance and surface area were found to be related to volume reduction (consolidation). These factors are important considerations for the engineer to design the appropriate size dewatering application using geotextile containment systems.

Data supports the conclusion that an additional nonwoven layer does not appreciably improve the filtering efficiency as measured using Total Suspended Solids for static dewatering applications. Given time, fine-grained materials contained within a single-layer, geotextile tube will dewater to a low moisture content.

FURTHER RESEARCH

The relationship of *in situ* viscosity to the rate of consolidation, settlement and style of geotextile tube warrants further research. While this parameter is probably not the most important in determining final dewatered characteristics, it may hold the key to optimizing the style of geotextile for a particular material such as sludge, dredged material, or lagoon waste. Testing of a wide variety of fine-grained materials need to be continued to distinguish which data are most important to collect prior to designing a geotextile tube dewatering project.

A comparison of accelerated laboratory test results to full size tube dewatering for the same fine-grained material will provide a reality check for the test. If the test accurately replicates tube dewatering, a time correlation between testing and field dewatering can be developed.

ACKNOWLEDGMENTS

The authors would like to acknowledge Synthetic Industries for supplying all necessary geotextiles for this project.

REFERENCES

American Association of State Highway Officials (AASHTO), 1990. "Guide Specifications and Test Procedures for Geotextiles," *Task Force Report #25*, AASHTO-AGC-ARTBA, Washington, DC.

Austin, D.N., Mlynarek, J. and Blond, E. (1997). "Expanded Anti-clogging Criteria for Woven Filtration Geotextiles," *Geosynthetics '97 Conference Proceedings*, March 11-13, 1997, Long Beach, CA, pp. 1123 – 1144.

Dunn, I.S., Anderson, L.R., and Kiefer, F.W. (1980). "Fundamentals of Geotechnical Analysis," John Wiley & Sons, New York.

Fowler, J., Bagby, R. and Trainer, E. (1996). "Dewatering Sewage Sludge with Geotextile Tubes." *Proceedings of the 49th Canadian Geotechnical Conference*, September 23-25, 1996, St. John's, New Foundland, Canada.

Gerry, G.S., and Raymond, G.P., (1983). "The In-Plane Permeability of Geotextiles," *Geotechnical Testing Journal*, ASTM, Vol. 6, No.4, December 1983, pp. 181-189.

Haliburton, T.A., (1977). "Research to Dewater Dredged Material," *9th Dredging Seminar*, Center for Dredging Studies, CDS Report No. 206, Sea Grant Report TAMU-SG-77-115, October 1977.

Koerner, R.M., (1994). "Designing with Geosynthetics," Third Edition, Prentice Hall, Upper Saddle River, NJ.

Leshchinsky, D. (1992). "Issues in geosynthetic-reinforced soil." *Proc. Int. Symp. On Earth Reinforced Pract.*, Balkema, Rotterdam. Kyushu, Japan, pp. 871-897.

Leshchinsky, D., Leshchinsky, O., Ling, H.I., and Gilbert, P.A. (1996). "Geosynthetic Tubes for Confining Pressurized Slurry: Some Design Aspects." *Journal of Geotechnical Engineering*, Vol. 122, No. 8, August 1996.

Miki, H., Yamada, T., Kokubo, H. Takahashi, I. and Sasaki, T., 1996. "Experimental Study on Geotextile Tube Dehydration method of Dredged Soil," *Geosynthetics: Applications, Design and Construction*, DeGroot, Den Hoedt and Termaat (eds), Balkema, Rotterdam.

Moo-Young, H., Meyers, T., and Townsend, D. (1998). "Evaluation of Geosynthetic Fabric Containers to Contain Contaminated Dredged Sediment," *Sixth International Conference on Geosynthetics*, 25-28 March, 1998, Atlanta, Georgia.

Salem, A.M., Krizek, R.J., and Azzouz, A.S., (1977). "Preliminary Consolidation and Compressibility of Dredgings," *9th Dredging Seminar*, Center for Dredging Studies, CDS Report No. 206, Sea Grant Report TAMU-SG-77-115, October 1977.

Schiereck, G.J., (1998). "Filter Structures," *Dikes and Revetments*, Pilarczyk (ed), Balkema, Rotterdam.

Terzaghi, K. and Peck, R. (1948), "Soil Mechanics in Engineering Practice," First Edition, John Wiley & Sons, New York.

Tosun, I., Yetis, U., Willis, M., and Chase, G., (1993). "Specific Cake Resistance: Myth or Reality?" *Water Science and Technology*, Vol. 28, No. 1, pp. 91–101, 1993.

U.S. Army Corps of Engineers (1997). "The Development and Demonstration of Dredged Material Containment Systems Using Geotextiles," Draft Technical Report.

A GRADIENT RATIO DEVICE FOR COMPATIBILITY TESTING IN CYCLIC FLOW

R. J. FANNIN
UNIVERSITY OF BRITISH COLUMBIA, CANADA
A. HAMEIRI
UNIVERSITY OF BRITISH COLUMBIA, CANADA

ABSTRACT

There is considerable variation in the empirical design guidance used for geotextile filtration applications, where flow is dynamic, pulsating or cyclic in nature. A new cyclic gradient ratio test device is described, with reference to the permeameter, loading system, hydraulic supply, a particle collection trough and flow measurement system. Specific emphasis is placed on design features to impose a head-controlled reversing flow through the permeameter. Discussion addresses the need for automated recording of the water head distribution, and hence value of gradient ratio, using pressure transducers.

INTRODUCTION

A distinction is made between unidirectional flow and reversing flow in filtration design using geotextiles. It is believed that a natural bridging network is induced in the soil adjacent to the geotextile during unidirectional flow: a filter zone develops progressively within the soil that is a reverse granular filter constructed from the in-situ soil (Lawson, 1982). This network may not develop under reversing flow, where the influence of changing direction of flow and associated seepage forces acts to destabilize such a network (Giroud, 1982; Kohler, 1993). Specific concerns address the change in effective confining stress that may induce a partial liquefaction of the soil, particularly under the relatively low magnitudes of vertical stress which are typical of erosion control structures.

A significant body of test data exists to describe soil/geotextile interaction for undirectional (steady state) flow, and validate design criteria for soil retention (Faure and Mylnarek, 1998). The two requirements are firstly an absence of continued piping of fine soils through the geotextile after formation of the filter zone, which leads to internal erosion, and

secondly entrapment of fine particles on the upstream face of the geotextile, which leads to clogging of its pores. In contrast, few data exist to describe behaviour under reversing flow. In this paper we describe a new gradient ratio test device that enables a cyclic flow to be imposed on the soil-geotextile filtration zone. The objective of the work is to critically evaluate the empirical relationships used for material specification in applications where cyclic flows dominate, such as marine construction and river erosion control. Experience gained in the design and fabrication of the test device is reviewed in the context of ASTM D5101.

EMPIRICAL DESIGN GUIDANCE

Design guidance is limited to empirical relationships that relate a characteristic pore opening size of the geotextile to one or more soil particles sizes. For example, in situations of dynamic, pulsating and cyclic flow that are typical of rock armour applications in erosion control Holtz et al. (1997) recommend for soil retention against piping:

$$O_{95} \leq 0.5\ D_{85} \tag{1}$$

where 0_{95} is the characteristic opening size of the geotextile and D_{85} is the characteristic particle size of the soil, irrespective of the soil gradation adjacent to the geotextile. They observe that "it is best to maintain sufficient weight or load on the filter to prevent particle movement".

Earlier USFHWA regulatory guidance (Christopher and Holtz, 1985) required

$$O_{50} \leq 0.5\ D_{85} \tag{2}$$

with a modification that:

$$O_{95} \leq D_{15} \tag{3}$$

if the soil can move beneath the geotextile and is coarse-grained ($D_{50} \geq 0.074$mm). The more recent change from O_{50} was made to facilitate practical specification documents (Holtz, 1998). The Canadian Geotechnical Society (CGS) Canadian Foundation Engineering Manual (1992) uses the latter modification of $O_{95} \leq D_{15}$ for coarse-grained soils and, for fine-grained soils ($D_{50} \leq 0.074$mm), requires:

$$O_{95} \leq 0.5\ D_{15} \tag{4}$$

$$O_{95} \leq 0.3\ \text{mm} \tag{5}$$

The CGS (1992) requirements yield a smaller opening size given their characterization of the soil by D_{15} rather than D_{85}. Further, the use of the Filtration Opening Size (FOS) from

hydrodynamic sieving or the Apparent Opening Size (AOS) from dry sieving is specifically acknowledged in design. In summary, there is considerable variation in the empirical relationships used for design. This is attributed to few laboratory studies of the behaviour, and no validation of the proposed relationships in any program of testing. One test method that is well-suited to these needs is the gradient ratio test, the development of which is briefly described below by way of an introduction to a new configuration of the device for cyclic testing.

THE GRADIENT RATIO TEST

Performance tests, such as the gradient ratio test (ASTM, 1996) are used to assess directly the compatibility of soil and geotextile in unidirectional (steady state) flow. Proposed by the U.S. Army Corps of Engineers in 1977, it was first published as a test method by ASTM in 1990. A rigid wall permeameter accommodates a cyclindrical soil sample and a geotextile specimen.

Measurements of hydraulic head are taken at several ports on the apparatus and used to establish the variation of hydraulic gradient through the soil and across the geotextile (see Fig. 1). Flow rate through the system is measured and used to calculate the permeability of the composite system. The gradient ratio is defined by the ratio of the hydraulic gradient in the soil-geotextile composite (i_{sg}) to that in the soil (i_s), where with reference to port locations 3, 5 and 7 (see Fig. 1):

$$GR_{ASTM} = i_{sg} / i_s = i_{57} / i_{35} \quad (6)$$

Early work by Haliburton and Wood (1982) led to an assessment of soil/geotextile compatibility based on the value of gradient ratio. A value less than one indicates a migration of adjacent fines through the geotextile leading to a more permeable zone immediately upstream of the geotextile. An unacceptable loss of fines is deemed to be a piping failure. In contrast, entrapment of any fines on or within the geotextile will lead to a less permeable zone, and a gradient ratio greater than one. A criterion of $GR_{ASTM} < 3$ has been proposed for clogging, but its application is limited by few test data (Christopher and Holtz, 1985).

In a recent development, Fannin et al. (1994) suggested an additional port, which is much closer to the geotextile than that specified in ASTM D5101, provides an enhanced index of i_{sg}. The position of port 6, a distance of 8mm above the top surface of the geotextile, yields a modified gradient ratio:

$$GR_{mod} = i_{67} / i_{35} \quad (7)$$

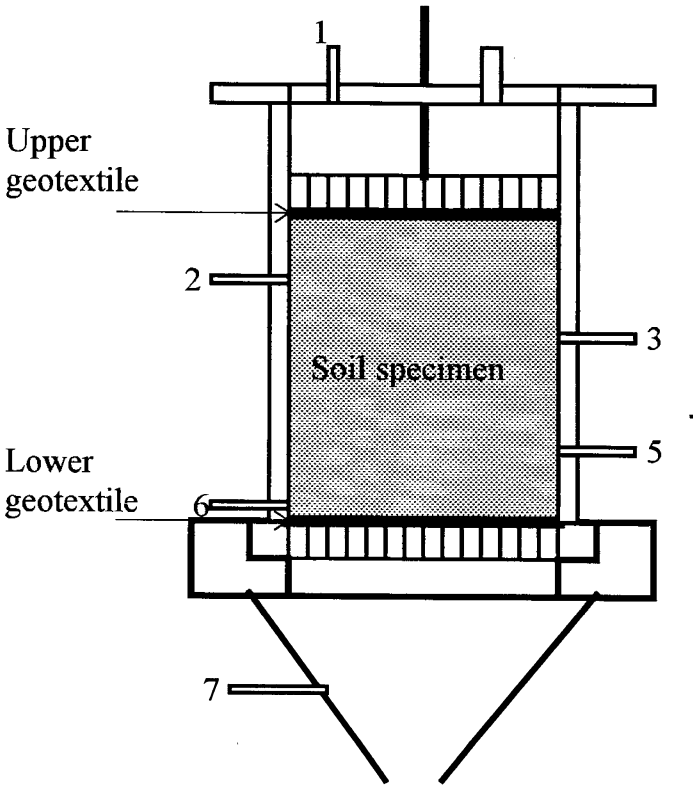

Port	Location
1	On top plate.
2	101mm above the geotextile.
3	75mm above the geotextile.
5	25mm above the geotextile.
6	8mm above the geotextile.
7	Below the sample.

Fig. 1: Gradient ratio test device: location of ports

which has been found to be a more sensitive indicator of flow restriction than GR_{ASTM}, and therefore easier to interpret. The use of such an additional port location is now receiving greater attention (Austin et al., 1997).

A CYCLIC GRADIENT RATIO TEST DEVICE

The test device comprises a rigid-walled permeameter which contains the soil specimen and geotextile sample; a loading system to apply a vertical confining stress; an hydraulic supply to impose cyclic flow through the device; a collection trough; and a flow measurement system. Components of the test device (see Fig. 2) are illustrated schematically in Fig. 3, and described in detail below.

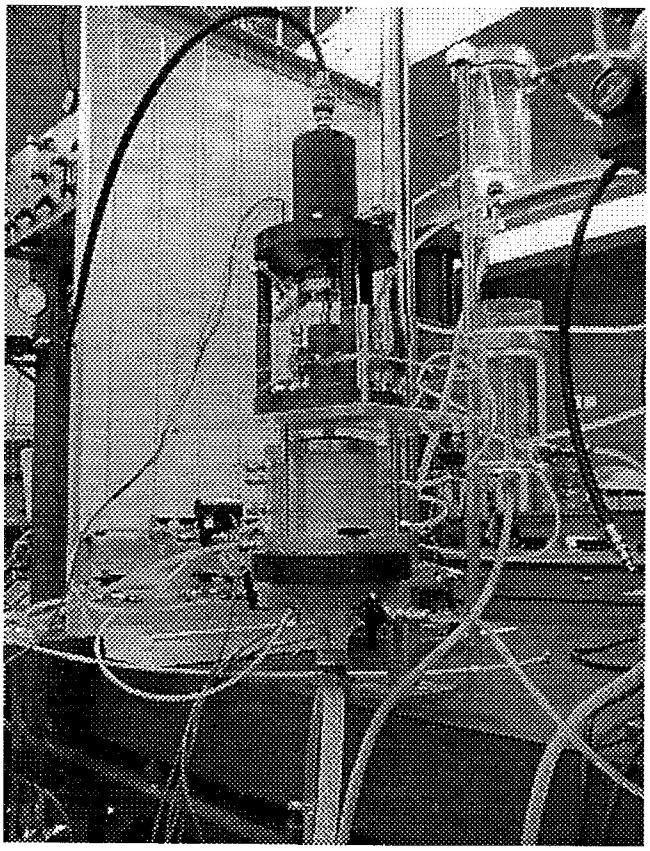

Fig. 2: A new cyclic gradient ratio test device

Permeameter

The permeameter is made of anodized aluminum and plexiglass. The rigid wall (a) is made of 8 mm thick plexiglass, to permit visual observations of the soil specimen during testing, and accommodates a specimen of diameter 102 mm and length approximately 125 mm. Visual observations have proved valuable to interpretation of test behaviour, especially for clogging of the geotextile.

The soil specimen has a geotextile sample placed above and below it (see Fig. 1). The lower geotextile seats on a coarse wire mesh placed on a rigid bottom plate (b) that is approximately 8 mm thick and perforated with many holes of 2 mm diameter on a triangular spacing of 3 mm. The upper geotextile is located between the soil and the top plate (c) connected to the loading piston. A circular insert to the plate is 6 mm thick, and also perforated with many holes of 5 mm diameter on a triangular spacing of 12 mm. A fine wire mesh is used to cover the lower surface of the insert where it is in contact with the geotextile. Water flow passes through large openings in the top plate and across the perforated insert. The cell top and base are made of anodized aluminum.

Manometer ports are located on the cell top, at four locations on the wall of the permeameter, and on the cell base (see Fig. 1). The locations are numbered 1 to 3, and 5 to 7, sequentially. The ports comprise a small hole with a 125 micron polyethylene filter. Water pressures are recorded with a series of differential pressure transducers. They are used to monitor the distribution of water head, and deduce the values of gradient ratio.

Loading system

A constant value of vertical stress is applied to the top of the soil specimen through the load piston (d). The clearance between the top platen and the walls of the permeameter is 50 microns. Air pressure is applied to the piston using a regulator. The cell top is clamped by three reaction bars to the cell base. The position of the load piston is monitored with a displacement transducer, to determine changes in sample length during testing.

Hydraulic supply

In laboratory testing of porous media to deduce permeability, the flow of water can be controlled in one of two ways: by a constant head device on the inlet and outlet of the permeameter (head-control), or by a flow pump across the permeameter (flow-control). The configuration of the cyclic gradient ratio test device uses head-control to reverse the direction of flow across the soil/geotextile interface. This option was selected in recognition of many construction applications that are governed by a head difference or hydraulic gradient across the filter zone.

Head-control is imposed by three constant-head tanks, termed the inlet (i), the inlet-outlet (i-o) and outlet (o) tank. The imposed hydraulic gradient is controlled, for a given soil specimen length (L), by the equidistant head difference (H) between the three tanks (see Fig. 3). The switching system employs a solenoid valve (s) that is computer-controlled. A downward hydraulic gradient in the test specimen has the inlet-outlet tank routed through the cell top, and discharge from the cell base routed to the outlet tank. Conversely, by switching the valve, an upward gradient is imposed by routing the inlet tank through the cell bottom and taking discharge flow from the cell top to the inlet-outlet tank. As a result, the inlet-outlet tank serves two functions, and the top of the specimen is maintained at a constant water head throughout the test.

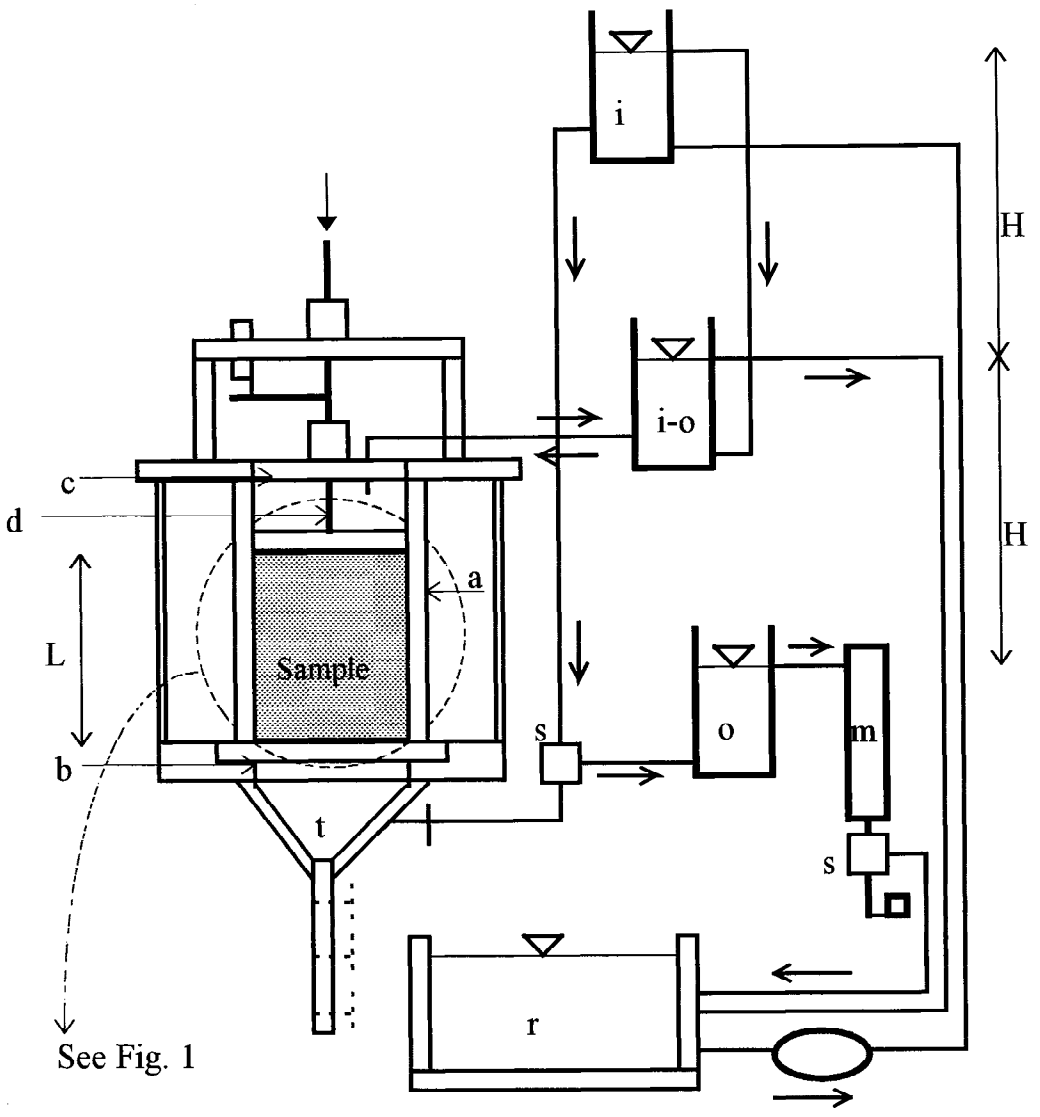

Fig. 3. Schematic view of the test device

Collection trough

Any study of soil retention criteria requires the particles that pass through the geotextile be gathered for characterization of size and gradation. Therefore a collector trough (t) is located below the cell base. It comprises a plexiglass funnel and sump of flexible polyethylene tube. Particles that migrate through the geotextile are directed by the funnel into the tube. A series of discrete samples can be captured at any time during sample preparation and testing by clamping across the tube to seal it in individual sections. After testing the tube is removed and the discrete

samples flushed from it section-by-section for particle size analysis. The transparent walls again allow for visual inspection of the behaviour.

Flow measurement system

The three constant-head tanks connected to the permeameter are recharged with deaired water, from a reservoir (r), by a peristaltic pump. Overflow water returns to the reservoir. Discharge water from the permeameter to the outlet constant-head tank is taken, by overflow, to a measuring tank (m) for determination of the flow rate. The rate is deduced from automatic recording of water head in that tank with time, using a pressure transducer. The tank is emptied periodically by a solenoid-controlled valve (s).

SUMMARY REMARKS

Attributes of a new gradient ratio test device that is designed to impose cyclic flow across the soil-geotextile filtration zone are described. A simple, but effective means to achieve head-control is presented. A computer-controlled data acquisition system reads the pressure transducers and displacement transducer with time. Data reduction yields a record of confining stress, specimen density, water head distribution (hence the gradient ratio), and flow rate (hence the permeability). Particle size analyses of material from the collector trough are made

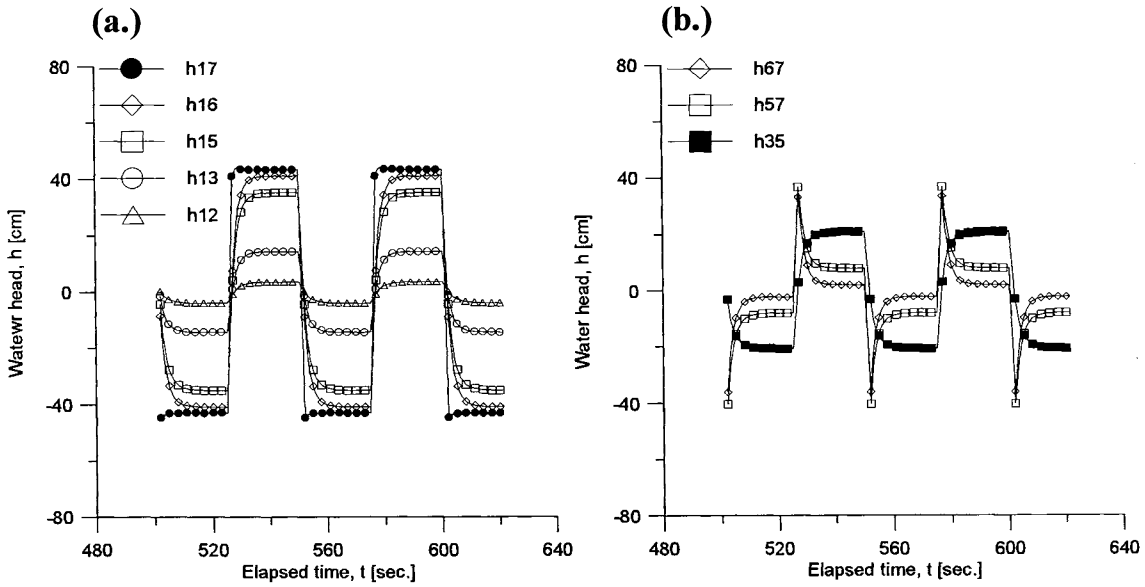

Fig. 4: Cyclic flow test data

automatically with a Sedigraph X-ray unit. Typical results are given in Fig. 4 to illustrate the variation of water head in the soil (h_{35}) and across the soil-geotextile composite zone (h_{57} and h_{67}), making reference to the port locations of Fig. 1. The system hydraulic gradient i_{17}=H/L=4 and flow reversal is imposed every 25s to yield a period T=50s.

A preliminary series of tests has been conducted to commission the test device. The following observations are made regarding the design and operation of such cyclic flow devices for evaluation of geotextile filtration applications:

- the automated recording of water pressure transducers (rather than manual reading of standpipe manometers) to measure the distribution of water head is essential: unlike manometers which require a volumetric flow in or out of the standpipe to define changes in head or pressure, the transducers operate with a negligible flow requirement and therefore rapidly detect transient pore-water pressures;

- the automated data collection allows for readings during the critical phase after flow reversal which is believed key to understanding the potential for development of stability.

ACKNOWLEDGEMENTS

This research is funded by the Natural Sciences and Engineering Research Council of Canada. The assistance of Harald Schrempp and Scott Jackson are gratefully acknowledged.

REFERENCES

ASTM D5101-96. Standard test method for measuring the soil-geotextile clogging potential by the gradient ratio. In 1996 Annual Book of ASTM Standards, Philadelphia, Pa.

Austin, D.N., Mylnarek, J. and Blond, E. 1997. Expanded anti-clogging criteria for woven geotextiles. Geosynthetics '97, Long Beach, California, March 11-13, 1997, pp.1123-1135.

Canadian Geotechnical Society, 1992. Canadian Foundation Engineering Manual, 3rd. edition. BiTech Publishers Ltd., Richmond, B.C.

Christopher, B.R. and Holtz, R.D. 1985. Geotextile Engineering Manual. U.S. Federal Highway Administration, Report FHWA-TS-86/203, National Highway Institute, Washington, D.C.

Fannin, R.J., Vaid, Y.P. and Shi, Y.C. 1994. Filtration behaviour of nonwoven geotextiles. Canadian Geotechnical Journal, No.31, pp.555-563.

Faure, Y. and Mlynarek, J. 1998. Geotextile-filter hydraulic requirements. Geotechnical Fabrics Report, Vol. 16, No. 4, Industrial Fabrics Association International, Roseville, Min., pp. 30-34.

Giroud, 1982. Filter criteria for geotextiles. In, Proceedings of the 2nd International Conference on Geotextiles, Las Vegas, Nev. Industrial Fabrics Association International, St. Paul, Min. Vol. 1, pp.103-108.

Haliburton, T.A. and Wood, P.D. 1982. Evaluation of U.S. Army Corps of Engineers Gradient Ratio test for geotextile performance. In, Proceedings of the 2nd International Conference on Geotextiles, Las Vegas, Nev. Industrial Fabrics Association International, Roseville, Min. Vol. 1, pp.97-101.

Holtz, R.D., Christopher, B.R. and Berg, R.R. 1997. Geosynthetic Engineering. BiTech Publishers Ltd., Richmond, B.C.

Holtz, R.D. 1998. Personal communication

Kohler, H.-J. 1993. The influence of hydraulic head and hydraulic gradient on the filtration process. In, Filters in Geotechnical and Hydraulic Engineering, edited by J. Brauns, M. Heibaum and U. Schuler. Karlsruhe, Germany, 20-22 October, 1992, Balkema, pp. 225-240.

Lawson, C.R. 1982. Filter criteria for geotextiles: relevance and use. ASCE Journal of the Geotechnical Engineering Division, 108(10), pp.1300-1317.

ANALYSIS OF EQUIPMENT LOADS ON GEOCOMPOSITE LINER SYSTEMS

DAVID J. KERKES, Ph.D., P.E.
CONSULTING GEOTECHNICAL ENGINEER, USA

ABSTRACT

The loads imposed on geosynthetics during installation are frequently the most severe that the materials will experience during their service life; however, they are among the most difficult to evaluate. This paper examines the loads imposed by track mounted and rubber tired vehicles spreading soil over the liner system during construction and proposes an analysis that uses three-dimensional sliding blocks for computing a factor of safety for the liner system under such loads, which takes into account the effect of the soil cover between the equipment and potential failure surface, as well as the effect of tensile forces in components of the liner above that surface. The solution algorithm, which is presented in some detail, can be executed using standard spreadsheet software. The limitations of the method are also discussed, and suggestions are made for using the method in light of the complex stress-strain behavior of composite liner systems.

INTRODUCTION

The realization that equipment loads need to be considered in the design of geocomposite liners is by no means a new idea and has been treated by McKelvey and Deutsch (1991), Druschel and Underwood (1993), McKelvey (1994), Corcoran and McKelvey (1995), as well as Koerner and Soong (1998). The methods that the author is aware of consider the problem in terms of two (an active and passive) sliding blocks, with the active block consisting of the entire slope and the passive block located at the toe. The positive effect of the passive block is sometimes referred to as "toe buttressing," and the equipment load is simply added to the active block. The limitation imposed by the location of the passive block, inclination of its base, and side force inclination between blocks, seems to preclude all but one type of potential failure surface. In this way, the passive block provides support to the active block irrespective of where the equipment may be located on the slope (i.e., a localized failure is not considered possible at any distance upslope of the passive block). The contention is made in this paper that a localized failure is possible at some point above the toe of the slope and that the forces in the immediate vicinity of the equipment need to be examined in this

regard. Furthermore, the forces associated with equipment loading are very much a function of the exact type of equipment working on the slope, and some of the specifics are discussed. A sliding block analysis is proposed that considers three (active, central, and passive) blocks above the potential failure surface, and the force associated with geosynthetic reinforcement is included in the analysis.

While the equations presented herein may initially appear to be complex, they are in fact quite straightforward and lend themselves well to solution using commercially available spreadsheet software. It is the availability of such software, with its built-in mathematical operators and interactive cells, that now enables engineers to formulate solutions of increasing complexity without the need to develop a program in a specific computer language, such as FORTRAN or BASIC. The nature of the solution algorithm will be briefly discussed; however, anyone comfortable with spreadsheets and macros will readily see how to develop an electronic worksheet to solve the equations. To assist the reader, the layout of a spreadsheet developed for this purpose is provided as a numerical example, which includes appropriate macro commands in Quattro-Pro.

LOADS IMPOSED BY CONSTRUCTION EQUIPMENT

The loads imposed by construction equipment depend on both the type of equipment and direction of travel on the slope. An analysis of these loads needs to consider the exact pieces of equipment being proposed for use in construction of the liner system, thus making the analysis quite site specific. While the subject of loads imposed by construction equipment has been treated in the literature, it appears that all of the forces are not always being considered. Let us first examine the case of a track mounted bulldozer spreading soil cover in the upslope direction as illustrated in Figure 1. The forces that must be overcome as the dozer moves up the slope are transferred to the underlying soil and

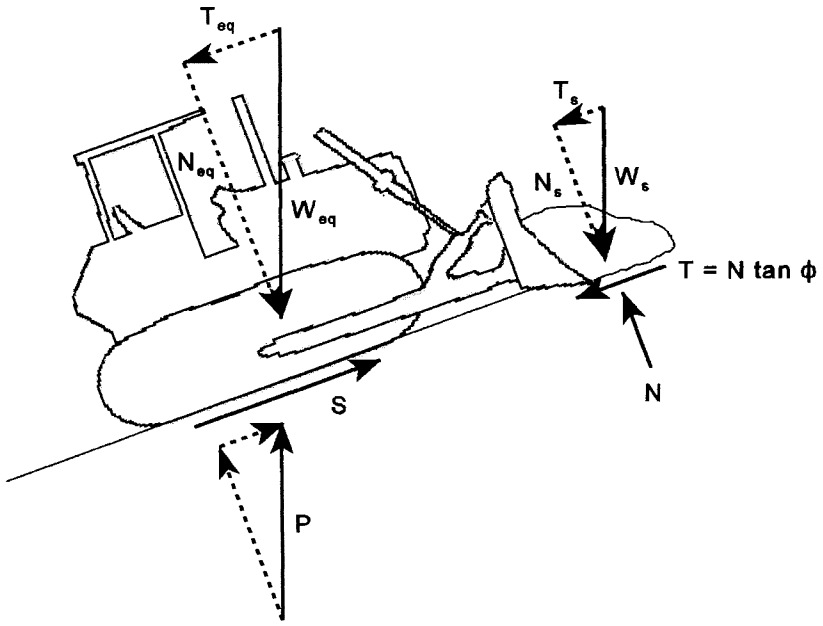

Figure 1: Forces Acting on a Bulldozer Traveling Upslope

geocomposite liner system by the tracks of the bulldozer. While the weight of the equipment (W_{eq}) is an obvious force that must be considered, let us not forget why the bulldozer is on the slope. The soil being spread by the dozer imposes certain forces that should also be considered, rather than simply assumed as being negligible. As the bulldozer spreads the soil, the dozer must overcome not only the weight component of the soil acting downslope against the blade (T_s), but the shear force in the soil itself as it is spread (N tan ϕ). By examining forces parallel to the slope it can be seen that, for the system to be in equilibrium there must exist a total resisting force (in the upslope direction) acting on the bottom of the tracks equal and opposite to the forces acting downslope (i.e., the weight components of the bulldozer (T_{eq}) and soil against the blade, and the shear force in the soil being spread). It is reasonable to assume that these forces are equally distributed to the tracks on each side of the bulldozer. It should be noted that, for convenience, the force P in Figure 1 can be taken simply as the weight of the bulldozer. In this way, the force equal and opposite to the tangential component of the bulldozer's weight is incorporated in P. The force S in Figure 1 is then equal and opposite to the sum of the weight component of the soil acting downslope against the blade plus the shear force in the soil pile being spread. Inertia forces can also be incorporated into the S term to account for acceleration and deceleration. For example, deceleration of the dozer after backing up (or traveling in the downslope direction) would result in a force in addition to the dozer's weight component that would act downslope when the bulldozer applies the brakes. Finally, to simplify the calculations, the bulldozer blade is assumed to be straight and frictionless (i.e., the soil pile does not increase the normal force beneath the dozer tracks). This assumption essentially maximizes the shear force within the soil being spread.

Let us now focus on the system of forces acting in the geocomposite liner system itself, specifically the soil cover immediately between the bulldozer track(s) and top of the first geosynthetic component. At this point it becomes convenient to model the problem in terms of three sliding blocks, as illustrated conceptually in Figure 2, with an active block (upslope of the dozer), a passive block (downslope of the dozer), and a central block (immediately beneath the track). Since the distance between bulldozer tracks will typically be larger than the depth of the soil cover being spread over the liner system, the system of sliding blocks illustrated in Figure 2 will develop beneath each of the two

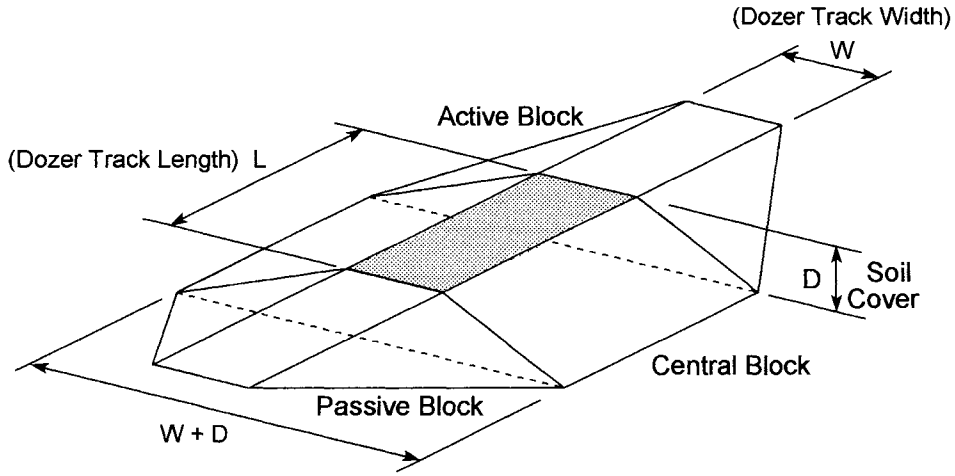

Figure 2: Sliding Blocks Beneath a Single Bulldozer Track

bulldozer tracks. It has been noted by Druschel and Underwood (1993) that soil arching mobilizes the soil between the tracks; however, the author is not convinced of this and the method proposed here ignores this potential effect. Thus, if it is assumed that the loads imposed by the equipment are equally distributed to each track, then a solution need only be developed for one set of blocks. Alternatively, one can also consider a critical combination of loads upon one track if such a condition were of interest to the designer.

It is reasonable to assume that the load imposed by the bulldozer is distributed down through the soil cover to the underlying liner component, and since the depths are typically very small a simple model has been used here employing the 1(H):2(V) approximation as presented in Winterkorn and Fang (1975) and elsewhere. As shown in Figure 2, the approximation has only been applied in the cross direction, wherein the contact area at the base of the central block is equal to the product of the contact length of the dozer track (L) and the width of the track plus depth of soil cover (W+D). The reader can refer to Poulos and Davis (1974) for a Boussinesq model should he/she wish to do so. For such analyses to be meaningful the engineer will need to use actual weights and dimensions for specific pieces of equipment, and such information is available from the manufacturer. Once the dimensions of the base of the central block have been determined, the three dimensional blocks in Figure 2 can be replaced by three dimensional prisms as illustrated in Figure 3, which greatly simplifies the calculation of the weights of the respective blocks.

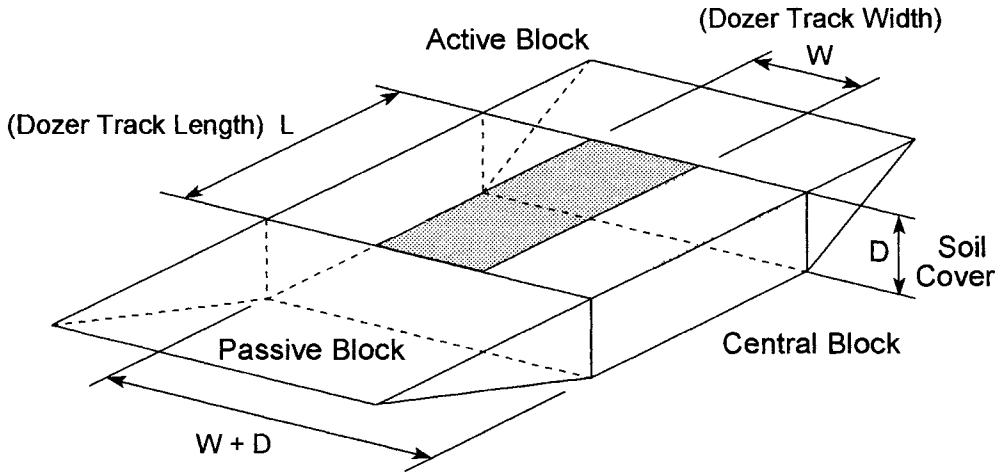

Figure 3: Prisms for Sliding Block Analysis

The independent and dependent variables in the problem will be addressed in detail in subsequent paragraphs, but before doing so let us examine some other loading conditions. Figure 4 illustrates the case of a bulldozer spreading soil while traveling downslope, and it is relevant to examine the forces that act in this problem. From Figure 4 it can be seen that, while the same set of forces exists as in the case of travel upslope, the forces do not act in the same way. Observe that the shear force in the soil pile being spread acts in the upslope direction, while the tangential component of the weight of soil pile does <u>not</u> contribute to the force S beneath the dozer track, since it does not pull on the

bulldozer blade. While acceleration of the bulldozer downslope is not likely to impart significant forces to the cover system, deceleration (braking) certainly does and, as previously noted, this force can be applied to the S term shown in Figure 4 as a percentage of the weight of the equipment. This system of forces would have to be compared to those that develop as the bulldozer spreads soil in the upslope direction.

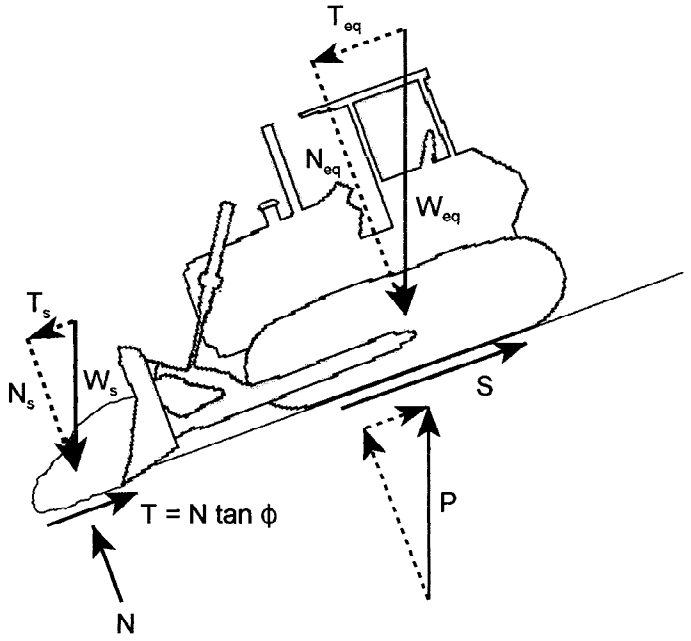

Figure 4: Forces Acting as a Bulldozer Travels Downslope

The system of forces associated with rubber tired equipment is similar, but not exactly the same as for track mounted equipment. Figure 5 illustrates the system of forces associated with a motor grader spreading soil in the upslope direction. As in the case of the bulldozer, acting downslope are the weight components of the grader and soil against the blade, and the shear force in the soil being spread. In addition, however, are the forces due to rolling resistance (R) at each of the grader's six tires. A basic discussion of rolling resistance is given by Beer and Johnston (1988) who show that the rolling resistance is a function of the radius of the tire, weight on the wheel, and coefficient of rolling resistance. Once again, by examining forces parallel to the slope it can be seen that for the grader to move upslope it must develop a total force greater than the forces acting downslope; however, this force is <u>not</u> distributed to each of the wheels of the grader. The force only acts against the wheels that are on actual driving axles; therefore, the number of driving axles must be established for the particular piece of equipment being analyzed. As in the case of the bulldozer, the engineer will need to obtain actual weights and dimensions for the specific pieces of rubber tired equipment, which must now include the details of the tires on the equipment. Now the forces that the equipment imparts to the geocomposite liner system are concentrated over a smaller area than in the case of track mounted equipment, and of specific interest is the loaded section width of the tire(s) on the actual driving axles, which can frequently be obtained from the manufacturer's product literature. Figure 6

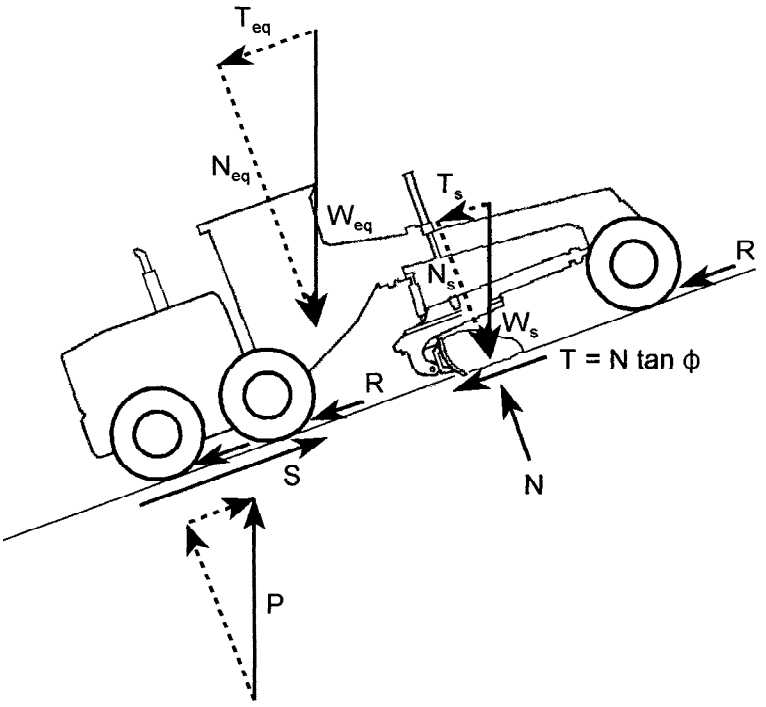

Figure 5: Forces Acting on a Motor Grader Traveling Upslope

illustrates the system of sliding blocks that develops beneath a single rubber tire on a driving axle. For this case the contact area at the bottom of the tire is taken as the square of the tire's loaded section width $(LSW)^2$ and the 1(H):2(V) approximation is applied in both directions to model the distribution of the load imposed by the tire down through the soil cover to the underlying liner component, which yields the dimensions of the base of the central block. In a manner similar to that of a motor grader, the reader can develop numerical models to consider the forces imposed by other types of rubber tired equipment, such as maintenance trucks and tractors, and the approach presented here can be extended to include compactors.

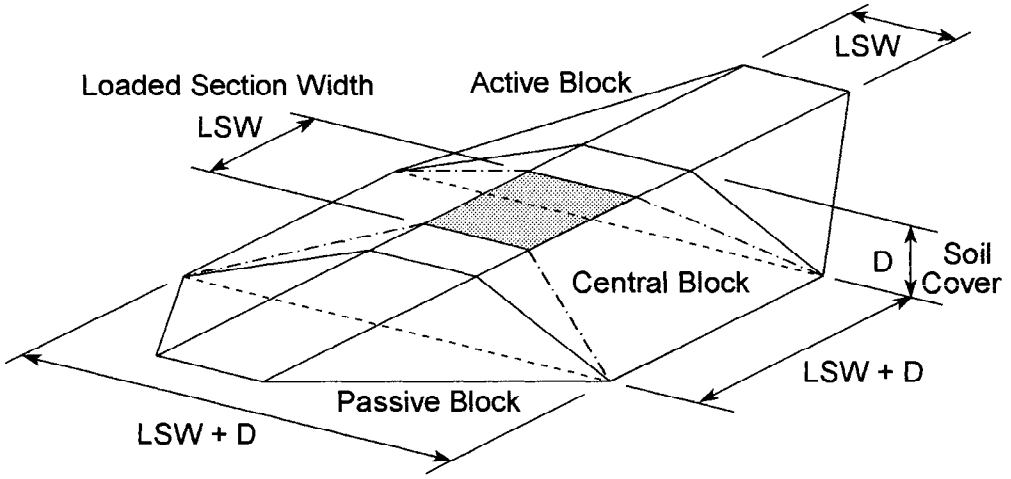

Figure 6: Sliding Blocks Beneath a Rubber Tire

SOLUTION ALGORITHM

Having examined the various forces imposed by the equipment operating on the cover system, let us now turn our attention to the forces acting in the cover itself. Figure 7 illustrates the three sliding blocks associated with a single bulldozer track and the respective forces acting on each block. This is the same set of sliding blocks that would act beneath a single tire of a motor grader, with the only difference being in the S and P terms acting on the central block. Note that any forces acting on the sides of the blocks (parallel to the direction of travel) have been ignored. These forces will be a function of the lateral stress against the sliding blocks, the friction angle of the cover soil, and area of the sides of the respective blocks; consequently, it is anticipated that they will be relatively small considering the shallow depth of soil cover. Nevertheless, it would not be too difficult to add these forces to the system of forces acting on the blocks illustrated in Figure 7 if the reader wishes to do so. The passive, central, and active blocks are designated as blocks 1, 2, and 3 respectively, and the blocks are inclined at angles ß, α (equal to the inclination angle of the slope), and θ respectively. The surface between the passive block and central block is designated as 4, and the surface between the central block and active block is designated as 5, both of which are assumed to be vertical. Note that the shear forces (T) that develop along the base of each block, as well as the interfaces between blocks, are mobilized shear strengths (denoted by the subscript m). The mobilized strength values are a function of the safety factor (F) and available strength values (soil friction angle ϕ, interface friction angle δ, and interface adhesion a), as shown in Equations 1 and 2 of Figure 7. The side force inclination between blocks is equal to the mobilized friction angle of the cover soil, following the

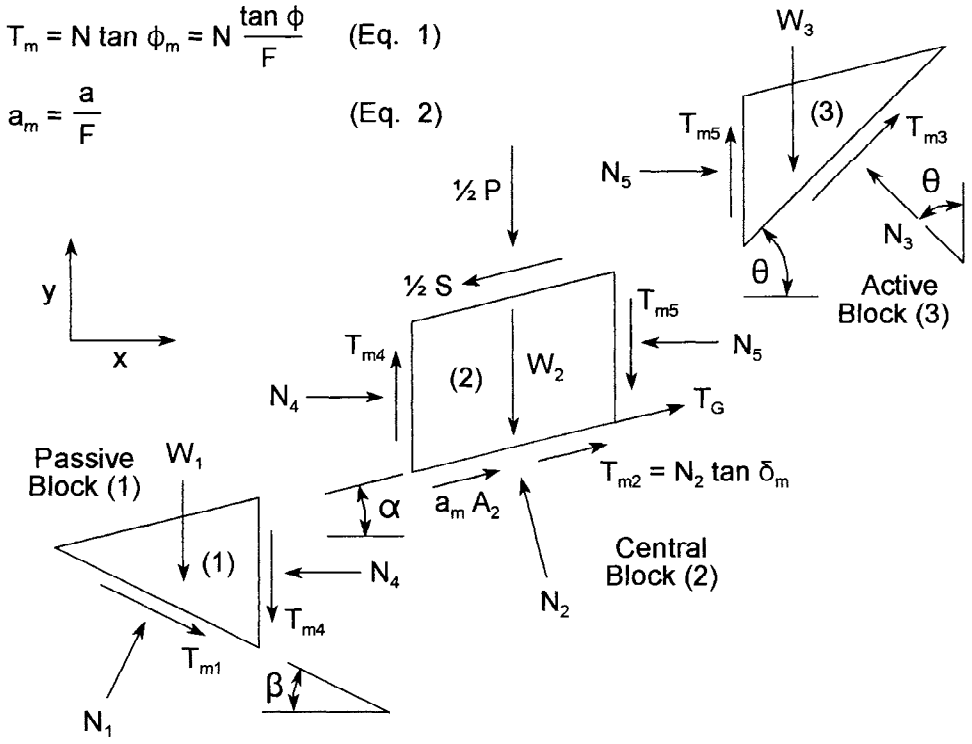

Figure 7: Sliding Blocks Beneath a Bulldozer Track

approach suggested by Sultan and Seed (1966). A force (T_G) is also shown acting at the base of the central block, and this force can be set as an independent variable to model the effect of tension in geosynthetic components in the liner system beneath the soil cover. It is imperative to note, however, that the force T_G can only develop if sufficient strength exists between the soil cover and geosynthetic in immediate contact with the cover through interface friction and/or adhesion (i.e., if slippage occurs along this interface, the underlying geosynthetics can provide no contribution to the stability of the cover system). Consequently, this is a criteria that must first be checked before a value for T_G can be applied to the analysis.

There are a number of independent and dependent variables associated with the problem, as can be seen from Figure 1 through 7. The designer must first establish the type and size of the equipment that will be spreading the soil on the slope and determine (or specify) the type and amount of cover soil that will be spread at the blade. The safety factor will also depend on the unit weight and depth of the soil cover (D in Figures 2, 3, and 6), the inclination angle of the slope (α in Figure 7), and the angles that the bases of the passive and active blocks make with the horizontal (ß and θ respectively in Figure 7). Regarding the depth of the cover soil, it is important to note that the depth used in the analysis should not be the final depth of the cover, but rather the depth of the first lift of soil spread by the equipment. Naturally, values for the strength parameters are also independent variables. From Figure 7 it can be seen that there are six (6) unknowns in the problem, these being the safety factor (F), and normal forces (N_{1-5}) acting on the bottom and interface surfaces of the blocks. Summing forces in the x (horizontal) and y (vertical) directions for each of the three blocks permits the development of expressions for each of the normal forces, and these equations are presented in Figure 8. Embedded in each of the equations, 3 through 8, is the unknown safety factor in the form of the mobilized strength parameters. A solution to these equations can be obtained as follows.

An initial value is assumed for the safety factor, and each of the respective normal forces are then computed using the expressions in Figure 8. It will be noted in Figure 8 that there are two expressions for the normal force (N_{5AB} and N_{5CB}) between the active and central blocks, and the initial assumption for the safety factor will generally produce two different values for that force. Obviously, the normal force can have only one value, and that value will be obtained for a unique value of safety factor. In other words, only one value for the safety factor will yield a correct solution to the equilibrium equations for any given set of independent variables, and a simple iterative process executed by means of a spreadsheet macro quickly converges on a unique value for the safety factor.

The method of halving the interval has been found to work quite effectively, and the algorithm consists of the following. Initial values are set in the spreadsheet for an upper limit and lower limit to the safety factor. For each iteration, the spreadsheet takes the safety factor as half the sum of the upper and lower limits, computes the mobilized strength values for the cover soil friction angle (ϕ_m) and interface friction angle (δ_m) using Figure 1, and for the interface adhesion (a_m) using Figure 2, and solves for the normal forces acting on the blocks using Equations 3 through 8. A comparison is then made of the computed values of N_{5AB} and N_{5CB}. If N_{5CB} is less than N_{5AB}, the spreadsheet copies the contents of the cell containing the safety factor (as a value) into the cell containing the upper limit

From the equilibrium equations for the Passive Block (Block 1) :

$$N_1 = \frac{W_1}{\cos\beta - \tan\phi_m \sin\beta - (\sin\beta + \tan\phi_m \cos\beta)\tan\phi_m} \qquad \text{(Eq 3)}$$

$$N_4 = N_1 (\sin\beta + \tan\phi_m \cos\beta) \qquad \text{(Eq 4)}$$

From the equilibrium equations for the Central Block (Block 2) :

$$N_2 = \frac{W_2 + \tfrac{1}{2} P - (a_m A_2 + T_G - \tfrac{1}{2} S)(\sin\alpha - \cos\alpha \tan\phi_m)}{\cos\alpha + \tan\delta_m \sin\alpha + (\sin\alpha - \tan\delta_m \cos\alpha)\tan\phi_m} \qquad \text{(Eq 5)}$$

$$N_{5CB} = N_4 + N_2 (\tan\delta_m \cos\alpha - \sin\alpha) + (a_m A_2 + T_G - \tfrac{1}{2} S)\cos\alpha \qquad \text{(Eq 6)}$$

From the equilibrium equations for the Active Block (Block 3) :

$$N_3 = \frac{W_3}{\cos\theta + \tan\phi_m \sin\theta + (\sin\theta - \tan\phi_m \cos\theta)\tan\phi_m} \qquad \text{(Eq 7)}$$

$$N_{5AB} = N_3 (\sin\theta - \tan\phi_m \cos\theta) \qquad \text{(Eq 8)}$$

Figure 8: Equations for the Normal Forces Acting on the Blocks

(effectively halving the interval), whereupon new values are computed for the safety factor, mobilized strength values, and normal forces acting on the blocks, which constitutes the information for the next iteration. Conversely, if N_{5CB} is greater than N_{5AB}, the spreadsheet copies the contents of the cell containing the safety factor (as a value) into the cell containing the lower limit, whereupon the next iteration is performed. This procedure converges on a safety factor quite rapidly. Figure 9 illustrates the general layout and macro commands (in Quattro-Pro) for a spreadsheet solution to the problem.

The data in Figure 9 is basically self explanatory and serves as an example illustrating the results of an analysis for a Caterpillar D6D bulldozer with low ground pressure tracks pushing 1.5 cubic yards of cover soil up a 3(H):1(V) slope.

Regarding the tensile force (T_G) in Equations 5 and 6, it should be noted that the force is treated as an external force acting on the central block, not a "mobilized" strength as defined in Equations 1 or 2. The tensile force is computed as the product of the tensile strength (in dimensions of force per linear dimension, such as kN/m or lb/in) and the width of the central block (W+D in Figure 2, or LSW+D in Figure 6). The following approach is recommended when considering this tensile force in the analysis. Begin by computing the safety factor with the tensile strength set at zero, rather than

Sliding Block Analysis with Surface Loads (P & S) and Geotextile Tensile Force (Tg)
Bulldozer Spreading Soil Upslope

			Safety Factor	F = 1.309
Unit Weight of Cover Soil	15.71	kN/cu m		
Depth of Soil Cover (D)	0.3	m	Errors ?	None
CAT D6D LGP Dozer	170	kN (total weight)		
Track Length (L)	2.90	m		
Track Width (W)	0.91	m		
Width at Interface (W+D)	1.21	m		
Contact Area at Interface	3.51	sq. m		

Beta =	15.00	deg =	0.262	rad
Alpha =	18.43	deg =	0.322	rad
Theta =	60.00	deg =	1.047	rad

½ P =	85.0	kN (per track)
½ S =	7.8	kN (per track)
Unit Tension	7.0	kN/m (geosynthetic)
Tg =	8.5	kN (Width at Interface * Unit Tension)

	Available (specified)				Mobilized (computed)			
Soil Cover Friction Angle	30.0	deg =	0.524	rad	23.8	deg =	0.416	rad
Interface Friction Angle	22.0	deg =	0.384	rad	17.2	deg =	0.299	rad
Interface Adhesion	0.0	kN/sq m			0.0	kN/sq m		

Block	Weight		Bottom Surface Area	
Passive (1)	1.58	kN		
Central (2)	16.54	kN	3.51	sq m
Active (3)	0.68	kN		

N(1) =	2.88	kN	Figure 8: Eq. 3
N(2) =	96.17	kN	Figure 8: Eq. 5
N(3) =	0.58	kN	Figure 8: Eq. 7
N(4) =	1.97	kN	Figure 8: Eq. 4
N(5)CB =	0.37	kN	Figure 8: Eq. 6
N(5)AB =	0.38	kN	Figure 8: Eq. 8

Method of Halving the Interval (Macro commands for Quattro-Pro)

```
MACRO \C    {LET Counter,0}{LET Upper Limit,10}{LET Lower Limit,0}{CALC}{BRANCH \X}
MACRO \X    {IF @ABS(N(5)CB-N(5)AB)<0.1}{BRANCH \N}
            {LET Counter,Counter+1}{IF Counter>35}{LET Message,"Convergence Error"}{QUIT}
            {IF N(5)CB<N(5)AB}{BLOCKVALUES F,Upper Limit}{BRANCH \X}
            {BLOCKVALUES F,Lower Limit}{BRANCH \X}
MACRO \N    {IF N(1)>0}{IF N(2)>0}{IF N(3)>0}{IF N(4)>0}{IF N(5)CB>0}{LET Message,"None"}{QUIT}
            {LET Message,"Side Force Error"}{QUIT}
```

Figure 9: Spreadsheet Example

some maximum allowable value. If an acceptable safety factor is obtained, there is no need to consider the effect of the geosynthetic. However, if the safety factor is unacceptable, input a nominal value for the tensile strength and compute the associated safety factor. Increase the tensile strength value in the analysis until the safety factor equals or slightly exceeds the minimum allowable safety factor, and then compare this "required tensile strength" to the material's allowable strength value. It is the author's opinion that this provides a more reasonable way of evaluating the interaction of the components in the cover system, enabling the designer to consider the respective levels of strain in each of the contributing components.

LIMITATIONS

The basic method proposed herein, though commonly used, has some inherent limitations that the designer should be aware of. The approach employs the limit equilibrium method; however, as is typically the case in sliding block analyses of this type, the solution considers only the conditions for force equilibrium. That is to say, the conditions of moment equilibrium are never examined.

A problem sometimes (though not frequently) encountered with the approach is the inability of the algorithm to converge on a solution. Modifying the macro to allow the engineer to examine the results one iteration at a time will often assist in identifying the trouble, and a slight modification to one of the variables will sometimes lead to an acceptable solution. The macro commands shown in Figure 9 contain a check that alerts the user when the spreadsheet encounters a problem with convergence.

Occasionally a negative value is computed for one of the normal forces acting on the blocks, most commonly the active block. While it is appropriate to check the equations in the spreadsheet for errors, the result is not necessarily due to an error in the algorithm. A negative value indicates that a tensile force is required to satisfy the conditions of equilibrium; consequently, such a result must be interpreted as unacceptable since no such tensile forces can in fact develop. For a solution to be acceptable, the normal forces cannot be negative. The macro commands shown in Figure 9 contain a check that alerts the user when a solution is obtained that produces a negative value for any one of the five normal forces.

It is relevant to note that the issue of strain compatibility is not addressed in any limit equilibrium method. Consequently, the results of the analysis proposed herein should be evaluated in concert with a review of the stress-strain curves for each component interface to determine if the mobilized strength values computed in the analysis are reasonable. In lieu of this approach, many members of the profession simply recommend the use of residual strength values.

The method does not directly yield a "minimum safety factor," since the safety factor is a function of the angles α, ß, and θ, as well as the other variables previously noted. While the angle α is generally fixed in the analysis as the inclination of the slope, ß and θ are independent variables that will affect the safety factor; thus, the designer will need to try several combinations for these angles.

SUMMARY

It is generally accepted by most designers that strength data used for final design should be obtained from laboratory tests on the materials actually intended for use in construction and should not simply be taken from the literature. Similarly, it would be inappropriate to ignore the details associated with the actual equipment planned for use in construction of the liner system, since the loads produced by such equipment frequently constitute the most severe conditions that the materials will experience during their service life. The method proposed here, which can be implemented using ordinary spreadsheet software, is a practical approach that considers many of the variables associated with the problem and allows the effect of these variables to be examined by extending a solution technique that has been used by the profession for many years in slope stability analyses.

REFERENCES

Beer, F. P., & Johnston, E. R. (1988) Vector Mechanics for Engineers - Statics, McGraw-Hill Book Co., New York

Corcoran, G. T. & McKelvey, J. A. (1995) "Stability of Soil Layers on Compound Geosynthetic Slopes," Proceedings of Waste Tech '95, New Orleans, LA, pp 301-314

Druschel, S. J, & Underwood, E. R. (1993), "Design of Lining and Cover System Sideslopes," Proceedings of Geosynthetics '93, Vancouver, Canada, pp 1341-1355

Koerner, R. M., & Soong, T-Y, (1998) "Analysis and Design of Veneer Cover Soils," Proceedings of the Sixth International Conference on Geosynthetics, Atlanta, GA, pp 1-23

McKelvey, J. A. (1991), "Consideration of Equipment Loading in Geosynthetic Lined Slope Design," Proceedings of the Eighth International Conference on Computer Methods and Advances in Geomechanics, Morgantown, WV, pp 1371-1377

McKelvey, J. A. & Deutsch, W. L. (1991), "The Effect of Equipment Loading and Tapered Cover Soil Layers on Geosynthetic Lined Landfill Slopes," Proceedings of the Fourteenth Madison Waste Conference, Madison, WI, pp 395-411

Poulos, H. G., & Davis, E. H., (1974) Elastic Solutions for Soil and Rock Mechanics, John Wiley & Sons, New York

Sultan, H. A., & Seed, H. B., (1966) "Stability of Sloping Core Earth Dams," Proceedings of the ASCE Conference on Stability and Performance of Slopes and Embankments, Berkeley, CA, pp 51-73

Winterkorn, H. F., & Fang, H-Y, (1975) Foundation Engineering Handbook, Van Nostrand Reinhold Co., New York

ASSESSMENT OF THE LONG-TERM PERFORMANCE OF POLYETHYLENE GEOMEMBRANE AND CONTAINERS IN A LOW-LEVEL RADIOACTIVE WASTE DISPOSAL LANDFILL

K. BADU-TWENEBOAH
SENIOR PROJECT ENGINEER, GEOSYNTEC CONSULTANTS, USA
L.G. TISINGER
PH.D. STUDENT, DEPARTMENT OF CHEMISTRY, MIAMI UNIVERSITY, USA.
J.P. GIROUD
SENIOR PRINCIPAL, GEOSYNTEC CONSULTANTS, USA
B.S. SMITH
SENIOR GEOTECHNICAL ENGINEER, CHEM-NUCLEAR SYSTEMS, INC., USA

ABSTRACT

This paper presents an evaluation of the long-term (500 years and more) performance of two polyethylene components of a low-level radioactive waste disposal landfill. The potential mechanisms of polyethylene deterioration are reviewed and the factors affecting these mechanisms are considered using data from studies conducted on polyethylene materials, such as geomembranes, pipes and cables. Analyses are performed to demonstrate that the polyethylene components of the landfill would perform their intended function of containment during the 500-year design period.

INTRODUCTION

A low-level radioactive waste disposal landfill was designed to include two polyethylene components: (i) a 1.5-mm thick high density polyethylene (HDPE) geomembrane used in the cover system of the landfill; and (ii) 9.5-mm thick linear medium density polyethylene (LMDPE) inner containers within reinforced concrete shells for the storage of the low-level radioactive waste. The functions of the HDPE geomembrane and LMDPE containers were infiltration control of precipitation falling over the cover system and protection of the concrete shells against the possible degrading effects of the chemical activity of the waste, respectively.

Since low-level radioactive waste landfills are typically designed to perform for a 500-year period or more, the authors were challenged by the regulatory agency to assess the long-term performance of the HDPE geomembrane and LMDPE containers. To do so, the potential mechanisms of aging and environmental deterioration of polyethylene were reviewed as a basis for assessing the long-term durability of the polyethylene geomembrane and inner containers.

An extensive literature survey was conducted. Data from studies conducted on polyethylene geomembranes as well as other polyethylene materials, such as pipes and cables, were utilized for the assessment of the impact of various mechanisms on the long-term performance of the HDPE geomembrane and LMDPE inner containers.

This paper presents the methodology and results of the assessment of the long-term performance of the two polyethylene components of the landfill. The case history presented in this paper is an example of the ultimate challenges placed in the United States before designers of geosynthetic components of containment systems used in applications where a very long design life is considered.

DESCRIPTION OF LANDFILL COMPONENTS

General Description

Figure 1 provides a schematic cross section of the low-level radioactive waste disposal landfill. The low-level radioactive waste is stored in high integrity containers composed of: (i) an outer reinforced concrete shell; and (ii) a 9.5-mm thick polyethylene inner container, which has the shape of a right circular cylinder. The high integrity containers are disposed in modules of concrete vaults of the landfill. Upon completion of disposal operations, a final cover system is constructed over the concrete vaults, as illustrated in Figure 1.

The Inner Container

The inner containers are made with a medium density polyethylene material having a density of approximately 0.935 g/cm^3, a yield strength of 18.6 MPa, and a break elongation of 400%. In addition, the inner container material contains ultraviolet (UV) energy stabilizers, but does not contain carbon black. The polyethylene inner container material is considered an LMDPE because according to ASTM D 1248, the terminology depends on the density of the resin: 0.926 to 0.940 g/cm^3 for LMDPE and above 0.940 g/cm^3 for HDPE. In the geomembrane industry, however, the terminology is traditionally based on the density of the geomembrane, which typically includes 2.5% of carbon black. A 2.5% carbon black content results in a geomembrane density equal to the resin density plus 0.012 g/cm^3 (Giroud, 1994a). As a result, a resin density of 0.935 g/cm^3 would lead to a geomembrane density of 0.947 g/cm^3; such geomembrane would be classified as HDPE even though it is made from an LMDPE resin. It should, therefore, be noted that the use of the terminology LMDPE, for the inner container material, and HDPE, for the geomembrane, does not imply that the resin used in the geomembrane has a higher density than the resin used in the inner containers.

An inner container has a minimum thickness of 9.5 mm; it is fabricated by a rotational molding process and therefore has no seams. After the waste is placed into the inner container, an LMDPE lid is thermally seamed to the inner container. The space between the inner container

sidewalls and the outer concrete shell is filled with a cementatious material after the inner container is filled with the waste.

The LMDPE inner container is not designed as a structural element of the high integrity container; this is provided by the outer reinforced concrete shell. According to Chem-Nuclear (1995a), the sole purpose of the LMDPE inner container is to serve as a "virtually impenetrable material against liquid flow from the radioactive material and a barrier protecting the concrete shell against the possible degrading effects of the chemical activity of the waste".

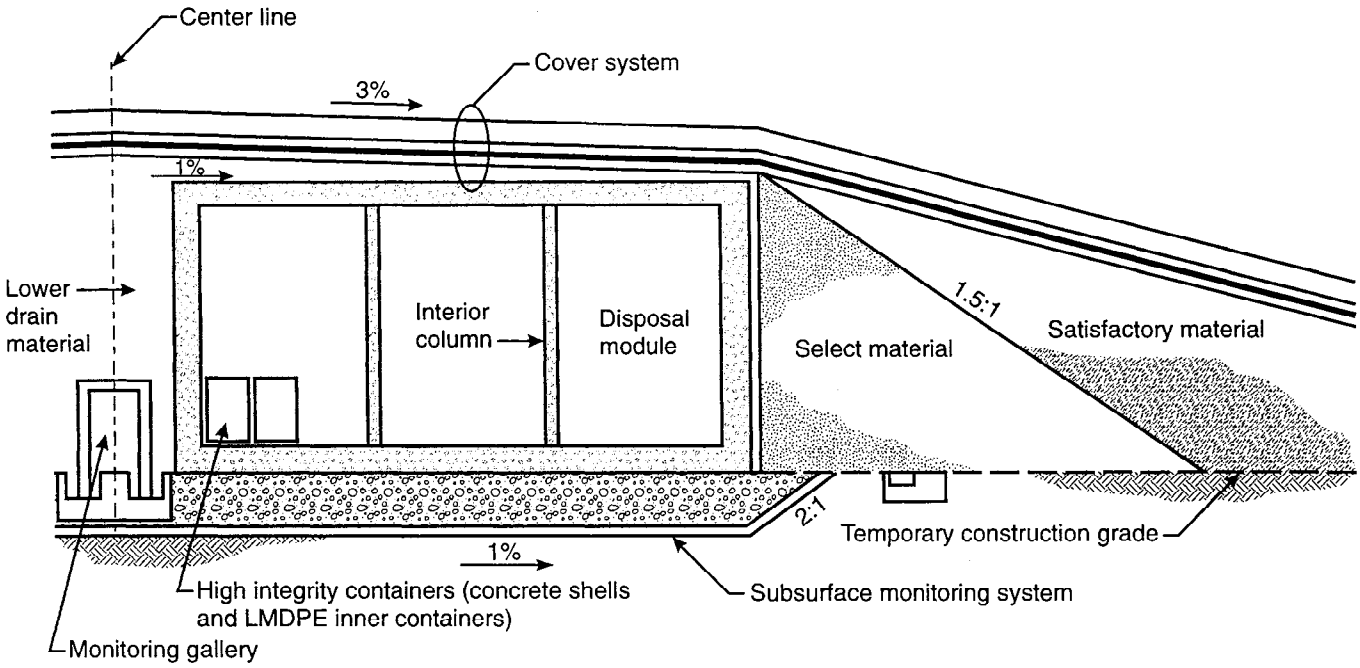

Figure 1. Schematic Cross Section of Landfill

The Cover System

The cover system profile is illustrated in Figure 2. The 1.5-mm thick HDPE geomembrane in conjunction with the geosynthetic clay liner (GCL) and 0.45-m thick low-permeability soil layer serve as a composite barrier to minimize or control infiltration of precipitation water into the concrete vaults of the landfill, thereby minimizing the risk for precipitation water to be in contact with the low-level radioactive waste. The drainage layers above and below the composite barrier also facilitate the control of infiltration into the landfill. Finally, the 1.2-m

thick layer of soil above the composite barrier provided protection to the geosynthetics components from the potentially damaging effects of erosion, vegetation, and burrowing animals.

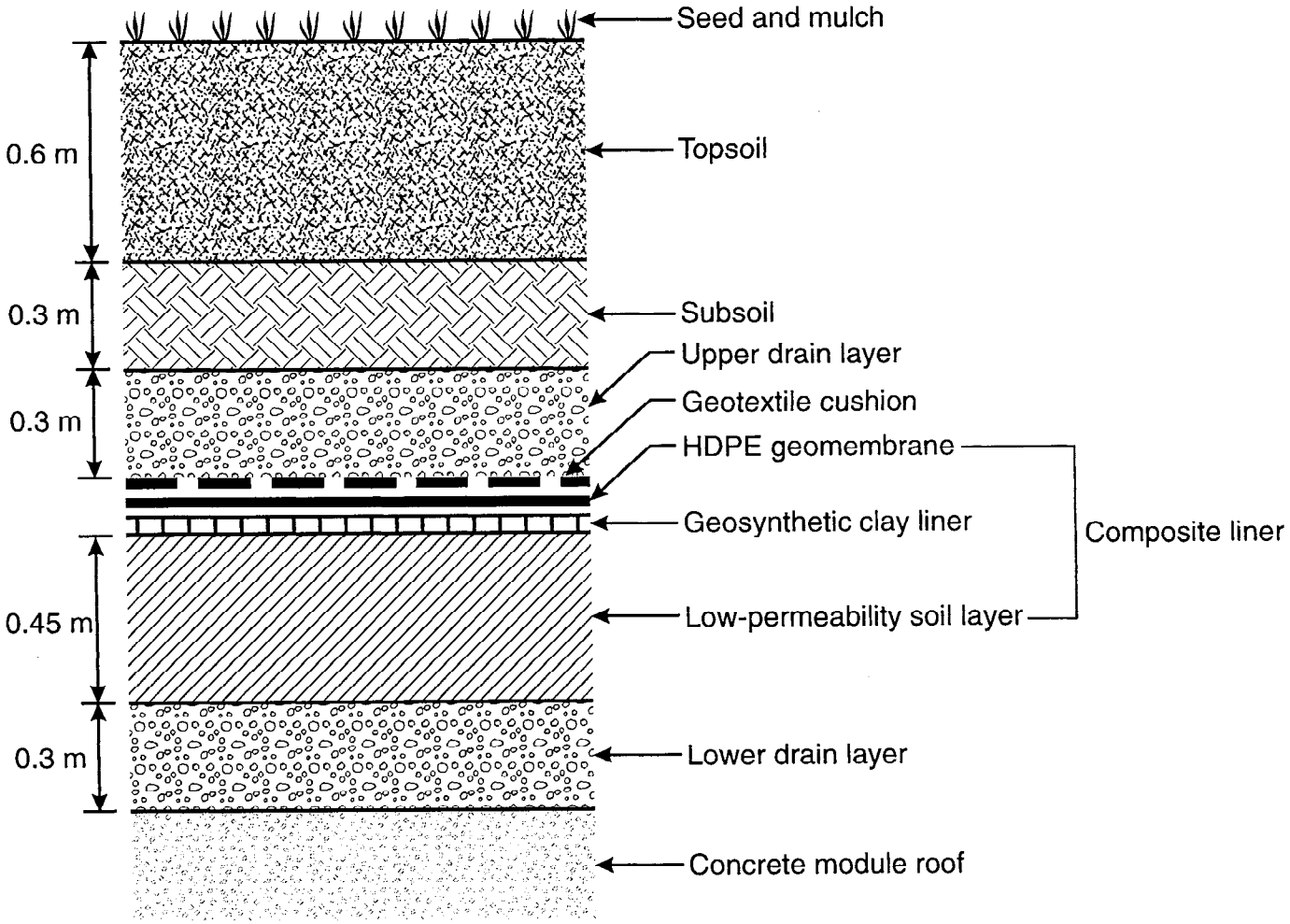

Figure 2. Cover System Profile

EVALUATION APPROACH

Background on Polyethylene

Polyethylene is the product of the polymerization reaction of the ethylene monomer (Brydson, 1982; Seymour and Carraher, 1981; Maraschin, 1996). Frequently, polyethylene materials are made by combining ethylene and low concentration levels of other monomers, such

as butene, hexene, and octene, under different conditions to produce different types of polyethylene. (These monomers are usually referred to as comonomers.) LMDPE may be made from three low-pressure polymerization reaction processes, gas-phase, slurry, and solution, resulting in a material that has a medium density (Maraschin, 1996). Similar to LMDPE, HDPE may be made from either slurry or gas phase process, generating a material having a high density (Maraschin, 1996). The specific comonomer that is used and its concentration in the polymerization reaction are often considered proprietary; however, in general, it is known that the comonomer is added to increase flexibility of the material. The resulting HDPE and LMDPE have many crystals of polyethylene within their structure. The crystals are very closely packed and virtually impenetrable; as a result, HDPE and LMDPE have extremely low permeability (Apse, 1989).

Polyethylene in HDPE and LMDPE materials has a highly stable molecular structure resulting from the absence of a reactive site, greatly limiting the ability of these materials to react with chemicals. Because of their extremely low permeability and the absence of a reactive site in their polyethylene molecules, these materials (HDPE and LMDPE) are very chemically inert and highly durable materials. Consequently, they can be expected to perform satisfactorily for a very long time.

Mechanisms of Deterioration

Polyethylene, like all synthetic materials may undergo deterioration due to internal (intrinsic) causes, often called "aging" or "natural aging", and deterioration due to external (environmental) elements. Such elements include chemicals, oxygen, microorganisms, heat, UV radiation, high-energy radiation (radioactivity), and mechanical actions (concentrated stresses due to materials in contact, stress cracking, abrasion, stresses due to structure deformation, thermal stresses, and direct actions of biological agents, e.g., animals and vegetation).

For the HDPE geomembrane, two mechanisms were deemed to have a potential impact on the long-term performance: oxidation and mechanical alteration (stress cracking, and action of biological agents). The impact of these mechanisms on the HDPE geomembrane is evaluated in this paper. For the LMDPE containers, the evaluation focuses on the only source of energy available, radioactivity.

Data Source

Data from studies conducted on geomembranes as well as other polyethylene materials, such as pipes and cables, were utilized for the assessment of each mechanism on the long-term performance of HDPE and LMDPE. An extensive data survey was conducted to assess the lifetime of the polyethylene geomembrane and containers when subjected to the mechanisms reviewed. Sources of information included various on-line databases, United States government-sponsored studies, in-house reports, technical papers, and publications from the polymer chemistry industry. To aid in locating references on the action of low-level radiation on

polyethylene materials, a comprehensive on-line search was conducted on the databases of RAPRA Technology Limited and Chem Abstracts. All references are provided at the end of this paper.

LONG-TERM PERFORMANCE OF HDPE GEOMEMBRANE

Exposure Conditions of HDPE Geomembrane

All of the deterioration mechanisms mentioned previously were reviewed with respect to the HDPE geomembrane, and many of them were eliminated. The HDPE geomembrane component of the cover system would be constructed over a GCL on top of a 0.45-m thick layer of low-permeability soil. Therefore, the HDPE geomembrane is not expected to be directly exposed to chemicals or to radioactivity from the landfill waste. Also, the presence of the 1.2-m thick layer of soil on top of the geomembrane should eliminate the effect of UV light and heat on the HDPE geomembrane. Since the cover system would be constructed on a stable foundation provided by the concrete vault, the potential impact of mechanical stress due to structure deformation on the HDPE geomembrane was considered to be negligible. Also, concentrated stresses due to materials in contact with the geomembrane are eliminated by the presence of smooth, protective materials next to the geomembrane: the geotextile cushion and the GCL. The fact that the geomembrane is overlain and underlain by materials such as granular drainage material, geotextile, GCL and compacted low-permeability soil should not promote biological actions by microorganisms. On the other hand, the impact of aging and biological agents may not be negligible and is discussed in this section. However, prior to discussing these two mechanisms, oxidation is discussed, even though the supply of oxygen to the geomembrane is extremely limited, because it is the main mechanism of deterioration of HDPE.

Oxidation of HDPE

Oxidation with Limited Supply of Energy. Oxidation of materials can result in both their softening and their embrittlement. Oxidation of HDPE is typically observed in cases where there is a significant supply of energy, a situation that is not expected in the landfill cover system. However, oxidation of HDPE samples, with or without antioxidants, has been found to occur to a limited extent in environments with very little energy and a limited supply of oxygen (Albertsson and Banhidi, 1980; Dolezel, 1967). Such environments are likely to be encountered by buried geomembranes. A small rate of oxidation of powdered HDPE was observed during long-term exposure to water and to soil, resulting in a mass loss of 0.07 percent per year (Albertsson and Banhidi, 1980). Because a powdered sample has an extremely large surface area compared to a typical 1.5-mm thick HDPE geomembrane, this rate translates into a 0.00001 percent mass loss per year in 1.5-mm thick HDPE geomembrane. With this rate of mass loss, it would take 10^7 years for the geomembrane to completely decay.

Lifetime Prediction. The lifetime of an HDPE geomembrane subjected to oxidation was predicted using Arrhenius modeling, which is the most common method for prediction of HDPE lifetime (Koerner et al., 1992). Arrhenius modeling uses a time-temperature superposition principle, in which a material is subjected to high temperature exposure, followed by a measure of some material property. This method assumes that the activation energy for a reaction is independent of temperature, allowing extrapolation of the behavior of the material at the high temperature to a behavior at lower temperature (Koerner et al., 1992). Results of Arrhenius modeling performed by Gray (1990), Howard and Gilroy (1969), Schneider (1989), and Koch et al. (1988) indicate that, with continuous exposure to oxygen, the lifetime of HDPE would vary from 400 to over 55,000 years. This range of 400 to 55,000 years, established for the case of a continuous supply of oxygen, can be considered as a lower boundary of the expected lifetime (due to oxidation only) of the geomembrane in the considered landfill where the oxygen supply is limited and little energy is available. Indeed, it was mentioned above that, with little energy and a limited supply of oxygen, it would take 10^7 years for the geomembrane to completely decay.

Molecules Susceptible to Oxidation. Albertsson and Banhidi (1980) indicated that the polyethylene molecules consumed by bio-oxidation (i.e., in biologically rich soils) are of very low molecular weight, residing at or near the surface of the HDPE material. These molecules are preferentially attacked because they are accessible. Higher molecular weight molecules, which are part of the amorphous/crystalline structure of HDPE, are not accessible and are therefore not attacked. Molecules of the amorphous/crystalline structure of HDPE provide HDPE with its performance properties, whereas the low molecular weight molecules located at the surface of the HDPE material do not (Wrigley, 1989; Koerner et al., 1990). Consequently, loss of molecules of the low molecular weight molecules should not have significant effect on the strength of HDPE (i.e., HDPE's performance should not be affected proportionally to mass loss).

Conclusion on Oxidation. From the foregoing discussions, it appears that: (i) polyethylene molecules most susceptible to oxidation are not those that govern the behavior of the geomembrane; and (ii) the expected lifetime of the HDPE geomembrane, due to oxidation and considering the limited oxygen supply in the considered landfill, should be much greater than 500 years. It will be seen in the following section that a faster deterioration may result from aging.

Aging of HDPE

Aging Mechanism. With time, semi-crystalline materials like HDPE undergo an increase in crystallinity without action from the environment (Wrigley, 1998; Moakes, 1976; Palermo and DeBlieu, 1983). This process is driven by the thermodynamic tendency of the polyethylene molecules to reduce their volume, which leads to gradual crystallization of polyethylene molecules

in the non-crystalline regions. This increased crystallinity causes a gradual increase in material's tensile strength and density, and a gradual reduction in the material's strain at yield (i.e., an increase in brittleness). A review of case histories on pipes and buried cables indicated that: (i) aging was not associated with signs of molecular deterioration, and the observed changes in mechanical behavior resulted from molecular reorganization; and (ii) aging resulted in a rate of loss of yield strain of 5 percent per 25 years of a typical observation period (Palermo and DeBlieu, 1983).

Lifetime Prediction. Using the rate of deterioration of 5 percent loss of yield strain per 25 years, one may predict that, after 500 years, the yield strain of the HDPE geomembrane will be either zero (linear relationship) or 36% of the original value (logarithmic relationship). Therefore, a lifetime on the order of 500 years can be predicted. This is the lifetime that was considered for this project since it was less than the lifetime determined assuming oxidation would be the main deterioration mechanism. This 500-year lifetime is consistent with the conclusion reached by an ad hoc committee of experts convened by the US Environmental Protection Agency that, because of HDPE's inertness and because of the innocuous conditions they are exposed when buried, such as in a waste disposal facility, HDPE geomembranes should last for hundreds of years (Haxo and Haxo, 1988).

Influence of Aging on the Development of Stress Cracking of the HDPE Geomembrane. Based on the foregoing discussions, an HDPE geomembrane is not likely to undergo significant molecular deterioration during the considered period of 500 years, but, as indicated above, molecular rearrangement could result in a decrease in yield strain of 5 percent every 25 years. Therefore, the geomembrane is expected to become stiffer as time elapses and, as a result, its susceptibility to stress cracking is expected to increase with time. As an attempt to predict when stress cracking should be assumed to occur, the following assumptions were made: (i) the climate at the site would drastically change in the future and become significantly colder, to the point that a temperature of –20°C would be possible; and (ii) stress cracking would occur at low temperature when the yield strain of the geomembrane is equal to, or less than, the tensile strain due to thermal contraction. While it is realized that the mechanisms of stress cracking and tensile rupture are different, it is known that HDPE geomembranes do exhibit stress cracking under extremely cold temperatures, i.e., temperatures at which they may rupture under very small strains under the biaxial tension that exist typically in the field. In other words, based on similarities between tensile rupture and stress cracking at low temperature, it is assumed that the environmental conditions likely to cause tensile rupture under low strain would also be favorable to the occurrence of stress cracking.

It was calculated that a tensile strain of 2.4% would result from the following mechanisms: (i) thermal contraction from 40°C to –20°C; (ii) shrinkage due to aging; and (iii) strain concentration next to seams. Considering a yield strain of 5% at –20°C under biaxial conditions, based on data provided by Giroud (1994b), and considering the decrease in yield strain of 5 percent every 25 years mentioned above, it was calculated that it would take 260

years (linear extrapolation) or 358 years (logarithmic extrapolation) for the yield strain of the geomembrane at –20°C under biaxial conditions to decrease from 5% to 2.4%. Therefore, an average value of 300 years was considered as the time when stress cracking could occur.

Influence of Aging on Infiltration through HDPE Geomembrane. Based on the foregoing discussions, an HDPE geomembrane is not likely to undergo significant molecular deterioration during the considered period of 500 years, but, as indicated above, molecular rearrangement could result in a decrease in yield strain of 5 percent every 25 years. This decrease in yield strain indicates a progressive stiffening of the geomembrane, which will decrease its ability to resist stresses on the long term, resulting in: (i) increase in defect size and number; and (ii) stress cracking, assumed to start after year 300 based on the rationale presented above.

Because of the expected absence of concentrated stresses, an increase in geomembrane stiffness seems more likely to increase the size of existing defects than the number of defects. A defect diameter of 2 mm and a defect frequency of 12.5 per hectare were considered at time zero, i.e., immediately after construction. These defect size and frequency are typically considered in landfill design. Various scenarios of defect size increase based on the yield strain decrease mentioned above were considered. Based on these scenarios, infiltration rate calculations were conducted using the leakage rate concepts and equations developed by Giroud and Bonaparte (1989a,b) and Giroud et al. (1989, 1992). The calculations resulted in an infiltration rate (expressed as an infiltration rate per unit area of the landfill cover) of 6.6×10^{-4} mm/year at year zero and an infiltration rate increase of 0.1 percent every year, hence an infiltration rate of 8.9×10^{-4} mm/year at year 300.

After that time, as indicated above, the mechanism of stress cracking was assumed to take place. Based on experience with stress cracks observed in the field with geomembranes having a low stress cracking resistance (which gives an idea of what would be stress cracking hundreds of years in the future with a modern geomembrane having a high stress cracking resistance) cracks with a 50 mm opening and located every 30 m were considered. The occurrence of stress cracking relieves stresses in the geomembrane, which may prevent any further stress cracking. Therefore, it was assumed that the size and number of cracks would be constant after 300 years. However, the rate of infiltration through the cracks was not constant because it was assumed that the GCL would progressively decay. Based on this scenario, infiltration rate calculations were conducted using the leakage rate equations developed by Giroud et al. (1992) for the case of infinitely long holes such as cracks. The calculations resulted in an infiltration rate (expressed as an infiltration rate per unit area of the landfill cover) of 6.3×10^{-2} mm/year at year zero and an infiltration rate of 4.6 mm/year at year 500.

It appears that the development of stress cracking resulted in a marked increase of the infiltration rate, with a maximum value of 4.6 mm/year at year 500. Accordingly, a design infiltration rate of 5 mm/year was used for the cover system for the entire period from year 0 to 500.

Conclusion on Aging. It appears from the above discussions that aging is the critical mechanism of deterioration of the geomembrane under the exposure conditions in the cover of the considered landfill. However, the geomembrane has been shown to be able to perform its intended function for a duration of up to 500 years.

Actions of Biological Agents

The impact of vegetation and other biological agents on the long-term performance of the cover system during the post-maintenance period was also evaluated. The technical literature (e.g., Hickey, 1963; Dedrick, 1975; Dexter, 1986; Landreth, 1991) was reviewed for data on the action of vegetation roots on geomembranes. The findings from the literature review were: (i) vegetation roots are not likely to penetrate through an intact geomembrane overlain by the typical soil thickness used in landfill cover systems; (ii) vegetation roots are more likely to develop laterally above the geomembrane than to penetrate through the geomembrane since they find nutrients above the geomembrane; and (iii) no reported data on roots enlarging an existing geomembrane defect were found.

The above observations were also confirmed by discussions with the technical staff of the local Soil Conservation Service (SCS) of the U.S. Department of Agriculture (USDA). There was however a concern of uprooting of trees during a severe storm event. If this occurred, the thickness of the cover soil could be locally reduced; or, in the worst case, the HDPE geomembrane could be locally exposed and thereby be susceptible to damage (e.g., tears and punctures). This concern resulted in the use of an increased thickness of soil layers above the geomembrane (i.e., 1.2 m compared to a typical thickness of 0.9 m for landfill cover systems incorporating geomembranes). Also, the design of the facility included an active maintenance program for the first 100 years following construction of the cover system. This program included periodic mowing and trimming of vegetation to minimize root growth, thereby reducing the risk of roots coming in contact with the geomembrane.

The increase in soil layer thickness above the geomembrane would also help against any damage by burrowing animals. Furthermore, the granular drainage layer would act as a barrier against burrowing (i.e. "biotic barrier").

LONG-TERM PERFORMANCE OF LMDPE CONTAINERS

Exposure Conditions of LMDPE Inner Containers

As the radionuclides decay, both energy from particles (alpha and beta) and gamma radiation energy are emitted. However, in the cases of the expected isotopes: (i) in typical low-level radioactive waste, the energy emitted from alpha particles is relatively small compared to the energies emitted from beta particles and gamma radiation; and (ii) alpha particles do not travel significant distances through the waste and most of them will therefore not reach the inner containers. Therefore, the energy from alpha particles can be neglected. The expected isotopes

in the waste emit primarily gamma radiation, which accounts for 80% of the total energy emitted, i.e. less than 40 Mrad. The amount of energy coming from beta particles in utility wastes is approximately 20% of the dose of gamma radiation, which is approximately 8 Mrad (Chem-Nuclear, 1995b). Therefore, the estimated total dose of radiation is less than 50 Mrad, which is below the 100 Mrad regulatory guideline. This 100 Mrad regulatory guideline was established to promote selection of polyethylene materials with extremely low risk of degradation under the exposure conditions expected in the high integrity containers. Because (i) the action of energy, on materials, from beta particles is the same as the action of energy from gamma radiation (Shalaby, 1979) and (ii) the emitted radiation is composed of mainly gamma radiation, this paper will discuss the impact of radioactivity on the LMDPE inner container in terms of gamma radiation, focusing on the total estimated dose of radiation, 50 Mrad.

Before and during its disposal, the LMDPE inner container was expected to encounter several potentially aggressive environmental elements in two stages. The first stage corresponds to the storage period and involves the potential exposure of the LMDPE inner container to the outdoors for a maximum period of 365 days. Under outdoor conditions, the LMDPE inner container could be subject to long-term exposure to UV radiation and heat. The second stage corresponds to the disposal period in which the inner container has the potential to be exposed to gamma radiation, chemicals, and mechanical stress for a maximum of 500 years. The impact of these mechanisms on the inner containers is evaluated in the following section.

Impact of Deterioration Mechanisms

First Stage. The evaluation of the LMDPE inner containers indicated that their long-term behavior should not be significantly impacted, during the first stage, by exposure to heat and UV radiation for 365 days. UV radiation, which is by far more aggressive at ambient temperatures than heat, does not penetrate below the surface of materials (Ciba-Geigy, 1987); therefore, the effect of UV radiation on the 9.5-mm thick inner containers was deemed negligible. On the other hand, heat can penetrate below the surface; however, at typical outdoor temperatures, its ability to energize oxidative degradation would be insignificant compared to that of UV radiation. A number of studies have been conducted which document the impact of extended outdoor exposure on the performance of polyethylene materials (Gilroy, 1985; Howard and Gilroy, 1969; Palermo and DeBlieu, 1983; Shelton and Wrigley, 1987; Ciba Geigy, 1987). These studies generally concluded that polyethylene materials containing antioxidants could withstand more than two years of continuous exposure without significant loss of design properties. Based on these studies, it is extremely improbable that the inner containers, which are very thick and contain antioxidants, would experience any significant reduction in performance after only 365 days of exposure outdoors.

Second Stage. During the second stage, the data reviewed indicated that the inner containers are resistant to the chemical constituents in the waste they are expected to contain (i.e., a waste that does not include organic solvents or oxidizing agents), and are also resistant to the temperatures

they are expected to be exposed to (Soo et al., 1986; USEPA, 1988; Whyatt and Farnsworth, 1990). The very small amount of oxygen available in the containers should affect the 9.5-mm thick containers even less than oxygen is expected to affect the 1.5-mm thick geomembrane; as it was previously shown that the effect of oxygen on the geomembrane is negligible, so is the effect of oxygen on the containers. In addition, the containers do not play any structural function; consequently, the expected maximum level of mechanical stress on the inner containers is very low and is far below the level that could have an impact on the long-term performance of the inner containers.

Based on the above discussion, only the effect of gamma radiation requires special attention in the case of the inner containers. Gamma radiation affects polyethylene in a way similar to UV radiation: it causes crosslinking in the amorphous regions (which increases crystallinity and density) and it provides energy that can be used for oxidation if there is oxygen available. A review of the literature has shown that, at the expected accumulated dose (< 50 Mrad), gamma radiation may actually enhance the performance of the inner container material by increasing slightly its density without having a deleterious effect on its ductility (Schonbacher, 1985; Bhateja and Young, 1983; Birkenshaw et al., 1989; O'Donnell and Whittaker, 1992; Fujimura et al., 1982; Portnoy, 1994; Ungar, 1981). There is even evidence that, at an accumulated dose of 108 Mrad, gamma radiation would not have a detrimental effect on the performance of the inner containers (Soo et al., 1986). Therefore, the conditions during the second stage of exposure of the inner containers are not conditions that have been determined to cause degradation of the inner container material at a rate greater than the expected rate of deterioration of the geomembrane, which was discussed in the previous section on lifetime prediction where it was determined that a 500-year lifetime could be predicted for the geomembrane.

Conclusion on the Impact of Deterioration Mechanisms. In summary, on the basis of the analyses presented in this section, the inner containers can be expected to maintain their function as a barrier, without release of its content for 500 years.

CONCLUSION

The mechanisms of polyethylene deterioration were reviewed and used to predict the long-term performance of an HDPE geomembrane and LMDPE containers used in a low-level radioactive waste disposal landfill. For the HDPE geomembrane, predictions based on stress cracking and aging were used to develop a scenario of geomembrane defects. Calculations performed to evaluate the rate of rainwater infiltration through the geomembrane defects showed that it was possible to demonstrate that the landfill cover system performance would be acceptable for 500 years. The LMDPE inner containers were evaluated on the basis of their durability under their expected environment, which would include heat and UV radiation during the first phase (storage, installation), and radioactivity during the second phase (operation).

Radioactivity was determined to be the only source of energy that could have a potential impact on the long-term performance of the containers; however, the effects of radioactivity were analyzed to have no significant impact during the 500-year design life.

ACKNOWLEDGMENTS

The support of GeoSyntec Consultants is acknowledged and, in particular, the authors are grateful to K. Holcomb and S.L. Berdy for assistance during the preparation of the paper.

REFERENCES

Albertsson, A.C. and Banhidi, Z.G. (1980), "Microbial and Oxidative Effects in Degradation of Polythene", Journal of Applied Polymer Science, John Wiley and Sons, New York, Vol. 25, pp. 1655-1671.

Apse, J.I. (1989), "Polyethylene Resins for Geomembrane Applications", Durability and Aging of Geosynthetics, Koerner, R.M., Editor, Elsevier, New York, pp. 159-176.

ASTM D 1248, "Standard Specification for Polyethylene Plastics Molding and Extrusion Materials", American Society for Testing and Materials, West Conschohocken, Pennsylvania, USA.

Bhateja, S.K. and Young, R.J. (1983), "Radiation-Induced Crystallinity Changes in Linear Polyethylene", Journal of Polymer Science: Polymer Physics Edition, John Wiley and Sons, New York, Vol. 21, pp. 523-536.

Birkinshaw, C., Buggy, M., Daly, S., and O'Neill, M. (1989), "The Effect of Gamma Radiation on the Physical Structure and Mechanical Properties of Ultrahigh Molecular Weight Polyethylene", Journal of Applied Polymer Science, John Wiley and Sons, New York, Vol. 38, pp. 1967-1973.

Brydson, J.A. (1982), "Plastics Materials", Butterworths Scientific, Boston, 800 p.

Chem-Nuclear Systems, Inc. (1995a), "Multi-Use Container High Integrity Container (MUC-HIC) Licensing Topical Report", Docket #WM-107 (CNSI-WM-107-P(A)), Revision 1.

Chem-Nuclear Systems, Inc. (1995b), "Internal Memorandum".

Ciba-Geigy (1987), "Light Stabilizers for Polyolefins", Ciba-Geigy Corporation, 35 p.

Dedrick, A.R. (1975), "Storage Systems for Harvested Water", Proceedings of Water Harvesting Symposium.

Dexter, A.R. (1986), "Model Experiments on the Behavior of Roots at the Interface Between a Tilled Seed-Bed and a Compacted Sub-Soil", Plant and Soil 95, pp. 149-161.

Dolezel, B. (1967), "The Resistance of Plastics to Micro-Organisms", British Plastics, pp. 105-112.

Fujimura, T., Arakawa, K., Hayakawa, N., Kuriyama, I. (1982), "Effect of an Additive on the Radiation Resistance of Polyethylene and Ethylene-Propylene Copolymer", Journal of Applied Polymer Science, John Wiley and Sons, New York, Vol. 27, pp. 2475-2482.

Gilroy, H.M. (1985), "Polyolefin Longevity For Telephone Service", Antec, pp. 258-264.

Giroud, J.P. (1994a), "Relationship Between Geomembrane Density and Carbon Black Content", Geosynthetics International, Vol. 1, No. 1, pp. 93-98.

Giroud, J.P. (1994b), "Quantification of Geosynthetics Behavior", Special Lecture, Proceedings of the 5th International Conference on Geotextiles, Geomembranes and Related Products, Singapore, Vol. 4, pp. 1249-1273.

Giroud, J.P. and Bonaparte, R. (1989a), "Leakage Through Liners Constructed with Geomembranes – Part I. Geomembrane Liners", Geotextiles and Geomembranes, Vol. 8, No. 1, pp. 27-67.

Giroud, J.P. and Bonaparte, R. (1989b), "Leakage Through Liners Constructed with Geomembranes – Part II. Composite Liners", Geotextiles and Geomembranes, Vol. 8, No. 2, pp. 78-111.

Giroud, J.P., Khatami, A., and Badu-Tweneboah, K. (1989), "Evaluation of the Rate of Leakage through Composite Liners", Geotextiles and Geomembranes, Vol. 8, No. 4, pp. 337-340.

Giroud, J.P., Badu-Tweneboah, K., and Bonaparte, R. (1992), "Rate of Leakage through a Composite Liner due to Geomembrane Defects", Geotextiles and Geomembranes, Vol. 11, No. 1, pp. 1-28.

Gray, R.L. (1990), "Accelerated Testing Methods for Evaluating Polyolefin Stability", Geosynthetic Testing for Waste Containment Applications, ASTM STP 1081, Koerner, R.M., Editor, American Society for Testing and Materials, Philadelphia, pp. 57-74.

Haxo, H.E. and Haxo, P.D. (1988), "Consensus Report of the Ad Hoc Meeting on the Service Life in Environments of Flexible Membrane Liners and Other Synthetic Polymeric Materials of Construction", EPA M86-155, 55 p.

Hickey, M.E. (1963), "Investigations of Plastic Films for Canal Lining", U.S. Bureau of Reclamation Report No. 19, 149 p.

Howard, J.B. and Gilroy, H.M. (1969), "Natural and Artificial Weathering of Polyethylene Plastics", Polymer Engineering and Science, Vol.9, No. 4, pp. 286-294.

Koch, R., Gaube, E., Hessel, J., Gondro, C., and Heil, H. (1988), "Long-Term Resistance of Dump Sealing Sheets of Polyethylene", EPA Report TR-88-0054, 42 p.

Koerner, R.M., Lord, A.E., and Hsuan, Y.H. (1990), "Long-term Durability and Aging of Geomembranes", Waste Containment Systems: Construction, Regulation, and Performance, Bonaparte, R., Editor, ASCE Geotechnical Special Publication No. 26, Proceedings of a Symposium held in San Francisco, CA, USA, pp. 52-83.

Koerner, R.M., Lord, A.E., and Hsuan, Y.H. (1992), "Arrhenius Modeling to Predict Geosynthetic Degradation", Geotextiles and Geomembranes, Vol. 11, No. 2, pp. 151-183.

Landreth, R.E. (1991), "The Resistance of Membranes in Cover Systems to Root Penetration by Grass and Trees", Proceedings of Geosynthetics '91, Atlanta, GA, USA, pp. 303-309.

Maraschin, N. (1996), "Polyethylene: Markets Expanding Very Rapidly and Technology Growing at Record Rate", Modern Plastics Encyclopedia '97, McGraw-Hill, New York, NY, pp. B3-B4.

Moakes, R.C. (1986), "*Long Term Natural Aging*", RAPRA Members Journal, Vol. 4, No. 2, Mar/Apr 1986, pp. 19-22.

O'Donnell, J.H. and Whittaker, A.K. (1992), "Composition and Crystallinity Effects in the Degradation of Ethylene-Propylene Copolymers by Gamma-Radiation", Ethylene-Propylene Copolymers, Marcell-Dekker, New York, pp. 1-10.

Palermo, E.F. and DeBlieu, I.K. (1983), "Aging of Polyethylene Pipe In Gas Distribution Service", A.G.A. Distribution Conference, Houston, TX, 12 p. plus 9 figures.

Portnoy, R.C. (1994), "The Response of Various Polyethylenes to High Energy Radiation", Proceedings from Antec '94, Society of Plastics Engineers, Vol. 3, pp. 2612-2618.

Schneider, H. (1989), "Long-Term Performamce of Polypropylene Geosynthetics", Durability and Aging of Geosynthetics, Koerner, R.M., Editor, Elsevier, New York, pp. 95-109.

Schonbacher, H. (1985), "How Plastics Perform Under Nuclear Radiation", Modern Plastics, McGraw-Hill, New York, pp. 64-68.

Seymour, R.B., and Carraher, C.E. (1981), "Polymer Chemistry An Introduction", Dekker, New York, 564 p.

Shalaby, S.W. (1979), "Radiative Degradation of Synthetic Polymers: Chemical, Physical, Environmental, and Technological Considerations", Journal of Polymer Science: Macromolecular Reviews, John Wiley and Sons, New York, Vol. 14., pp. 419-458.

Shelton, W.S., and Wrigley, N.E. (1987), "Long-Term Durability of Geosynthetics Soil Reinforcement", Proceedings of Geosynthetics '87, New Orleans, LA, U.S.A., Vol. 2, pp. 442-455.

Soo, P., Arora, H., Swyler, K.J., Becker, W., and Sobel, E. (1986), "The Effects of Environment and Gamma Irradiation on the Mechanical Properties of High Density Polyethylene Topical Report", Office of Nuclear Regulatory Research, NUREG/CR-4607 BNL-NUREG-51991 AN, 86 p.

Ungar, G. (1981), "Review: Radiation Effects in Polyethylene and n-Alkanes", Journal of Material Science, Vol. 16, No. 10, pp. 2635-2656.

USEPA (1988), "Lining of Waste Containment and Other Impoundment Facilities", EPA/600/2-88/052, 12 sections and 14 appendices.

Whyatt, G.A. and Farnsworth, R.K. (1990), "The High pH Chemical and Radiation Compatibility of Various Liner Materials", Geosynthetic Testing for Waste Containment Applications, ASTM STP 1081, Koerner, R.M., Editor, American Society for Testing and Materials, Philadelphia, pp.110-124.

Wrigley, N. E. (1989), "The Durability and Aging of Geogrids", Durability and Aging of Geosynthetics, Koerner, R.M., Editor, Elsevier, New York, pp. 110-134.

ENVIRONMENTAL STRESS CRACKING IN GEONETS MANUFACTURED FROM HIGH DENSITY POLYETHYLENE

JOHN SIEBKEN - NATIONAL SEAL COMPANY, USA
DON CUNNINGHAM - NATIONAL SEAL COMPANY, USA

ABSTRACT

This paper presents the results of research into environmental stress cracking of geonets.

In the first section, the resistance to environmental stress cracking (ESCR) was evaluated for sheet and plaques made from the geonets.

In the second section, three geonet samples were manufactured for the evaluation. One sample was manufactured from geomembrane-grade polyethylene resin. A second sample was manufactured from a higher density polyethylene resin used in the blow molding industry. A third sample was manufactured using a 50/50 blend of the first two.

Specimens from each sample were placed under a compressive load of 718 kN/m^2 in a vessel containing a solution of 10% surface-active agent and 90% water at a temperature of 50° C. Specimens were removed periodically, and examined to determine the extent of environmental stress cracking and tested to determine the flow capacity of the geonet. The data indicates that the extent of environmental stress cracking observed in the geonets is related to the density of the resin.

INTRODUCTION

Geosynthetics used in landfill applications are expected to perform for long periods of time under harsh conditions. Much effort has been expended researching the durability of the materials in use. Some geosynthetics, however, have received more attention in certain areas than others.

The result of this focus has been positive in that polyethylene resins have been developed for geomembranes that have superior resistance to environmental stress cracking.

On the other hand, it appears that little attention has thus far been paid to environmental stress cracking in geonets manufactured from HDPE. The only reference to any kind of cracking in geonets discovered by the authors was reported by Slocumb, Demeny, and Christopher (1986) as an interesting observation in their research into the creep characteristics of geonets.

Perhaps the lack of attention is due to the function of the material. Geonets are intended to convey a liquid (sometimes a gas), and a few cracks here and there probably won't prevent the material from fulfilling this function. Slocumb noted that brittle products prone to fracture should not be selected, but that even geonets with fractured strand junctions will continue to perform.

It follows that if stress cracking exists at all, then how much can be expected in geonets? As with the geomembranes, the ESCR of geonets will depend on the polyethylene resin used in their manufacture.

Our goal in this research was to study the ESCR of geonet materials and how this might affect the flow capacity of the geonet.

ESCR EVALUATION OF GEONETS CURRENTLY IN USE

We have evaluated the ESCR of three geonets currently in use. They are designated here as Manufacturer A, Manufacturer B, and Manufacturer C. All three materials were bi-planar geonets as are typically found on the market.

The resin used in the geonet from Manufacturer A is also used to manufacture geomembrane by a cast-sheet extrusion process. The geomembrane has been extensively tested by the single point notched constant tensile load (SP-NCTL) ESCR test per ASTM D 5397. The resin used by Manufacturer A typically has an SP-NCTL ESCR time to failure in excess of 200 hours.

There was only enough geonet from two samples of material from Manufacturer B to make plaques approximately 2.3 mm thick. The plaques were tested according to ASTM D 5397 in the same manner as the material from Manufacturer A. The specimens from both sample plaques had failure times in excess of 200 hours.

Geonet from Manufacturer C was processed with a grinder, and the resulting chips made into 1.45 mm thick by 300 mm wide sheet on a laboratory extruder. Specimens from the sheet were then tested according to ASTM D 5397 and ASTM D 1693 Environmental Stress-Cracking of Ethylene Plastics. In the ASTM D 1693 test, bent specimens with a controlled imperfection on one surface are exposed to a surface-active agent (10% Igepal CO630 and 90% water) at 50 °C and monitored until cracking is observed.

The specimens of Manufacturer C material tested according to ASTM D 5397 had an average failure time of 0.8 hours. For the Manufacturer

C material tested according to ASTM D 1693, specimens were tested with a machine direction orientation and a cross-machine direction orientation. Cracks were observed in the cross-machine direction specimens after about 6 hours, and in the machine direction specimens after about 25 hours.

It has been our experience that materials exhibiting failure times of greater than 200 hours in the SP-NCTL ESCR test do not fail in the ASTM D 1693 test, even after many thousands of hours of exposure. Based on that experience, the ASTM D 1693 test was not conducted on the materials from Manufacturer A or Manufacturer B. The ESCR results are summarized in Table 1.

Table 1. ESCR Failure Times

	Failure Time (hours)	
Material	ASTM D 5397 (SP-NCTL)	ASTM D 1693
Manufacturer A	>200	NA
Manufacturer B	>200	NA
Manufacturer C	0.8	25 hrs - Machine Direction 6 hrs - Cross-Machine Direction

LABORATORY EVALUATION OF ESCR IN GEONETS UNDER COMPRESSIVE LOAD

Two polyethylene resins, designated resin 1 and resin 3, and a 50/50 blend of those resins, designated resin 2, were used to manufacture geonet for a laboratory evaluation of geonet ESCR while under a compressive load. The density, melt index for two load conditions, and melt flow ratio for the resins are shown in Table 2.

Table 2. Resin Properties

Resin	Density (natural resin) (kg/m^3)	Melt Index (190/2.16) (g/10 min)	Melt Index (190/21.6) (g/10 min)	Melt Flow Ratio
1	938	0.27	21.5	78 : 1
2	944	0.39	34.3	89 : 1
3	965	0.76	62.6	82 : 1

The data in Table 2 indicates that resin 1 has a lower density, a higher molecular weight and a narrower molecular weight distribution than resin 2 or 3.

Three geonet samples were produced from the three resins. The mass per unit area and the thickness of the geonets are shown in Table 3.

Table 3. Geonet Laboratory Sample Physical Properties		
Geonet Designation (by resin)	Mass per Unit Area (g/m^2) (nominal)	Thickness (mm)
1	976	Avg: 5.95 SD: 0.038
2		Avg: 5.80 SD: 0.041
3		Avg: 5.90 SD: 0.036

Fifteen, 30.5 cm by 30.5 cm specimens were sampled from each geonet roll. Ten specimens from each material were immersed in a solution of 90% water and 10% Igepal CO630 at a temperature of 50°C, and subjected to a compressive load of 718 kN/m^2. The specimens were stacked in the baths with separating layers of 550 g/m^2 non-woven, polyester geotextile.

Five of the specimens for each geonet material were evaluated for water flow capacity in accordance with ASTM D 4716 Determining the (In-plane) Flow Rate per Unit Width and Hydraulic Transmissivity of a Geosynthetic Using a Constant Head. The conditions for the test included a profile of steel plate/geonet/steel plate, a compressive load of 718 kN/m^2, a seating time under compressive load of 1 hour, and a hydraulic gradient of 1.0 .

Two specimens of each geonet type were removed from the bath after exposure times of 500, 1000, 1500, 2000, and 2500 hours. These specimens were cleaned, evaluated for extent of environmental stress cracking, and tested for flow capacity using the same conditions applied to the unexposed specimens. The results of the flow rate testing are shown in Table 4. The results are also presented graphically as average flow rate versus bath immersion time in Figure 1.

Table 4. ASTM D 4716 Flow Rate Result Summary						
Geonet	Flow Rate (x 10^{-3} m^3/sec-m)					
	Unexposed	After 500 Hours Under Load	After 1000 Hours Under Load	After 1500 Hours Under Load	After 2000 Hours Under Load	After 2500 Hours Under Load
1	#1 1.550 #2 1.620 #3 1.370 #4 1.220 #5 1.560 Avg:1.460 SD: 0.170	#1 0.800 #2 0.831 Avg:0.816 SD: 0.022	#1 0.609 #2 0.683 Avg:0.646 SD: 0.052	#1 0.697 #2 0.487 Avg:0.592 SD: 0.148	#1 0.631 #2 0.635 Avg:0.633 SD: 0.003	#1 0.583 #2 0.702 Avg:0.643 SD: 0.084
2	#1 1.650 #2 1.560 #3 1.640 #4 1.600 #5 1.730 Avg:1.640 SD:0.006	#1 0.987 #2 1.030 Avg:1.010 SD: 0.003	#1 1.110 #2 0.825 Avg:0.968 SD: 0.202	#1 0.747 #2 0.866 Avg:0.807 SD: 0.084	#1 1.060 #2 0.721 Avg:0.891 SD: 0.240	#1 0.730 #2 0.446 Avg:0.588 SD: 0.201
3	#1 1.830 #2 1.790 #3 1.680 #4 1.730 #5 1.770 Avg:1.760 SD: 0.060	#1 0.810 #2 1.040 Avg:0.925 SD: 0.163	#1 0.706 #2 0.532 Avg:0.616 SD: 0.123	#1 0.483 #2 0.372 Avg:0.428 SD: 0.078	#1 0.641 #2 0.491 Avg:0.566 SD: 0.106	#1 0.622 #2 0.439 Avg:0.531 SD: 0.129

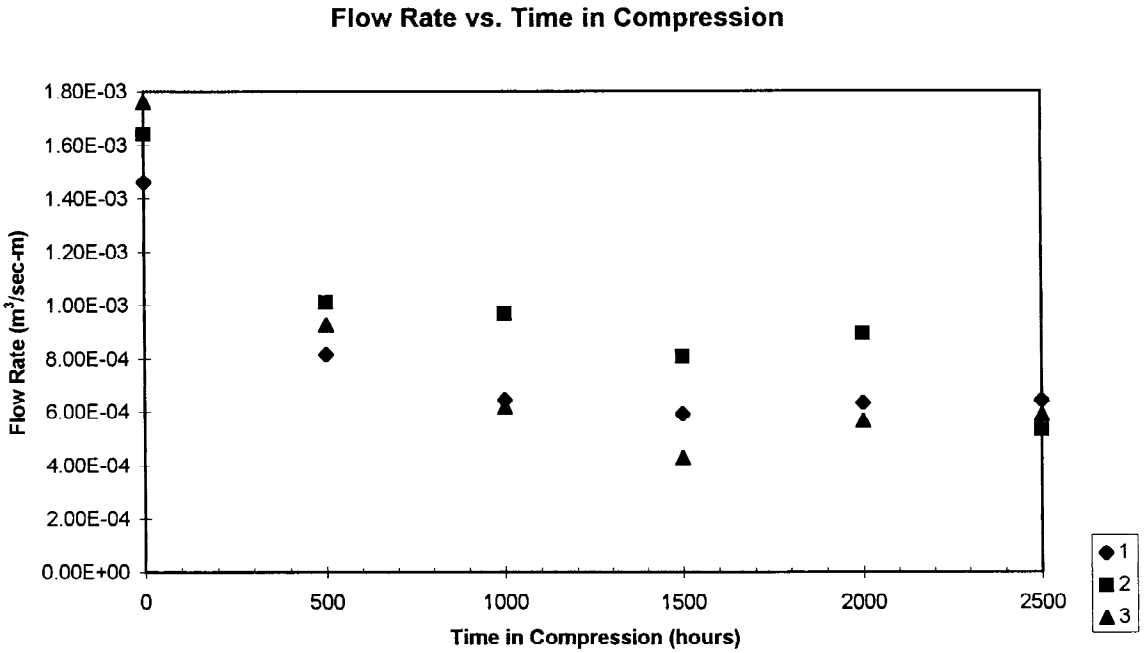

Figure 1. Flow Rate vs. Time in Compression

The geonet specimens were examined under 15X magnification for environmental stress cracking over the course of the exposure. To quantify the extent of cracking, a template containing five open areas was placed over each specimen. Each opening in the template had an area of approximately 6.5 cm^2. The number of individual cracks observed was counted for each area, and normalized to the number of strand intersections visible in an area. The resulting stress crack frequency for each geonet is shown in Table 5. The results for geonets 2 and 3 are shown graphically in Figure 2.

Table 5. Number of Cracks per Geonet Strand Intersection

Geonet	After 500 Hours in Bath	After 1000 Hours in Bath	After 1500 Hours in Bath	After 2000 Hours in Bath	After 2500 Hours in Bath
1	0	0	0	0	0
2	2	2	2	3	4
3	5	6	8	12	11

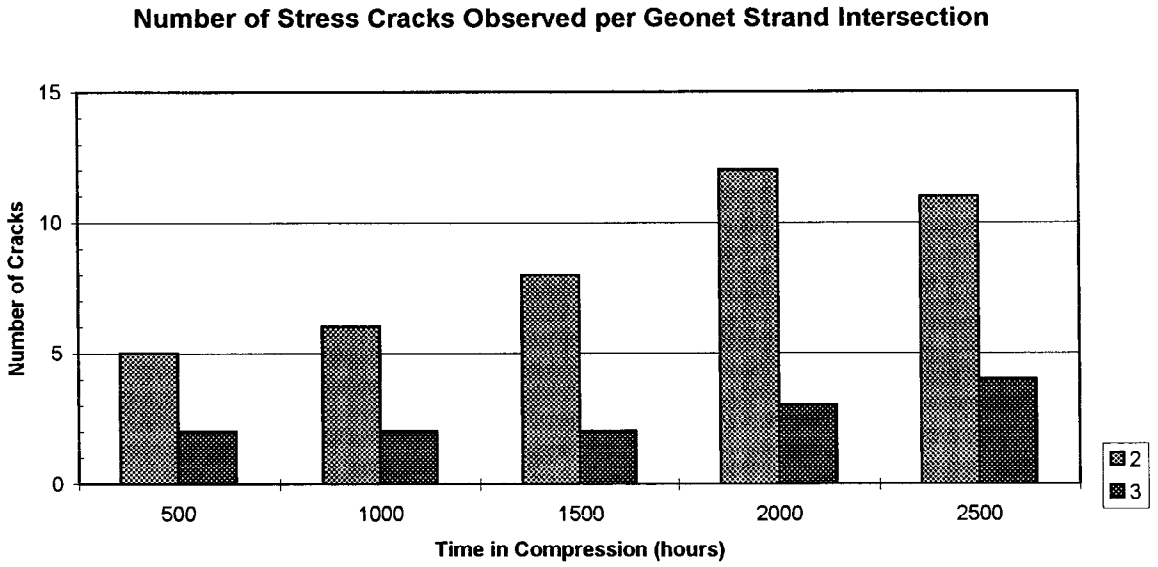

Figure 2. Number of Cracks per Strand Intersection Viewed

Samples of the resin used to manufacture the geonet samples were also formed into 2 mm thick sheet. The sheet was then evaluated for SP-NCTL ESCR per ASTM D 5397 as described previously. The results are consistent with the rest of the ESCR data in this section. The ESCR of the sheet samples can be categorized as Resin 1>Resin 2>Resin 3. The results of the SP-NCTL ESCR tests are summarized in Table 6.

Table 6. ASTM D 5397 Single-Point NCTL-ESCR

Material	Average Time to Failure for 5 Specimens (hours)
Resin 1	>200
Resin 2	5.5
Resin 3	0.6

DISCUSSION

It is clear from the data presented that geonets can stress crack while under compressive load. In this evaluation, the resins with a higher density cracked extensively. Examples are shown in Figures 3 and 4. Figure 3 shows a magnified view (15X) of cracked geonet strands. The geonet in the figure was made with Resin 3 and is shown after 2000 hours of immersion.

The geonet in Figure 4 was also made with Resin 3, and is shown after 1000 hours of immersion. The cracking was so severe that several pieces of geonet fell off from around the edges. The resulting non-uniform specimen caused concern about how the edges might affect the flow rate tests. To restore the uniformity of the flow path, geonet edges with missing pieces were filled with wax. This meant that some of the specimens had a narrower width than others in the test. However, the flow rates are normalized for width and the results are not believed to have been biased by sealing the edges of the geonet specimens that fell apart.

The flow rate results suggest that some improvement can be gained by using higher density polyethylene resins to make geonets. Slocumb (1986 et al) reported that the largest portion of transmissivity loss when a geonet is under compression is because the geonet strands roll over. One would expect a stiffer material to be more resistant to strand roll-over. The data also suggests that this initial advantage can disappear over time as environmental stress cracking progresses in the geonet, effectively accelerating the roll-over of the geonet strands.

The potential for environmental stress cracking in the field looks to be greater for at least one geonet currently on the market. In a 1993 article, Hsuan, Koerner, and Lord reported the NCTL ESCR ductile-brittle transition times for 21 as-manufactured HDPE geomembranes and 7 field-exhumed HDPE geomembranes that had evidenced stress cracking problems.

Overall, the ductile-brittle transition times ranged from 4 hours to 5000 hours. All 7 of the field-exhumed HDPE geomembranes with stress cracking problems had ductile-brittle transition times of less than 100 hours. This led to the current ductile-brittle transition time recommendation of >100 hours for HDPE geomembranes.

An SP-NCTL ESCR time of 200 hours or more is recommended by Koerner in Designing with Geosynthetics, 4^{th} ed. (1998) to ensure that the ductile-brittle transition time for a polyethylene resin will be greater than 100 hours. Clearly, the geonet from Manufacturer C will have a ductile-brittle transition time a great deal less than 100 hours. It may also have stress cracking problems in the field, like the HDPE geomembranes reported by Hsuan et al.

What might be the consequences of a stress-cracked geonet in the field? A reduction of flow capacity has been demonstrated. Given the severity of stress cracking observed, it is conceivable that with

enough time the material may become polyethylene aggregate instead of geonet. Speculation regarding other areas of concern arising from stress cracked geonets, slope stability for example, is left to the reader.

CONCLUSIONS

- ESCR, as a property of polyethylene, is applicable to geonets as well as geomembranes.
- There are geonets on the market manufactured from polyethylene resins that have very good and very poor ESCR.
- It has been shown that HDPE geonets manufactured from polyethylene with poor ESCR can crack severely while under a compressive load in a bath meeting the solution and temperature conditions of ASTM D 5397.
- Stiffer HDPE geonets have more resistance to strand roll-over under load, resulting in higher flow rate values when tested per ASTM D 4716. The advantage can be negated when stress cracking occurs, and the strands roll over more easily.
- The results of this research lead the authors to suggest that HDPE geonets manufactured from poor ESCR polyethylene resin not be used in designs where environmental stress cracking of the geonet may have a negative impact on the function of the liner system.

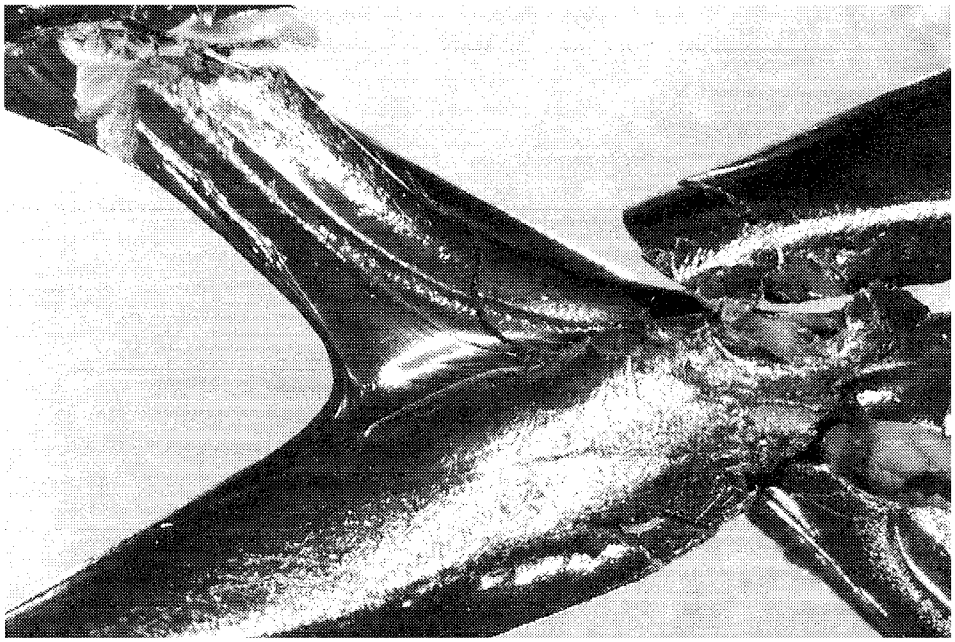

Figure 3. Cracks in Geonet at Strand Intersection

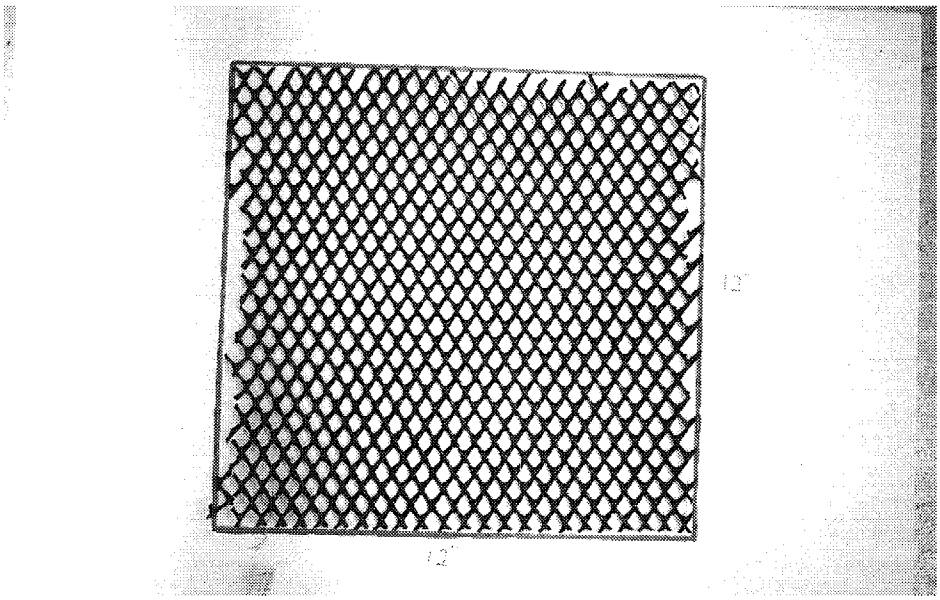

Figure 4. Geonet Specimen After 1000 Hours

REFERENCES

ASTM D 1693-70, (1993) "Standard Test Method for Environmental Stress Cracking of Ethylene Plastics", Annual Book of ASTM Standards, ASTM, West Conshohocken, PA, USA.

ASTM D 4716-95, (1998) "Standard Test Method for Environmental Stress Cracking of Ethylene Plastics", Annual Book of ASTM Standards, ASTM, West Conshohocken, PA, USA.

ASTM D 5397-95, (1998) "Standard Test Method for Environmental Stress Cracking of Ethylene Plastics", Annual Book of ASTM Standards, ASTM, West Conshohocken, PA, USA.

Koerner, R.M., (1998) "Designing with Geosynthetics, Fourth Edition", Prentice Hall, New Jersey, USA.

Hsuan, Y.G., Koerner, R.M., and Lord, A.E., Jr.. (1993) "Stress Crack Resistance of High Density Polyethylene Geomembranes", J. Geotechnical Eng. Div., ASCE, Vol. 119, No. 11, pp. 1840-1855.

Slocumb, R.C., Demeny, D.D., and Christopher, B.R., (1986) "Creep Characteristics of Drainage Nets", Superfund '86, Washington, D.C.

Acknowledgements

The authors would like to thank Brian Tomlinson of BT Technology, Inc. for the construction of the geonet compression devices.

UNPROTECTED PP LINER FOR STORAGE OF PAPER MILL BLACK LIQUOR IN COLD REGION

BOMBARDIER L., JETTÉ D., PICHÉ M. and **ROLLIN A.**
SOLMERS INTERNATIONAL, LONGUEUIL, CANADA

ABSTRACT

Black liquor at 90°C produced in a Southern Ontario paper mill is stored during winter time in a open pond lined with a reinforced Polypropylene geomembrane 1,14 mm thick. During the construction phase of the pond (maximum capacity of 62,500 m^3), a quality assurance quality program for the liner installation was implemented and was followed by an electrical leaks detection survey. The design and selection criteria for the liner, particularly the PP geomembrane specific installation parameters, advantages and limitation, are discussed. The advantages and difficulties encountered during installation are presented, and an analysis of the leaks detected during the CQA program is presented.

INTRODUCTION

A corrugated-paper medium, fluted as a middle layer in the walls of container board, is manufactured by Norampac at its mill in Trenton, Southern Ontario, Canada. One of the by-products issued from this industrial process, called black liquor, is pumped year-round since 1971 into three large holding ponds located at the site. The liquor, at an average temperature of 90°C and of pH fluctuating from 5.5 to 8.4, must be transferred daily in these ponds at a rate of 150 m^3/d through a 2" diameter pipe. This operation is feasible during the winter months because the black liquor freezes below –5°C, while ambient temperatures typically remain above –20°C.

In the past, it has been found economical to store black liquor in simple earthen lagoons excavated in an impervious stratum (natural till) surrounded by 3H:1V dikes constructed of sand and gravel with an impervious sandy till core. In order to increase the environmental integrity of the lagoon, it was decided to line the ponds with a synthetic material to minimize soil infiltration of the black liquor to the surrounding soil. One of the three existing lagoons, the White Water Lagoon, pond C (east section), measuring approximately 138 by 215 meters and 5

meters in depth, has been separated in two ponds by an intermediate dike. The east pond has been abandoned, now overgrown with vegetation, and is to be designed to contain future production of the black liquor of maximum capacity of 55,000 m^3. The bottom and slopes of the pond total an area of approximately 18,000 m^2 (bottom area of 10, 000 m^2).

The back liquor at 90°C must be stored in this open pond at a rate of 150,000 liters per day, even during the winter period. The liquor composition is approximately 76% water, 5% inorganic material (mostly sodium carbonate), 17% soluble organic components and 2% of particulate matter as fine wood and bark fragments. Also, 7,500 to 11,000 liters of a nitric acid washing solution must be pumped every two weeks into the pond.

This paper will present the specifics of design and construction criteria related to the geosynthetics installation and the quality assurance program implemented. Particularly the PP geomembrane specific installation parameters and advantages will be discussed and the difficulties encountered during installation will be presented. Data gathered during the leak detection program will be presented and analyzed.

DESIGN CONSIDERATIONS

Many restraints had to be taken into consideration for the design of the lined pond such as maintaining the initial geometry of the pond, balancing the volumes between cut and fill materials to avoid backfill importation, avoiding rock excavation (the localization of the bedrock level has been estimated to be less than 2 meters below the existing lagoon bottom level), creating a low point to empty the pond whenever needed, selecting suitable synthetic liner that can sustain extreme thermal gradients and resisting nitric acid attacks.

A drainage trench consisting of clean stone and a 6" diameter HDPE perforated pipe wrapped by a 150 g/m^2 geotextile, was installed under the flexible membrane liner to control the water pressure from water table upraising and to intercept infiltration. Following a 0,5% longitudinal slope and combined to a 15 cm thick sand layer lying under the liner with bottom lateral slopes of 1%, this drainage system was necessary to evacuate the water-table pressure lifting the liner in empty cell conditions. The drainage pipe is connected to a 60" circular concrete manhole equipped with a pump and floats to return to the cell any collected water or black liquor that could have leaked through the liner system. A black liquor collector system, consisting of plastic pipe, a sump pump and a low point, was installed on the slope in the pond to insure collection of the liquor and to maintain a minimum residual head of 0,30 m black liquor at bottom.

As shown schematically on Figure 1, the interior slopes of the pond have been steepened to 2,8H:1V following a stability analysis and to stockpile the backfill material needed for the reshaping of the cell bottom. The existing intermediate dike was enlarged to allow for the construction of the anchor trench (120 x 76 cm) and its height increased to optimize the volume of black liquor stored.

Because thermal conditions creating great thermal shocks whenever the hot liquid, at 90°C, is transferred into the pond lined with a synthetic liner at a freezing temperature, minimum temperature of -20°C, a reinforced Polypropylene geomembrane 1.14 mm thick was selected to be installed on the bottom and slopes of the pond. A nonwoven polypropylene geotextile 400 g/m^2 (3,5 mm thick) and 1450 N tensile strength has been sandwiched between the geomembrane and a layer of 150 mm of sand as protection layer against puncture.

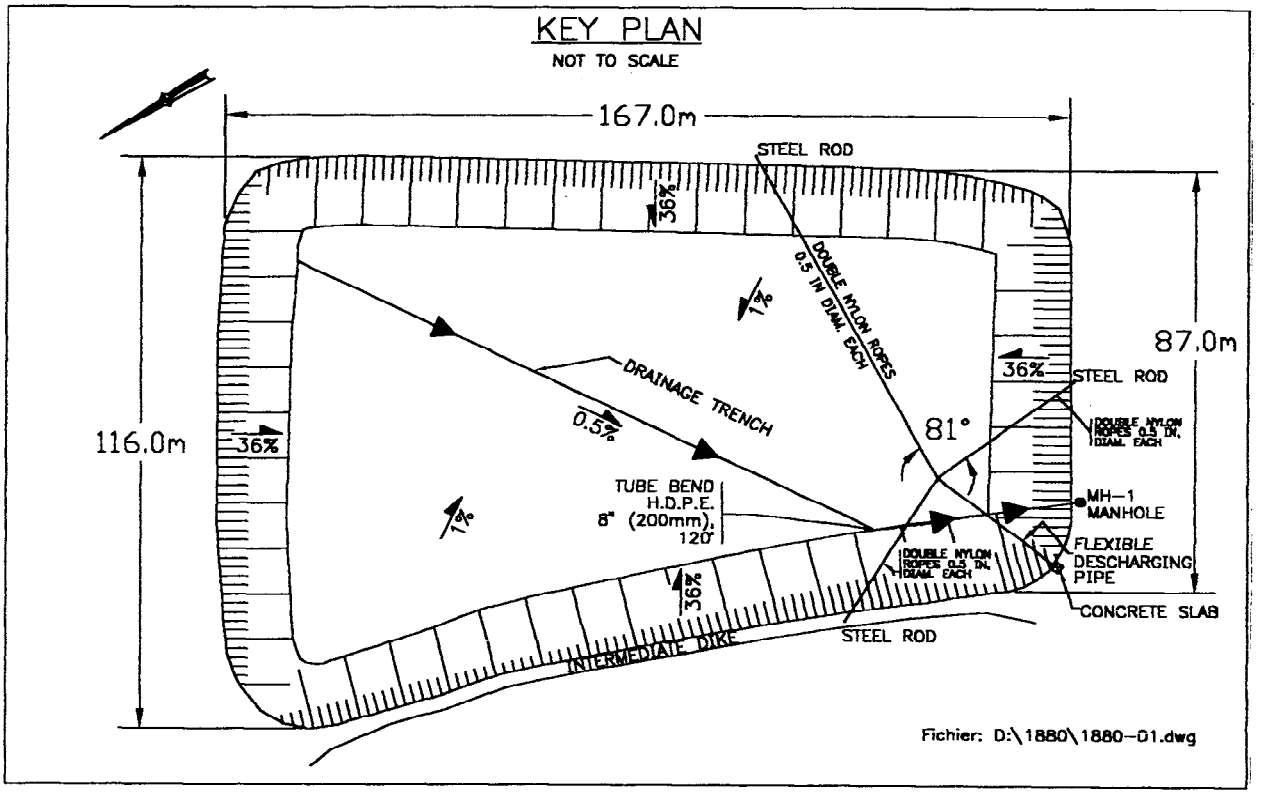

Figure 1. Schematic top view of the cell

During the construction phase, a construction quality assurance (CQA) program was implemented for the liner installation. It included an electrical leak detection survey on the uncovered geomembrane during installation. The total bottom covered area was checked for leak detection using a developed technique capable of detecting small holes and faulty welds on the exposed PP geomembrane.

LINER SELECTION

Past experience

Many geomembranes are commercially available but few can resist so great thermal shock whenever the hot liquid, at 90°C, is transferred into the pond lined with a synthetic liner at a freezing temperature lower than -20°C. The types of geomembranes used as liners in black

liquor lagoons have been butyl rubber, polyvinyl chloride (PVC), chlorosulfonated polyethylene (CSPE) and high density polyethylene (HDPE) (Peggs 1993). From 1984 till 1993, HDPE liners appears to have replace CSPE that has provided the best service.

The HDPE membranes were selected because of their resistance to potential chemical attack from the black liquor and associated soap and 20% nitric acid solutions. A number of HDPE geomembrane lining systems installed at several pulp and paper mills for the containment of hot black liquor during servicing of recovery boilers have failed after being in service for less than one year (Peggs 1993). At one site, the failure was due to environmental stress cracking in the presence of the black liquor and associated soap solutions. As an additional limitation, the HDPE geomembrane manufacturers are recommending a maximum temperature fluctuation less than 70°C and are specifying that a heat absorption system be installed whenever the temperature fluctuation is forecasted to be greater.

Recently, polypropylene geomembranes have been proposed as replacements for HDPE to extent the service lives of installations (Peggs 1993). In this paper, study of PP characteristics related to require performance is presented.

Mechanical properties

Flexible polypropylene has demonstrated outstanding tensile and impact performance, very high flexibility, low temperature behavior, environmental/chemical resistance and durability (Kilius 1993, Shah 1993). Its elongation at failure (over 150%) gives a high ability to conform to differential settlements in earth containment works. Thick non-reinforced PP sheets can resist point stress over rough substrates. The reinforced PP geomembrane resin density is equal to 0.91 g/cm^3 (Sageos 1997).

Chemical resistance

Results of the tests performed on the chemical resistance of geomembranes immerged for 21 days in a black liquor at 70°C (Peggs 1993) are presented in Table 1. The analysis of the initial and final property values of immersed HDPE, VLDPE and PP geomembranes is indicating that the polypropylene geomembrane resistance to the black liquor attack is acceptable. Its lower crystalline content dramatically reduces any risk of environmental stress cracking making it a good candidate for the containment of surface-active chemicals such as those found in hot black liquor.

The chemical resistance of PP geomembranes to organic solvents was tested (Shah 1993). No significant detrimental effect from exposure to saturated solutions of these solvents was detected.

Dimensional stability

To minimize stresses resulting from important expansion and contraction of the liner during its service life, the geomembrane thermal stability must be very high. The ASTM-D696 standard procedure is usually used and results obtained from such a test are presented in Figure 2 (JPS 1993).

Table-1: Chemical resistance of liners exposed to black liquor (Peggs 1993)

GEMEMBRANE CHANGE IN PROPERTIES AFTER EXPOSURE TO BLACK LIQUOR					
PARAMETER	INITIAL PP	FINAL PP	CHANGE (%) PP	HDPE	VLDPE
Mass (g)	15.718	15.721	0.02	0.03	0.24
Thickness (mils)	40.7	41.1	1.0	-0.5	-1.72
Dimension					
-Roll Direction (in.)	3.896	3.907	0.28	-0.03	0.00
-Cross Roll (in.)	6.772	6.721	0.75	0.22	0.00
Tensile					
-Break Stress (psi)	2409	2438	-1.1	8.0	21
-Break Elongation (%)	1152	1084	-5.9	-7.0	78
Oxidation Temperature (^{0}C)	244.96	243.44	-0.62	-2.00	-4.00
Composition					
-Polymer/Adds. (%)	96.9	96.89	0.01	-	-
-Residue (%)	3.10	3.11	0.32	-	-
-Combustible (%)	2.76	2.76	0	-	-
					-
Onset of decomposition (^{0}C)	291.8	289.6	-0.8	-	-
Infrared Spectrum	-	-	no change	no change	no change

The maximum and minimum displacement per 30.5 meters length of geomembrane when exposed to a 32°C change in temperature for VLDPE, HDPE, PP and reinforced PP geomembranes are compared. It can be observed from the obtained results that the linear coefficient of PP samples are lower than both PE products: the PP reinforced liner has deformed 692% less than the PE sample and 240% less for flexible PP. The reinforced PP is expected to

expand less enabling the membrane to lay-flat with minimum undulations or wrinkles in the sheet resulting in outstanding dimensional stability.

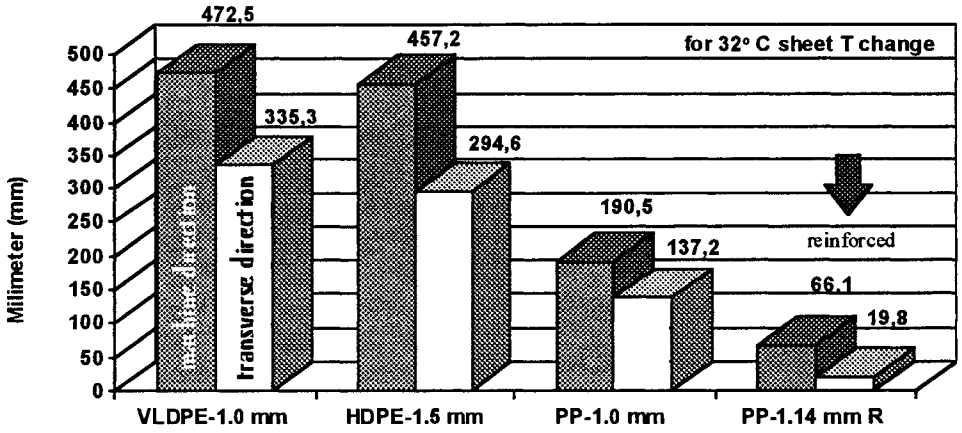

Figure-2: Geomembranes thermal dimensional stability

Factory-fabricated panels

Flexible liners such as PVC, PP and scrim-reinforced PP liners are lightweight allowing the flexibility to fabricate very large panels while minimizing field seaming, providing simpler assembly plan and easiness in field installation. From in plant controlled welding characteristics, homogeneous wedge seams with consistent peel and shear strength can be obtained easily. The number of pre-welded sheets constituting a panel must be limited to obtain a workable weight panel for transportation, field installation and overlapping using available equipment and manpower.

Figure 2. Photograph of PP panel carried to the site

From past experience, the maximum panel size should be limited to 1400 m^2 or approximately 1,400 kg (Solmers 1997) to avoid the use of heavy mobile equipment on the site to transport and lay down the panels. As shown in Figures 2 and 3, the pre-fabricated PP panels were transported to the edge of the slopes and then manually installed on pond slopes and bottom without the use of heavy equipment circulating on the bottom and slopes of the pond.

Figure 3. Photograph of PP geomembrane panel deployment

Field welding

The PP sheets have a wide window of welding parameters double wedge equipment. Wedge welding machine speeds can be obtained with an acceptable temperature window ranging 300 to 500°C as shown in Figure 4.

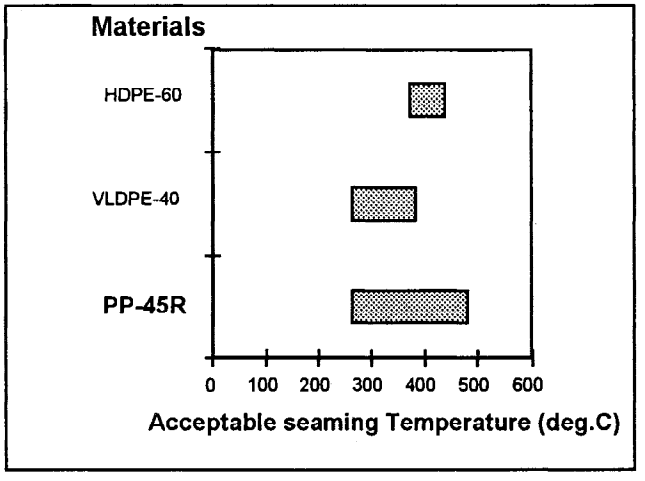

Figure 4. Seaming temperature window

The prefabricated panels were welded using dual seam welding machines operating at speed ranging from 1.23 to 1.98 m/min and at temperature fluctuating from 413 to 504°C. The PP geomembrane was welded with an equivalent procedure as being developed for HDPE sheets welding at a higher speed. Calibration tests performed on trial seams indicated acceptable average shear and peel resistances (14.8 kN/m for the peel resistance and 18.9 kN/m for the shear resistance) (shown in Figure 5) greater than the supplier recommended values.

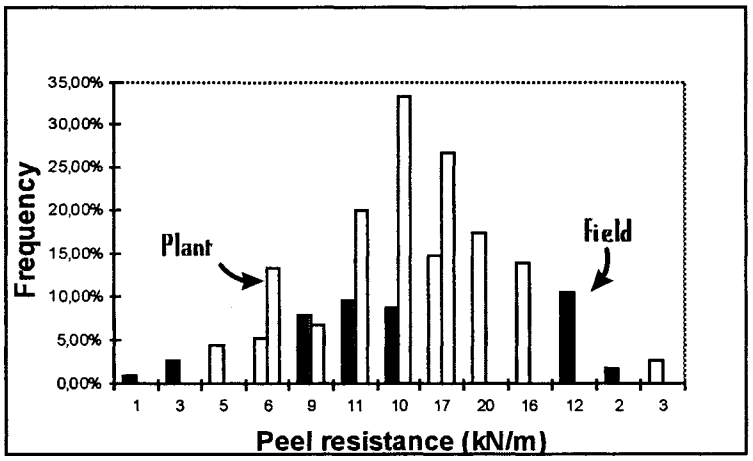

Figure 5. Peel resistance of PP seams

At specific areas and for repair patches, hot air hand welding was performed. With an overlap of 150 mm, the upper surface of the sheet and the lower face of the patch were heated and then press together manually using a hand roller.

LINER DESIGN AND INSTALLATION

A written and knowledgeable-prepared CQA plan including the review of the design drawings, approval of the installer QC procedures, the inspection of the geosynthetic products before their installation, on-site seam testing program and a leak detection survey was approved by the client. As stipulated in the CQA program, the installer assembly plan was reviewed prior to proceed with a quality control program during the entire period of installation consisting in ensuring the integrity of the geotextile and the liner and the quality/resistance of the liner seams. Conformity tests were performed by an independent laboratory on material delivered on site and on performed seams.

A total length of 1,303 meters of double and single-track fusion seams were performed and tested for continuity using the air lance and vacuum box non-destructive tests. The CQA program requested destructive shear and peel seam testing after each 130 meters of seaming.

During installation, less waves and wrinkles were observed resulting from temperature changes due to the great thermal stability of the liner. Also it was found easier to install the panels on top of the slopes and in the anchorage trenches as a result of the liner flexibility.

The main disadvantage during installation was related to the low friction between the PP liner and the geotextile. Because of the high friction resistance between these two materials, the membrane was sticking to the geotextile making it difficult to install. A specific geotextile with a calendered surface in contact with the liner should be used in the future for easiness of installation.

LEAK DETECTION SURVEY

A leak detection technique was used to locate leaks in the polypropylene uncovered geomembrane (Rollin 1998 and 1999). An electrical potential, 24 DC voltage, is applied between a water puddle and the conductive soil sub-grade layer. The PP geomembrane being an electrical insulator, no electrical current is conducted in the absence of leaks. As water flows through a leak, a current is immediately detected by an audio signal, informing the operator of the presence of a perforation in the geomembrane. The main advantage of the technique is the possibility to detect leaks in liner seams and sheet (100% of lined area) as work progressed during the installation phase. The geo-electrical survey rate of approximately 400 m^2/h per operator does not affect the installation work schedule and allows for a rapid quality control of the installer's work (Figure 6).

Figure 6. Photograph of an operator surveying the pond liner

Water is usually supplied by gravity from a tank truck parked at the top edge of the pond or cell. The low voltage and current used with this technique do not involve any risk for the operator. Approximately 11,000 m^2 of liner have been surveyed, an area corresponding to the bottom area of the pond (67% of the total lined area). As described in Table 2, a total of six (6) leaks were detected in location as shown in Figure 7. Except for a faulty manufactured seam, all other leaks are the results of human activities: two knife cuts, one wedge overheating and two holes resulting from pliers used during non-destructive testing of seams. PP liner being less resistant to knife cuts and equipment piercing than HDPE membrane, greater care must be taken during its installation. A photograph of the faulty seam is presented in Figure 8.

Table 2: Leak types and dimensions

Type of detected leak	Leak size (mm^2)
Manufactured seam	< 2
Knife cut	2 to 10
Knife cut	> 10
Pliers damage during installation	< 2
Pliers damage during installation	> 10
Wedge overheating	2 to 10

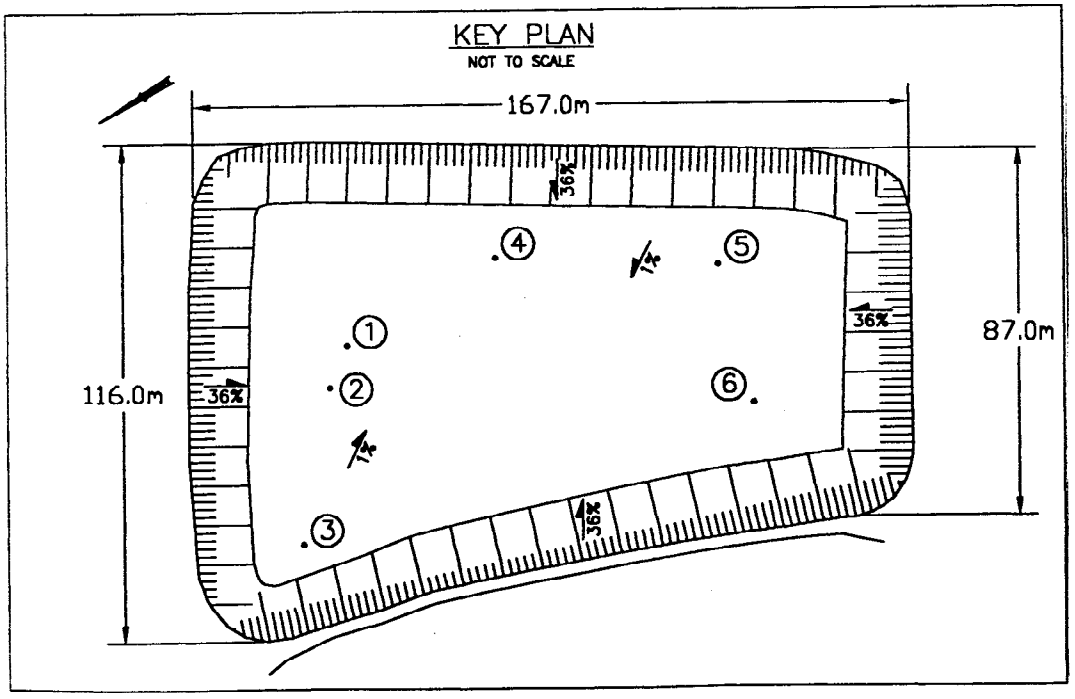

Figure 7. Leaks location from electrical detection system

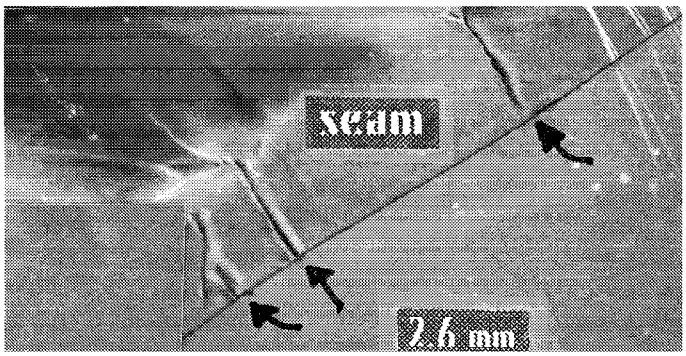

Figure 8. Photograph of a faulty manufactured seam

The leak density of 5.24 leaks/ha is greater than expected from the strict CQA program implemented, the high quality of the sub-grade material used and the presence of a geotextile sandwiched between the liner and the sub-grade soil (Rollin 1999). It is interesting to point out that no holes were found during the survey resulting from poor quality of the sub-grade material or from equipment movement on the liner. All leaks resulted from human operations.

The average size of the leaks is 15 mm^2. A leakage rate of 29,000 l/d-ha (11,921 m^3 per year) has been estimated using equations proposed by Giroud and Bonaparte (1989) and taking into account a 2.5 m hydraulic head and the presence of a 0.30 m thick sand drainage layer of 1×10^{-3} m/s permeability.

$$Q = C_B \, a \, \sqrt{2 \, g \, h} \, ,$$

Where $a = 1.5$ E-5m^2,
$h = 2.5m$,
$g = 9.8$ m/s^2
C_B = dimensionless coefficient related to the shape of the edge of the aperture ; for sharp edge, $C_B = 0.6$),

In detecting and repairing the leaks found during the implementation of the electrical leak detection survey, almost 12 millions liters of black liquor per year were diverted from migrating through the liner. This volume of liquid is equivalent to 19% of the reservoir's capacity.

The number of leaks found during this electrical leak detection survey performed after rigorous Construction Quality Assurance Program stresses the need to improve existing programs. Greater care must be exercised during construction phase for high quality of sub-grade and cover soil materials, accuracy of installation of liner on sub-grade soil, and inspection of welds in vicinity of pipe penetration, sumps and at repair patches. The electrical leak detection system

has demonstrated its validity and usefulness and should be included in a construction quality assurance program.

MONITORING

The pond was in operation before the 1997 winter months and a monitoring visit was done in June 1998 to survey the pond liner and drainage accessories. The overall performance of the pond was excellent and the monitoring of the liquid pumped from the drainage system installed under the liner indicates that the liquid is exempt of the black liquor color.

A HDPE 200 mm diameter pipe used to pump the black liquor from and in the pond collapsed under the sump pump action and had to be replaced by a steel pipe. The HDPE floating drums platform to which a Hypalon flexible pipe used to fill the pond is attached has been functioning well. A security procedure was implemented to insure that at all time a minimum depth of 0.30 m of liquid must be maintained in the pond to prevent contact between the floating platform and the liner.

CONCLUSION

The Polypropylene reinforced geomembrane did resist the great thermal shock during the first nine (9) months of operation where the hot black liquid, at 90°C, was transferred into the pond at a freezing temperature lower than -20°C. PP liner appears to have replaced successfully other synthetic liners that have provided poor service in the past. The PP membrane was selected because of its dimensional stability to very large temperature fluctuations and for its resistance to potential chemical attack from the black liquor and associated soap and 20% nitric acid solutions.

The prefabricated PP panels were welded using dual seam welding machines operating at speed varying from 1.23 to 1.98 m/min and at temperature fluctuating from 413 to 504°C. It was notice that the PP sheets have been welded more rapidly using an equivalent procedure has being developed for HDPE sheets welding.

Approximately 11,000 m^2 of liner have been surveyed by an electrical leak detection technique. A total of six (6) leaks were detected at the bottom of the pond. Except for a faulty manufactured seam, all other leaks were the results of human activities: two knife cuts, one wedge overheating and two holes resulting from pliers used during non-destructive testing of seams. PP liner being less resistant to knife cuts and equipment piercing than HDPE membrane, greater care must be taken during its installation. In detecting and repairing the leaks found during the survey, almost 12 millions liters of black liquor per year were prevented from migrating through the liner. The electrical leak detection system has demonstrated its validity and usefulness and should be included in a construction quality assurance program.

The overall performance of the pond was excellent during the winter months and the monitoring of the liquid pumped from the drainage system installed under the liner indicates that the liquid is exempt of the black liquor color. The usefulness of such a drainage system is to permit a long-term follow-up of the facility.

ACKNOWLEDGEMENTS

The authors wish to acknowledge the contribution of Greig Graham, Project Coordinator, Terrafix, Gordon E. Tripp, Superintendent of Eng. and Douglas R. Beemer, Project Engineer, Norampac, for their technical support.

REFERENCES

Giroud J.P. and Bonaparte R. (1989),"Leakage through Liners Constructed with Geomembranes, Part II: Composite Liners", Geotextiles and Geomembranes, vol. 8, no 2, pp 71-112

JPS Elastomerics Corp (1993), "Stevens Popypropylene Geomembranes", technical brochure.

Kilius D.E. (1993), "Cold Temperature Performance of Polypropylene Geomembrane and Seams", proceedings GRI 1993, pp 191-201, December.

Peggs I., Lewis D.R., and Dewijn T. (1993), "Geomembranes for the Containment of Pulp and Paper Mill Hot Black Liquors: Problems and Remediation", proceedings Geosynthetics'93, IFAI, St-Paul, pp .

Peggs I., Lewis D.R., Kilius D.E. and Dewijn T. (1993), "Geomembrane Liners for Black Liquor Lagoons: Problems and Remediation", proc. Canadian Pulp and Paper Association, technical section, Pacific Coast and Western Branches, Whistler, pp 1-6, May.

Rollin A.L. and Jacquelin T. (1998), "Geomembranes Failures: Lessons Learned from Geo-Electric Leaks Surveys", Lessons Learned from Geomembrane Failures, JPG Editing, to be published

Rollin A.L., Marcotte M., Jacquelin T. and Chaput L. (1999), "Leak Location in Exposed Geomembrane Liners using an Electrical Leak Detection Technique", proceedings Geosynthetics'99, Boston, March, to be published.

Shah A. and Frobel R.K. (1993), "Poplypropylene Geomembranes – The Alternative Containment Solution", proceedings Geosynthetics'93, IFAI, St-Paul, pp 1081-1092.

Sageos (1997), "Domtar, White Water Lining", technical report, project S234-001, October

Solmers (1997), "White Water Lagoon Lining", technical report, project 97-1756, November

OVERCOMING THE OBSTACLES: INSTALLATION OF A GEOSYNTHETIC COVER SYSTEM OVER HAZARDOUS WASTE PITS

Kenneth R. Daly
GeoSyntec Consultants, Huntington Beach, California, USA
James A. McKelvey, III
GeoSyntec Consultants, Huntington Beach, California, USA

ABSTRACT

A case history on the final closure of twelve hazardous waste pits at a site in Southern California is presented. The closure system consisted of a geosynthetic cover system overlying the pits and a low permeability soil cut-off wall serving as a vertical barrier along the perimeter of the pits. The project presented obstacles that had to be overcome during the design and construction phases of the closure system. The physical and chemical characteristics of the waste material contained within the pits posed unique challenges for both components of the closure system. Acidic refinery sludges and petroleum-laden drilling muds were the major constituents of the waste. Some of these components exhibited poor shear strength and were susceptible to appreciable settlement. As the closure system was required to have a 100 year design life, the acidic nature of the waste also posed durability concerns for the closure system components. Design and construction was also complicated by the objectionable odor of the waste, as waste disturbance would result in complaints from the adjacent community. Design and construction obstacles were further compounded by geometric site constraints.

Despite the obstacles encountered during the design and construction of the closure system, the project was completed on schedule without any major incidents. In addition to providing protection of the environment, the closure system provided an appealing end use in the form of a park-like setting containing a three hole expansion of the adjacent golf course. By discussing the major obstacles encountered during this project, and how these obstacles were overcome, insight for similar projects will be provided.

1. INTRODUCTION

1.1 Background

The McColl Site contains 12 unlined disposal pits on an approximate 8.8 hectare (22 acre) inactive waste disposal facility parcel in Fullerton, California. The pits contain approximately 55,000 m^3 (73,000 yd^3) of acidic refinery sludges and petroleum-laden drilling muds. The sludges were generated from the production of high-octane aviation fuel, and were placed in the disposal pits during the 1940s. Disposal of the drilling muds within the pits occurred during the 1950s and 1960s. Upon completion of disposal activities, approximately 0.3 to 1.5m (1 to 5 ft) of overburden soil was placed over the 8.5 to 16.8 m (28 to 55 ft) thickness of waste within the pits.

Residential developments border the site to the east and south. Along the site's western boundary is a golf course and a regional park, and a four-lane highway borders the northern boundary. As shown in Figure 1, the Site is divided into three areas containing the unlined pits: Los Coyotes, Upper Ramparts and Lower Ramparts.

The physical and chemical character of the refinery sludges and drilling muds within the pits has changed since initial deposition. The waste materials and the byproducts thereof exist in solid, liquid, and gaseous states. Site investigations performed during the design phase found that the distribution of the various waste constituents varied throughout the site. The waste material was characterized in the twelve pits as: a hard, solid material similar to asphalt; a viscous tar-like material; and the drilling muds. The viscous tar-like material was mobile and had seeped to the surface of the overburden soil at approximately fifty locations since initial deposition. The general area adjacent to the McColl Site underwent appreciable development throughout the 1970s and 1980s. Consequently, numerous complaints from the expanded community residents were received by regulatory agencies regarding odors emanating from the site. This prompted the McColl Site to be placed on the United States Environmental Protection Agency's National Priorities List (NPL) in 1982.

1.2 Scope of the Project

The primary objectives of the final closure system of the McColl Site were: long term isolation of the waste; minimization of rainwater infiltration; control of gases emitted from the waste; and compatibility with the expected end use of the site. A cover system, including a gas collection and treatment system, was designed and constructed to provide long term isolation and minimize infiltration. A subsurface vertical barrier around the pits, consisted of a low permeability soil cut-off wall, minimizing outward lateral waste migration and inward lateral migration of surface liquid. Slope stability improvements were required to mitigate several unstable slopes adjacent to the pits. In addition, surface water controls at the site were enhanced. As the focus of this paper is on the design and construction of geosynthetic components of the final closure system, discussion of the low permeability soil cut-off wall and surface water management improvements will not be presented.

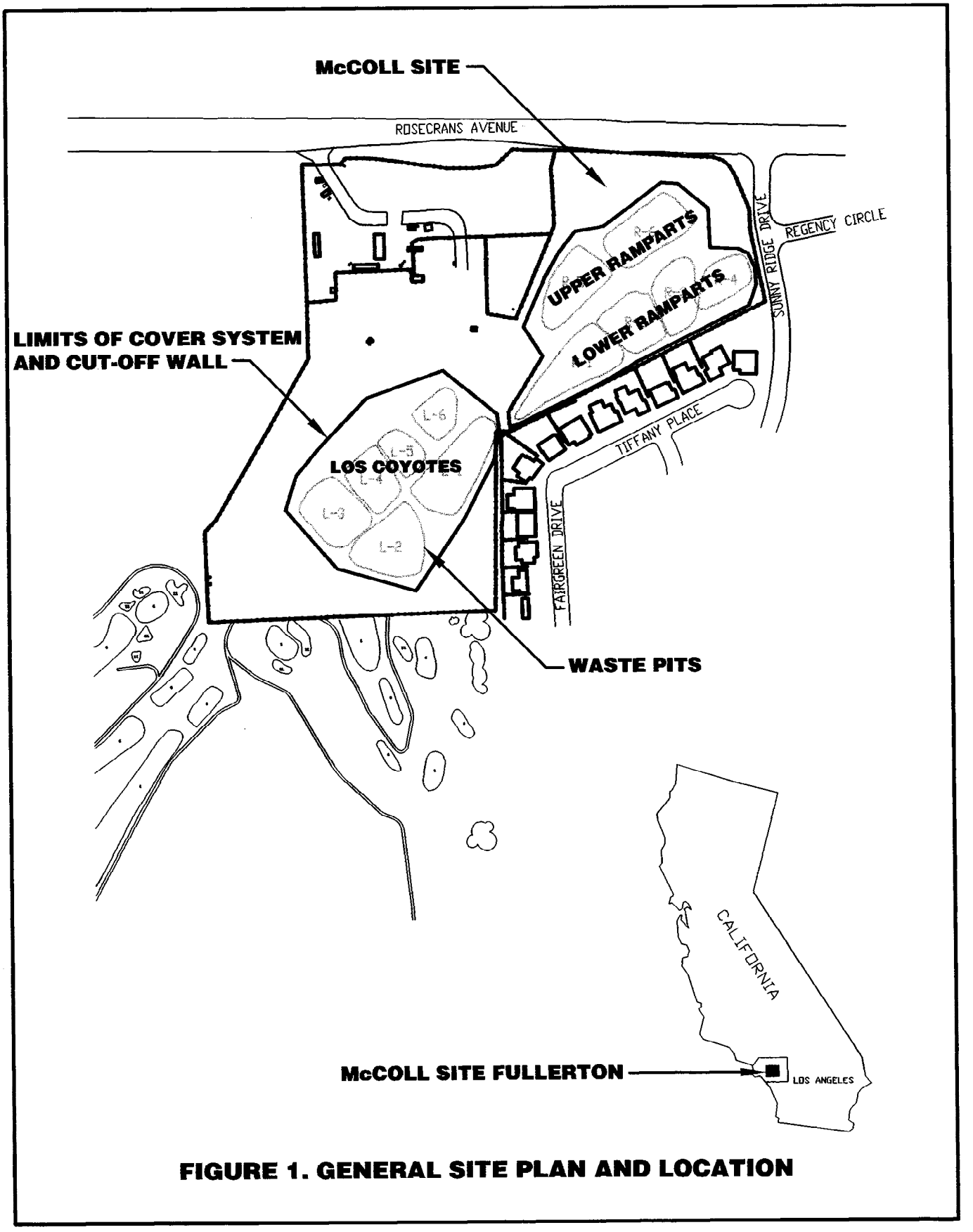

FIGURE 1. GENERAL SITE PLAN AND LOCATION

1.3 Design Considerations

As previously discussed, the waste material throughout the pits included a viscous tar-like material and soft drilling muds. These materials were not present in equal proportions nor were they evenly distributed within the pits. In consideration of these physical waste characteristics, the cover system was required to sustain overall settlement and differential settlement. Pits in the Lower Ramparts area contained a high percentage of drilling muds and therefore the weight of the cover system in this area needed to be minimized to reduce the potential for settlement and possible bearing capacity problems.

The refinery sludges and subsequent byproducts thereof within the waste possessed a low pH and high concentrations of organic sulfur, aromatics, and hydrocarbons. Site investigations indicated that the average pH of these waste materials was 3.5, ranging from 1 to 8.1. It was felt during the design that the durability of the final closure system components could be adversely impacted by the chemical characteristics of the waste. Accordingly, an extensive chemical compatibility program was undertaken to assess the impact, if any, of the waste materials on the cover system components.

In some locations of the site, waste material existed as close as 3 m (10 ft) to the site property line. The proximity of the waste material to the property boundary presented space limitations to construction of the cover system. In addition, the aforementioned space limitations were compounded by steep slopes. These existing slopes were steeper than 2H:1V (horizontal:vertical) locally along the southerly perimeter of the site, and between the Upper and Lower Ramparts areas. The stability of these slopes was of concern to both the construction and long-term integrity of the final closure system.

The expected end use of the site was to expand the adjacent golf course by constructing three golf course holes over the Los Coyotes and Upper Ramparts areas. In the Lower Ramparts area, the end-use would consist of a park-like setting. Accordingly, the design of the final closure system needed to accommodate loadings and grading features associated with the end-use, as well as maintenance and golf course operations.

2. APPLICATION AND BENEFITS OF GEOSYNTHETICS

2.1 Geosynthetic Applications

Conventional construction materials and techniques were replaced with geosynthetics for many aspects of the closure system at the McColl Site. A geosynthetic clay liner (GCL) was utilized as the low permeability barrier of the composite cover system in lieu of a compacted clay liner (CCL). Geosynthetic reinforcement of the cover system was employed as opposed to stabilizing soft waste materials to adequately support the cover system. Geosynthetic reinforced earth structures rather than conventional crib or retaining walls were employed to stabilize slopes. In addition, a geocomposite was used in place of a granular drainage layer. In consideration of project specific conditions, the application of geosynthetic alternatives was often more suitable and cost effective than their conventional counterparts. The project specific conditions and subsequent benefit of utilizing geosynthetics is discussed further below.

2.2 Benefit of Geosynthetics

Cover systems in the United States for closure of waste facilities typically incorporate a composite barrier layer comprised of a compacted clay liner (CCL) beneath a geomembrane. The availability of sufficient quantities of on-site material suitable for construction of a CCL was questionable. Issues regarding site access, material storage, noise restrictions, construction traffic, and costs were also of concern. Furthermore, as previously discussed, the weight of the cover system needed to be minimized in the Lower Ramparts area and the constructibility of a CCL on the steep slopes would be problematic. In consideration of these project specific conditions, a GCL provided a more suitable alternative for use as the low permeability component of the composite barrier than a CCL.

Design considerations included the ability of the cover system to sustain settlements attributed to the soft nature and inhomogenous distribution of the waste materials. Excessive settlements of the waste materials under the final closure system loads could induce undesirable stresses in the geomembrane barrier, disturb surface water management controls, and alter the final surface grades of the golf course. To mitigate these concerns, geosynthetic reinforcement was required beneath the cover system.

Two types of geosynthetic reinforcement were used. The type of geosynthetic reinforcement used was dependent on the overburden stresses associated with the proposed cover system and the physical characteristics of the waste material in the pits. Cellular confinement reinforcement (geocell) was proposed for the Lower Ramparts area as this material would provide the needed reinforcement for the light-weight cover system. The Los Coyotes and Upper Ramparts areas did not contain drilling muds and would require appreciable soil overburden to provide the golf course grades. Geogrid reinforcement of the cover system was proposed in these areas.

Several areas of the site required slope stabilization. In addition, space limitations coupled with the slopes along the southerly boundary of the site necessitated construction of working platforms for construction of the low permeability soil cut-off wall. To address these issues, three reinforced earth structures were constructed on the site. One structure provided the working platform for cut-off wall construction. This structure supported an excavator with a gross operating weight of 1,100 kN (124 tons). Another structure was required to span the cut-off wall while buttressing the slope and waste pits behind the structure. This structure needed to sustain deformation while maintaining its integrity. This obstacle was overcome by selecting a geosynthetic-reinforced earth structure with a flexible fascia. In comparison to traditional retaining walls alternatives such as or reinforced concrete or crib walls, each geosynthetic-reinforced earth structure permitted landscaping of the fascia, which was considered more aesthetically pleasing than traditional alternatives.

3. GEOSYNTHETIC DESIGN

3.1 Cover System

Two different cover systems were used at the site depending on the physical characteristics of the waste material in the pits and the anticipated end use of the area. The two cover systems were referenced as the golf course cover system (Los Coyotes and Upper Ramparts areas) and the open space cover system (Lower Ramparts area). Both cover systems employed similar geosynthetic components. The primary component of the cover system was the barrier layer, comprised of a 40 mil HDPE

geomembrane over a GCL. The GCL was comprised of sodium bentonite adhered to a HDPE geomembrane carrier. To mitigate the potential degradation of the GCL's sodium bentonite component associated with long term exposure to the acidic waste, and to provide redundancy in waste isolation, the GCL would be installed with the geomembrane carrier side down. The cover system was generally comprised of, from top to bottom, a protection layer, a drainage layer, a barrier layer, a gas collection layer, a reinforced foundation layer, and an unreinforced foundation layer. Details of the two cover systems are illustrated in Figure 2 and are discussed further below.

3.1.1 Golf Course Cover System

The golf course cover system was required to incorporate a means of protecting the geosynthetic components of the barrier layer from intrusion or excavations associated with golf course operations and maintenance. Protection of the geosynthetic barrier layer was achieved by means of a mechanical barrier layer. The mechanical barrier layer consisted of a 0.3 m (1 ft) thick layer of hard, durable, and rounded cobbles placed over the geosynthetics of the barrier layer. In addition, the mechanical barrier layer functioned as the required drainage layer. A geotextile cushion was used to protect the geosynthetic barrier layer from the cobbles of the mechanical barrier/drainage layer.

The geogrid-reinforcement required to support the soil overburden associated with golf course landscaping consisted of two layers of uniaxial reinforcement placed orthogonal to one another. This design permitted up to 4.6 m (15 ft) of fill for golf course landscaping.

3.1.2 Open Space Cover System

The design of the open space cover focused on minimizing the weight of the cover system, hence reducing settlement, and providing adequate reinforcement. As this area would not be subjected to golf course operations and maintenance, the mechanical barrier layer to intrusion or excavations was not required. Further weight reduction of the open space cover system was attained by using a geocomposite, as opposed to a granular material, for the drainage layer.

As the light-weight cover system was anticipated to minimize overburden-induced settlement of the waste, less displacement would be available to mobilize the strength of the reinforcement. The three-dimensional cellular confinement system (geocell) provided more stiffness than the two-dimensional sheet reinforcement and was able to effectively distribute construction loads as well as the weight of the cover system.

Due to space constraints along the southerly portion of the site, design of the open space cover system had to accommodate placement of the geomembrane portion of the cover system over a soldier pile wall. Puncture analyses performed using the method presented by Giroud et al., 1995, indicated that the effective puncture mechanism would be reduced by beveling the edges of the lagging boards as indicated in Figure 3. Furthermore, a geotextile cushion was required beneath the geomembrane. As shown in Figure 3, stable earthen material existed between the waste pit and the soldier pile wall, therefore stresses in the geomembrane associated with differential settlement of the waste were not anticipated at the top of the soldier pile wall.

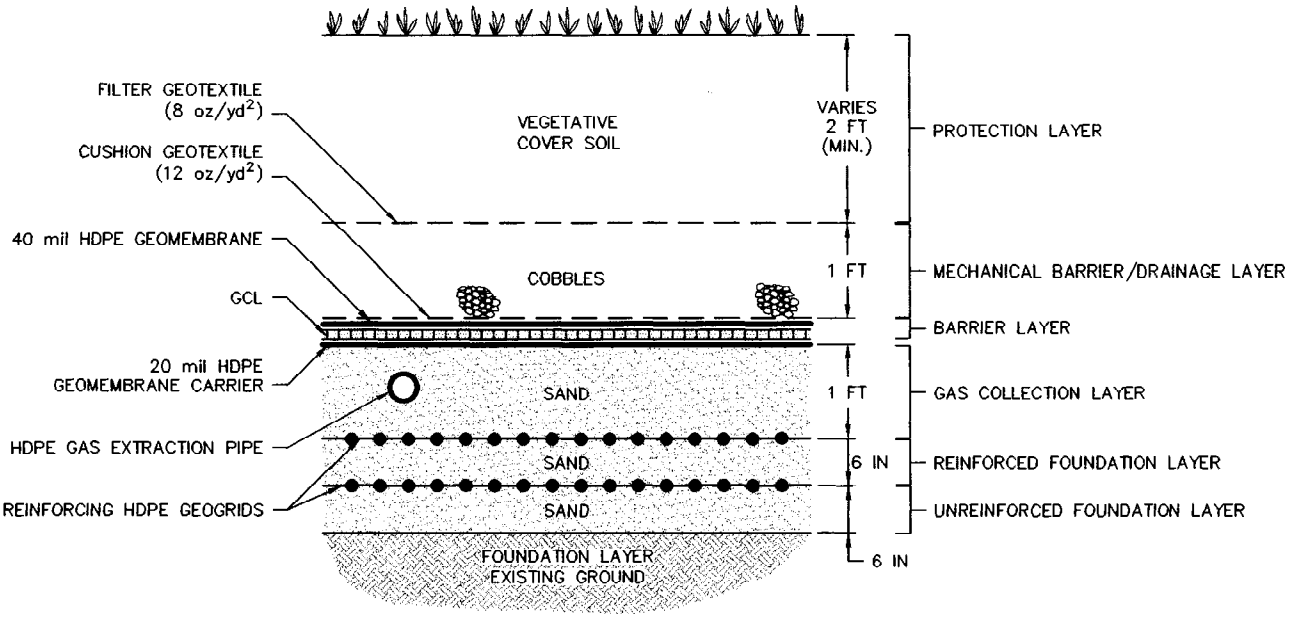

COVER SYSTEM - GOLF COURSE

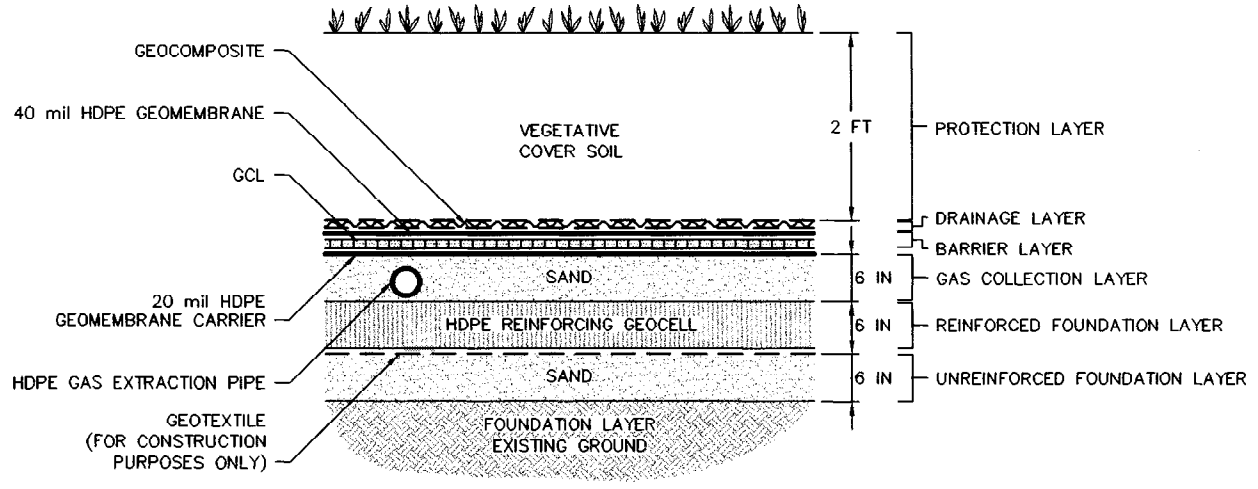

COVER SYSTEM - OPEN SPACE

FIGURE 2. COVER SYSTEM DETAILS

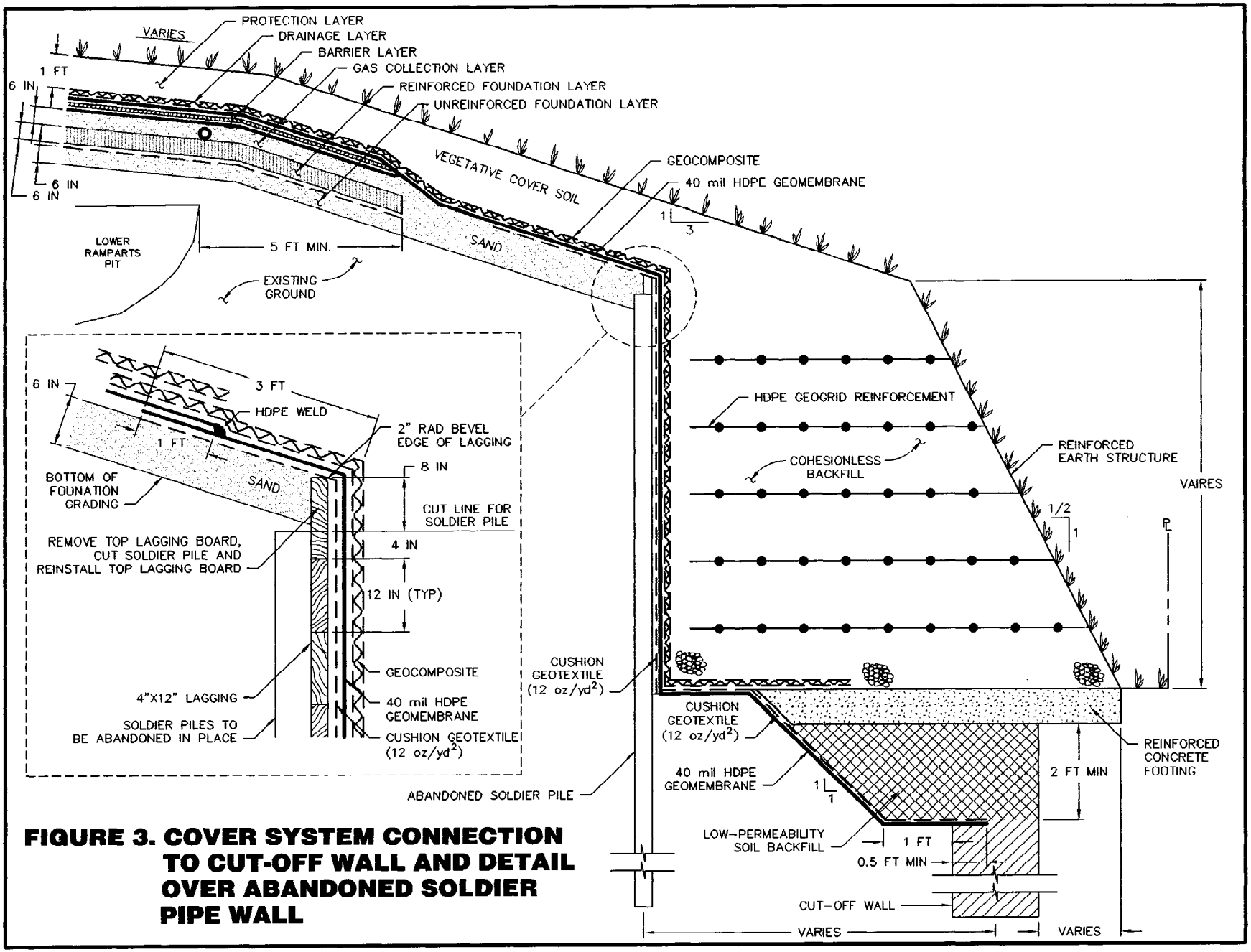

FIGURE 3. COVER SYSTEM CONNECTION TO CUT-OFF WALL AND DETAIL OVER ABANDONED SOLDIER PIPE WALL

3.2 Cover System Connection with the Cut-Off Wall

The main objective for the final closure system was to provide long term waste isolation. The cover system would provide vertical waste isolation, while the low permeability soil cut-off would provide lateral waste isolation. To provide continuity between the vertical and lateral barriers, the cover system/cut-off wall connection illustrated in Figure 3 was designed. Continuity was attained by sealing the geomembrane portion of the barrier within the cut-off wall. The connection design incorporated a trench along the top of the cut-off wall, which permitted the geomembrane to be "keyed" into the cut-off wall. The "key" was subsequently backfilled with low permeability soil providing intimate contact, and hence continuity, between the geomembrane and the low permeability soil of the cut-off wall.

3.3 Chemical Compatibility

Due to the chemical characteristics of the waste material at the McColl Site, it was critical that the chemical compatibility of geosynthetic components with the waste material be evaluated and accounted for in design. Based on the low pH of the waste, polyethylene materials were selected. However, there was concern that organic compounds in the waste could be soluble in polyethylene, hence reducing strength and increasing ductility. Furthermore, the possibility environmental stress cracking resulting from oxidation of the polyethylene in the presence of waste was of concern.

Prior to development of the final design, the chemical compatibility program was completed. The chemical compatibility study considered both chemical exposure and environmental stress cracking on the polyethylene materials proposed for use at the site. While the results of exposure testing indicated that the polyethylene materials would initially soften upon contact with waste derived liquids, degradation of the polymer would not be expected . Results of environmental stress cracking tests suggested that the stress crack resistance of materials would be adequate following exposure. Based on results of the chemical compatibility program, the design of the reinforcement materials included appropriate reduction factors. In applications where prolonged exposure was considered to be possible, reduction factors up to fifty percent were employed in relevant design properties such as tensile strength and puncture resistance.

4. GEOSYNTHETIC CONSTRUCTION

4.1 Cover System Reinforcement

Though most aspects of the geosynthetic installation of the cover system at the McColl Site were typical there were some unique features. Of particular mention are installation of the geosynthetic reinforcement layer of the cover system and the vertical installation of HDPE geomembrane over a soldier pile wall. Due to the complexity of the site and project schedule constraints, extensive coordination was required during construction. Furthermore, in order to meet the project schedule, phased construction was necessary in portions of the final closure system, which presented some obstacles.

The reinforcement layer of the golf course cover system consisted of two layers of uniaxial HDPE geogrid placed orthogonally to one another. The two layers of geogrid were separated by 152 mm (6 in) of sand. The reinforcement layer was constructed on a prepared sand foundation layer (Figure 2).

Permanent connections at the end of each roll of geogrid were provided by Bodkin joints. Neither permanent nor temporary (for construction) connections were provided at the sides of each roll of geogrid. This required additional care to prevent side to side separation of rolls while placing the sand layer over the geogrid. Geogrid panels were prestressed during placement of the overlying sand by anchoring one end of the panel with sand while pulling the other end taught with the bucket of a backhoe. A special yolk was constructed such that the backhoe could tension the geogrid without damage. The yolk consisted of a steel rod which slipped through the geogrid. Rope or chains were attached at each end of the rod and secured to the bucket of the backhoe.

Similar to the reinforcement layer of the golf course cover system, the geocell reinforcement of the open space cover system was founded on a prepared foundation of sand. However, a geotextile was placed on the prepared foundation prior to installation of the geocell to provide a suitable foundation for geocell installation (Figure 2). Though no rigorous mechanical connection was specified for joining geocell panels, geocell panels were connected with staples prior to subsequent sand infilling and backfilling. Observations during construction indicated that it was beneficial to maintain a uniform distribution of the overburden material while infilling and backfilling over the geocell.

To minimize potential problems associated with the soft characteristics of the waste material, provisions were included in the technical specifications limiting equipment loading during specific phases of construction. Maximum allowable ground pressures for tracked vehicles and rubber wheel vehicles were specified. Special measures, including the use of structural mats to attenuate ground pressures, were required for equipment exceeding allowable ground pressures.

4.2 Vertical Cover System Construction

Due to space limitations along the southerly portion of the site, a soldier pile wall was constructed to create a working pad for excavation of the cut-off wall (Figure 4). Subsequently, it was necessary to extend the geomembrane over the soldier pile wall to tie-in with the cut-off wall. Construction of the reinforced-earth structure (RES) in front of the soldier pile wall and overlying the cut-off wall was complicated. A construction detail illustrating the design of the soldier pile wall / cover system / cut-off wall / RES is presented in Figure 3. The soldier piles were trimmed below the elevation of the top lagging boards and edges of the lagging boards were beveled to minimize their impact on the integrity of the geomembrane. Two layers of geotextile cushion were then installed to protect the overlying geomembrane from puncture.

It was anticipated that construction of the RES would tend to pull the geomembrane panels draped over the soldier pile wall downward, which could develop undesirable tension in the geomembrane. During the design phase, it was considered that by carefully sequencing the construction of this detail, tension of the geomembrane could be minimized. First, the panels of geomembrane extending over the soldier pile wall and connecting to the cut-off wall would be installed. These panels would not to be connected with the remainder of the cover system until completion of the RES. As the end of the geomembrane panels were free to displace during construction of the RES, the potential for geomembrane tension would be alleviated.

Contrary to the original construction sequence, unforeseen events required that the geomembrane installation be completed in its entirety prior to construction of the RES (Figure 5). To preclude

development of unacceptable tension in the geomembrane, a relief cut was made in the geomembrane along the top of the soldier pile wall prior to construction of the RES. Geomembrane straps were then welded to the geomembrane at regular intervals on either side of the tension relief cut. The straps were installed with enough slack to permit displacement of the geomembrane while preventing the geomembrane from slipping over the soldier pile wall. In addition, tension resulting from displacement of the panels during construction of the RES was concentrated in the straps and not the panels themselves. A photograph of the completed RES constructed over the liner system, cut-off wall, and soldier pile wall is illustrated in Figure 6.

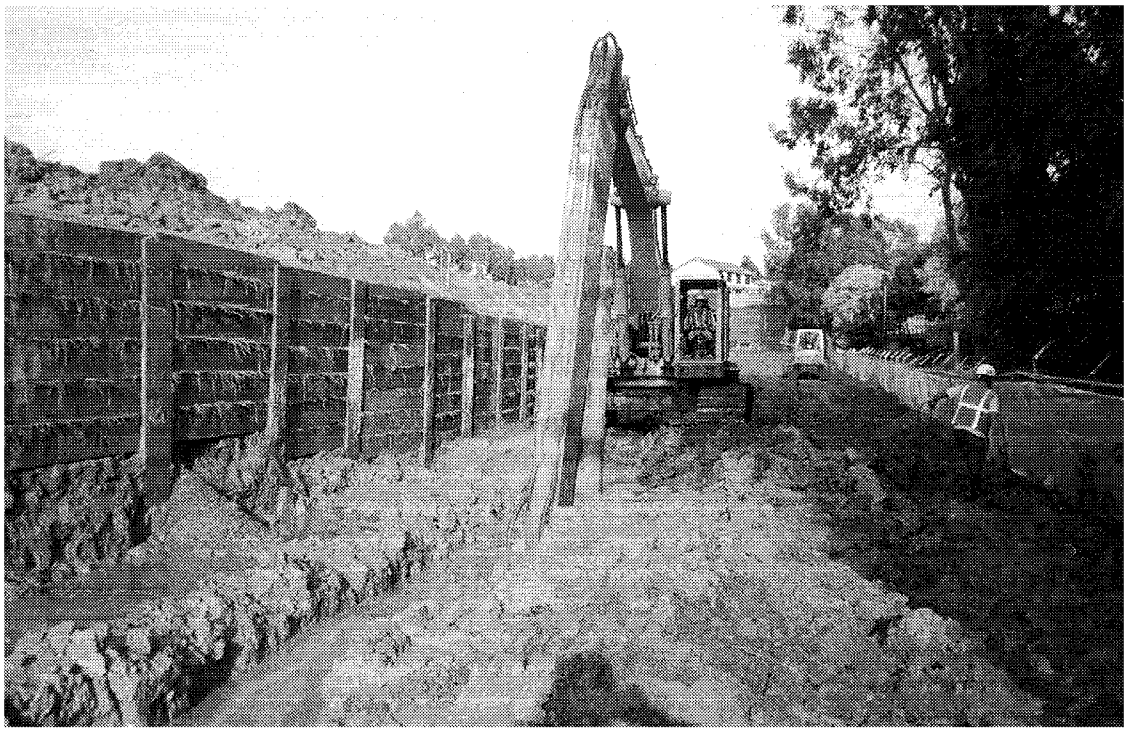

Figure 4. Soldier Pile Wall and Working Pad for Excavation of the Low Permeability Soil Cut-Off Wall

5.0 CONCLUSIONS

In consideration of project specific conditions, the application of geosynthetic alternatives was often more suitable and cost effective than their conventional counterparts. Replacing a traditional compacted clay liner with a GCL and using geocomposite material in place of an aggregate drainage layer helped minimize the settlement concerns. Geosynthetic reinforcement of the cover system was used to strengthen and support the cover system as opposed to stabilizing the waste material to provide sufficient bearing capacity to support the cover. Geosynthetic reinforced earth structures provided effective alternatives to crib or retaining walls in stabilizing slopes and creating working pads.

In addition to the demonstrated benefits of using geosynthetics, observations during design and construction for closure of the McColl Site provided several lessons. In regards to design, it was learned that actual chemical compatibility testing of materials is required for competent design. The exposure testing performed to evaluate chemical compatibility provided a rational basis for the use of appropriate reduction factors during design. Observations during construction indicated that the technique used to

tighten the geogrid reinforcement of the golf course cover system proved successful and the geogrid panels were not damaged during installation. It was learned that connections of adjacent geogrid panels would facilitate fill placement over the geogrid, as less care would be required to minimize separation of adjacent panels.

Figure 5. Completed Cover Installation over the Soldier Pile Wall

While not explicitly discussed in the paper, the success of this project and the ability to overcome the obstacles associated with this project was largely based upon the open communication between the design engineers, construction managers, contractors and concerned regulatory agencies. During the design phase of the project, "over-the-shoulder" meetings were held on regular intervals between the design team, client representatives and regulatory agencies, which allowed the design to be optimized while addressing concerns associated with the project. This open communication extended into construction by introducing the new members to the project (i.e., the contractors and construction managers) to the over-the-shoulder meetings, which allowed unforeseen obstacles during construction to be easily overcome.

6.0 ACKNOWLEDGEMENTS

The authors would like to acknowledge the parties involved with the successful design and construction of the closure system at the McColl Site including the concerned regulatory agencies (i.e., USEPA, CalEPA-DTSC). Parsons Engineering Science of Pasadena, California, and GeoSyntec Consultants, of Huntington Beach, California provided design, engineering, procurement, and construction management services. Construction was completed by Smith Environmental Technologies Corporation, of Torrence, Califorinia, and Lovco Construction of Long Beach, California.

Figure 6. Completed Reinforced Earth Structure over the Liner System, Cut-Off Wall, and Soldier Pile Wall

REFERENCES

Giroud, J.P., Sodelman, K.L., Pelte, T., and Beech, J.F., "Design Method to Prevent Geoemembrane Failure in Tank Corners", GeoSynthetics International, Vol. 2, No. 6, 1995, pp. 971-1018.

CONNECTION CAPACITY OF PRECAST CONCRETE SEGMENTAL UNITS AND GEOGRIDS: TESTING AND DESIGN CONSIDERATIONS

MICHAEL BERNARDI, PE
STRATA SYSTEMS INC., USA

BLAISE FITZPATRICK, PE
FITZPATRICK ENGINEERING ASSOCIATES, USA

ABSTRACT

The use and acceptance of Segmental Retaining Walls (SRW) with geosynthetic reinforcement is rapidly increasing in North America. In addition to external and internal stability considerations, analysis of the facing stability is also required. As part of the facing stability analysis, the connection pullout strength of the geosynthetic reinforcement between courses of precast concrete blocks is determined in the laboratory and the results of the tests are applied to determine the Factor of Safety against connection failure at all geosynthetic locations in an SRW. The paper will review the design considerations at the connections for the various design methodologies as well as the performance criteria associated with these methodologies.

The paper will also examine the connection capacity test method. A comparison of the results obtained from the different testing equipment will be made and the impact to the design will be pointed out. Connection failure will be addressed in terms of geosynthetic rupture and geosynthetic pullout.

The information provided in this paper has been normalized and reflects the results of testing with PVC coated polyester geogrid in combination with precast concrete segmental block units.

INTRODUCTION

The use of Segmental Retaining Walls (SRW) is becoming increasingly popular in North America. The use of soil reinforcement elements in the design and construction of SRWs has made it possible to erect retaining walls well in excess of 10 meters.

Several design methodologies have appeared over the last two decades. Three of the more widely used design methods in North America can be found in the following documents:

- National Concrete Masonry Association (NCMA), Design Manual for Segmental Retaining Walls, Second Edition;

- Federal Highway Administration (FHWA) Demonstration Project 82, (DEMO 82) Report No. FHWA-SA-96-071, Mechanically Stabilized Earth Walls and Reinforced Slopes, Design and Construction Guidelines; and

- Association of State Highway and Transportation Officials (AASHTO), Standard Specifications for Highway Bridges, and 1997 Interims (AASHTO T-15).

The methods described in the Demo 82 and AASHTO T-15 documents are essentially identical. Although there are significant differences between the methods described in the NCMA manual and the last two, the overall approach is similar. This paper will discuss the geosynthetic/modular block connection capacity requirement of the local facing stability component of the analysis. The paper will present and discuss the following topics related to the connection capacity issue:

- testing equipment and protocol;
- current design approach for determining the allowable design strength of a geosynthetic; and
- data interpretation and design implications.

TESTING EQUIPMENT AND PROTOCOL

Conceptually, the connection capacity test is simple. A layer of reinforcement of a given length is placed between two courses of block. The blocks are installed in the same way as they would be in the field. A normal load is applied and maintained to the column of blocks in an attempt to reproduce the confining pressures of the units located above the reinforcement. The reinforcement is then pulled out from between the blocks at a constant rate. The test is concluded when the reinforcement has either pulled out from between the blocks, when the reinforcement has ruptured, or when a combination of pullout and rupture has occurred. The test is repeated at different normal loads. For a given load, the pullout capacity is recorded as a function of displacement. The load displacement curves in Figure No. 1 illustrate typical results for a series of normal loads in a facing connection test.

The test is carried out in accordance with the NCMA Test Method SRWU-1, or the method described in Appendix A.3 of the DEMO 82 document. The Demo 82 test method is identical to the NCMA test method, with a few modifications. Typically, the test is carried out in either a "pullout box"-type apparatus or within a structural frame.

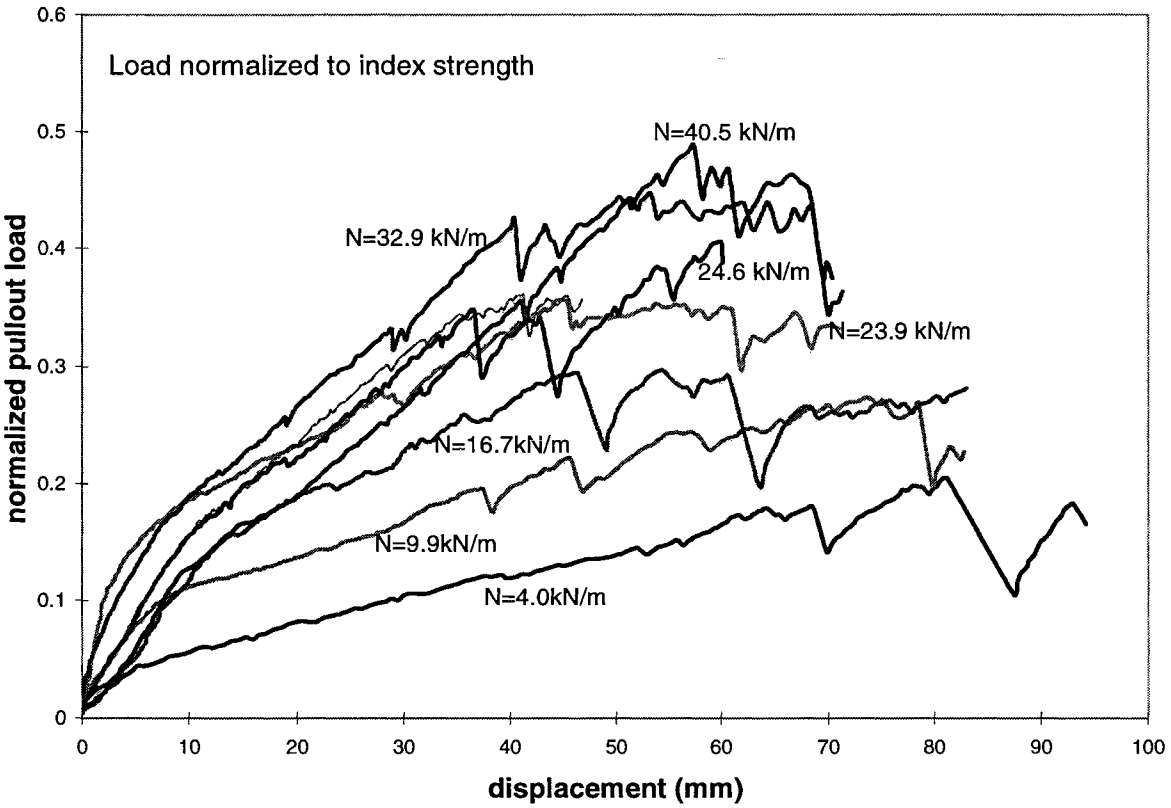

Figure No. 1. Typical Load-Displacement Curves for a Series of Normal Loads

From the information obtained in the load displacement curves, the peak displacement values are then plotted against the corresponding confining normal loads to produce the connection capacity curves as shown on Figure No. 2. The connection capacity curves are used to determine the facing connection strength for both the peak criterion and the serviceability criterion, if applicable.

The connection strength can then be taken directly from the connection capacity curves and, once applicable reduction and safety factors have been applied, will be used in design if it is less than the long-term allowable strength of the geosynthetic. In determining the connection strength from the connection capacity curves, the equivalent normal load can be equal to no more than the hinge height of the structure. The hinge height of a given segmental block system is a function of the batter or setback of the SRW and the depth of the precast concrete block.

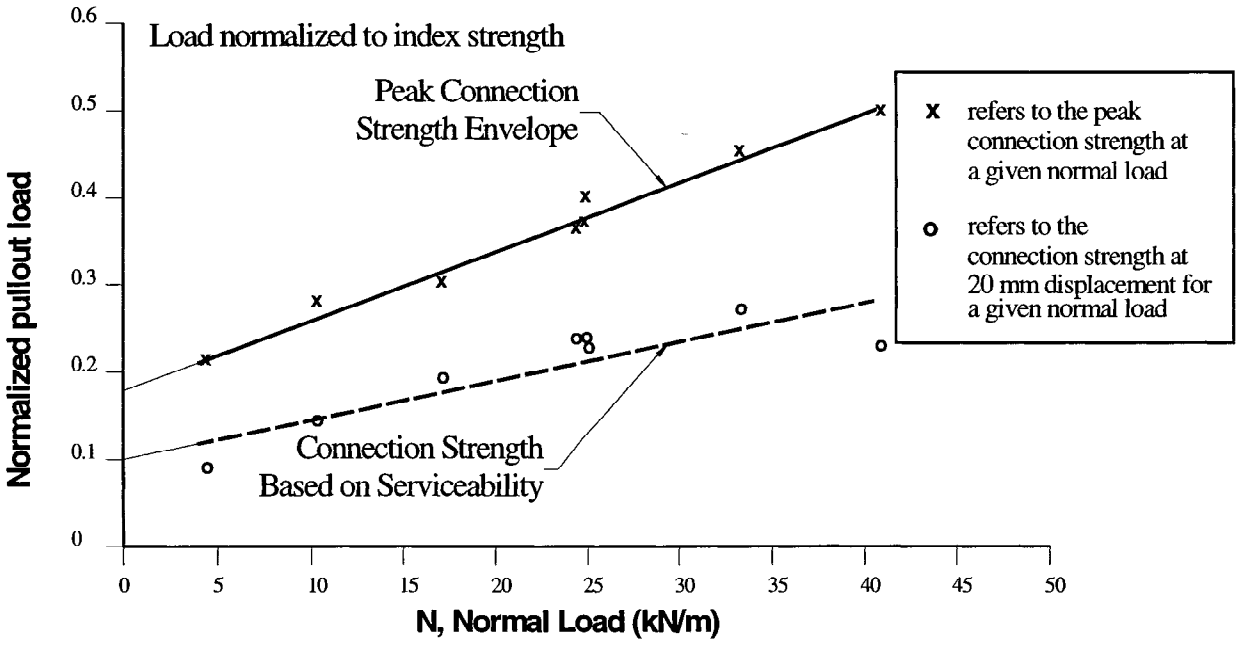

Figure No. 2. Connection Capacity Curves as a Function of Normal Load

The connection capacity curves, as shown in Figure No. 2, are unique to every SRW block/geosynthetic combination, and may also be unique to the testing laboratory. The connection capacity curves shown in Figure No. 3 is an example of the variability of the test results obtained from two laboratories.

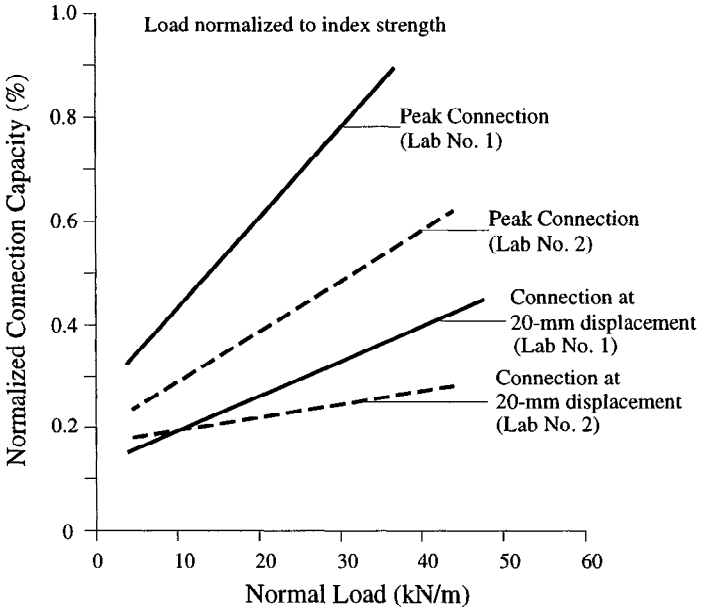

Figure No. 3. Comparison of Connection Capacity Curves for Identical Block/Geogrid Combination carried out at Different Testing Laboratories

The pairs of connection capacity curves shown in Figure No. 3 are the results of tests carried out on identical blocks and with the same geogrid reinforcement. The variability of the results, especially at higher normal loads, is significant. The intent is not to discredit the test, but rather to point out anomalies which may significantly impact designs of SRWs. Since connection capacity tests are rarely repeated, it is difficult to say how sensitive a block/geosynthetic combination is to testing at different laboratories.

CURRENT DESIGN APPROACH

In the facing connection stability analysis, it is conservatively assumed that the maximum tensile force that the connection must resist is the applied tensile force calculated at the failure surface. The NCMA defines the allowable long-term connection strength of a given geosynthetic/modular block combination as the least of the following values:

- the peak connection strength divided by an overall factor of safety;
- the connection strength based on serviceability; or
- the allowable long-term strength of the geosynthetic.

In the NCMA definition, the distinction between geosynthetic rupture and geosynthetic pullout as the mode of failure at the facing connection is not made. AASHTO and DEMO 82 treat connection at the face of retaining walls somewhat differently. Unlike the NCMA method, both the AASHTO and DEMO 82 methods have made a distinction between a rupture failure and pullout failure. In addition, AASHTO and DEMO 82 have modified the serviceability requirement. Instead of measuring the pullout capacity at the 20-mm displacement from the back of the block, it is implied that the deflection is measured from the end of the reinforcement at the front of the block. The AASHTO and DEMO 82 methods calculate the long-term allowable connection strength of a given geosynthetic/modular block combination as the least of the following values:

- the peak connection strength (based on either rupture or pullout failure);
- the connection strength based on the modified serviceability requirement; or
- the allowable long-term strength of the geosynthetic.

The method requires that, for connection rupture, the following relationships for determining the allowable long-term connection strength, T_{ac}, be satisfied:

$$T_{ac} \leq \frac{T_{ult} \times CR_u}{RF_{CR} \times RF_D \times 1.5} \qquad \text{(Eq. 1)}$$

and,

$$CR_u = \frac{T_{ultc}}{T_{lot}} \qquad \text{(Eq. 2)}$$

where T_{ult} is the Minimum Average Roll Value (MARV) of the ultimate strength of the reinforcement as per ASTM D4595, RF_{CR} is the reduction factor for creep, RF_D is the reduction factor for environmental aging, T_{ultc} is the peak connection strength from the rupture load displacement curves, and T_{lot} is the ultimate strength of the specific lot of geosynthetic used in the connection test (as per ASTM D4595). Note that Eq. 1 includes RF_{CR}, the reduction factor for creep. This equation is similar to the equation used to calculate the allowable long-term design strength of the geosynthetic reinforcement. In the latter, it is assumed that the geosynthetic will be subjected to a sustained load for the entire duration of the design life of the structure. The RF_{CR}, which is a function of the design life of the structure, is applied to the equation to ensure that the geosynthetic will not fail due to rupture prior to the design life. If the mechanism at the connection causes the connection to fail in rupture, then the RF_{CR} must be applied. It also implies that a load, which will result in creep failure of the geosynthetic during the design life of the structure, can be sustained at the connection.

Similarly, the method requires that, for connection pullout, the following relationships for determining the allowable long-term connection strength, T_{ac}, be satisfied:

$$T_{ac} \leq \frac{T_{ult} \times CR_S}{1.5} \qquad \text{(Eq. 3)}$$

and,

$$CR_S = \frac{T_{sc}}{T_{lot}} \qquad \text{(Eq. 4)}$$

where, T_{sc} is the peak connection strength from the pullout load displacement curves.

Note that Eq. 3 does not contain the RF_{CR}. In this instance, it is assumed that a load, which will result in creep failure of the geosynthetic during the design life of the structure, cannot be sustained at the connection.

FAILURE MODES

The definition of rupture and pullout in the AASHTO and Demo 82 documents; however, are not entirely clear. Although the documents do refer to the load displacement curves for determining whether the connection is a rupture connection or a pullout connection, there are no specific criteria on which to base the definitions.

It is submitted that the photograph in Figure No. 4 and the corresponding load displacement curve presented in Figure No. 5 are examples of geosynthetic pullout failure for the reasons stated below:

a) The peak connection strength occurs at a relatively large displacement. For this particular sample, the peak connection strength occurs at a displacement of 80 mm.

Furthermore, the test is terminated at a displacement of nearly 100 mm, with a decrease in pullout load of less than 16 percent of the peak pullout load. The peak connection strength is followed by an abrupt decrease in strength of the connection, but there is recovery of strength for the given confining pressures. This is indicative of pullout of the reinforcement from between the blocks.

b) Many of the machine direction ribs are still intact. In the test, twenty (20) of the twenty-three (23) machine direction ribs remained intact after completion of the test.

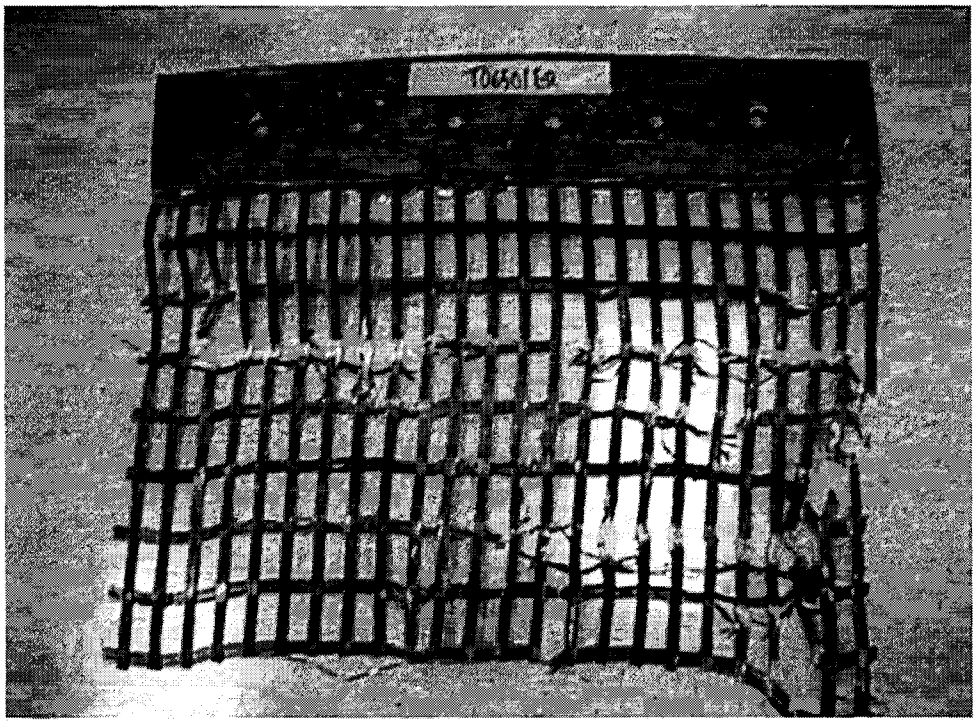

Figure No. 4. Photograph of geogrid reinforcement after completion of connection capacity test (pullout failure)

It is also important to note that the peak connection strength (Figure No. 5) occurs at a pullout load that is less than the creep reduced strength of the geosynthetic. The peak connection occurs at approximately 50 percent of the ultimate strength of the geosynthetic, whereas the creep reduced strength occurs at 62 percent of the ultimate strength of the reinforcement. Therefore, the sustained load at the connection for this particular normal load would not lead to geosynthetic failure, assuming a 100-year design life.

Compare the condition of the geogrid in Figure No. 4 and the condition of the geogrid shown in Figure No. 6. The majority of the machine direction ribs have clearly been severed for almost the entire width of the sample.

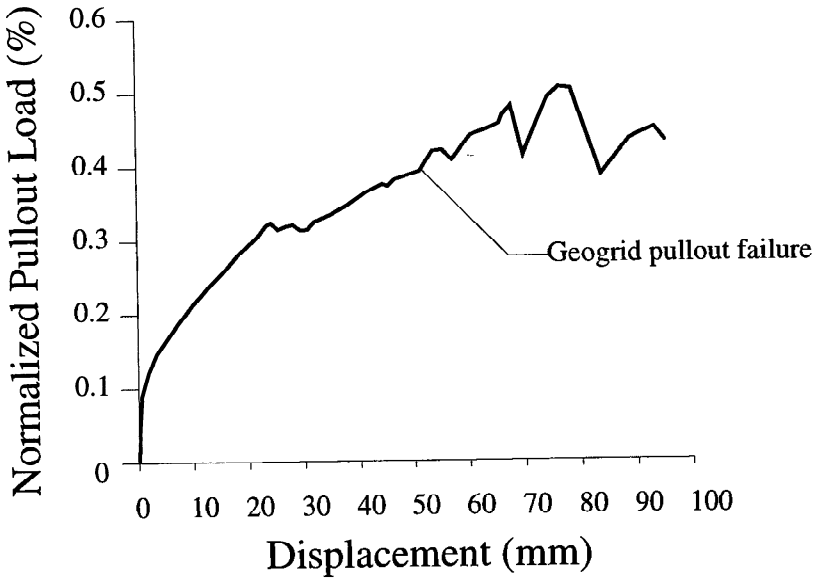

Figure No. 5. Corresponding load-displacement curve for test in Figure No. 4

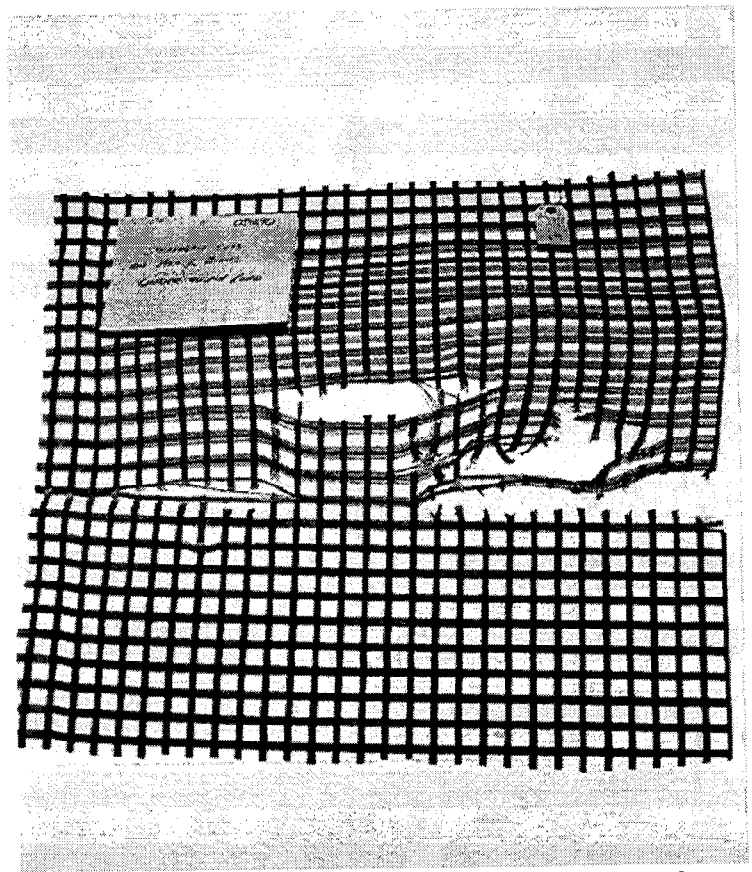

Figure No. 6. Photograph of geogrid reinforcement after completion of connection capacity test (rupture failure)

Compare also the load-displacement curve in Figure No. 7 with the one in Figure No. 5. In order to emphasize the comparison, the curves are presented on the same graph in Figure No. 8. The peak connection strength is achieved at lower displacements and the post-peak decrease in pullout load is more abrupt with no recovery in connection strength. Also note that, for this particular test, the peak strength is achieved at a level which is greater than the creep reduced strength of the geosynthetic. In this case, the sustained load at the connection can result in geosynthetic rupture failure during the design life of the structure.

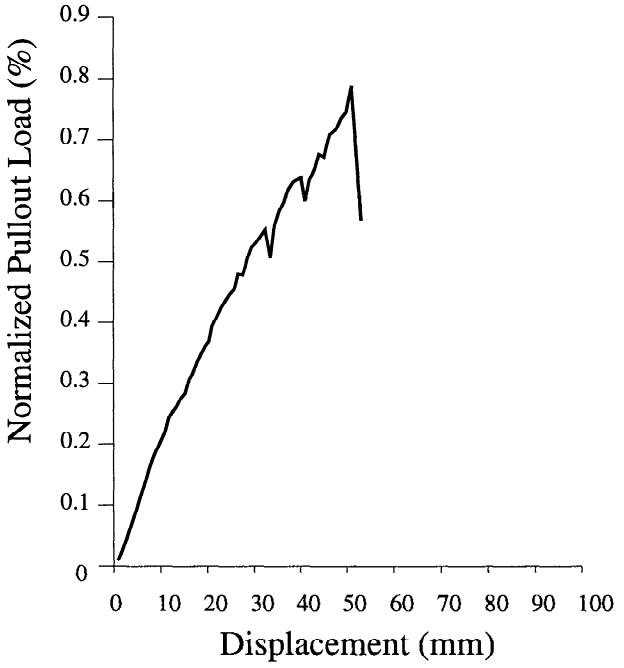

Figure No. 7. Corresponding load-displacement curve for test in Figure No. 6

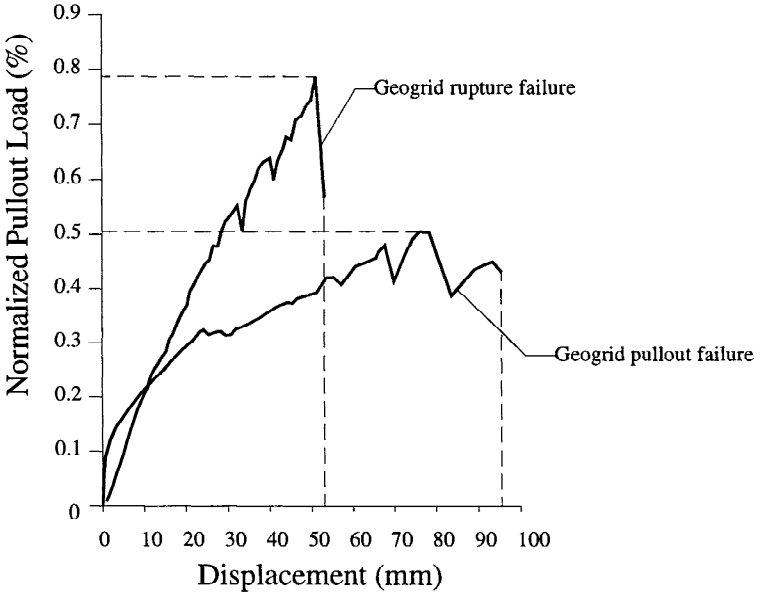

Figure No. 8. Typical load displacement curves illustrating rupture and pullout failure.

DATA INTERPRETATION AND DESIGN IMPLICATIONS

It has been shown that, except for the construction of the connection capacity curves (Figure No. 2), very little interpretation is required for calculating the long-term allowable connection strength for a given segmental block/geosynthetic combination when considering the NCMA method. Although the design implications that relate directly to the interpretation of the facing connection test and results are significant, the rules of interpretation are clear and lead to little confusion.

The same cannot be said for the AASHTO and DEMO 82 approach. The interpretation of the facing connection test and results, and the distinction between rupture and pullout failure of the connection test, are crucial because the design implications are significant. As indicated previously, additional reduction factors are applied to the calculation of the long-term allowable connection strength of the segmental block/geosynthetic combination if the mode of failure of the connection is rupture of the geosynthetic. Simple examination of the connection capacity curves (Figure No.2) is not sufficient to classify failure of the connection as rupture or pullout. Examination of the load displacement curves leads to a more accurate evaluation of the mode of failure.

Calculation of the long-term allowable connection strength for a given block/geosynthetic system based on the AASHTO and Demo 82 documents is simple if the mode of failure is clearly rupture or clearly pullout for the given system. However, it is likely that both pullout and rupture occur within the same series of tests for a given system. It is likely that pullout failure will occur at low to medium normal loads, and that rupture failure will occur at high normal loads. This may lead to misinterpretation of results and lead to improper calculation of the long-term allowable connection strength of the block/geosynthetic combination.

CONCLUSIONS

The facing connection test has been reviewed in light of two commonly used methodologies; that is, the NCMA method and the AASHTO and DEMO 82 methods. The following conclusions can be drawn.

a) The NCMA design manual provides an approach to facing connection that does not require the designer to take into account the mode of failure of the connection. It is assumed that the Factor of Safety applied to peak connection strength takes into consideration the applicable reduction factors when determining the long-term connection strength of the block/geosynthetic system.

b) The AASHTO and DEMO 82 documents provide an approach to facing connection that requires the designer to make a distinction between geosynthetic rupture and geosynthetic pullout as failure modes. An accurate description of both failure modes is required and a precise set of criteria must be established to differentiate both modes of failure. This is

particularly important when the connection capacity curve for a specific block/geosynthetic combination may reflect both geosynthetic rupture failure and geosynthetic pullout failure.

RECOMMENDATIONS

As an initial evaluation, it is suggested that the failure criteria be based on the shape of the load displacement curves, as shown in Figure No. 9. The following characteristics of the curve should be taken into account:

- the displacement to peak connection strength;
- the post-peak behavior of the load displacement curve, which includes both the recovered connection capacity of the system as well as the time or displacement for the connection to recover;
- the total displacement of the geosynthetic; and
- the value of the peak load, regardless of the failure mode. If the peak load is less than the creep reduced strength of the geosynthetic, no reduction factor for creep need be applied. If it is greater, then a value no greater than the creep reduced strength of the geosynthetic should be used.

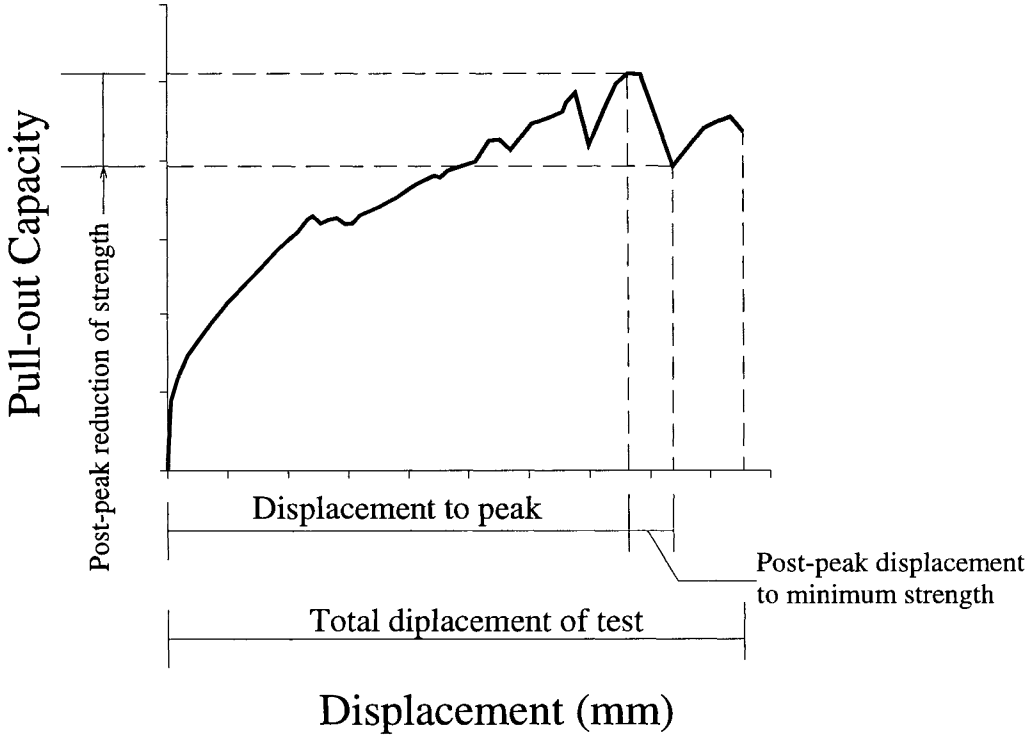

Figure No. 9. Load displacement curve showing suggested criteria for connection evaluation

FURTHER RESEARCH

The need for further research in the analysis of facing connection is great, not so much from a connection strength perspective, but from an actual applied load perspective. Conservative assumptions have been made from the load side of the equation, which have made the overall factor of safety of segmental retaining walls unusually high. Presently, full-scale segmental retaining walls are being constructed and monitored so those design concerns such as connection loads, facing connection strength, and hinge height can be analyzed. Design engineers can then attribute the attention that these concerns truly deserve.

ACKNOWLEDGEMENT

The authors would like to acknowledge the contribution of John Paulson. His suggestions and comments were truly invaluable.

REFERENCES

AASHTO, 1996, *Standard Specifications for Highway Bridges, with 1997 Interims*, American Associations of State Highway and Transportation Officials, Fifteenth Edition, Washington, DC, USA

ASTM Standards on Geosynthetics, 1995, *Standard Test Method for Tensile Properties of Geotextiles by the Wide-Width Strip Method, Designation: D 4595 - 86,* American Society for Testing and Materials, Fourth Edition, West Conshohocken, PA, USA

Bathurst, R.J. and Simac, M.R., 1993, *Laboratory Testing of Modular Unit-Geogrid Facing Connections,* STP 1190 Geosynthetic Soil Reinforcement Testing Procedures (S.C.J. Cheng, editor) American Society for Testing and Materials, (Special Technical Publication), West Conshohocken, PA, USA

NCMA, 1996, *Design Manual for Segmental Retaining Walls,* National Concrete Masonry Association, Second Edition, Herndon VA, USA

INSTALLATION DAMAGE TESTING, SENSITIVITY ASSESSMENT AND DERIVATION OF RF_{ID}

C. JOEL SPRAGUE, SAM ALLEN, AND SCOTT THORNTON
TRI/ENVIRONMENTAL, INC., AUSTIN, TX, USA

ABSTRACT

There is currently no accepted laboratory simulation of installation damage, and, therefore, field trials continue to remain the state of practice. Therefore, a procedure originally developed and reported by Watts and Brady (1994) for applying installation damage to geosynthetics which allows for exhumation of the test samples while avoiding unintended damage was adopted. A review of the test procedure is provided with typical results for a range of geosynthetics and soil types. Additionally, a proposed approach to interpreting the data is presented that uses regression analysis to compare different variables and their relative relationship to retained strength. Clearly, mass per unit area, which has been thought to be directly related to the level of installation, is not always the most important variable. The regression relationships can be used to normalize the data to reflect project-specific conditions. The normalized installation damage results appear to compare favorably with RF_{ID} values recommended by Elias, et.al. (1997).

INTRODUCTION

There is no currently accepted laboratory simulation of installation damage. Thus, a convenient field method has been adopted for applying installation damage to geosynthetics. The method, which allows for exhumation of the test samples while avoiding unintended damage, was developed and reported by Watts and Brady (1994) of the Transport Research Laboratory in the United Kingdom. Several different geosynthetics have been tested using the same soils and testing procedures. The resulting data and, more importantly, the interpretation of the data is presented.

MATERIALS

A number of geotextiles and geogrids have been tested as shown in Table 1. All geosynthetics were tested in the machine direction. Typically, the geosynthetics were exposed to a range of three soils/aggregates described as sand, sandy gravel, and flexible base course. The soils/aggregates were classified as sub-angular to angular. The grain size distributions are shown in Table 2.

Table 1. Geosynthetics Tested for Installation Damage

Geosynthetic Designation	Geosynthetic Description
Grid A	Acrylic Coated PET Grid
Grid B	PVC Coated PET Geogrid
Grid C	PVC Coated PET Geogrid
Grid D	PVC Coated PET Geogrid
Textile A	PET Woven Geotextile

Table 2. Soil/Aggregate Gradations (percent passing by weight)

(Sieve No.)/Size	Sandy Gravel	Sand	Flexible Road Base
(1-3/4) 44.5 mm			100
(1-1/4) 31.5 mm	100	100	91
(7/8) 22 mm	95		82
(3/8) 9.5 mm	55		55
(#4) 4.75 mm	47	99	43
(#10) 2 mm	37		
(#40) 0.425 mm	24	22	25
(#200) 0.75 mm	2	4	

SAMPLING AND SPECIMEN SELECTION

Each set of tensile tests of an exposed style of geosynthetic was compared with tensile tests of the same style of the geosynthetic in an unexposed, or baseline, condition. A specific sampling procedure was followed that assured that individual baseline specimen populations were developed from the same region of the roll width as those specimens dedicated to installation damage exposure. In this way, tensile specimens were not representative of the roll width, but instead were specific to a defined region within the roll width.

This approach was accomplished by cutting five coupons (four for exposure and one for baseline) measuring approximately 1.1 m x 1.3 m (42 in. x 52 in.) in sequence along the roll length. This technique captured common yarns/ribs in the tested specimens to minimize variation. Each coupon yielded 5 candidate specimens for testing for a total of 20 potential specimens. The coupons and candidate specimens were selected prior to exposure and installed in accordance with a defined sampling plan. Exposure coupons were laid within the exposure lane in consecutive order, each representing five specimens. Thus, the exposure lane was constructed with specimens 1 through 20. Upon exhumation of the exposed coupons, specimens were cut and tested in accordance with the hierarchy shown in Figure 1.

Exposure Coupon 1					Exposure Coupon 2					Exposure Coupon 3					Exposure Coupon 4				
1	2	3	4	5	11	12	13	14	15	6	7	8	9	10	16	17	18	19	20
Exposed Specimen Testing Order →																			
First specimens tested										Specimens tested if needed									

Figure 1. Specimen Numbering and Layout

A minimum of nine exposed specimens from each testing condition were systematically selected for testing from the 20 candidate specimens. The test results were averaged and compared to the average of six baseline specimens. Additional exposed specimens were tested if needed to assure a coefficient of variation of less than five percent.

EXPOSURE PROCEDURE

Since compaction typically occurs parallel to the face of retaining walls and the contour lines of slopes, the fabric direction to be evaluated (normally the machine direction) was placed perpendicular to the running direction of the compaction equipment (see Figure 2).

To initiate the exposure procedure, four steel plates each measuring 1.1 m x 1.3 m (42 in. x 52 in.), equipped with lifting chains, were placed on a flat clean surface of hardened limestone rock. An 0.2 m (8 in.) layer of soil/aggregate was then placed over the adjacent plates and compacted. Next, each of four samples of geosynthetic was placed on the compacted soil over an area corresponding to an underlying steel plate. To complete the installation, the second layer of soil was compacted over the geosynthetic (see Figure 4). To guide and contain the compaction process, braced railroad ties defined the long edges of the installation. The lifts and degree of compaction conformed to good commercial practice.

All soils were placed in single lifts and compacted to a thickness between 0.15 and 0.20 m (6 and 8 in.). Compaction was accomplished using a 0.80 m (31 in.) wide ride-on roller providing a static load of 11.6 kN (2600 lbs) and a vibratory force of 32.6 kN (7326 lbs). All compaction and exhumation procedures were performed under the supervision of a qualified lab technician. Laboratory soil classification and field thickness and density measurements were made by a qualified geotechnical technician. The following construction quality control measurements were followed during exposure.

- Proctor and sieve analyses were performed on each soil/aggregate.
- Thickness measurements were made before and after compaction.
- Density/moisture content measurements were made on each lift using a nuclear density gage to confirm that densities exceeding 90% of modified Proctor (per ASTM D 1557) were being achieved.
- Additionally, the number of equipment loadings (i.e. passes) were recorded for each exposure and corresponding soil compaction effort.

Figure 2: Panel Layout

Figure 3: Application of Second Layer of Soil

Figure 4: Secondary Compaction and Quality Control Testing

Figure 5. Exhumation via Lifting Plates

To exhume the geosynthetic, railroad ties were removed and one end of each plate was raised with lifting chains (Figure 5). After raising the plate to about 45°, soil located near the bottom of the leaning plate was removed and the plate was struck with a sledge hammer to loosen the fill. The covering sand/aggregate was then carefully removed from the surface while rolling the geosynthetic away from the soil. This procedure assured a minimum of exhumation stress.

SPECIMEN PREPARATION AND WIDE WIDTH TENSILE TESTING

Upon removal from the exposure site, exposure coupons were allowed to dry. Coupons were then cleaned by removing surface soil via light hand sweeping. Soil trapped within a geotextile's structure was not removed by washing and or otherwise stressing the geotextile. No soil was able to penetrate into any of the grid structures. No additional cleaning was performed and specimens were cut and tested in their soiled condition.

The evaluation of RF_{ID} was based on the results of wide width tensile tests per ASTM D 4595, *Standard Test Method for Tensile Properties of Geotextiles by the Wide-Width Strip Method.* In the case of geogrid samples, ASTM D 4595 was modified to incorporate their structure. For implementation of ASTM D 4595 the laboratory utilizes capstan grips which require specimen lengths of 1.1 m (42 in.). The specimens were tested using an Instron Model 5583 tension/compression machine equipped with capstan roller clamps. Strain was monitored using an Epsilon extensometer mounted on the specimen via prongs for geotextiles and quick-release clips for geogrids. Pretest slack removal around the roller grips was limited to application of a fifty pound preload immediately prior to testing each specimen. After exposure was complete, all baseline and exposed wide width tensile tests were performed during the same testing period.

TEST RESULTS

Test Data

To adequately evaluate installation damage, it is necessary to collect as much data on the materials and installation as possible. Tables 3 and 4 provide relevant laboratory and field data associated with the installation damage exposures.

Table 3. Data on the Reinforcement

Reinforcement			
Product	Mass per Unit Area (g/m^2)	Uncoated Mass per Area (g/m^2)	Coating Mass per Area (g/m^2)
Grid 1A	181	122	59
Grid 1B	195	139	56
Grid 1C	372	264	108
Grid 2A	248	110	138
Grid 2B	516	165	351
Grid 2C	412	200	212
Grid 3A	205	122	83
Grid 3B	234	142	134
Grid 3C	276	207	69
Grid 4A	157	72	85
Grid 4B	216	102	114
Grid 4C	283	130	153
Grid 4D	375	220	155
Textile 1A	458	458	0
Textile 1B	712	712	0
Textile 1C	915	915	0

Table 4. Installation-Related Test Data

	Sand			Sandy-Gravel			Flexible Base		
Product	Lift Thickness (m)	Comp-action (% Mod. Proctor)	Strength Retained (%)	Lift Thickness (m)	Comp-action (% Mod. Proctor)	Strength Retained (%)	Lift Thickness (m)	Comp-action (% Mod. Proctor)	Strength Retained (%)
Grid 1A	0.20	101.90	90.00	0.20	101.10	89.70	0.20	93.40	96.80
Grid 1B	0.20	104.10	88.30	0.20	97.60	91.10	0.20	96.00	95.90
Grid 1C	0.20	101.30	87.70	0.20	98.90	90.40	0.20	95.10	100.00
Grid 2A	0.20	95.60	91.60	0.19	97.50	87.90	0.19	95.20	82.80
Grid 2B	0.20	95.00	93.10	0.19	98.60	90.60	0.19	95.20	93.70
Grid 2C	0.20	94.70	90.10	0.15	96.90	80.60	0.19	95.00	84.60
Grid 3A	0.20	104.50	81.70	0.20	98.90	77.20			
Grid 3B	0.20	104.30	86.60	0.20	100.50	78.40			
Grid 3C	0.20	103.10	91.20	0.20	100.70	83.20			
Grid 4A	0.20	102.20	98.80	0.20	98.50	85.70	0.20	95.60	97.40
Grid 4B	0.20	102.70	87.30	0.20	100.80	85.30	0.20	93.90	94.20
Grid 4C	0.20	104.30	95.50	0.20	99.90	95.10	0.20	93.60	90.10
Grid 4D	0.22	103.75	88.50	0.20	101.90	97.40	0.20	97.00	88.40
Textile 1A	0.20	98.90	77.30	0.18	97.60	74.50	0.18	96.10	75.00
Textile 1B	0.15	105.00	70.40	0.18	100.20	76.40	0.15	93.70	74.10
Textile 1C	0.15	105.00	65.80	0.18	99.50	71.70	0.18	93.20	75.60

Interpretation of Results

The results of installation damage testing are presented in terms of retained strength for the given exposure condition. This means that, strictly speaking, the results only apply directly to projects involving the same geosynthetic, soil, lift thickness, and compactive effort. Well, clearly the intent of installation damage testing is to provide more broadly useful results. To this end, it is important to interpret the results in light of the variables involved and provide a mechanism, if possible, to extend the test results to other related conditions.

While it has been widely proposed that installation damage is directly related to the mass per unit area of the tested geosynthetic, our results did not support this. Rather, it became apparent that the relationship between installation damage and the testing variables is much more complex. Various relationships were studied using regression analysis in an attempt to discover the most significant relationship(s) for each tested geosynthetic. Tables 5a and 5b provide a summary of the various relationships examined and the associated correlation coefficients (R^2) that were determined by regression analysis. Table 6 calculates "normalized" retained strength values using the regression relationships with the highest correlation coefficients defined in Tables 5a and 5b. When required, the "normalized" stress ratio used in the calculation is for a installation condition of 90% modified Proctor compaction and 8 inch lifts (i.e. 90 / 8 = 11.25).

Table 5a. Retained Strength (x) vs. Selected Relationship (y) Analysis - Grids

Geosyn-thetic	Soil	Vs. Mass per Unit Area	Vs. Coating Mass per Unit Area	Vs. Coating Ratio	Vs. Stress Ratio	Vs. Stress Ratio Coating Ratio	Vs. Stress Ratio Coating Mass
Grid 1	Sand	y = -1.9715x + 182.16 R^2 = 0.5579	y = -0.4808x + 44.82 R^2 = 0.4421	**y = 1.6873x - 119.59** **R^2 = 0.8924**	y = -0.01x + 13.687 R^2 = 0.0042	y = -0.0233x + 2.4933 R^2 = 0.7458	y = 1.0749x - 88.889 R^2 = 0.363
	Sandy-Gravel	y = 0.295x - 19.316 R^2 = 0.0043	y = -0.0621x + 7.8027 R^2 = 0.0025	y = -2.7495x + 278.57 R^2 = 0.8158	**y = -0.3125x + 40.65** **R^2 = 0.9784**	y = 0.0265x - 1.9788 R^2 = 0.7379	y = 0.0859x - 1.5604 R^2 = 0.0009
	Flex. Base	y = 1.4061x - 129.83 R^2 = 0.9257	y = 0.3953x - 36.382 R^2 = 0.9746	y = -0.2285x + 52.316 R^2 = 0.0534	y = -0.0026x + 12.112 R^2 = 0.0012	y = 0.0026x + 0.1408 R^2 = 0.0307	**y = -0.8873x + 92.498** **R^2 = 0.9958**
Grid 2	Sand	y = 1.019x - 81.771 R^2 = 0.1475	y = 1.3633x - 117.98 R^2 = 0.4126	= 5.5107x - 446.37 R^2 = 0.926	y = 0.0125x + 10.742 R^2 = 0.1071	**y = -0.0184x + 1.8956** **R^2 = 0.9384**	y = -0.2477x + 24.682 R^2 = 0.1726
	Sandy-Gravel	y = 0.1032x + 2.6525 R^2 = 0.018	y = 0.261x - 15.643 R^2 = 0.1799	y = 1.4283x - 64.953 R^2 = 0.7399	y = -0.1939x + 30.433 R^2 = 0.8931	**y = -0.0092x + 1.0352** **R^2 = 0.9735**	y = -0.0648x + 7.8742 R^2 = 0.1214
	Flex. Base	y = 0.5982x - 40.499 R^2 = 0.7715	**y = 0.5345x - 39.621** **R^2 = 0.9625**	y = 1.3525x - 59.31 R^2 = 0.8464	= 0.001x + 12.602 R^2 = 0.1301	y = -0.0047x + 0.627 R^2 = 0.805	y = -0.1452x + 14.756 R^2 = 0.8046
Grid 3	Sand	**y = 0.2201x - 11.999** **R^2 = 0.984**	y = -0.0415x + 5.9984 R^2 = 0.3571	y = -1.6049x + 173.82 R^2 = 0.8021	y = -0.0183x + 14.577 R^2 = 0.8416	y = 0.0198x - 1.3207 R^2 = 0.777	y = 0.0988x - 3.0776 R^2 = 0.4006
	Sandy-Gravel	y = 0.3237x - 18.725 R^2 = 0.9503	y = -0.087x + 9.3348 R^2 = 0.701	**y = -2.6655x + 247.17** **R^2 = 0.9881**	y = 0.0283x + 10.254 R^2 = 0.5298	y = 0.0339x - 2.3208 R^2 = 0.9863	y = 0.2193x - 12.19 R^2 = 0.8141
	Flex. Base	y = 0.5982x - 40.499 R^2 = 0.7715	**y = 0.5345x - 39.621** **R^2 = 0.9625**	y = 1.3525x - 59.31 R^2 = 0.8464	y = 0.001x + 12.602 R^2 = 0.1301	y = -0.0047x + 0.627 R^2 = 0.805	y = -0.1452x + 14.756 R^2 = 0.8046
Grid 4	Sand	y = -0.2595x + 31.608 R^2 = 0.2704	y = -0.0725x + 10.444 R^2 = 0.1631	y = 0.6546x - 9.9666 R^2 = 0.3357	y = 0.0299x + 9.945 R^2 = 0.2152	y = -0.0029x + 0.5253 R^2 = 0.3346	y = 0.1057x - 6.1594 R^2 = 0.2823
	Sandy-Gravel	**y = 0.4057x - 29.268** **R^2 = 0.8525**	y = 0.1455x - 9.4861 R^2 = 0.848	y = -0.6438x + 109.11 R^2 = 0.4188	y = 0.0161x + 11.067 R^2 = 0.3179	y = 0.004x - 0.1167 R^2 = 0.4367	y = -0.139x + 16.187 R^2 = 0.7454
	Flex. Base	y = -0.6594x + 68.617 R^2 = 0.9419	**y = -0.2414x + 26.07** **R^2 = 0.9753**	y = 1.031x - 44.798 R^2 = 0.4492	y = -0.0095x + 12.76 R^2 = 0.0382	y = -0.0058x + 0.7768 R^2 = 0.4061	y = 0.239x - 18.736 R^2 = 0.9225

Table 5b. Retained Strength (x) vs. Selected Relationship (y) Analysis - Textiles

Geosyn.	Soil	Vs. Mass per Unit Area	Vs. Stress Ratio	Vs. Stress Ratio / Mass per Area
Textile 1A	All	y = -0.6897x + 70.323 R^2 = 0.828	y = -0.1726x + 26.531 R^2 = 0.8404	y = -0.0425x + 4.2004 R^2 = 0.9982
Textile 1B	All	y = -1.5429x + 134.99 R^2 = 0.2909	y = 0.0124x + 13.237 R^2 = 0.0232	y = -0.0252x + 2.6073 R^2 = 0.9992
Textile 1C	All	y = 3.0263x - 206.17 R^2 = 0.1141	y = -0.2168x + 31.197 R^2 = 0.0235	y = -0.0162x + 1.7072 R^2 = 0.9603

Table 6. Normalized Retained Strengths

	Sand		Sandy-Gravel		Flexible Base	
Product	Normalizing Relationship	Normalized Strength Retained (%)	Normalizing Relationship	Normalized Strength Retained (%)	Normalizing Relationship	Normalized Strength Retained (%)
Grid 1A	Coating Ratio	90.1	Stress Ratio	94.1	Stress Ratio / Coating Mass	96.9
Grid 1B	Coating Ratio	87.8	Stress Ratio	94.1	Stress Ratio / Coating Mass	96.5
Grid 1C	Coating Ratio	88.0	Stress Ratio	94.1	Stress Ratio / Coating Mass	100.3
Grid 2A	Stress Ratio / Coating Ratio	92.0	Stress Ratio / Coating Ratio	90.6	Coating Mass per Unit Area	81.8
Grid 2B	Stress Ratio / Coating Ratio	94.0	Stress Ratio / Coating Ratio	94.5	Coating Mass per Unit Area	93.5
Grid 2C	Stress Ratio / Coating Ratio	91.1	Stress Ratio / Coating Ratio	88.8	Coating Mass per Unit Area	85.8
Grid 3A	Mass per Unit Area	82.0	Coating Ratio	77.5	Coating Mass per Unit Area	78.7
Grid 3B	Mass per Unit Area	85.9	Coating Ratio	78.0	Coating Mass per Unit Area	79.2
Grid 3C	Mass per Unit Area	91.6	Coating Ratio	83.3	Coating Mass per Unit Area	78.0
Grid 4A	None*	98.8	Mass per Unit Area	83.6	Coating Mass per Unit Area	97.6
Grid 4B	None*	87.3	Mass per Unit Area	87.8	Coating Mass per Unit Area	94.1
Grid 4C	None*	95.5	Mass per Unit Area	92.7	Coating Mass per Unit Area	89.2
Grid 4D	None*	88.5	Mass per Unit Area	99.4	Coating Mass per Unit Area	89.1
Textile1A	Stress Ratio / Mass per Area	79.2	Stress Ratio / Mass per Area	79.2	Stress Ratio / Mass per Area	79.2
Textile1B	Stress Ratio / Mass per Area	82.2	Stress Ratio / Mass per Area	82.2	Stress Ratio / Mass per Area	82.2
Textile 1C	Stress Ratio / Mass per Area	79.6	Stress Ratio / Mass per Area	79.6	Stress Ratio / Mass per Area	79.6

* No acceptable general relationship was identified with which to normalize, therefore, "raw" results are used.

DISCUSSION

Installation damage varies with soil type, lift thickness, and degree of compaction. Each unique combination of these variables will result in a specific level of damage to a given geosynthetic. And, since each individual material application will involve a unique combination of soil type and associated lift and compaction requirements, a unique reduction factor is most appropriate.

Project-specific installation damage factors can be determined from related testing data using normalization. Normalization is a way of adjusting available test data based on documented relationships between variables to reflect project-specific conditions.

The technical approach included careful monitoring of construction variables (especially lift thickness and compaction) during testing to facilitate the normalization of results to any similar project specification.

Compacted lift thicknesses used in installation damage testing ranged from 0.15 to 0.20 m (6 to 8 in.) and compaction percentages ranged from 90 to 100+ percent of modified Proctor compaction. Field data is essential for the determination of unique reduction factors for other similar conditions. Regression analysis can be used to establish the relationship(s) between variables.

Table 7 presents the range of normalized reduction factors determined for the tested geosynthetics.

Table 7. Summary of Normalized Installation Damage Reduction Factors

Geosynthetic Type	Sand		Sandy-Gravel		Road Base	
	Normalized % Retained	RD_{ID}	Normalized % Retained	RD_{ID}	Normalized % Retained	RD_{ID}
Grid 1A	90.1	1.11	94.1	1.06	96.9	1.03
Grid 1B	87.8	1.14	94.1	1.06	96.5	1.04
Grid 1C	88.0	1.14	94.1	1.06	100.3	1.00
Grid 2A	92.0	1.09	90.6	1.10	81.8	1.22
Grid 2B	94.0	1.06	94.5	1.06	93.5	1.07
Grid 2C	91.1	1.10	88.8	1.13	85.8	1.17
Grid 3A	82.0	1.22	77.5	1.29	78.7	1.27
Grid 3B	85.9	1.16	78.0	1.28	79.2	1.26
Grid 3C	91.6	1.09	83.3	1.20	78.0	1.28
Grid 4A	98.8	1.01	83.6	1.20	97.6	1.02
Grid 4B	87.3	1.15	87.8	1.14	94.1	1.06
Grid 4C	95.5	1.05	92.7	1.08	89.2	1.12
Grid 4D	88.5	1.13	99.4	1.01	89.1	1.12
Textile1A	79.2	1.26	79.2	1.26	79.2	1.26
Textile1B	82.2	1.22	82.2	1.22	82.2	1.22
Textile 1C	79.6	1.26	79.6	1.26	79.6	1.26

The reduction factors presented in Table 7 uniquely represent the following conditions:

- Sand and Sandy-gravel (See Figure 1 for PSD Curves)
- 8 inch compacted lifts
- 90% modified proctor density

The installation damage testing results appear to compare favorably with RF_{ID} values recommended by Elias, et.al. (1997) as shown in Table 8.

Table 8. Comparison to Historical Values

Source	Cohesive Soils	Sand	Sandy-Gravel	Flexible Base
Elias, et. al. (1997)	1.05 - 1.20	1.10 - 1.40	1.40 - 2.20	Not done
TRI Testing	Not done	1.01 – 1.26	1.01 – 1.39	1.00 – 1.28

CONCLUSIONS

While it is commonly held that more massive geosynthetics are more resistant to installation damage, this relationship did not commonly emerge from this testing. Rather, it appears that other phenomena may more significantly effect results. The coating plays a crucial role in a geogrid's resistance to installation damage. Coating thickness may vary from style to style or may be variable within a given style. Testing seems to indicate that the amount of coating more than mass per unit area relates to the damage of geogrids. Additionally, the amount of stress applied during installation is an important variable which can be normalized for project-specific compaction and lift thickness specifications.

Yet, it was not always possible to find satisfactory relationships between the variables of installation and retained strength. This may mean that more testing variables need to be tracked and documented, or perhaps some of the materials are too variable to constitute a family of products. Still, it appears that in many cases installation damage results can be normalized to project-specific requirements providing a more appropriate and, perhaps, lower reduction factor than might generally be used.

REFERENCES

Elias, et al (1997), "FHWA technical note on the degradation-reduction factors for geosynthetics", Geotechnical Fabrics Report, August, pp. 24-26.

Watts, G.R.A. and K.C. Brady (1994), " Geosynthetics: Installation Damage and the Measurement of Tensile Strength", Proceedings of the Fifth International Conference on Geotextiles, Geomembranes, and Related Products, Singapore, pp. 1159-1164.

PROPERTIES OF COATED FIBERGLASS GEOGRID

JOHN PAULSON, P.E.
STRATA SYSTEMS,INC., USA

ABSTRACT

Fiberglass filament has been used for tensile strength applications for years. Fiberglass filament exhibits excellent tensile strength, modulus and creep resistance, but exhibits poor abrasion characteristics as demonstrated in the flex test, a manual test applied to individual yarns. Past uses for this fiber in textiles have been with coated or laminated scrims, where flexural resistance is not an in-service need. Use has been limited in geosynthetics because of difficulties in manufacturing, installation and in-service conditions.

This paper presents a new category of coated fiberglass product with strength at very low strain and little creep strain, while exhibiting excellent resistance to installation and in-service stresses. The yarn discussed has been coated during yarn production but prior to use in manufacturing geogrids.

Geogrid rib tensile strength and load-strain characteristics are presented and compared with several currently available reinforcement materials. Installation damage field trial results on the finished geogrid are also presented. Tensile creep and stress rupture test results are presented, along with the behavioral differences in this yarn when compared with conventional yarn and polymer types.

Properties used to determine Long Term Design Strength (LTDS) reduction factors are presented and discussed, along with a summary of future work suggested to further define this new reinforcement material.

INTRODUCTION

Glass fiber is the dominant reinforcement used in enhancing the performance of many polymeric composites. This is due to its high

specific tensile strength and modulus at relatively low cost. For this reason, glass fiber reinforced polymeric composites have found extensive use in automotive, construction, marine, electrical, and consumer applications.

In spite of key performance attributes of glass fibers suitable for many geosynthetic applications such as reinforcement, their penetration in this market segment has been negligible because of concerns regarding abrasion resistance.

The specific tensile strength (strength divided by specific gravity) of coated glass fiber yarn is about ten fold higher and the specific tensile modulus about five fold higher than those of polypropylene or polyester filaments used in soil reinforcement applications. Modulus of fiberglass yarn is 10-20 times greater than Polyester (PET) and high density polyethylene (HDPE). Figure 1 shows characteristic load-strain curves for PET, HDPE and glass fiber.

Geotechnical design utilizing geosynthetic reinforcement has been used in North America since the early 1970's. The first applications were geotextile walls built by the US Forest Service (Stewart, et.al,1971) and in reinforcement of embankments over soft soils (Fowler et.al.,1987). These embankment applications used woven polypropylene and polyester fabrics that exhibited ultimate strengths at strains of 12-20 %, with design strengths assumed to be in the 5-10 % range. The significant width of a typical embankment of 50 meters could result in total deformations of 2 meters or more. This deformation did not consider the additional strain over time, or creep that polymers (high-density polyethylene HDPE) exhibit. Deformation performance may be improved if a high strength, very low strain reinforcement element were to be introduced into these structures. Figure 1 depicts conceptual comparative load-strain behavior of PET, HDPE, and fiberglass.

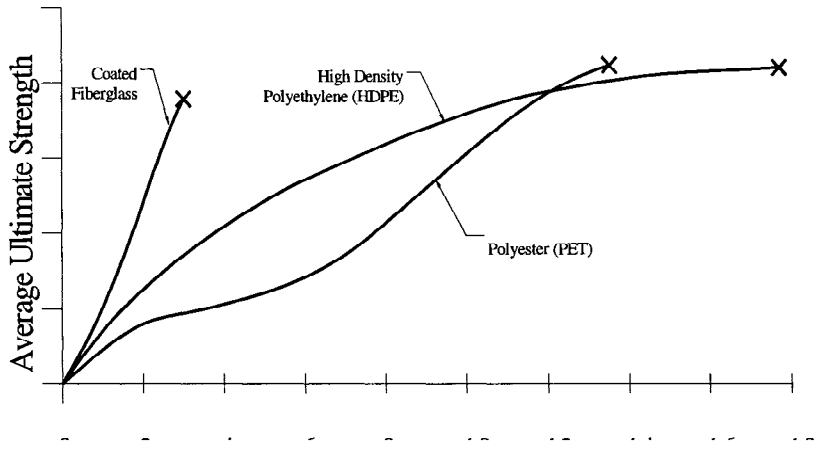

Figure 1. Conceptual Tensile Strength vs Strain Results: PET vs HDPE vs Fiberglass

LITERATURE REVIEW

Girgis (1991) introduced the concept of fiberglass yarns for geosynthetics. In this reference the coated glass fiber product, Hercuflex™, and process was presented.

Martine (1993) reported on long term tensile creep and stress rupture testing of unidirectional fiberglass reinforced composites. Tension creep specimens were loaded to values of 40%, 50% and 60 % of the short-term ultimate strength range. The only creep strain noted was attributed to the polyester resin encapsulating the glass fiber.

Stress rupture testing was performed on 24 specimens with loads of 50 to 66% of short term ultimate strength. These tests showed a sharp drop off in strength initially, followed by a relatively flat stress rupture envelope slope thereafter.

Miyata (1996) presents the first published use of fiberglass yarn in a geogrid form. This geogrid is produced by impregnating high tensile strength continuous bundles with vinyl-ester resin which are then molded to give the grid geometry. Although the material discussed therein is not a coated fiber or knitted material, the stress-strain characteristics indicative of fiberglass are demonstrated. Tensile strength test results showing 2.2 % strain at ultimate load are presented for a family of geogrids. Stress rupture behavior of glass fiber is presented by Miyata (1996) as well as a reduction factor for the short-term ultimate strength to be used to prevent rupture.

FIBER DESCRIPTION

The fiber described herein uses a coated yarn technology in which the individual glass filaments in a yarn bundle are impregnated with a polymeric coating material. This provides the yarn with enhanced abrasion resistance making it potentially suitable for use in geosynthetic applications. This coated yarn combines the properties of glass fiber: low elongation (~3%), no creep, high tensile strength, high tensile modulus, and thermal stability with those of the coating to provide flexibility and abrasion resistance (Girgis 1991).

This yarn can then be processed into geogrids or geotextiles by conventional textile processing methods such as beaming, weaving, knitting etc. A secondary polymeric coating may be applied after grid fabrication to further enhance product structural integrity, junction strength and to give added protection for enhanced durability under installation and other environment conditions. This coating is similar to what is presently used to coat knitted polyester geogrid products.

TESTING PROGRAM

Geogrid.

The structure developed and used for this project used the yarn described above, which was knitted and PVC coated. This process closely followed a knitted, coated geogrid product commercially available. This geogrid uses polyester yarn. A close up of the knitted structure is shown on Figure 2.

A testing program was undertaken to quantify physical properties of the yarn, the knitted ribs and the finished geogrid. This section will describe the test program, summarize the results, and present comparisons to conventional yarn strength and property testing.

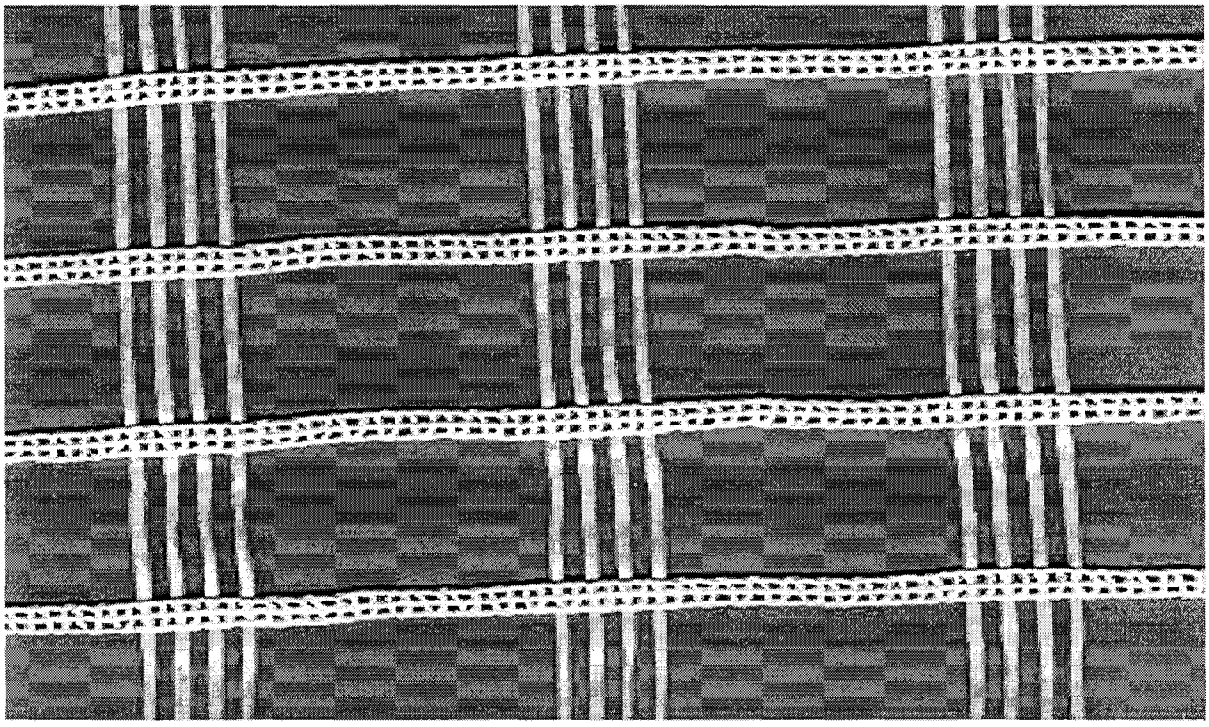

Figure 2. Knitted Geogrid Structure

Tensile Strength - Fiber and Rib.

The yarn producer had developed testing methods and results for this yarn. Because of the very high modulus and low strains at failure, tensile testing on this material is sensitive to clamping and other attachment devices. The goal of the following individual yarn test program was to replicate the tensile strength and modulus results obtained from the yarn producer. Once yarns could be successfully

tested knitted ribs were then tested. Several grips were evaluated, including wedge clamps, and single and multiple roller clamps.

It was found that the best result was obtained when very smooth surfaced multiple roller grips were used. Various surfaces were applied to the roller type grips in an attempt to achieve the highest test results. Chrome plating of the roller grips turned out to provide the lowest friction surface, and coupled with several wraps, became the preferred clamping procedure.

Single rib tensile strengths consisting of 3 yarn bundles per rib were then attempted. Test procedure GRI:GG1 was used. Table 1 summarizes the individual yarn and single rib break strength results and the respective efficiency.

The efficiency is defined as the reported test result divided by the theoretical maximum tensile strength, determined by summing the fiber tensile strengths. Yarn and rib strength efficiencies from this testing are around 88%.

TABLE 1. Yarn and Knitted Rib Strength Results

	Tensile (ave)	elongation %
Yarn	104 lb	2.2-3.0
Rib	365 lb	2.2-3.0
Efficiency	88 %	100 %

Wide Width Tensile Testing.

Wide width strip tensile testing, in accordance with ASTM D4595 was attempted but was found difficult to perform on this extremely high modulus fiber geogrid. Specimens 20 cm wide as well as 10 cm specimens were attempted, with little success.

Where yarn to single rib efficiencies are 88-90%, wide width specimens tested to date reveal an efficiency of about 50 %. This is because all yarns and ribs in a wide width specimen do not pick up load equally during the test. Because of the difficulty in wide width testing, single rib test results will be used to determine tensile strength properties.

Installation Damage.

Fiberglass has historically performed poorly when subjected to repeated flexural loading. The flex test, typically performed by manually bending an individual yarn back and forth will result in yarn breakage when subjected to only a few flexural cycles. The coated fiberglass yarn will withstand thousands of cycles of this test.(PPG 1992.

The fragility of this coated yarn was investigated using installation damage testing of a full size geogrid specimen, performed on full width samples to quantify this fragility.

The test setup consisted of a 1.5 meter wide by 6 meter long test platform where compaction of the overlying fill was achieved with heavy construction equipment. This procedure was developed and reported by Watts and Brady (1994). Installation damage was imparted by compaction a relatively aggressive aggregate described as flexible crushed surfacing base course. The aggregate was classified as sub-angular to angular. Compaction efforts to density levels of 90 - 95 % of modified proctor density (ASTM D1557) were achieved. This material had a maximum dry density of 134.7 pcf and optimum moisture content of 8.0%. The material gradation is listed in Table 2 below.

Table 2. Gradation of Graded Flexible Base

US Standard Sieve size, Sieve no.	% Passing
1-3/4"	100
1-1/4"	91
7/8"	82
3/8"	55
No. 4	43
No. 10	34
No. 40	25

Tensile strengths of each individual rib across a roll width, before and after exposure, were measured. Results are graphically shown on the Figure 3.

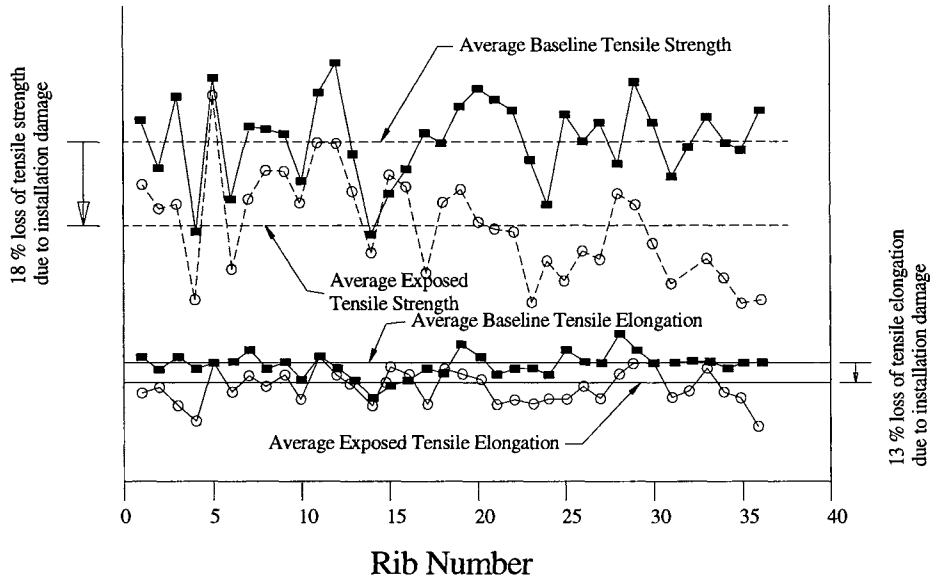

Figure 3. Baseline and Exposed Strength and Elongation

The top portion of this figure plots the unexposed individual rib tensile strength taken from ribs across the full roll width, as well as the "after exposure" tensile strength of the same rib position on the roll. The lower portion depicts the relative elongation at failure for unexposed and exhumed specimens. The average strength reduction is about 15%, for an RF_{id} of 1.17 - 1.22.

Durability

Because of its inorganic nature, glass is one of the more durable materials for use in soil environments. The resistance of glass to chemical attack is excellent, making it ideal for long term reinforcement applications (Girgis 1991).

Tensile Creep or Rupture

Creep rupture performance of geosynthetics can be evaluated using one of two approaches: long duration creep testing, and stress rupture testing.

Long term (minimum duration of 10,000 hrs ASTM 5262) tensile testing is performed at varying load levels while measuring strain over time.

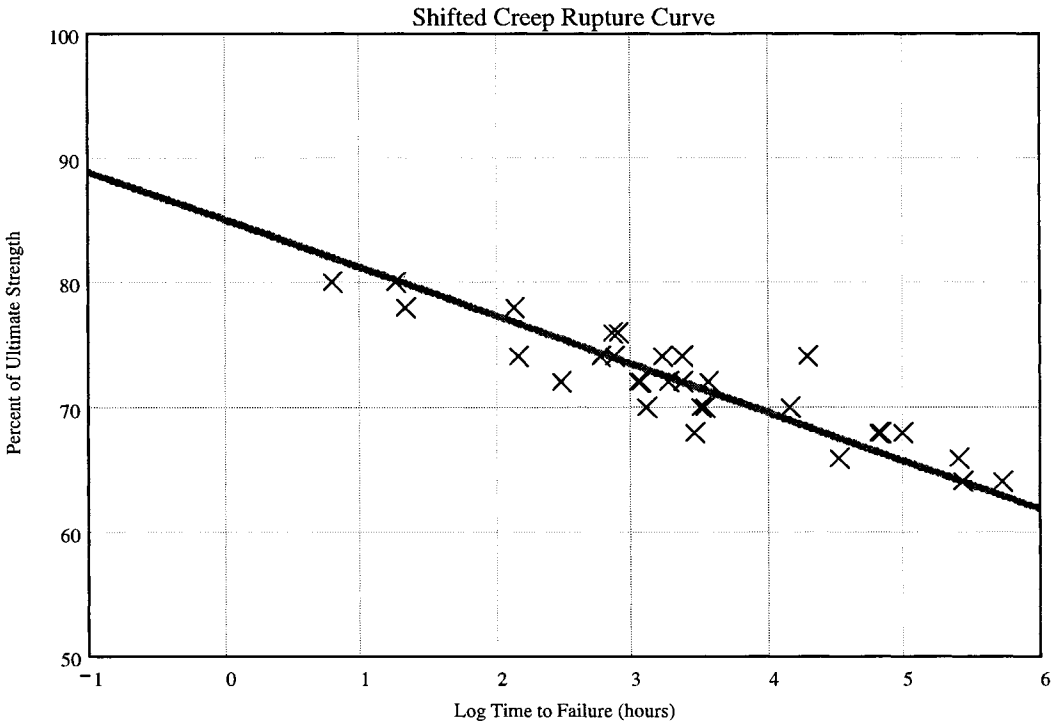

Figure 4. Typical Stress (%) vs Log Time to Rupture Plot for PET

The second method of evaluating creep rupture behavior is stress rupture testing, wherein specimens are loaded to failure at very high load levels, with time to failure measured. A stress rupture envelope is generated as a plot of percentage of ultimate tensile strength versus time to failure.

Figure 4 shows a typical stress rupture result for polyester yarn. ASTM D5262 procedure is used, with the test series beginning with the higher approximate ultimate strength percentage, then progressively reducing the load level.

Figure 5 shows the average stress rupture results, both from a fiber/matrix product, (Martine,1993) and from the glass fiber product developed herein.

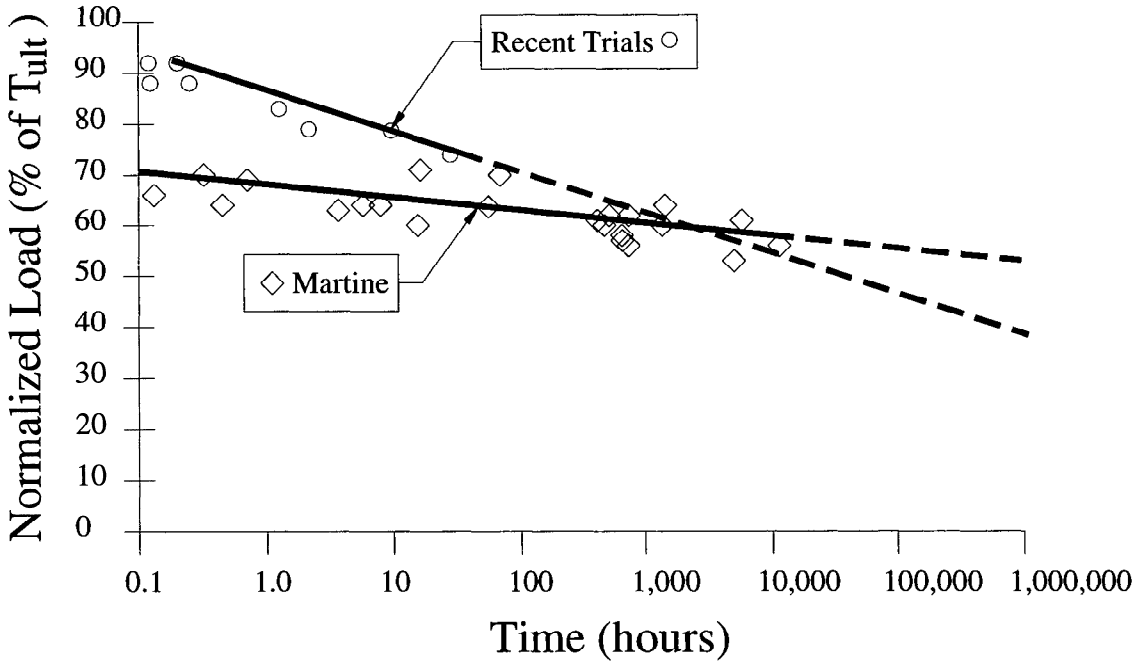

Figure 5. Stress Rupture Testing: Current Product, and Martine (1993)

While results cannot be directly compared to the knitted geogrid coated fiber, they demonstrate the behavior of this fiber in sustained tensile testing. Of interest is the slope of the respective failure envelopes, which is relatively flat from Martine (1993)and steeper for the recent trials.

Stress rupture testing for the new product experienced testing difficulties when long time duration loads were attempted. The slope of the stress rupture failure envelope was much steeper. The primary cause for this is thought to be poor clamping, because of the observed yarn and rib breaks at the clamp yarn/interface. It is believed that this is a clamping technique issue, not a yarn weakness. Work is

continuing to refine this clamping arrangement to allow accurate long duration testing of this material.

SIGNIFICANCE OF HIGH MODULUS GEOGRID REINFORCEMENT

The coated glass fiber reinforcement geogrid operates at working strain levels of approximately 1%, as opposed to 5 % or even higher initial strains commonly used in polymeric reinforcement design. This section discusses several examples of potential low strain benefit applications.

Significant strain under load may result in undesirable deformations in a reinforced soil structure. These strains induce high deformations and soil structure movements. Several examples where lower working strains may improve performance are:

- Embankments over soft ground, where strains of 5 % may result in significant lateral deformations and vertical settlement. Lower working strains would decrease lateral deformations and could reduce differential settlement.

- Veneer reinforcements when strains under load exert undesirable downlope movement and shear forces into the geomembrane and geomembrane seams.

- Tall geogrid reinforced retaining walls where lateral deformations may become visible. Current design procedures are conservative: thus measured strains in existing walls are typically much lower than what was assumed in design. As this conservatism diminishes, higher loads and consequent higher strains will result.

Benefits of Low/No Creep

Long term creep adds additional deformations to the reinforced structure. Olefin based reinforcement may exhibit additional time dependent strains higher than the elastic strains initially caused from loading. The total strain vs time comparison shown in figure 6 reveal that significant post-construction strains are possible. None of these strains occur when the glass fiber reinforcement is used.

Future Work

Further research is ongoing to better ascertain the stress rupture behavior of the coated fiberglass yarn material. The work by Martine (1993) indicates a relatively flat stress rupture curve compared with the recent test results. The potential reduction factor for creep rupture may vary from 50% from Martine (1993) to 40 % from recent efforts. This needs to be clarified with future testing. Additionally, more work on clamping the high modulus, glass fiber yarn

to allow accurate and more appropriate testing is the focus of future efforts.

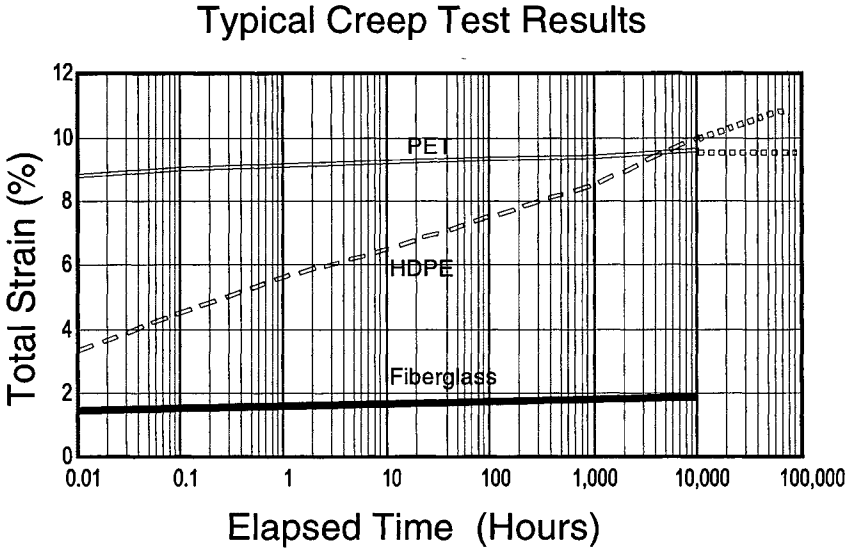

Figure 6. Comparative Strain vs time creep behavior of HDPE, PET and Fiberglass

CONCLUSIONS

Glass fiber reinforcement holds promise for future reinforcement uses. Testing to date reveals strains at working loads of 1 %. Time dependent strains of about 0.01% per decade at working loads of about 40 % of ultimate effectively eliminate time dependent deformations as a design consideration for fiberglass based geogrids. This will be further verified with future work.

Testing of fiberglass geogrid is different from composite materials of conventional materials. New clamping arrangements must be developed to deal with this new geosynthetic fiber.

ACKNOWLEDGEMENTS

PPG provided the yarn characteristic data, and educated the author on the properties of glass fiber yarn for reinforcement. Thanks to John Burke for supporting this work.

TRI Environmental worked tirelessly testing this new and different material. Special thanks go to Scott Thornton, and Sam Allen.

Finally, thanks go to Mike Bernardi who spent hours discussing the benefits of low strain materials, and for his insightful comments.

REFERENCES

Miyata, K. "Walls Reinforced with Fiber Reinforced Plastic Geogrids in Japan" Geosynthetics International Journal - 1996,Vol.3, No. 1 pp 1-11

Martine, E. "Long Term Tensile Creep and Stress Rupture Evaluation of Unidirectional Fiberglass Reinforced Composites", 48th Annual Conference Composites Institute, February 8-11,Session 9-A/1-4, 1993

Girgis, Mikhail M. "Impregnated Fiber-Glass yarn for High Strength Geosynthetic Reinforcement", American Chemical Society Annual meeting, Miami, FL. PP.337-350,1991

PPG Hercuflex Brochure, "Hercuflex Fiber Glass Strand",2049F, 1/92

Watts & Brady, "Installation Damage Procedure",4th International Conference on Geotextiles, IGS and IFAI, The Hague, Netherlands, 1990

Stewart, J.,Williamson, R. and Nohney, J. "Guidelines for Use of Fabrics in Construction and maintenance of Low Volume Roads", USDA Forest Service, Portland, OR also FHWA Report No. FHWA-TS-78-205, 1977

Fowler, J. , Koerner, R.M., "Stabilization of Very Soft Soils using Geosynthetics", Geo'87, New Orleans, LA pp.289-300 1987

Geosynthetics '99 Author Index

Geosynthetics '99 Author Index

Geosynthetics '99 Subject Index

Geosynthetics '99 Subject Index